UNCLASSIFIED

ORNL-2379
Reactors–Power
TID-4500 (13th ed.)

cy-8

HOMOGENEOUS REACTOR PROJECT

QUARTERLY PROGRESS REPORT

FOR PERIOD ENDING JULY 31, 1957

OAK RIDGE NATIONAL LABORATORY
OPERATED BY
UNION CARBIDE NUCLEAR COMPANY
A Division of Union Carbide and Carbon Corporation
UCC
POST OFFICE BOX X · OAK RIDGE, TENNESSEE

UNCLASSIFIED

Printed in USA. Price $5.00 cents. Available from the

Office of Technical Services
U. S. Department of Commerce
Washington 25, D. C.

ORNL-2379
Reactors—Power
TID-4500 (13th ed.)

Contract No. W-7405-eng-26

HOMOGENEOUS REACTOR PROJECT

QUARTERLY PROGRESS REPORT

For Period Ending July 31, 1957

Project Director – R. B. Briggs
Associate Director – C. E. Winters

Homogeneous Reactor Test – S. E. Beall
Reactor Design and Analysis – J. A. Lane
Engineering Development – J. A. Lane
Reactor Materials Research – E. G. Bohlmann
Chemical Engineering Development – D. E. Ferguson
Supporting Chemical Research – E. H. Taylor
Analytical Chemistry – M. T. Kelley

DATE ISSUED

SEP 27 1957

OAK RIDGE NATIONAL LABORATORY
Operated by
UNION CARBINE NUCLEAR COMPANY
A Division of Union Carbide and Carbon Corporation
Post Office Box X
Oak Ridge, Tennessee

ORNL-2379
Reactors–Power
TID-4500 (13th ed.)

INTERNAL DISTRIBUTION

1. C. E. Center
2. Biology Library
3. Health Physics Library
4. Metallurgy Library
5-6. Reactor Experimental Engineering Library
7-9. Central Research Library
10-14. Laboratory Records Department
15. Laboratory Records, ORNL R.C.
16. G. M. Adamson
17. J. E. Baker
18. S. E. Beall
19. A. M. Billings
20. D. S. Billington
21. E. P. Blizard
22. E. G. Bohlmann
23. C. J. Borkowski
24. G. E. Boyd
25. J. C. Bresee
26. F. R. Bruce
27. W. D. Burch
28. C. A. Burchsted
29. A. D. Callihan
30. D. W. Cardwell
31. W. L. Carter
32. G. H. Cartledge
33. R. A. Charpie
34. R. D. Cheverton
35. H. C. Claiborne
36. W. E. Clark
37. T. E. Cole
38. E. L. Compere
39. D. D. Cowen
40. S. Cromer
41. F. L. Culler
42. J. S. Culver
43. J. S. Drury
44. W. K. Eister
45. L. B. Emlet (K-25)
46. D. E. Ferguson
47. J. H. Frye, Jr.
48. C. H. Gabbard
49. J. L. Gabbard
50. W. R. Gall
51. H. E. Goeller
52. A. T. Gresky
53. J. C. Griess
54. E. Guth
55. P. A. Haas
56. P. H. Harley
57. P. N. Haubenreich
58. J. W. Hill
59. C. J. Hochanadel
60. A. Hollaender
61. A. S. Householder
62. G. H. Jenks
63. W. H. Jordan
64. S. I. Kaplan
65. P. R. Kasten
66. C. P. Keim
67. M. T. Kelley
68. R. B. Korsmeyer
69. K. A. Kraus
70. J. A. Lane
71. W. J. Leonard
72. R. E. Leuze
73. S. C. Lind
74. R. B. Lindauer
75. R. S. Livingston
76. M. I. Lundin
77. R. N. Lyon
78. J. L. Marsh (C&CCC, South Charleston)
79. H. F. McDuffie
80. J. P. McBride
81. H. A. McLain
82. R. A. McNees
83. J. R. McWherter
84. O. Menis
85. E. C. Miller
86. C. S. Morgan
87. K. Z. Morgan
88. E. J. Murphy
89. M. L. Nelson
90. J. P. Murray (Y-12)
91. L. F. Parsly
92. Sigfred Peterson
93. M. L. Picklesimer
94. L. R. Quarles
95. W. D. Reel
96. P. M. Reyling
97. R. C. Robertson
98. A. M. Rom
99. M. W. Rosenthal
100. H. C. Savage

101. C. H. Secoy
102. C. L. Segaser
103. E. D. Shipley
104. M. J. Skinner
105. R. W. Stoughton
106. A. H. Snell
107. I. Spiewak
108. C. D. Susano
109. J. A. Swartout
110. E. H. Taylor
111. D. G. Thomas
112. P. F. Thomason
113. M. Tobias
114. D. S. Toomb
115. W. E. Unger
116. R. Van Winkle
117. B. Weaver
118. A. M. Weinberg
119. E. P. Wigner (consultant)
120. G. C. Williams
121. J. C. Wilson
122. C. E. Winters
123. F. C. Zapp
124. ORNL – Y-12 Technical Library, Document Reference Section
125. HRP Director's Office, Y-12

EXTERNAL DISTRIBUTION

126. F. C. Moesel, AEC, Washington
127. Houdry Corporation (Attn: G. A. Mills)
128. Division of Research and Development, AEC, ORO
129-135. TISE for P.A.R.P.
136-661. Given distribution as shown in TID-4500 (13th ed.) under Reactors–Power category (75 copies – OTS)

Reports previously issued in this series are as follows:

ORNL-527	Date Issued, December 28, 1949
ORNL-630	Period Ending February 28, 1950
ORNL-730	Feasibility Report – Date Issued, July 6, 1950
ORNL-826	Period Ending August 31, 1950
ORNL-925	Period Ending November 30, 1950
ORNL-990	Period Ending February 28, 1951
ORNL-1057	Period Ending May 15, 1951
ORNL-1121	Period Ending August 15, 1951
ORNL-1221	Period Ending November 15, 1951
ORNL-1280	Period Ending March 15, 1952
ORNL-1318	Period Ending July 1, 1952
ORNL-1424	Period Ending October 1, 1952
ORNL-1478	Period Ending January 1, 1953
ORNL-1554	Period Ending March 31, 1953
ORNL-1605	Period Ending July 31, 1953
ORNL-1658	Period Ending October 31, 1953
ORNL-1678	Period Ending January 31, 1954
ORNL-1753	Period Ending April 30, 1954
ORNL-1772	Period Ending July 31, 1954
ORNL-1813	Period Ending October 31, 1954
ORNL-1853	Period Ending January 31, 1955
ORNL-1895	Period Ending April 30, 1955
ORNL-1943	Period Ending July 31, 1955
ORNL-2004	Period Ending October 31, 1955
ORNL-2057	Period Ending January 31, 1956
ORNL-2096	Period Ending April 30, 1956
ORNL-2148	Period Ending July 31, 1956
ORNL-2222	Period Ending October 31, 1956
ORNL-2272	Period Ending January 31, 1957
ORNL-2331	Period Ending April 30, 1957

HRP QUARTERLY PROGRESS REPORT

SUMMARY

PART I. HOMOGENEOUS REACTOR TEST

1. HRT Operations

Repairs and modifications to the HRT system were made throughout the quarter. Following an inspection of flanges for stress cracks, a total of 120 flanges were replaced or remachined, and a complete set (12,000 ft) of leak-detector lines was installed. Bellows assemblies were replaced in all the system low-pressure valves.

Other work performed concurrently on the reactor included preparation of an iodine removal bed for insertion ahead of the fuel recombiner, installation of the nuclear instruments and fuel-storage-tank recombiner, and modification of the reactor piping to minimize diaphragm-pump malfunctioning.

Operating staff activities included analyzing the reactor behavior in connection with the preparation of the HRT Operating Manual, preparation of test procedures, and reporting on previous reactor tests.

An analysis of the behavior of gases in the high-pressure system indicates that it is impossible, even at high oxygen injection rates, to ensure excess oxygen in that system if bubble letdown in excess of 1 to 2 liters/min is permitted. Letdown of gas-saturated liquid alone, however, permits the maintenance of a moderate oxygen excess with reasonable injection rates, while keeping the estimated xenon poisoning effect below 2%.

A portable refrigeration unit was constructed for remote-maintenance activities; it has adequate capacity to freeze plugs in the 4-in.-OD, 0.469-in.-wall reactor piping while the shield is flooded with water.

2. HRT Design

An iodine-removal bed was designed to minimize iodine poisoning of the platinum catalyst in the fuel recombiner and to reduce xenon poisoning in the reactor. An independent leak-detector system was designed to serve several large flanges which cannot be replaced. A capillary flowmeter system for all leak-detection systems was designed which will increase the speed and accuracy of locating leaking flanges.

Final modification of the design of the primary refrigeration system was completed, and all equipment necessary to increase the capacity of the system was ordered. Recommendations were made relative to cleaning and storage of the steam and cooling-water systems.

The fuel and blanket feed-pump discharge piping was redesigned to permit venting of the pumps should they become gas-bound. The piping modification included improving the reliability of the feed supply for the purge pumps, providing gas-venting lines for the feed pumps, and repiping the blanket pressurizer to limit the need for blanket diaphragm-pump operation. The flange development program was completed, with the conclusion that the ring-joint flanged closure will give satisfactory service in the HRT so long as certain restrictions on machining, etc., are observed.

3. HRT Component Development

The 400A-1 and 300A pumps continued to circulate uranyl sulfate solution without difficulty. Tests of shaft-seal mixing in the 400A-2 pump showed that purge flow reduced the amount of mixing across the seal; zero mixing has not been achieved.

Feed-pump loops continued to operate without failures during the quarter; however, there were two purge-pump diaphragm failures, one at 596 and one at 946 hr. A method of relieving gas binding of feed pumps was developed. Check-valve trim of Star J balls vs type 17-4 PH seats proved satisfactory in both water and uranyl sulfate. In the Ohio State University fatigue program, cold-worked type 347 stainless steel was found to be subject to corrosion fatigue but annealed material was relatively immune.

Materials procurement by Babcock & Wilcox for the HRT spare heat exchanger is scheduled for completion in August, at which time fabrication will begin.

The HRT mockup terminated a 1580-hr run with 0.04 m UO_2SO_4 because of a tube failure in the Foster Wheeler 80-kw heat exchanger. The failure was a result of pitting in a tube plugged with corrosion products. Following repairs, the mockup started another run.

The HRT fuel and blanket recombiners were successfully operated to demonstrate that no significant loss of platinum had occurred since installation.

4. HRT Reactor Analysis

At some time in the future, the HRT may be operated with a thorium oxide blanket. Several nuclear characteristics of the reactor were estimated for various slurry concentrations in the blanket region. A conversion ratio of 0.6 appears possible with a blanket thorium concentration of 250 g/liter and a 280°C average temperature. The reactivity change associated with complete settling of this slurry would be about 0.15 Δk_e. A core temperature rise from 280 to about 340°C would be required to compensate for this reactivity addition.

5. HRT Controls and Instrumentation

The letdown valves are being reduced in size, and the plug material is being changed from Stellite No. 6 to 17-4 PH stainless steel to prevent the corrosive attack found in initial HRT operation. Pitting attack on the flanges of the bellows assemblies necessitated the replacement of the bellows assemblies in the low-pressure valves. A frequency-response analysis indicated that $\frac{3}{8}$-in. tubing is the optimum size for speed of response for the line connecting the pneumatic amplifier to the letdown valves.

Prototype linear differential transformers of a more radiation-resistant construction were received and will be tested as to suitability for use on the reactor displacement-type liquid-level transmitters.

The necessary instrument and controls engineering work covering revisions to the feed pumps and to the steam refrigeration, leak-detector, and purge-water systems was completed.

6. HRT Processing Plant

All components of the low-pressure system of the HRT processing plant were tested individually, and a test of the integrated system demonstrated its operability. Tests of interest included demonstration of the separability of the H_2O and D_2O systems and a series of tests in which more than 99.5% of simulated corrosion products was dissolved in the dissolver system.

Difficulties in sealing six valve flanges were remedied by remachining and realigning the flanges. The Swagelok connectors on the tantalum nozzles of the dissolver were sealed by substituting lead ferrules for the tantalum ferrules on two of the five connectors.

The low heat transfer of the tantalum-lined stainless steel dissolver was remedied by adding mercury to the space between the liner and the dissolver shell. The dissolver jacket was divided to form two sections; the upper one may be cooled with water while the lower one is steam-heated during the dissolution cycle. The cooling of the upper jacket provides total condensation, permitting increased boilup rates, which supply the vigorous evaporation necessary for complete dissolutions of the solids.

Calculations of the expected performance of the HRT charcoal beds indicate that the activity discharged to the stack is strongly dependent on the inert-gas flow rate. At 5 Mw reactor power and the arbitrary stack discharge limit of 80 curies/day, a maximum of 318 cc/min of oxygen sweep gas can be accommodated per absorption bed. Short-circuiting of gases in the charcoal bed can substantially reduce this number. The beds will be tested for the presence of voids that would contribute to such short-circuiting.

PART II. REACTOR DESIGN AND ANALYSIS

7. HRE-3 Design

Preliminary flowsheets and design data were prepared for HRE-3, a 60-Mw thorium breeder reactor. A preliminary design for an oxygen pressurizing system was analyzed, and conceptual studies of the reactor-vessel configuration were started.

8. Reactor Analysis

Nuclear characteristics associated with spherical reactors in the size range likely for HRE-3 were evaluated. Based on two-group calculations, breeding ratios between 1.09 and 1.12 appear possible for 9-ft-dia reactors having a 4-ft-dia core, with blanket thorium concentrations between 500 and 1000 g/liter. These values for the breeding ratio would be lower by about 0.03 if xenon were not removed from the core system. The increase in breeding ratio if there were no neutron absorptions in the core tank, H_2O, and copper would be about 0.02, 0.005, and 0.005, respectively. If the surface of the core system corroded to a depth of 0.001 in. and the soluble corrosion products were distributed uniformly

throughout the fuel solution, the associated decrease in breeding ratio would be about 0.03 for a reactor with a 4-ft-dia core. If no corrosion products were present, a 9-ft-dia reactor having a 4-ft-dia core and a blanket thorium concentration of 1000 g/liter would require about 220 days to generate an amount of fuel in the blanket equal to the core-system inventory.

The breeding ratio for several spherical, thorium breeder reactors was evaluated on the basis of a multigroup model, and the results were compared with those of two-group calculations. The two-group method gave breeding ratios about 5% higher than did the multigroup method. This difference was due primarily to the values for η^{23} in the resonance region; resonance absorptions in fuel were not considered in the two-group model.

The breeding ratio and wall power density were calculated for some two-region cylindrical reactors. Comparison of these two-group results with those for two-region spherical reactors having the same core volume indicate that breeding ratios are nearly the same for these geometries. Maximum wall power densities were always higher for the cylindrical reactors.

Oracle codes were written for determining the nuclear characteristics of two-region, time-dependent, thorium breeder reactors and of two-group, N-region reactors and for evaluating the zero- and first-order Bessel functions of the second kind.

PART III. ENGINEERING DEVELOPMENT

9. Development of Fuel-System Components

The 20-cfm canned-motor blower was operated for 1462 hr without any noticeable bearing wear. Repair of the 4000-gpm Byron Jackson pump was completed.

Parts of the two oxygen compressors were returned to the manufacturers for revision.

A multipump testing facility for 10-gpm feed pumps is under construction, and pump components are being ordered and fabricated. A direct water drive for a feed pump was operated; the life of the water cylinders was short.

A ring-gasketed titanium-to-stainless-steel flange joint was designed, and a prototype will be subjected to a thermal-cycle test. Delivery of titanium-lined pipe by Crane Company is expected in two to three months; Pfaudler Company had further difficulty with tubing for their titanium-lined heat exchanger.

A large thermal-cycle test facility is being constructed, and components are being purchased for a heat exchanger test, which will be made in this system.

Testing of six tube bundles containing type 347 stainless steel tubes, nickel-plated tubes, and normal-bore and counterbored tube sheets in chloride–oxygen–boiler water environments was completed. Some indications of intergranular attack were found but no confirmed stress-corrosion cracking was found.

10. Development of Reactor Slurry Systems

Turbulent-flow pressure-drop measurements were made over a velocity range of 4 to 47 fps with a slurry containing 570 g of thorium per kilogram of H_2O and having a yield stress of 0.03 lb/ft^2 and a coefficient of rigidity of 2.2 centipoises.

Laminar flow pressure drop calculations were extended from the previously reported Hedström number of 10^7 to a value of 10^{15}.

A capillary sampler-viscometer is being constructed which can be attached to high-pressure loops to give pseudo-shear diagrams of the slurry at the loop operating temperature while samples are being taken.

A Foxboro electromagnetic flowmeter was tested in a low-temperature slurry loop for a total of 100 hr and found to give accurate readings with a slurry of 800 g of thorium per kilogram of H_2O concentration. A suitable high-temperature insulator must be found before this instrument can be used at 300°C.

A parametric study was made of the effect of slurry rheological properties on the heat exchanger design and pumping requirements to remove 1 Mw of heat from various thorium oxide slurries.

In particle-size degradation tests the Waring Blendor was used to produce slurries which formed cakes of varying degrees of cohesion when the slurry was air dried.

Water and slurry were circulated for more than 2200 hr during the quarter in loops S, T, and 200A. Run 200A-11, which had accumulated 2100 hr at the end of the last quarter, was terminated at the end of 2303 hr because of noisy pump operation. The slurry was easily flushed from the system. The handling characteristics and the generalized attack rate at 300°C for the sulfated thorium–½% uranium oxide slurry are similar to those observed

for the sulfated thorium oxide slurry. The sphere-forming tendencies of two different batches of thorium oxide were compared in runs 200A-12 and -13. In both runs spheres of 20 to 25 μ in diameter were formed in less than 55 hr of circulation.

Spheres of 20 μ in diameter were formed in T loop in 13 hr of circulation. After 47 hr, 0.3 wt % of sodium metasilicate was added in an attempt to disintegrate the spheres. The silicate was ineffective although circulation was continued for an additional 68 hr, before the run was terminated by pump failure. Parts of the impeller were caked.

The changes to the HRT blanket test system described in the last quarterly report were completed, and the system was started up (run SM-3). At a loop flow of 350 gpm and an inlet nozzle velocity of about 32 fps, the slurry appears to be well suspended and in motion throughout the blanket at all concentrations up to the present charge level of 238 g of thorium per kilogram of H_2O. The maximum operating temperature is 200°C. After shutdown the settled bed, which was as dense as 840 g of thorium per kilogram of H_2O, was resuspended within 20 sec after the pump had started. Samples taken from the blanket and circulating loop were generally of slightly lower concentration than that estimated from the thorium charge, although gamma scans of the blanket failed to reveal any massive accumulations.

11. Instrument and Valve Development

A pressure transmitter suitable for direct connection to 640°F reactor process lines was tested and found to have an accuracy of 2% and a natural frequency of 375 cps. This high-frequency response performance will be advantageous in reactor kinetic studies to determine the effectiveness of the pressurizer in damping reactivity excursions.

A pneumatically-powered-bellows valve actuator rated for thrusts to 12,000 lb was received for evaluation as to suitability for use on 2-in. control valves in 2000-psi service. By relocation of parts, the actuator can be set up to open or close the valve upon loss of actuating air pressure. Hardenable noble-metal alloys supplied by Baker & Company, plates of aluminum oxide and tungsten carbide by Linde, and Kennametal cemented tungsten carbide compositions are being evaluated as valve-trim materials.

PART IV. REACTOR MATERIALS RESEARCH

12. Solution Corrosion

The second all-titanium loop, 100A loop H, was placed in operation during the past quarter and has operated satisfactorily for more than 400 hr with uranyl sulfate solution at 250°C and approximately 1000 psi.

Loop I was modified to provide close control of oxygen concentration in the circulating solution in order to study the effect of various oxygen concentrations on corrosion under dynamic conditions.

A fourth test of the mockup of the Zircaloy-2–stainless steel transition joint used in the HRT reactor vessel was completed. No additional mechanical deflections of the bellows were made, but 50 additional thermal cycles of the unit were carried out. The joint and bellows functioned properly and were leaktight. Pitted areas on the bellows which developed during the first runs filmed over and stopped corroding.

The series of long-term runs at 200, 250, and 300°C with the solution proposed for use in the HRT was concluded. The tests were for approximately 20,000 hr at each temperature. It was shown that once the oxide film formed on the pins during the first test, no measurable corrosion occurred in subsequent exposures. Stainless steel and titanium stress specimens exposed during about the latter 13,000 hr of these tests gave no evidence of stress-corrosion cracking.

In a study of the effect of heat treatment on corrosion of type 347 stainless steel, it was found that areas heated above 1950°F have somewhat lower critical velocities and lose more weight during film formation than do those annealed at 1950°F.

Pretreatment of stainless steel specimens for 100 hr at 250°C with oxygenated water containing 100 or 200 ppm chromium(VI) as chromium trioxide decreased initial weight losses on subsequent exposure to uranyl sulfate solutions at lower temperatures but could not be depended on to increase the critical velocities.

Oxygen exhaustion in runs at 200, 250, and 280°C with 0.17 m UO_2SO_4 containing less than 3 ppm chloride did not produce stress-corrosion cracking of stressed type 347 stainless steel specimens during short exposures.

At low flow rates, increasing sulfuric acid concentrations in 0.17 *m* UO_2SO_4 at 250°C increased the extent of corrosion of type 347 stainless steel during film formation and increased the corrosion rate at 70 fps.

Failure of a ½-in. type 347 stainless steel pipe in 0.04 *m* UO_2SO_4 containing 0.02 *m* D_2SO_4 and 0.005 *m* $CuSO_4$ in heavy water was observed when the solution was heated above the two-liquid-phase separation temperature. Apparently the pipe was severely corroded when small quantities of the heavy phase came in contact with the steel. This failure illustrates the necessity of preventing two-liquid-phase separation even in dilute solution.

Studies of the stress-corrosion cracking of type 347 stainless steel in boiling halide-containing uranyl sulfate solutions have shown that chloride concentrations between 25 and 500 ppm produced cracking of type 347 stainless steel during exposure times of 25 to 500 hr. Under the same conditions, bromide ions did not produce cracking, although severe subsurface attack was found in highly stressed areas. Studies have also shown that uranyl ions conjointly with chloride ions influence the susceptibility to cracking.

Stress-corrosion tests in high-temperature water have shown that cracking occurs with chloride concentrations between 25 and 100 ppm, with either high or low oxygen concentrations, at starting pH values between 2.8 and 10.5 and at temperatures between 200 and 300°C. At 200 and 250°C, cracking seemed to occur faster and more frequently than at 300°C.

Several alloys of zirconium were corrosion tested in simulated HRT core solution at 300°C. The following alloys exhibited very good corrosion resistance: 5% Pt–95% Zr, 10% Pt–90% Zr, and 5% Pd–95% Zr. Other alloys tested were considerably less resistant than Zircaloy-2.

Type 347 stainless steel, surface hardened either by Malcomizing or Thermospray 16-C, corroded excessively in uranyl sulfate solutions, even at 80°C. Hastelloy R-235, Multimet, and Timken 16-25-6 demonstrated a high degree of corrosion resistance to simulated HRT core solution at 300°C. Under the same conditions, types 431 and 414 stainless steel corroded excessively; even at boiling temperatures, these two alloys corroded at rates as high as 7 mpy. Type 202 stainless steel has shown a high corrosion resistance to most reactor-associated environments. In tests run to date, its corrosion resistance has been equal to that of type 347 stainless steel.

Type 420 stainless steel hardened to R_C 50 to 52 corroded excessively in 90°C uranyl sulfate solution of the composition used in in-pile loops. At 25°C, the corrosion rate was much less. In similar environments, both type 17-4 PH stainless steel and Stellite No. 6 corroded at negligible rates.

13. Slurry Corrosion

Venturi flowmeters have been installed in the pressurizer mixing line and main circulating line of loop BS. Operation of similar flowmeters previously installed in loop CS has been useful and essentially trouble-free.

Dynamic-corrosion data and operating experience are reported for seven thorium oxide slurry runs in 100A pump loops at 300°C, with circulating concentrations ranging between 404 and 740 g of thorium per kilogram of water, operating times from 13 to 579 hr, and with the use of thoria preparations calcined at temperatures from 550 to 1600°C.

The thoria calcined at 550°C circulated well, did not cause operating difficulties at a concentration of 404 g of thorium per kilogram of water, and gave low corrosion rates.

Material calcined at 650°C plugged slow-flowing loop regions in two runs, when the concentration was taken above 750 g of thorium per kilogram of water. Corrosion was not excessive.

Circulation of previously pumped 800°C-calcined thoria in a hydrogen atmosphere gave increased corrosion rates at velocities above 40 fps, with lighter attack at lower velocities.

Micropulverized, 800°C-calcined thoria, of 1-μ original particle size circulated satisfactorily, showing relatively high loop corrosion rates during the early part of the run and being reduced in particle size to 0.5 μ only slowly. Specimen corrosion was normal.

A special batch of thoria, calcined at 1600°C, was tested in two loop runs. Circulation properties and resuspension characteristics appeared excellent, and no caking was noted. Corrosion rates were low. The thoria was not reduced from its original particle size of 1.3 μ.

Sodium metasilicate additions resulted in increased corrosion of type 347 stainless steel and titanium by circulating thorium oxide slurries in toroid tests at 250°C.

Special preparations of thoria spheres and of thorium-uranium oxide were circulated as slurries at 250°C in toroids. The larger spheres were degraded. Corrosion rates were generally low.

A test of 1026 hr duration in toroids at 250°C indicated a general decrease in corrosion rate by circulating slurries with extended time.

In tests of heating and cooling systems for temperature control of an in-pile toroid apparatus, an air-water mixture was used as the coolant medium and Nichrome resistance wire for heating. Cooling and heating capacities up to 1600 w were demonstrated in preliminary tests in the gear-driven rotator model. The rotated-arms model was revised to reduce vibration and to be of suitable dimensions for in-pile use.

14. Radiation Corrosion

The construction of loop L-4-18 was completed, and the loop is now in operation in beam hole HB-4. Loop L-2-19 is being constructed.

Development of a loop for operation in the ORR is nearing completion, and component parts are being fabricated. Some development and experimental work is yet to be done on the core tank and the circulating pump.

The tenth and eleventh in-pile loop experiments, L-2-15 and L-4-16, were completed. These stainless steel loops were exposed in LITR beam holes HB-2 and HB-4, respectively. Both experiments employed 0.17 m UO_2SO_4, and the main-stream temperature in the experiments ranged from 278 to 280°C. The over-all stainless steel corrosion rates of the two experiments based on oxygen-consumption data were 1.3 and 0.5 mpy, respectively. Zircaloy-2 corrosion rates in the core coupon holders varied from 1.9 mpy at 1.3 w/ml to 15.4 mpy at 19.2 w/ml. The corrosion rate at these conditions is expressed reasonably well by the following equation:

$$R = 1.04P\left(1 - e^{-95/R^{1.5}}\right),$$

where

R = corrosion rate, mpy,
P = power density, w/ml.

Analyses of the scale from various parts of loop L-4-16 indicated that zirconium corrosion products were distributed throughout the loop as a constituent of the scale.

Exposure of stainless steel loop L-2-17 in LITR beam hole HB-2 was completed. The UO_2SO_4 concentration was 0.04 m, the same as that proposed for the HRT. The main-stream operating temperature was 300°C. The over-all stainless steel corrosion rate based on oxygen data was 0.8 mpy.

Fabrication and testing of four in-pile autoclaves for radiation-corrosion studies in the LITR were completed during the past quarter. The number of coupon-type corrosion specimens to be included in the new HB-5 rocking autoclave was reduced from nine to six to improve the flow of fuel solution around the specimens during in-pile operation.

The pressure excursion observed in previously reported experiments Z-13 and Z-22 may be explained by a loss of copper from solution rather than by hydrogen absorption as previously suggested. An attempt was made to analyze three Zircaloy-2 specimens from three different in-pile autoclave experiments for hydrogen content. The method appeared to give results which were uncertain by 20 to 30 ppm. A specimen from the MTR experiment with water and a hydrogen atmosphere was the only one that exhibited a significant increase in hydrogen content over that of a control specimen. Comparison of weight-loss and oxygen-consumption data indicates that no hydrogen pickup has occurred during LITR exposures of Zircaloy-2 to solutions at appreciable fission power densities.

Three Zircaloy-2 MTR experiments which contained solutions free of uranium are discussed, and corrosion data are presented. Chemical analysis of the solution from MTR experiment 15-7, which was with water and an oxygen atmosphere contaminated with nitrogen, indicates that most of the nitrogen was oxidized to nitrate during exposure.

15. Metallurgy

Studies of the transformation kinetics and mechanisms of the Zr-Nb-X alloys showed that the transformation characteristics are quite complex. The hardening constituent in these alloys was tentatively identified as a body-centered niobium-rich phase, supersaturated with zirconium, whose composition changes with aging time toward that predicted by the phase diagram for the equilibrium niobium phase. A double (possibly triple) aging peak was observed for the Zr–15% Nb alloy at 350°C. Additions of 1% Al, ½% Cu, 2% Th, and 2% Mo to the Zr–15% Nb alloy delay for more than 2 hr the formation of the hardening phase on beta-

quench-and-reheat aging. The addition of 5% Mo prevents its formation for at least two weeks at all temperatures. Tests of Zr–15% Nb specimens aged at 400°C for 2 hr and then at 600°C indicated that the hardness decreases to the initial as-quenched hardness; thus the hardening phase, formed at 400°C, redissolves at 600°C (or some intermediate temperature) instead of coarsening as would be expected.

No change in tensile properties of Zircaloy-2 was found either from radiation damage or from hydrogen pickup after subsize specimens were irradiated at 280°C in a uranyl sulfate corrosion test loop to a fast (>1 Mev) flux of about 2×10^{19} nvt.

Rather than embrittling as had been feared, the impact strength of A-55 titanium to which various amounts of hydrogen had been added increased with aging at 300°C.

Titanium welds were made in RC-70A 2½-in.-dia sched-40 pipe with RC-40A and RC-55A filler metal. Metallographic and mechanical evaluation indicated sound welds. The hardness and strength were somewhat greater than those of weldments made with RC-40A and RC-55A base metal, while the ductility was somewhat less.

Contracts were signed for two programs related to reactions between metals and aqueous solutions. The Aerojet General Corp. will obtain a comparison between the reactions of zirconium with water and with uranyl sulfate solutions. The Stanford Research Institute will endeavor to determine the limiting conditions for sustaining reactions of titanium with aqueous solutions. Early results have shown that titanium disks broken by a buildup of oxygen pressure to about 2000 psi ignite and that the reaction is sustained.

It was concluded that the recent failures in the bolts, nuts, and ferrules of the HRP flange test loop were caused by cadmium embrittlement. Flanges which have been in contact with cadmium-plated hardware do not appear to have been harmed.

PART V. CHEMICAL ENGINEERING DEVELOPMENT

16. Uranyl Sulfate Fuel Processing

Tests with actual HRT charcoal showed the adsorptive capacity of the charcoal for fission-product rare gases at 25 to 100°C to be less than predicted by extrapolation of lower temperature data. Charcoal containing 5 to 6% water, the amount present in a sample of HRT charcoal, had only about 75% of the adsorptive capacity of the same material dried at 100°C. The presence of a small channel in a horizontally placed HRT trap could decrease the breakthrough time of the trap by a factor of 10.

In the low-pressure system of a homogeneous reactor the stability of iodate is decreased by increasing the sulfuric acid concentration. In the HRT mockup, iodine introduced into the high-pressure system rapidly moved to the low-pressure system. There it was absorbed on the catalytic recombiner and impaired the operation of the recombiner. Protection of the recombiner by a silver absorber located ahead of the recombiner and regeneration of a poisoned catalyst bed by operation at 650°C were demonstrated.

Simulated HRT corrosion-product solids suspended in uranyl sulfate solutions disappeared at 275°C, presumably by agglomeration and settling, but reappeared quantitatively in suspension after the solution had been cooled to room temperature. Irreversible adsorption in the absence of surfaces grossly hotter than the solution did not appear to occur. The rapid disappearance of solids in suspension in loop A can be attributed almost entirely to collection of these solids in the back of the pump.

Tests with a segmented steam jacket on the glass-lined vessel for dissolution of fission and corrosion products prior to sampling showed that two-cycle operation gave over 99.5% dissolution.

The Henry's law constant for krypton solubility in water and 0.02 *m* UO_2SO_4 shows a linear dependence on temperature but departs from linearity in the case of 0.04 *m* UO_2SO_4 solutions.

Uranium losses due to adsorption on simulated HRT fission and corrosion product solids can be held to 0.2% by washing such solids with either water or dilute sulfuric acid. Uranium losses during the subsequent steps of UO_4 precipitation and washing can be held to 0.25% by performing the operations at 2°C.

17. Uranyl Sulfate Blanket Processing

Essentially all the plutonium formed by LITR irradiation of 1.4 *m* UO_2SO_4 under oxygen pressure at 250°C in titanium bombs was either in solution or adsorbed on the bomb walls. Only insignificant amounts were found as a loose precipitate. Part

of the adsorbed plutonium was readily removed by contacting at 85°C with nitric acid containing Ce(IV). However, the plutonium was removed completely only by repeated descaling with strong acids, which badly corroded the base metal. Most of the neptunium remained in solution; some was adsorbed on the bomb walls, but only insignificant amounts appeared in the precipitate.

Loop P-1 was operated for 180 hr in a UO_2SO_4 solution containing 330 g of uranium per kilogram of H_2O.

18. Thorium Oxide Slurry Development

A slurry of 800°C-fired thorium-uranium oxide (U/Th mole ratio = 0.005/1) prepared from the coprecipitated oxalates and containing 20,000 ppm of MoO_3 and 3000 ppm sulfate, added as $Th(SO_4)_2$, was irradiated for 247 hr at 300°C in the LITR with no visible damage.

In out-of-pile studies on the catalytic recombination of hydrogen-oxygen mixtures by slurries (500 g of thorium per kilogram of H_2O) containing 0.05 m MoO_3, slurries of thorium-uranium oxides calcined at 1000°C for 16 and 24 hr and at 1600°C for 24 hr had high catalytic activities (>>10 moles of H_2 per hour per liter). Slurries of the mixed oxides calcined at 800°C for 24 hr and at 1000°C for 4 hr had low catalytic activities even after treatment with hydrogen.

A ¼-in.-ID glass elbow flowmeter was evaluated for possible use with thorium oxide slurries. With slurries of specific gravities of 1.8 and 1.5 the velocity vs ΔH in terms of head of fluid flowing was log-log linear. The same calibration was applicable with water as the flowing fluid.

Slurry hindered-settling rates, from room temperature to 300°C, decreased with decreasing particle size. Settling rates increased with increasing slurry temperature. Additional factors other than a simple decrease in water viscosity appeared to be involved. Silicate addition slowed the rate at all temperatures and changed the shape and increased tne slope of the temperature-dependence curve.

The settling rate, from room temperature to 300°C, for slurries of oxide prepared from oxalate precipitated at 10°C and fired at 1000 to 1600°C, was greatest for the 1200°C material. Oxide fired at 1600°C and pumped in a 100A loop settled more rapidly and showed much greater flocculation than the unpumped material.

In studies on calcination-temperature effects on thorium oxide, firing at 1000 to 1600°C did not affect the average particle size. For oxides of approximately the same particle size the abrasive characteristic, measured with the jet-impingement slurry abrasion tester, increased with increasing calcination temperature and showed a linear logarithmic dependence on reciprocal firing temperature ($°K^{-1}$). This would appear to associate the increase in the abrasive characteristic with increasing crystallite size. Oxides fired at 1400°C for 64 hr and at 1600°C for 12 hr resisted degradation in impingement tests; those fired at 1400°C for 12 hr and at 1600°C for 2 hr, as well as lower fired oxides, were degraded. Grinding the oxides in a mortar, blending as a slurry in a Waring Blendor, and subjecting slurries to ultrasonic treatment did not markedly affect the particle size of the oxides prepared from oxalate precipitated at 10°C and fired at 1000 to 1600°C.

Thoria microspheres with an average diameter less than 10 μ (wet) were prepared by a gel technique. Calcined to oxide, these beads will be less than 3 μ in diameter.

Preliminary tests of thorium oxalate preparation with a jet-mixer indicate that it is possible to produce submicron ThO_2 by this method and that the particle size can be controlled by varying the mixing conditions.

19. In-Pile Slurry Loop

In the in-pile slurry loop program – a joint effort of the Pennsylvania Advanced Reactor Project and ORNL – Westinghouse will design and fabricate the loops, and ORNL will install and operate the loops in the ORR and will segment the loops in cells now being prepared in Building 3026.

A mockup of a proposed loop design constructed at Westinghouse was operated in preliminary room-temperature tests with water.

A special shielding plug for the ORR was designed to accommodate the in-pile slurry loop, and design work was begun on equipment chambers that will be installed at the face of the reactor.

PART VI. SUPPORTING CHEMICAL RESEARCH

20. Aqueous Systems at Elevated Temperatures

A semi-micro phase-study apparatus was used to relate composition, liquid fraction filling of quartz sample tubes, and critical temperature of the SO_3-H_2O system. The T_c-vs-composition curve showed a maximum of 665°C just below 0.5 mole fraction of SO_3. A platinum-lined steel pressure

vessel employing a movable bimetallic pressure-transmitting diaphragm was designed to measure pressures of the highly corrosive solutions in the critical region.

The densities of heavy-water liquid and saturated vapor at elevated temperatures up to the critical point were determined from observations in quartz tubes on the fractional filling at high temperature as a function of fractional filling at room temperature. The desired densities were then obtained through mass-balance equations involving the known phase densities at room temperature.

The effect of $CuSO_4$ and H_2SO_4 on the homogeneous catalysis of the hydrogen-oxygen recombination was studied at 200°C to make comparisons with previously reported observations at 175°C and to improve the estimation of catalytic activity and apparent hydrogen solubility. The maximum apparent hydrogen solubility occurred again at ~ 0.05 *M* acid, but, in contrast to the relations at 175°C, the catalytic activity at 200°C appeared to be inversely related to the acidity over the whole range (0.01 to 0.20 *M* H_2SO_4).

Further work was done on the determination of temperatures of precipitation for dilute solutions in the system UO_2SO_4-$CuSO_4$-$NiSO_4$-H_2SO_4-H_2O; the method previously described, involving sampling and analysis of mixtures equilibrated in titanium bombs, was used. The method gave consistent results for mixtures in which $3CuO{\cdot}SO_3{\cdot}2H_2O$ was the first precipitate, but only rough information where the primary precipitate was $2UO_3{\cdot}SO_3{\cdot}5H_2O$. In general, the precipitation temperatures were found to be considerably lower, by ~ 25 to 65°C, than values previously obtained by visual observation in quartz tubes.

21. Radiation Chemistry

Hydrogen yields from the Co^{60} gamma-ray radiolysis of aqueous solutions are lowered by the presence of nitrate ion. The hydrogen yield in dilute nitrate solution may be expressed by the following equation $G(H_2) = -0.40[NO_3^-]^{1/3} + 0.45$. The suppression of the hydrogen yield by NO_3^- is interpreted as experimental evidence for the reaction of hydrogen atoms with the nitrate group.

PART VII. ANALYTICAL CHEMISTRY

22. Analytical Chemistry

Two improved methods were developed for the separation and estimation of the aluminum content of contaminated slurries of thorium oxide. One method is based on multiple solvent extraction followed by a colorimetric determination of the aluminum complex of 8-quinolinol, while the other is based on the measurement of the radiant intensity of an extract of thenoyltrifluoroacetone when aspirated in a flame spectrophotometer.

In the further development of methods for the analysis of solutions of uranyl sulfate, improved methods are reported for the estimation of zinc polarographically and for the determination of ruthenium flame-photometrically.

CONTENTS

PART V. CHEMICAL ENGINEERING DEVELOPMENT

PART VI. SUPPORTING CHEMICAL RESEARCH

PART VII. ANALYTICAL CHEMISTRY

Part I

HOMOGENEOUS REACTOR TEST

S. E. Beall

1. HRT OPERATIONS

S. E. Beall

H. F. Bauman
N. A. Brown[1]
J. R. Buchanan
J. R. Engel
J. D. Flynn
D. F. Frech
T. H. Gladney[1]
R. H. Guymon
R. J. Harvey
P. N. Haubenreich
J. W. Hill, Jr.
R. W. Jurgensen[2]
S. I. Kaplan
J. O. Kolb
H. M. McLeod
R. M. Pierce
D. M. Richardson
G. W. Rivenbark
H. K. Search[3]
A. J. Sharenberger
W. Terry
K. W. West
R. Van Winkle

1.1 REACTOR OPERATIONS

The major effort on the reactor system during the report period was the replacement of defective materials.

1. The results of the dye-penetrant examination of all HRT flanges for stress cracks, begun in April, led to the replacement or remachining of 83 high-temperature flanges and 37 low-temperature flanges in the reactor system, out of a total of 259 flanges inspected. These flanges, together with 12,000 ft of new leak-detector tubes, were installed during the period.

2. An inspection of the low-pressure valves, after their removal from the system in June, revealed serious pitting and some cracking in the stainless steel disks to which the bellows are welded. New bellows assemblies were secured, and all low-pressure valves in the system are being refitted with the new units (see also Sec. 5.1.2).

3. Investigations during the previous quarter confirmed the fear that galvanized or cadmium-plated bolts would deteriorate at reactor temperatures, because of diffusion of the plating into the bolts, with the formation of brittle intermetallic compounds. Consequently, a complete replacement set of bolt material was ordered, and all plated nuts were cut from the reactor flanges. Final assembly of the piping will be delayed for a short time by late arrival of the new materials.

During the replacement of the materials described above, many other revisions were being made, including the installation of the nuclear instruments and the fuel-storage-tank recombiner. An iodine-recovery bed packed with silvered alundum Raschig rings is being fabricated for installation in the fuel low-pressure system. The unit will be located in the fore end of the recombiner casing to scavenge fission-product iodine from the off-gas stream and to prevent poisoning of the recombiner bed (see also Sec. 2.5).

Several piping changes, dictated by supporting development work and by previous operating experience, were also made. These included the installation of chemical treatment and sampling facilities for the steam system, completion of an enclosed demineralized-water loop to supply the reactor coolers, and a series of modifications designed to eliminate past difficulties with gas-binding of the diaphragm pumps.

During the repair period, members of the operating staff were engaged in a critical evaluation of the reactor behavior, in conjunction with the preparation of the HRT Operating Manual. In addition, numerous test procedures and analyses of previous experimental data were prepared. Several of these were released for distribution, and are listed below:

1. N. W. Curtis and S. I. Kaplan, *Leak Test Procedure for HRT Service Steam System*, ORNL CF-57-6-52 (June 11, 1957).

2. J. R. Engel, *Radiation Level in the Stator Region of the HRT Fuel Circulating Pump*, ORNL CF-57-7-25 (July 3, 1957).

3. D. F. Frech, *Fuel Purge Pump Cooler Performance Test*, ORNL CF-57-6-28 (June 6, 1957).

4. D. F. Frech, *Fuel Feed Cooler Performance Test*, ORNL CF-57-6-40 (June 12, 1957).

5. P. N. Haubenreich, *Effects of Letdown Rates and Oxygen Injection Rates on Xenon Poison Level and Excess Oxygen Concentration in the HRT*, ORNL CF-57-5-100 (May 31, 1957).

6. T. E. Haynes and R. Van Winkle, *September, 1956 Measure of Radiation Level of HRE Fuel System Components After Storage for 27 Months*, ORNL CF-57-6-26 (June 5, 1957).

---

[1] On loan from TVA.

[2] On loan from American Gas and Electric Co.

[3] On loan from Pennsylvania Power and Light Co.

7. S. I. Kaplan, *Drying Procedure for HRT Process Piping*, memorandum dated June 20, 1957.
8. S. I. Kaplan, *Leak Test of HRT Shield* (procedure), memorandum dated June 26, 1957.
9. S. I. Kaplan, *HRT Helium Leak Test Procedure*, memorandum dated July 18, 1957.
10. J. D. Perret, Jr., *Liquid Level Calibration of Fuel and Blanket Heat Exchangers*, ORNL CF-57-6-27 (June 6, 1957).
11. R. Van Winkle and J. D. Flynn, *Blanket Entrainment Separator Performance*, ORNL CF-57-6-58 (June 13, 1957).
12. R. Van Winkle and R. R. Wiethaup, *Observed Performance of the Fuel Sample Cooler*, ORNL CF-57-6-17 (June 3, 1957).
13. R. Van Winkle and R. R. Wiethaup, *Observed Net Heat Loss from the HRT High-Pressure System*, ORNL CF-57-6-20 (June 4, 1957).
14. R. Van Winkle and R. R. Wiethaup, *Oxygen Concentration in Fuel and Blanket High-Pressure Systems, HRT Run 7*, ORNL CF-57-6-56 (June 12, 1957).
15. R. Van Winkle and R. R. Wiethaup, *Testing of Adsorptive Capacity of Charcoal Beds*, ORNL CF-57-6-119 (June 4, 1957).
16. R. R. Wiethaup and R. Van Winkle, *Typical Performance of Letdown Heat Exchangers*, ORNL CF-57-7-55 (July 8, 1957).
17. R. R. Wiethaup and R. Van Winkle, *Blanket Pressurizer Level Change When Draining Condensate from the Blanket Heat Exchanger*, ORNL CF-57-6-58 (June 13, 1957).

1.1.1 Effects of Letdown Rate and Oxygen Injection Rate on Xenon Poison Level and Excess Oxygen Concentration

Calculations indicate[4] that it is impossible, even at high oxygen injection rates, to ensure an excess of oxygen in the HRT fuel solution if the bubble letdown rate is more than 1 or 2 liters/min. It is believed necessary to have an excess of O_2 present to prevent the reduction of uranium and excessive corrosion in stagnant lines where the radiolytic gas can be completely recombined by the copper in the fuel solution. If, on the other hand, no bubbles are allowed to form, a reasonable excess oxygen concentration can be maintained with an oxygen injection rate which would not tax the capacity of the off-gas system by excessive dilution of the fission-product gases in the charcoal beds. Results of the calculations are shown in Fig. 1.1. The bubble letdown rate is the volume flow rate of wet gas leaving the circulating stream at the gas separator. The excess oxygen is the total oxygen less that which would be required to combine with all the dissolved hydrogen. As the letdown rate increases, the total dissolved oxygen drops below the stoichiometric concentration because of the greater solubility of the hydrogen (lower Henry's law constant).

If the production of radiolytic-gas bubbles is suppressed to preserve an adequate concentration of oxygen, the concentration of gaseous fission products in the high-pressure fuel solution will also build up. However, it is estimated that the poisoning effect of the Xe^{135} will be reduced to less than 2% by liquid letdown alone, without iodine removal in the low-pressure system. With the

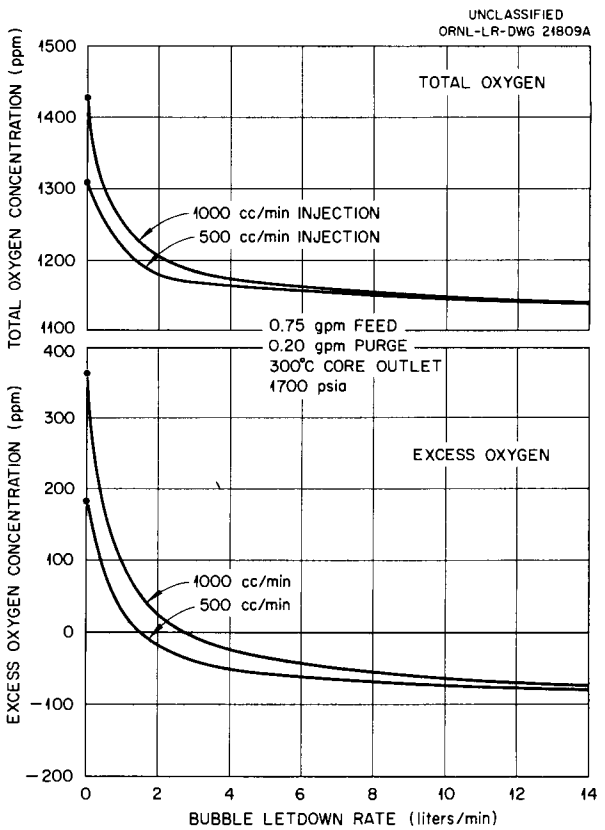

Fig. 1.1. Effect of Gas Letdown on Total and Excess Oxygen Concentrations.

[4] P. N. Haubenreich, *Effects of Letdown Rates and Oxygen Injection Rates on Xenon Poison Level and Excess Oxygen Concentration in the HRT*, ORNL CF-57-5-100 (May 31, 1957).

iodine adsorption bed installed ahead of the catalytic recombiner, the xenon poison level should be less than 1% without any bubble letdown. The effect of bubble letdown rate and oxygen injection rate on xenon poison level in the absence of an iodine adsorption bed is shown in Fig. 1.2.

1.1.2 Portable Refrigeration System for Remote Maintenance

During the April 1957 underwater-maintenance period, the existing HRT refrigeration system was found to be inadequate to freeze ice plugs in the $3\frac{1}{2}$-in. piping at the fuel circulating pump. To ensure a convenient means of freezing these lines, a portable refrigeration system was constructed which utilizes the mixing of dry ice and Amsco 125-82 solvent to achieve a sufficiently cold mixture for direct circulation to the freeze coils. A single-stage centrifugal pump, rated at 40 gpm with a 95-ft head and powered by a 3-hp electric motor, is used to circulate the cold Amsco.

The following general conclusions were derived from the testing of the portable system:

1. The system is rugged and dependable. A continuous run of 72-hr duration was made to demonstrate the reliability of the system.

2. The system is simple and flexible. Extremely low temperatures, approaching –85°F, can be achieved, while any higher temperature can be held by controlling dry-ice input.

3. The system is reasonably economical to operate. During the 72-hr run, dry ice was used at an average rate of 78 lb/hr. At the current price of dry ice to the Laboratory of 2.5 cents/lb, the cost for dry ice is $1.95/hr.

4. The system will successfully freeze ice plugs in 4-in.-OD, 0.469-in.-wall piping submerged in water.

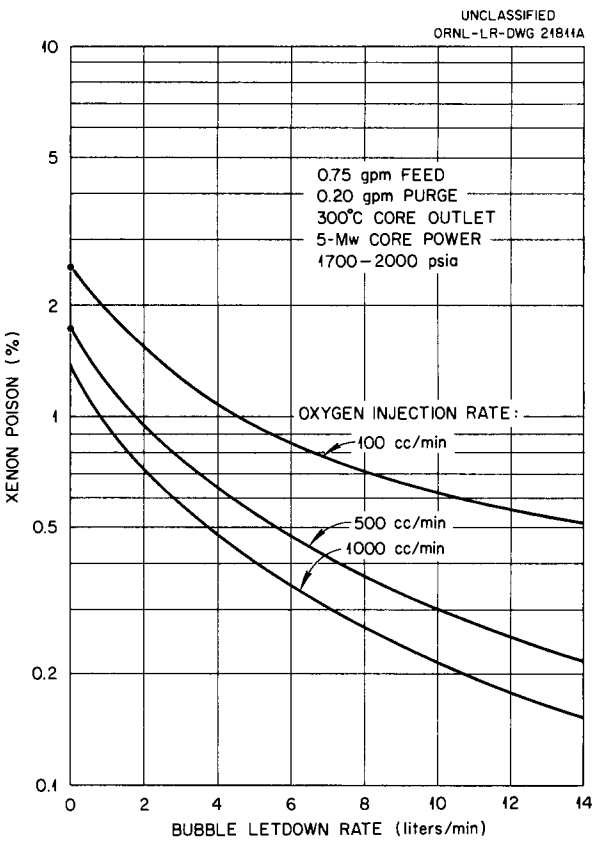

Fig. 1.2. Effect of Gas Letdown on Xenon Poison Level.

2. HRT DESIGN

W. R. Gall M. I. Lundin

F. C. Bowen[1]
C. A. Burchsted
R. D. Cheverton
C. J. Claffey
C. W. Collins
E. H. Gift
E. M. Guglielmo
H. A. McLain
R. C. Moren[2]
A. C. Phillips[1]
R. G. Pitkin[1]
R. C. Robertson
J. N. Robinson
W. Robinson
R. E. Schappel
C. L. Segaser
D. D. Tarr[1]
W. L. Wright
F. C. Zapp

2.1 REFRIGERATION SYSTEM

The capacity of the installed primary refrigeration system proved to be inadequate for simultaneous operation of several freeze jackets and the cold traps. The design of the system was modified (Fig. 2.1) to increase the capacity from an estimated 20,000 Btu/hr to about 79,000 Btu/hr (at −40°F evaporating temperature).[3-5] The design temperature of the secondary refrigerant, Amsco,[6] was also lowered from −30°F to −40°F, because experiments had indicated that improved freeze-jacket operation was obtainable with the lower temperature. At the −50°F evaporator temperature required for the lower Amsco temperature, the capacity of the primary system will be 57,000 Btu/hr.

Freon-22 will replace Freon-12 as the primary refrigerant in the modified system. The present 15-hp single-stage condensing unit will be replaced with a 25-hp two-stage unit, and a forced-circulation shell-and-tube evaporator will be substituted for the submerged-coil evaporator. The instrumentation for the refrigeration system will also be modified. The new control panel will be a graphic type with indicator lights to show which cold traps are being refrigerated. Flowmeters and additional thermocouples will be added to permit better estimation of the refrigeration capacity being developed by the primary system, and an improved timing system will provide complete programing of the chilling and defrosting cycles of the cold traps.

2.2 WATER TREATMENT

Fouling of the steam and cooling-water systems, resulting from extended operation of the HRT without chemical treatment of the water in those systems, indicated the desirability for such protection in future operations of the reactor.

2.2.1 Steam System

The problem of chemical treatment of boiling water in a radiation field was discussed with several water-treatment specialists.[7,8] It was concluded that hydrazine, which had been recommended for the control of oxygen concentration,[6] should be tried first because it will not introduce solids into the system; however, should it break down too rapidly under the radiation, it may be supplemented with, or replaced by, potassium sulfite. The sulfite treatment has the disadvantages of foaming and introducing solids, thus requiring more frequent blowdown of the heat exchangers. A coordinated phosphate treatment, using mono-, di-, or tri-potassium phosphate, or any combination of two of the three, will be used for pH control.[6]

2.2.2 Reactor Cooling-Water System

Potassium chromate will be used as a corrosion inhibitor in the closed cooling-water loop serving the stainless steel components in the reactor

---

[1] On loan from Vitro Engineering Co.

[2] On loan from Westinghouse Electric Corp.

[3] W. R. Gall *et al.*, *HRP Quar. Prog. Rep. Oct. 31, 1955*, ORNL-2004, p 11–13.

[4] W. R. Gall *et al.*, *HRP Quar. Prog. Rep. April 30, 1956*, ORNL-2096, p 17–18.

[5] F. C. Zapp, *HRT Process Flowsheets (Revision III)*, ORNL CF-55-5-156, Rev. III, p 10 (Jan. 30, 1957).

[6] W. R. Gall *et al.*, *HRP Quar. Prog. Rep. Jan. 31, 1957*, ORNL-2272, p 27.

[7] H. A. McLain, *Treatment of the HRT Steam System Water*, ORNL CF-56-11-132 (Nov. 29, 1956).

[8] W. R. Gall *et al.*, *HRP Quar. Prog. Rep. April 30, 1957*, ORNL-2331, p 19.

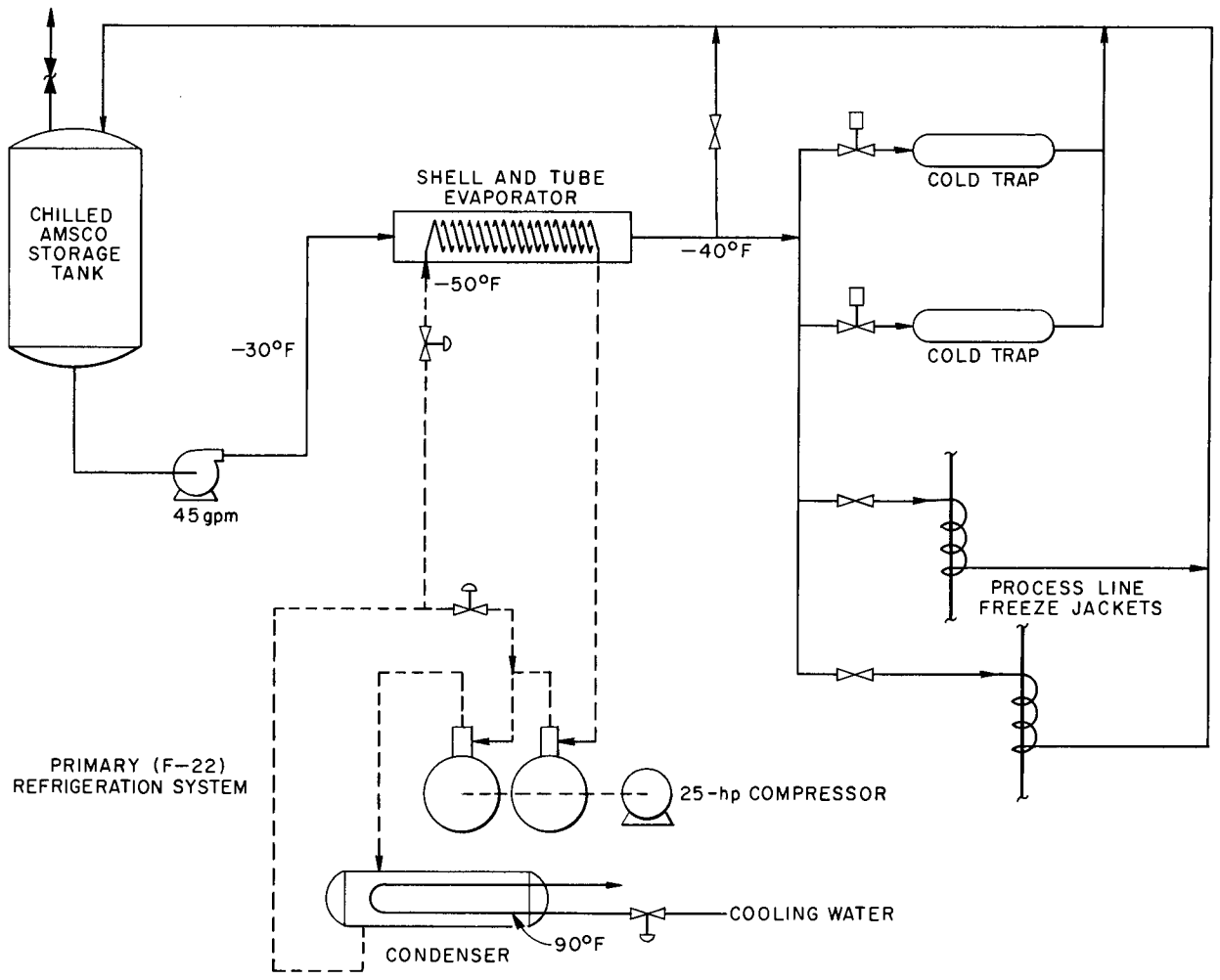

Fig. 2.1. Modified HRT Refrigeration System.

cell.[9] Because the chromate will decompose under radiation if the pH falls below 8, the pH of the water in the system will be maintained between 9 and 10.

2.2.3 Cooling-Tower Water System

A mixture of sodium chromate and sodium phosphate may be used to inhibit corrosion in the cooling-tower water circuit used to cool the water in the closed reactor water loop. If this treatment is used, the concentration of the chromate (CrO_4) and phosphate (PO_4) will be maintained between 20 and 25 ppm, and the pH of the water will be held between 6 and 7; a pH lower than 6 would result in appreciably higher corrosion rates, and a pH higher than 7 would cause the precipitation of calcium phosphates. Chlorinated phenols will be used for the control of algae in the cooling tower and will be added only as required to hold down algae formation.[10]

[9] H. A. McLain, memo to W. R. Gall, *Treatments for the HRT Closed Cooling Water and Cooling Tower Water System*, July 16, 1957.

[10] H. A. McLain, R. E. Aven, and R. C. Robertson, *HRT Cooling Water System Modification*, ORNL CF-56-8-152 (Aug. 23, 1956).

2.3 CLEANING AND STORAGE OF THE STEAM AND COOLING-WATER SYSTEMS

Operation of the steam system and closed cooling-water loop of the HRT over an extended period without adequate water treatment will necessitate that those systems be cleaned prior to further operation of the reactor. An inhibited phosphoric acid solution (10% H_3PO_4 + 0.2% Rodine-20) will be used for this purpose. Circulation of the cleaning agent will be followed by a 0.1% phosphoric acid rinse, a neutralizing rinse with 0.5% trisodium phosphate, and flushing with water. Potable water will be used during the cleaning and neutralizing operations, but steam condensate will be used for final flushing to minimize the concentration of chloride ion in the system.[11]

After cleaning, both systems will be kept full of water at all times while awaiting further operation of the reactor and during any future extended period of shutdown; that is, they will be maintained in wet storage. The storage solution for the steam system will be either condensate or demineralized water containing 100 ppm of hydrazine; the solution for the closed cooling-water loop will be condensate or demineralized water containing 1000 ppm of potassium chromate. These storage solutions will require periodic circulation to disperse pockets in which the inhibitor has become depleted.

2.4 STEAM-SYSTEM WATER SAMPLING

Continuous analysis of the concentrations of dissolved hydrogen and oxygen in the water circulated in the steam system was recommended to determine the effectiveness of oxygen control agents added to the water. A recorder and two Cambridge-type dissolved-gas analyzers, one for hydrogen and one for oxygen, will be used to monitor the samples drawn from the existing sample cooler.

Because the water in the heat exchangers will probably become radioactive, it will also be necessary to revise the present means of sampling the water from the exchangers. Water samples will be drawn directly from the exchangers, through a cooler, to the waste-evaporator sampler or a similar sampling device. An additional Cambridge dissolved-gas analyzer, shielded for radiation, will be required to monitor these samples for dissolved oxygen.

2.5 LEAK-DETECTOR SYSTEM

Because of the extreme difficulty of replacing certain of the major component flanges, an independent leak-detector system was designed to serve the fuel inlet and outlet flanges of the pressure vessel, the main heat exchanger head flanges, and the circulating-pump flanges.[12] The system is similar to the existing high- and low-pressure leak-detector systems, except for the addition of return lines from the heat exchanger head flanges and the reactor-vessel dome (fuel outlet) flange. The return lines will permit future sampling of the leak-detection fluid for the presence of chlorides, plus subsequent flushing of the system if the necessity is indicated; they will also permit a change from a static to a circulating system should it appear desirable. For the present, the return lines will be capped where they enter the control room. The leak-detection fluid will be D_2O, with overpressure provided by a mixture of helium and hydrogen. An excess of hydrogen will be maintained to suppress the presence of oxygen due to radiolytic decomposition of D_2O.

An improved indicating system, incorporating a capillary-tube flowmeter, was designed to supplement the present leak-detector indicating systems and to be installed on the independent system described above. This system will be used primarily during reactor shutdown for the rapid location of leaking flanges. The flowmeter is capable of measuring flow rates as low as 7.7 cc/day and as high as 385 cc/day; about 2 min will be required to obtain a reading of 99% of the actual rate of flow (i.e., rate of leak). The method of determining the location of a leak by alternately valving-off segments of the system remains unchanged. The measuring device of the new indicating system is a standard differential-pressure cell. Figure 2.2 is a view of the indicating system, showing the differential-pressure cell, a cutaway of the flowmeter, and the leak-detector-system header.

[11] H. A. McLain, *Chemical Cleaning and Storage of the HRT Steam and Closed Cooling Water Systems*, ORNL CF-57-6-36 (June 5, 1957).

[12] E. A. Mason and H. A. McLain, *Circulating Leak Detector System for HRT Flanges*, ORNL CF-57-4-38 (April 9, 1957).

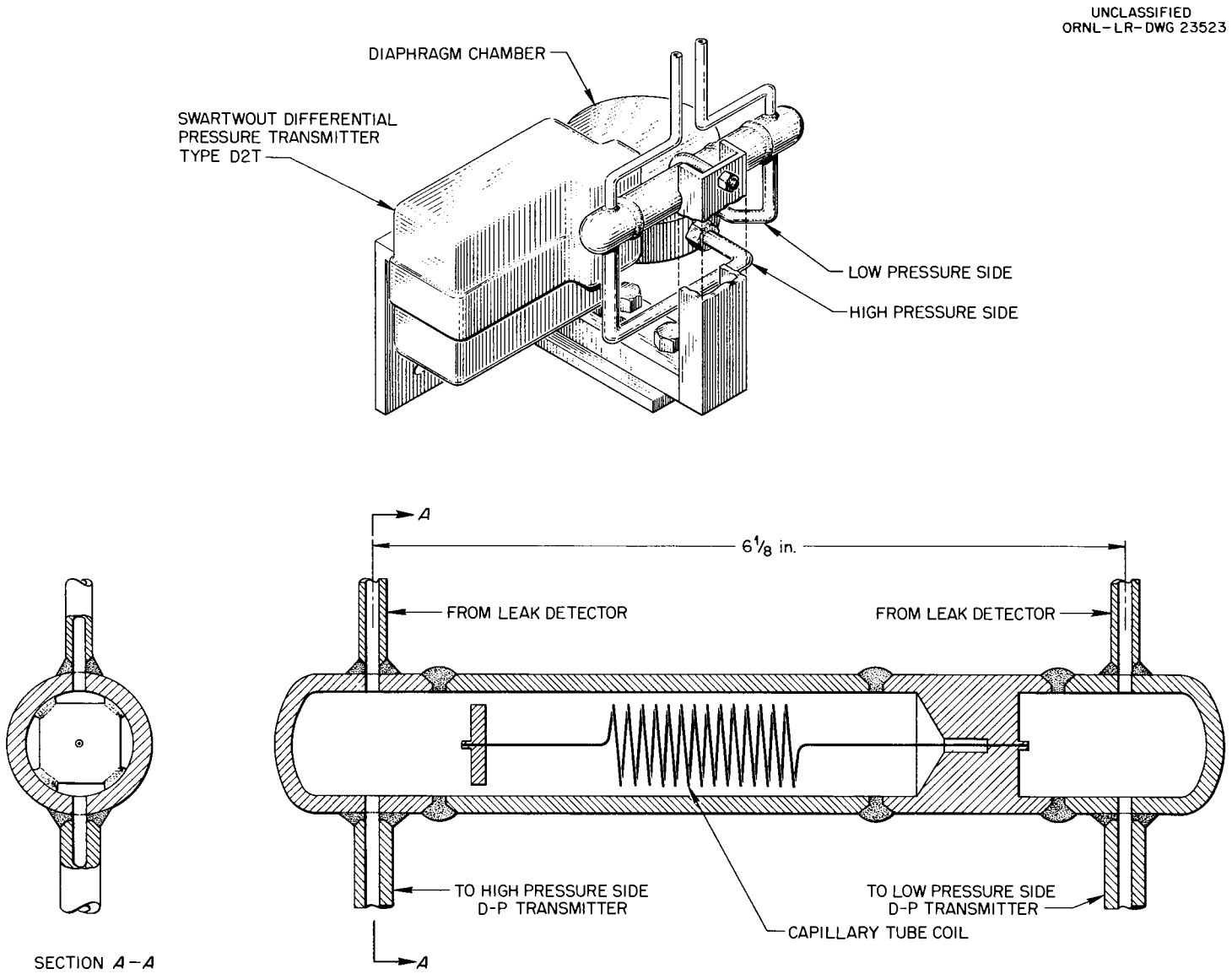

Fig. 2.2. Capillary-Tube-Flowmeter Leak-Indicating System.

2.6 IODINE REMOVAL

The fuel recombiner was redesigned to incorporate an iodine-removal bed to minimize iodine poisoning of the platinum catalyst in the recombiner. The bed, a 12-in.-ID × 36-in. cylinder packed with ½-in. silvered Raschig rings, will be inserted below the existing recombiner (Fig. 2.3). In addition to removing essentially all the iodine from the entering gas-and-steam mixture, the bed is also expected to lower the xenon concentration of the reactor system. Because I^{135}, the precursor of Xe^{135}, will be held on the bed until it decays, the xenon thus formed will be able to return to the high-pressure system only through the condensate. Since the distribution coefficient of xenon at 65°C is 13.4, 93% of the xenon entering the recombiner-condenser will pass off to the charcoal bed. With no gas letdown and with an oxygen injection rate of 500 cc/min, the Xe^{135} poison fraction in the HRT would be about 2%; the addition of the iodine-removal bed should reduce the poison fraction to 0.6%, under the same conditions.

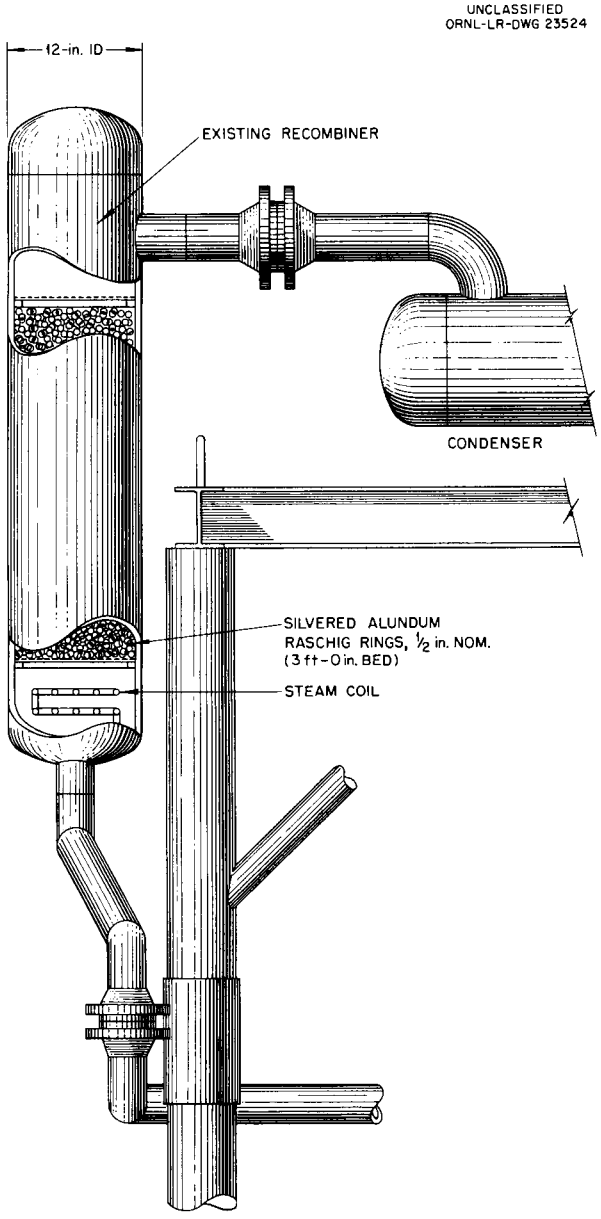

Fig. 2.3. HRT Iodine-Removal Bed.

The addition of the iodine bed will increase the pressure drop in the low-pressure system by less than 0.2 psi, which is not expected to affect the normal operation of the system. At equilibrium, the heat production rate of the iodine decay will be approximately 33,000 Btu/hr, sufficient to raise the temperature of the gas by 144°F. It is expected that the higher temperature of inlet gas will improve the efficiency of the recombiner. Removal of this heat during shutdown periods will be accomplished by cooling coils within the bed.

The iodine-removal bed may have a life of about 40,000 hr, based on available data, which indicate that the iodine concentration of the bed can reach 1.3×10^{-4} g-mole of I_2 per square foot.

2.7 FLANGE DEVELOPMENT PROGRAM

The investigation of ring-gasket flanged joints for the HRT is essentially complete. It is concluded that this type of joint will give satisfactory performance in the HRT provided that

1. closer tolerances and better finishes are maintained on both flange groove and gasket than are required by the ASA standard; the pitch diameter of both ring and groove is machined to a tolerance of ±0.0010 in., as opposed to the ASA tolerance of ±0.005; the angular tolerance on the sides of the groove and on octagonal rings is maintained at ±15 min of arc, as compared to ±½ deg required by ASA; a 32-μin.-rms finish is maintained on the seating surfaces of both flange groove and ring;
2. the hardness of the face of the flange groove is a minimum of R_B 84 or Brinnel 160, and the hardness of the ring-joint gasket is a maximum of Brinnel 140 (these requirements are covered in HRP specifications 201a and 202a);

3. adequate precautions are taken in all stages from initial machining to final installation to protect the seating surfaces of both rings and grooves from scratches or other damage;
4. flange bolts are increased in length and equipped with ferrules or nut-ferrules to provide increased elasticity;
5. the flanges are insulated with approximately ten layers of aluminum foil or the equivalent;
6. flange bolts are initially tightened to a stress of approximately 45,000 psi ± 10%.

The torque wrench is an adequate tool for tightening the flange bolts, since recent tests indicate that it is capable of reproducing indicated bolt loads within 9% of the actual load as determined with an extensometer.

After thermal cycling, the above bolt stresses will drop off, approaching an asymptotic value of about 30,000 psi. This asymptotic value is, for all practical purposes, reached after three thermal cycles. If all other conditions specified above are met, no retightening of the bolts is necessary.

Two each of ½-in. 1500-lb, 1-in. 2500-lb, 2-in. 2500-lb, and 3½-in. 2500-lb flanged joints were used in the tests which resulted in the conclusions above. The temperature-pressure cycle was under saturation conditions, with a maximum pressure of 2000 psi and minimum temperatures from 20 to 100°C. Maximum heating and cooling rates were 55°C/hr, and the test loop was maintained at the high and low temperature of each cycle long enough for equilibrium conditions to be reached throughout the flanges. Pressure differentials across the leakage paths of the flanges ranged from 15 to 2000 psi. A leak rate of less than 1 cc of water per day at room temperature was considered acceptable for the tests. It must be noted that the flanges in the test facility were not subjected to the pipe moments and torques which will be encountered in operation of the HRT.

Two series of tests were made which indicated that, providing the above limitations are observed, a flanged joint may be opened and reassembled at least four times, with either the same or a newly machined ring gasket, and subjected to at least nine thermal cycles between each reassembly without excessive leakage occurring in any part of a cycle. No difference in leak rate was observed to be due to the type of ring gasket used, and it was concluded that rings with either oval or octagonal cross sections are equally suitable for ring-joint flange closures; however, they cannot be used interchangeably on reassembly of the same joint. In the first series of tests the same gasket was reinstalled in each flange on reassembly, and the gasket was rotated 90 deg to prevent reseating at the same point.[13] In the second series a newly machined ring of the same type was installed on each reassembly. No significant difference in leak rates was observed in the second series, but some indication of galling or surface abrasion not observed in the earlier series was found. Whether the condition was the result of using newly machined rings or was caused by the repeated use of the same non-machined flanges is not known; whatever the cause, it had no significant effect on leakage.

Recent tests to determine the reliability of the torque wrench for tightening flange bolts showed a maximum deviation of average indicated-bolt-load from average actual-bolt-load, as determined by an extensometer, of about 9%. Prior to this particular series of tests the same bolts and nuts had been tightened and loosened about ten times, a molybdenum disulfide lubricant being used each time before tightening. For the series of tests noted, particular care was taken to clean and relubricate the threads. The results gave much less deviation than those previously obtained with the same nuts and bolts.[14] It is possible that the continued use of the same nuts and bolts had conditioned them prior to making the latest tests; if this is the case it may be necessary to similarly condition replacement nuts and bolts for the HRT.

2.8 PIPING ALTERATIONS

The fuel and blanket feed-pump piping was redesigned to permit venting of the pumps should they become gas-bound. Vent lines, containing high-pressure remotely operated valves, were installed from the pump discharge lines (lines 110 and 210, respectively, for the fuel and blanket pumps) to the dump tanks. Special check valves are located in the discharge lines to prevent loss of system pressure during venting. These valves employ a high-lift ball as a means of minimizing seat wear on alternating strokes of the feed

[13] W. R. Gall *et al.*, *HRP Quar. Prog. Rep. April 30, 1957*, ORNL-2331, p 19.

[14] W. R. Gall *et al.*, *HRP Quar. Prog. Rep. Jan. 31, 1957*, ORNL-2272, p 25.

pumps. Also included in this alteration was the addition of a high-pressure oxygen-addition orifice, which should provide better dispersion of the oxygen gas which is fed into the feed-pump discharge at this point.

Improving the reliability of the reactor diaphragm pumps was approached by: (1) assuring a constant feed supply, (2) providing a means of relieving the cause of pump stoppage, and (3) limiting the use of pumps during operation. The purge pumps, which formerly were supplied from a standpipe below the recombiner condensers, will now draw directly from the condensate tanks. A constant feed supply will be maintained by utilizing the present condensate weight recorders as level controllers. Condensate will be available to the feed pumps as before, except that during dilution, the condensate supply to these pumps will first pass through the feed cooler, instead of flowing directly to the pumps. A further effort to minimize the chances for diaphragm-pump difficulties was made in the blanket system by modifying the blanket pressurizer, so that it can be supplied directly from both the blanket high-pressure circulating loop and the purge-pump feed from the low-pressure system. A $\frac{1}{2}$-in. circulation line was added between the standpipe and the heated leg header of the blanket pressurizer. This line will make it unnecessary to operate the blanket, feed, or pressurizer purge pumps except when filling the loop or when making up leakage to the low-pressure system.

Drawings showing piping changes necessary to accommodate the installation of rupture-disk assemblies to supplement the main-heat-exchanger relief valves were completed. The relief valves on both water and steam sides of the heat exchangers were relocated to permit the insertion of rupture-disk assemblies upstream of the valves.

3. HRT COMPONENT DEVELOPMENT

I. Spiewak

J. M. Baker
R. Blumberg
J. S. Culver
C. H. Gabbard
B. A. Hannaford
P. H. Harley
P. G. Herndon
E. C. Hise
J. C. Moyers
I. K. Namba
D. L. Snyder
D. E. Willis

3.1 PUMP DEVELOPMENT

3.1.1 400A-1 Pump and Loop

The 400A-1 Westinghouse pump, which contains a titanium impeller and a stainless steel thermal barrier with a titanium wear-ring insert, has operated for 10,965 hr since the thermal barrier was welded to the stator flange. For 10,722 hr, a solution of 0.04 *m* UO_2SO_4, 0.005 *m* $CuSO_4$, and 50 mole % excess H_2SO_4 has been circulated at 255°C. Solution analyses indicate an average over-all loop corrosion rate of 0.07 mpy for the run.

3.1.2 400A-2 Pump and Loop

The 400A-2 Westinghouse pump was used in an attempt to determine the extent of mixing through the shaft seal between the hot end of the pump and the motor cavity. Indications are that a mixing flow of 2 liters/hr was present with no purge flow. Mixing occurred at a rate of 0.2 to 0.4 liter/hr with purge flow in the range of 4 to 35 liters/hr. The lower suction ports in the rotor shaft were plugged in order to determine their effect on the mixing rate. With the ports plugged and with no purge flow, a mixing flow of only 0.9 liter/hr was indicated; with a purge flow of 12 liters/hr, the mixing flow was reduced to 0.03 liter/hr.

3.1.3 300A-1 Pump

The 300A-1 pump has operated in the HRT mockup since the revised thermal-barrier seal weld was made for a total of 1735 hr: 142 hr with 0.13 *m* UO_2SO_4 solution at 260°C, 376 hr with 1.3 *m* UO_2SO_4 solution at 260°C, and 1217 hr with 0.04 *m* UO_2SO_4 solution at 280 to 300°C. Occasional instantaneous power irregularities have been noted, but the pump continues to function satisfactorily.

3.1.4 HRT Fuel and Blanket Circulating Pumps

Titanium labyrinth inserts and impellers were installed on the HRT circulating pumps. The thermal barriers were seal-welded into the stator housings.

3.2 FEED PUMPS

3.2.1 Feed-Pump Test Loops

Endurance testing of various diaphragm materials in uranyl sulfate and water is continuing in test loops 1 and 2 and in the HRT mockup. Testing of full-sized feed-pump check valves using type 17-4 PH seats was begun in these loops also. No feed-pump diaphragm failures were experienced during the quarter. Table 3.1 lists the test duration for all pump heads now in operation.

Two heads in the HRT mockup have had failures of the blanked-off nipple on the intermediate side of the head. In these failures, longitudinal cracks about $\frac{3}{4}$ in. long extended equally into the nipple and the base metal of the head. Similar nipples will not be permitted on future heads; other nipples connecting the check valves and intermediate line were reinforced to prevent future failures.

The mockup feed pump was equipped with a duplex reciprocating drive unit consisting of a Milton-Roy power end and two ORNL-designed pulse-generating cylinders. This drive operates with considerably less noise and shock than the Scott & Williams drive unit.

Several methods of relieving gas-bound pump heads were tried. The only method that was completely satisfactory in venting gas from the head and the suction line is shown in Fig. 3.1. This method was thoroughly tested on the HRT mockup and is being installed on the HRT feed pumps.

3.2.2 Purge Pumps

Two purge-pump diaphragm failures occurred during the quarter: one on the HRT mockup and one on purge-pump test loop No. 1. These failures

occurred at 596 and 946 hr, respectively. Both diaphragms were made from a batch of sheet stock which has given uniformly poor results.

The head from the mockup was replaced with a rebuilt head containing 100-mesh screens and a 0.019-in. annealed diaphragm with mechanically polished surfaces. Two other heads are being rebuilt: one with an Allegheny Ludlum alloy AM-350 diaphragm and the other with a full-hard type 347 stainless steel diaphragm. These two heads will be life-tested by using a new Scott & Williams P-2 drive unit.

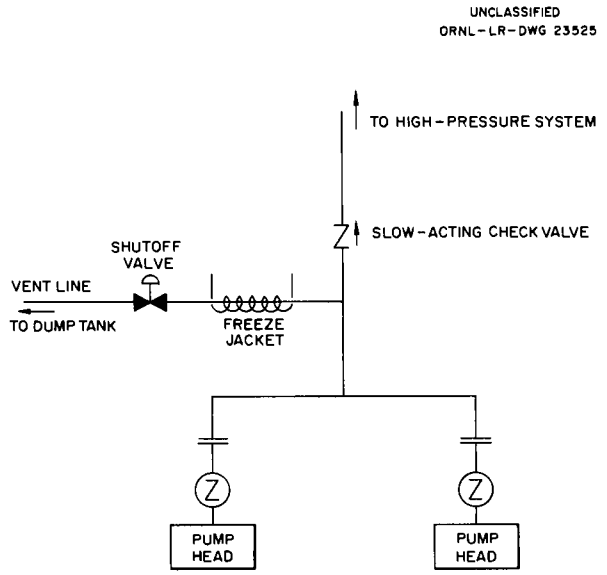

Fig. 3.1. Feed-Pump Venting System.

3.2.3 Check-Valve Material Test

Testing of various check-valve material combinations is continuing. The following materials successfully passed 250-hr screening tests in water:

Balls	Seats
Star J	17-4 PH
Star J	Carpenter 20
Star J	347 Stainless Steel
Kennametal K 501	Kennametal K 501

In addition, the Star J balls vs 17-4 PH seats ran 1700 hr in both water and 10-g/liter uranyl sulfate solution without developing static leakage.

It was found that Stellite 6 seats prerun in uranyl sulfate or prelapped can withstand a distilled-water environment better than new seats, which fail in less than 200 hr. It is believed that minute water leaks cause corrosion-erosion failure; the pretreatment eliminates such leaks temporarily.

Table 3.1. Duration of Tests of Feed-Pump Heads Currently Operating

Head Location	Diaphragm	Test Duration (hr)
Feed-pump loop No. 1 (water)		
East	0.031-in., annealed, liquid-blasted finish	1608
West	0.019-in., annealed	5940
Feed-pump loop No. 2 (UO_2SO_4)		
South	0.031-in., annealed, mirror finish	2424
North	0.031-in., ¼ hord, as-rolled finish	2424
HRT mockup (UO_2SO_4)		
South	0.022-in., ¼ hard, polished	4808
North	0.031-in., ½ hard, as-rolled finish	1384
Valve test loop	0.031-in., annealed	248

3.2.4 Corrosion Fatigue Tests

The corrosion fatigue program at Ohio State University is approximately one-third complete. Endurance limits obtained thus far for type 347 stainless steel are listed in Table 3.2. There is a great reduction in the fatigue life of the hardened materials in uranyl sulfate, but annealed stock is affected only slightly.

Tentative conclusions are that annealed type 347 sheet should be used for fuel feed pumps and that hardened stock may be superior for distilled-water pumps.

Tests are being continued on types 347 and 316 ELC stainless steel and on Allegheny Ludlum AM-350.

3.2.5 HRT Replacement Feed and Purge Pumps

A full set of four feed-pump heads and four purge-pump heads is being manufactured at ORNL. These heads contain 100-mesh screens to protect the diaphragms from dirt. The feed-pump diaphragms are annealed 0.031-in. type 347 stainless steel; purge-pump diaphragms are annealed 0.019-in. type 347. Fuel-feed check valves contain Stellite Star J balls and Stellite 3 seats; all other seats are type 17-4 PH. Check valves will be pretested in development loops prior to installation on the heads.

3.3 HRT SPARE HEAT EXCHANGER

Materials for the HRT spare heat exchanger are either on hand or scheduled for August delivery. Ninety-five per cent of the Babcock & Wilcox shop drawings have been reviewed and approved by ORNL. Welding and inspection procedures are being resolved by discussions between Babcock & Wilcox and ORNL personnel.

The specifications require that the heat exchanger be subjected to a thermal-cycle test. Calculations of the transient temperature behavior of the shell while the tubes are thermally cycled between 380 and 580°F were carried out. It was shown that the temperature change in the shell would not exceed 0.5°F per minute during any part of the test, which would induce a temperature gradient of 2.5°F across the shell. This produces a negligible thermal stress.

During the first six or seven cycles of the test, the maximum shell temperature would increase during successive cycles but would stabilize at about 480°F after this period. While the temperature variation of the heat exchanger tubes would be 200°F during any cycle, the steady-state shell variation would be 20 to 25°F.

3.4 HRT MOCKUP

3.4.1 Mockup Operation

During the report period, the HRT mockup completed a 1580-hr run in which 0.04 *m* UO_2SO_4, 0.02 *m* H_2SO_4, 0.005 *m* $CuSO_4$, and 50 ppm O_2 were circulated at 1700 psi and 280°C. The run was terminated because a leak developed between the primary and secondary regions of the loop heat exchanger. This failure is discussed in detail in Sec. 3.4.2.

The generalized corrosion rate observed during this run was 1.25 mpy based on nickel analyses of the solution. The uranium concentration was quite erratic, and following the run, 980 g of solids, containing 650 g of uranium and 45 g of

Table 3.2. Endurance Limit (10^7 Cycles) of Type 347 Stainless Steel Sheet

Temper	Endurance Limit (psi)		
	In 0.04 *m* UO_2SO_4 at 60°C	In Water at 60°C	In Air at Room Temperature
Annealed	34,000		39,000
¼ hard	30,000		
½ hard	32,000	57,000	67,000
¾ hard	33,000		
Full hard	43,000		

copper, was found in the horizontal leg connecting the pressurizer and the circulating system. Since there was no net loss of uranium from solution, it is surmised that the uranium had been precipitated somewhere in the system during the previous 1.3 *m* UO_2SO_4 test. It apparently redissolved during the 1580-hr run (accounting for the erratic uranium analyses) and reprecipitated at the solution-water interface in the pressurizer. Hydrolysis of UO_2SO_4 in this region had been noted in previous runs when insufficient excess H_2SO_4 was present.

Failures in feed-pump capped nipples and a purge-dump diaphragm during the run are described in Secs. 3.2.1 and 3.2.2, respectively. None of these failures resulted in shutdown of the system.

The loop heat exchanger was replaced, pending construction of a duplicate, with Calrod heaters placed around the high-pressure circulating system to give a total of 60 kw. Three dead-end sections of ½-in. pipe were welded into the high-pressure system to explore possible oxygen-depletion effects in future runs.

Another run with 0.04 *m* UO_2SO_4 was then started in the mockup; it has continued for 155 hr to date.

3.4.2 Mockup Heat Exchanger

The 80-kw heat exchanger[1] built by Foster Wheeler for the HRT mockup failed after 10,165 hr of operation. One of the tubes developed a sizable leak, approximately 8 in. from the upper end of the tube. An initial examination revealed that 11 (including the one which failed) of the 37 tubes comprising the tube bundle had become plugged with solids and that the remaining tubes were heavily scaled. The solids were predominantly Fe_2O_3. The quantity of solids was so large that they evidently were deposited as a result of corrosion elsewhere in the system. Since a change in heat-transfer behavior was observed during the period when 1.3 *m* UO_2SO_4 was run in the mockup, it is believed that the solids were deposited at that time. The heat exchanger was connected in a bypass line which permitted a flow of 100 gpm before plugging began.

The tube in which the failure occurred and two other tubes, one plugged and one open, were carefully sectioned and visually examined. The failure, shown in Fig. 3.2, was caused by a large pit

[1] W. L. Ross and L. F. Goode, *HRP Quar. Prog. Rep. July 31, 1954*, ORNL-1772, p 42–43.

Fig. 3.2. Tube Failure in HRT Mockup Heat Exchanger.

which developed on the primary side of the heat exchanger. Numerous other pits were observed in other areas of the failed tube and in the two other typical tubes. Examples of these are shown in Fig. 3.3.

Materials for building another similar heat exchanger at ORNL are on hand.

3.4.3 Iodine Injection Tests

Samples taken from the partially poisoned HRT-mockup recombiner[2] showed that between 50 and 87% of the iodine injected into the system had deposited rather uniformly on the platinized alundum catalyst.

A silvered alundum bed was placed upstream of the recombiner, and KI was again injected into the high-pressure fuel system. Virtually all the iodine was trapped in the two alundum beds; about 90% was found on the silvered alundum. The silvered bed did not prevent partial poisoning of the platinized alundum catalyst. It is believed that poisoning can be eliminated by increasing the mass-transfer surface of silvered alundum; this will be explored in future runs. It was found that the poisoned catalyst can be regenerated by permitting its temperature to rise to 650°C.

[2] I. Spiewak *et al.*, *HRP Quar. Prog. Rep. April 30, 1957*, ORNL-2331, p 30.

3.5 HRT RECOMBINERS

The HRT fuel and blanket recombiners were successfully operated to demonstrate that no significant loss of platinum had occurred since installation. In addition, runs were made to determine recombination efficiencies at low gas concentrations and low steam diluent flows. Table 3.3 summarizes the data. At high stoichiometric gas concentrations, recombiner efficiency was 100%. At low concentrations, as much as 50 cc of hydrogen per minute left the system in the off-gas stream. In order to recombine this gas, a 5-in.-long roll of platinized wire mesh was inserted into a steam-jacketed section of 1-in. off-gas piping. The hydrogen and oxygen recombined by this section raised the over-all efficiency to virtually 100%.

Fig. 3.3. Typical Pitting in Tubes of HRT Mockup Heat Exchanger.

Table 3.3. Test of HRT Recombiners

Entering Stream				Exit Stream			
				Hydrogen			
Steam Flow (lb/hr)	Stoichiometric Gas Concentration (%)	Excess Oxygen (%)*	Excess Oxygen (cc/min)	Concentration (%)	Flow (cc/min)	Temperature (°F)	Recombination Efficiency
Blanket-System Recombiner							
120	0.08	105	300	0.6	2	250	99.7
120	0.80	25	700	6.8	48	260	99.2
120	0.80	25	710	3.0	22	265	99.6
120	0.80	55	1,575	3.4	54	260	99.1
200	8.0	20	9,900	0.0	0	635	100.0
300	8.0	63	49,300	0.0	0	690	100.0
Fuel-System Recombiner							
120	0.08	110	300	1.0	3	230	99.5
120	0.80	15	450	7.2	32	260	99.5
300	8.0	60	48,100	0.0	0	670	100.0

*Based on quantity of stoichiometric gas.

4. HRT REACTOR ANALYSIS

P. R. Kasten

C. W. Nestor, Jr. M. W. Rosenthal

4.1 EFFECT OF BLANKET THORIUM CONCENTRATION ON HRT NUCLEAR CHARACTERISTICS

The thorium blanket experiment is one of three major experiments which may be performed in the HRT. In this test, the initial thorium concentration will influence the nuclear characteristics and behavior of the reactor. Based on two-group calculations, results were obtained for the conversion ratio as a function of blanket thorium concentration and were obtained also for the reactivity addition associated with complete removal of thorium from the blanket region. Although not reliable on an absolute basis, the results indicate the magnitude of the effects involved.

4.1.1 Conversion Ratio

The initial conversion ratio of the reactor with U^{235} as fuel is shown in Fig. 4.1 as a function of blanket thorium concentration. Since the conversion ratio is a direct measure of the rate of U^{233} production, the values in Fig. 4.1 indicate the relative rates at which the U^{233} concentration (in *grams per liter*) would build up in the blanket. At 250 g of thorium per liter the rate would be about three-fourths that at 1000 g of thorium per liter. However, when the concentration is expressed as *grams of* U^{233} *per gram of thorium*, the relative rate of U^{233} buildup would be greater at the lower thorium concentrations, being nearly three times as great at 250 g of thorium per liter as at 1000 g of thorium per liter. Thus, for a given time of reactor operation, the accuracy by which conversion ratio can be determined may be greater at the lower thorium concentrations.

4.1.2 Reactivity Effects Associated with Settling of Slurry

The amount of reactivity, Δk_e, which would be added to the HRT if all the thorium in the blanket were suddenly removed is plotted in Fig. 4.2 as a function of initial thorium concentration. The Δk_e associated with a concentration of 250 g of thorium per liter is seen to be over one-half that associated with 1000 g of thorium per liter; also, the reactivity addition resulting from a specified *fractional* decrease in thorium concentration does not change appreciably with different initial thorium concentrations. Therefore, in studying the stability and safety of two-region reactors, the

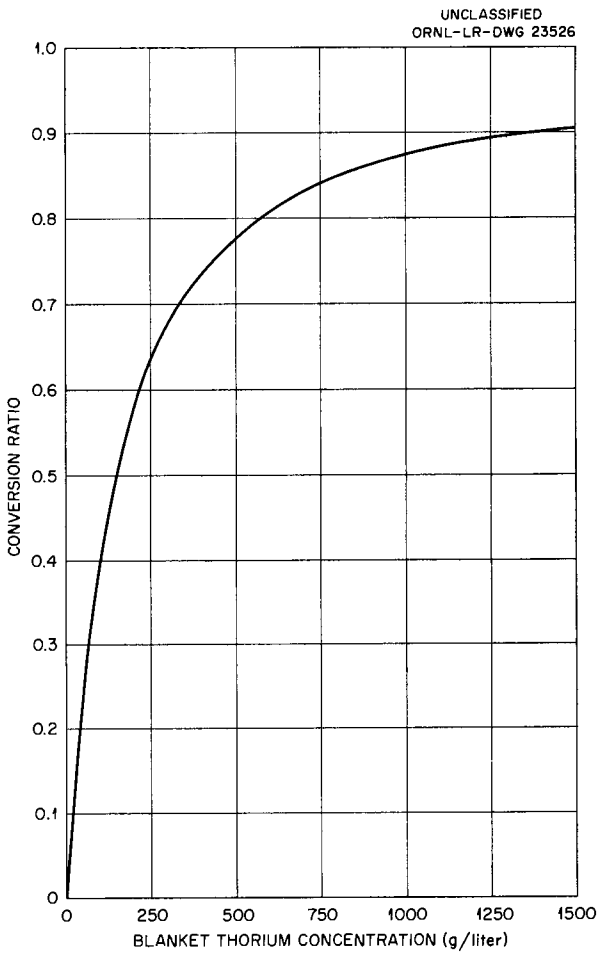

Fig. 4.1. Conversion Ratio vs Blanket Thorium Concentration in HRT. Fuel, U^{235}; temperature, 280°C.

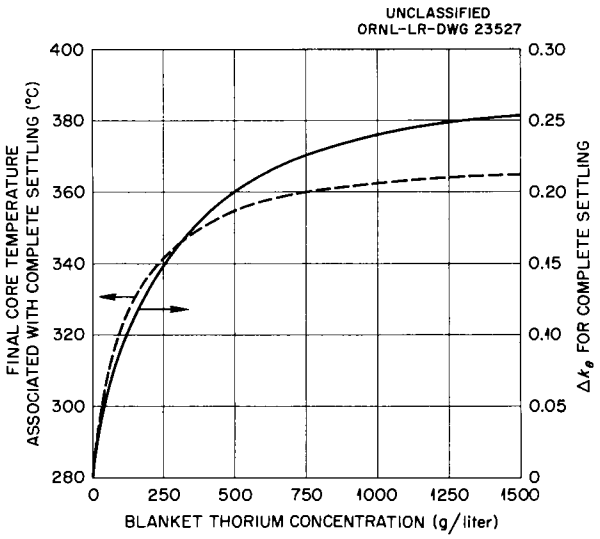

Fig. 4.2. Reactivity and Temperature Changes Associated with Complete Settling of Slurry in HRT Blanket.

information which could be obtained with 250 g of thorium per liter in the HRT blanket should be comparable with that obtained with a concentration of 1000 g of thorium per liter.

Although the amount of reactivity tied up in slurry may be large, experimentally determined settling rates are sufficiently low that the resultant rates of reactivity increase should not be hazardous. However, to compensate for the reactivity addition, the core temperature may rise to values which necessitate dumping the reactor. The dashed curve of Fig. 4.2 indicates the magnitude of the temperature rise that would be required to compensate for the reactivity addition if all the thorium in the blanket were removed and no other action took place to reduce the reactivity. In practice, the operator would make the reduction by diluting the fuel in the core. Should this be insufficient, he would stop power withdrawal and begin dumping the reactor.

5. HRT CONTROLS AND INSTRUMENTATION

D. S. Toomb

E. H. Bell
A. M. Billings
J. C. Gundlach
R. L. Moore
R. M. Pierce[1]
W. P. Walker[2]
K. W. West
H. D. Wills

5.1 COMPONENT AND SYSTEM TESTING

5.1.1 Letdown Valves

In the shakedown operation of the HRT much difficulty was experienced with corrosion of the Stellite No. 6 plugs of the letdown valves. The wear was localized near the seating cones because the valves were oversized for the operating conditions.[3] Erratic behavior of Stellite No. 6 in 5 wt % nitric acid and in distilled water at 80°C with an overpressure of 150 psi of oxygen has been noted in static corrosion tests.[4]

New bellows assemblies with Armco 17-4 PH stainless steel plugs hardened to R_C 35 to 40 will be installed for the next series of reactor runs. These valves will be sized as follows:

	C_v-¾ Open	C_v-Full Open
Fuel-system letdown	0.03 linear	0.1 nonlinear
Blanket-system letdown		0.04 linear

The fuel-system letdown-valve taper was machined with a discontinuity to provide for a maximum flow of 15 cfm of radiolytic gas, which may be required under some circumstances. These valves will possibly be retained for uranyl sulfate operation if concurrent tests in the development loops are satisfactory.

5.1.2 Low-Pressure-System Valves

Inspection of the low-pressure valves revealed deep pitting and some stress cracking (similar to that caused by chlorides) on the flanges of the bellows assemblies. The valve is shown in Fig. 5.1, and typical pitting attack in Fig. 5.2. The bellows assemblies were replaced in all the low-pressure valves.

5.1.3 Pressurizer-Level Control Loop

An HRT letdown-valve control loop was simulated by a 1:2 pneumatic amplifier and 30 ft of tubing connecting the valve actuator and the amplifier. An analysis[5] of the frequency response of the loop indicated that ⅜-in. tubing is the optimum size for response, although there was very little difference between ¼-, ⅜-, or ½-in. tubes.

5.2 DEVELOPMENT

5.2.1 Liquid-Level Transmitters

Prototype linear differential transformers suitable for sensing displacer (float) motion in the HRT level transmitters were received from the G. L. Collins Company and the Crescent Engineering Company. The transformers are designed to be radiation resistant by the elimination of all organic material and are suitable for operation at 300°C. The Collins transformer, shown at the far right of Fig. 5.3, is wound with copper wire insulated with ceramic material, and the leads are brought through the stainless steel housing by ceramic-to-metal seals. The Crescent unit, shown at the center of Fig. 5.3, is wound with ceramic-insulated silver wire, and the leads are brought through the stainless steel housing by compression-type seals. The transformers presently in use, shown at the left of Fig. 5.3, were fabricated at ORNL and are wound with Sprague Electric Co. Ceroc T wire on American Lava Corporation Lava forms. The new units, which should be more radiation resistant than those presently installed, will be thoroughly tested before final evaluation.

---

[1] On loan from TVA.

[2] Consultant from University of Virginia.

[3] A. M. Billings, *HRT Letdown Valves*, ORNL CF-57-6-25 (June 5, 1957).

[4] J. L. English *et al.*, *Quarterly Report of the Solution Corrosion Group for the Period Ending April 30, 1957*, ORNL CF-57-4-55, p 41.

[5] B. M. Rothleder, G. Melikian, and C. E. Shaw, *Control System Analysis*, KT-281 (May 8, 1957).

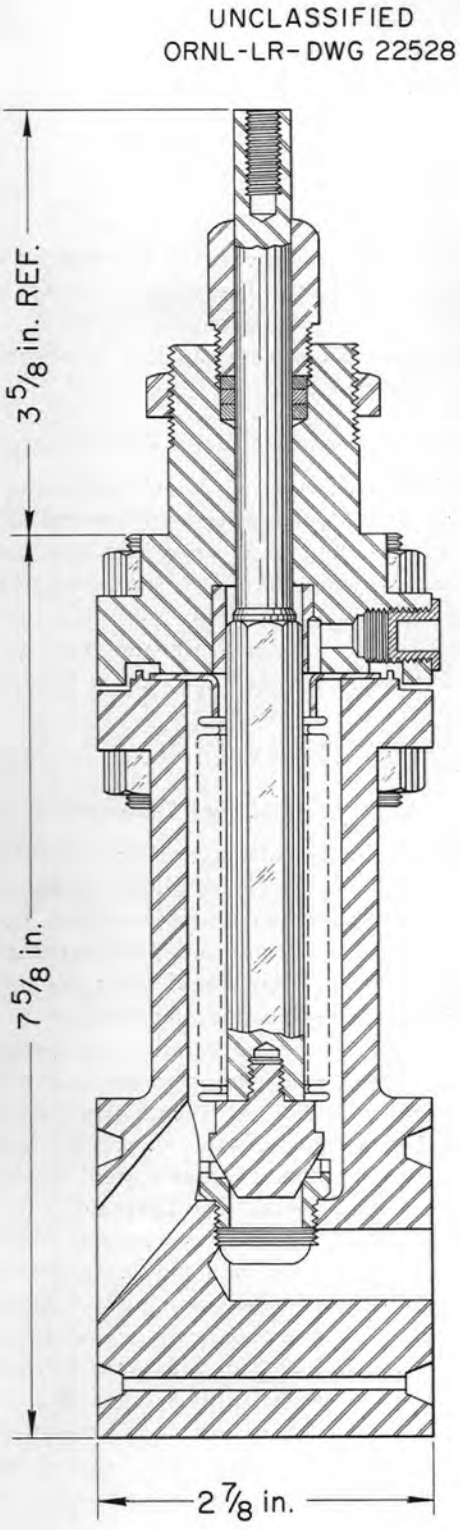

Fig. 5.1. Low-Pressure Valve.

Fig. 5.2. Pitting Attack on Low-Pressure-Valve Bellows Head.

5.3 DESIGN

The necessary instrument and controls engineering work was completed covering the following revisions and additions to the plant system:

1. the addition of remotely actuated valves to bleed accumulated gas from the feed pumps,
2. the addition of remote speed control for the fuel steam-system feed-water pump,
3. the addition of pumps to inject chemical additives to the feed-water streams,
4. the increase in capacity of the refrigeration system used to cool the off-gas-system cold traps and to freeze-off process lines for maintenance operations,
5. the revision of the leak-detector system to include differential-pressure transmitters for measuring leakage flows by the measurement of the pressure drop across a length of capillary tubing,
6. the revision of the condensate control system to permit purge water to be drawn from the condensate tanks.

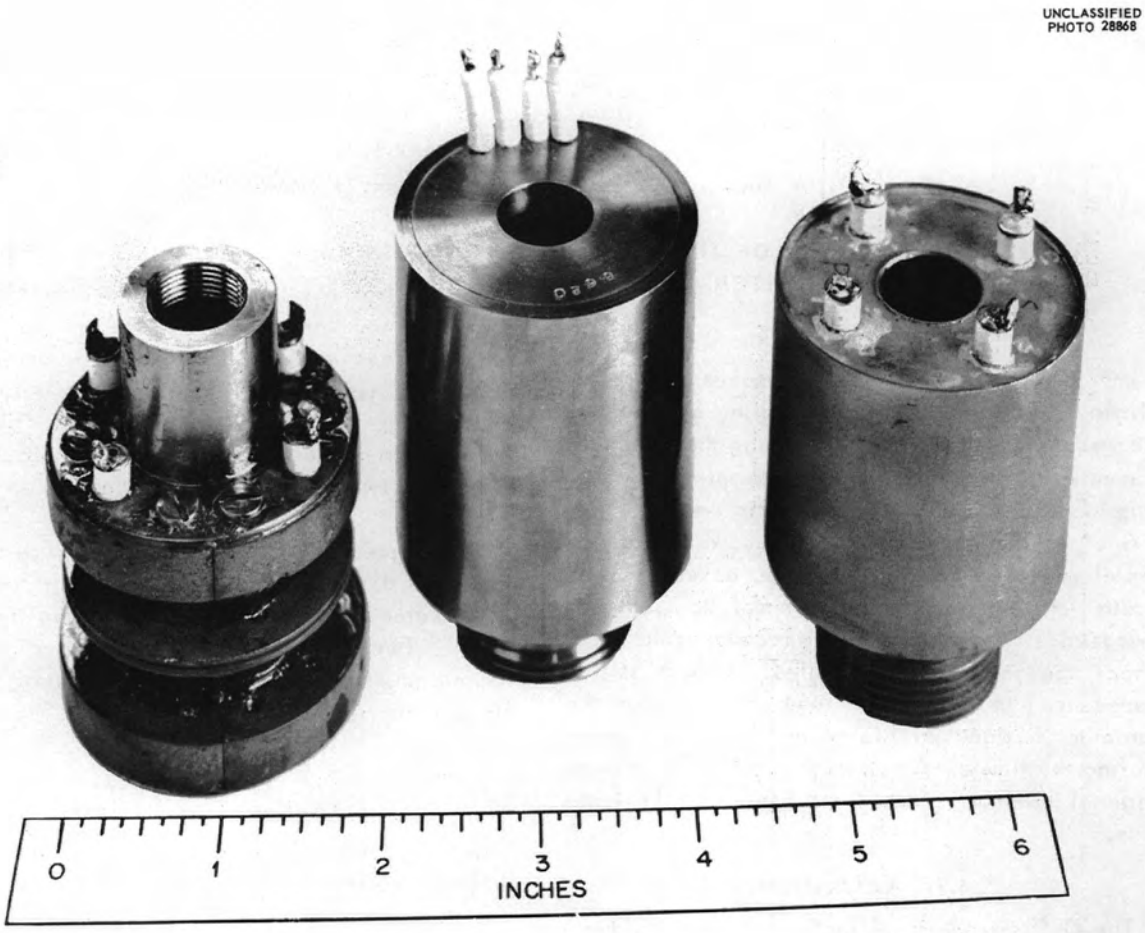

Fig. 5.3. Prototypes of Differential Transformers for HRT Liquid-Level Transmitters.

6. HRT PROCESSING PLANT

W. E. Unger W. D. Burch P. A. Haas
W. L. Albrecht L. H. Chase A. M. Rom
T. A. Arehart R. W. Horton W. F. Schaffer
N. C. Bradley C. S. Lisser J. W. Snyder
N. A. Brown F. C. McCullough R. H. Winget

6.1 FINAL ASSEMBLY OF THE LOW-PRESSURE SYSTEM

6.1.1 Leak Check

Improperly machined gasket grooves and poorly aligned flanges prevented the sealing of six valve flanges. Remachining and realigning these flanges corrected this difficulty. The completed system was then given a 500-psi hydrostatic test.

One of the tube-to-flange liner welds on the tantalum-lined dissolver flange assembly was again cracked during an attempt to seal the Swagelok fittings.[1] Following repairs in the local shops the assembly was sealed, although it was necessary to substitute lead ferrules for the tantalum ferrules on two of the five tubes penetrating the flange. A helium leak test with 100-psi internal pressure showed all fittings to be leak-free.

6.1.2 Calibrations

The D_2O storage level instruments – a Baldwin-strain-gage-type weigh cell and the thermal-level probe – were calibrated. Based on observations throughout this operating period, the weigh cell should indicate volumes to within 1 liter, and the thermal probe should indicate volumes to within 2 to 3 liters. The storage tank holds 40 liters. The bubbler-type liquid-level instruments on the decay tanks and dissolver were calibrated also.

The Potter turbine-type flowmeters have not proved reliable for measurement of boilup rates from the dissolver and decay tanks. Excessive bearing wear, resulting either from dirt particles or from the nonlubricating conditions (superheated steam), caused the turbine to turn erratically. However, these measurements are not absolutely essential to plant operation, and replacement of the meter would not be necessary if difficulty developed during operation.

[1] W. R. Gall *et al.*, *HRP Quar. Prog. Rep. April 30, 1957*, ORNL-2331, p 43–44.

6.2 FLUSHING AND CLEANING PROCEDURES

The system was treated with the standard three-step, flushing and cleaning procedure, consisting of a process water flush to remove any foreign debris, a trisodium phosphate solution rinse for degreasing, and a pretreatment with 5% HNO_3. Samples from the acid treatment showed that no off-grade material had been incorporated in the system.

All low-pressure leak-detector lines were checked for chloride contamination by soaking for 24 hr with water and draining and analyzing the solution. Two of the 42 lines showed minor contamination, the water from them containing 4.8 and 10 ppm chlorides.

6.3 DISSOLVER

6.3.1 Heat-Transfer Tests

Unacceptably low heat-transfer rates noted during preliminary water boiling tests of the tantalum-lined dissolver were attributed to air space, which measured 15 to 20 mils, between the tantalum liner and steel vessel. Addition of mercury to the space increased the over-all coefficient from 5 to about 75 Btu/hr·ft^2·°F. Previous tests had also pointed out the need for violent agitation of the dissolver contents and additional refluxing capacity. The two needs were met by dividing the jacket into two sections (Fig. 6.1). In the lower section, all the heat applied enters at the bottom, and the bubbles rising from the vessel bottom provide the required agitation. With cooling water flowing through the upper section, complete reflux is possible within the dissolver, thus preventing the entrainment of liquid from the dissolver.

6.3.2 Corrosion

The acceptably low corrosiveness of mercury and Cerrolow-117 (an alternate to mercury) at 260°C was determined by exposing coupons of tantalum to mercury and to Cerrolow-117 contained in sealed type 347 stainless steel capsules. After 500-hr exposure metallographic examination showed no

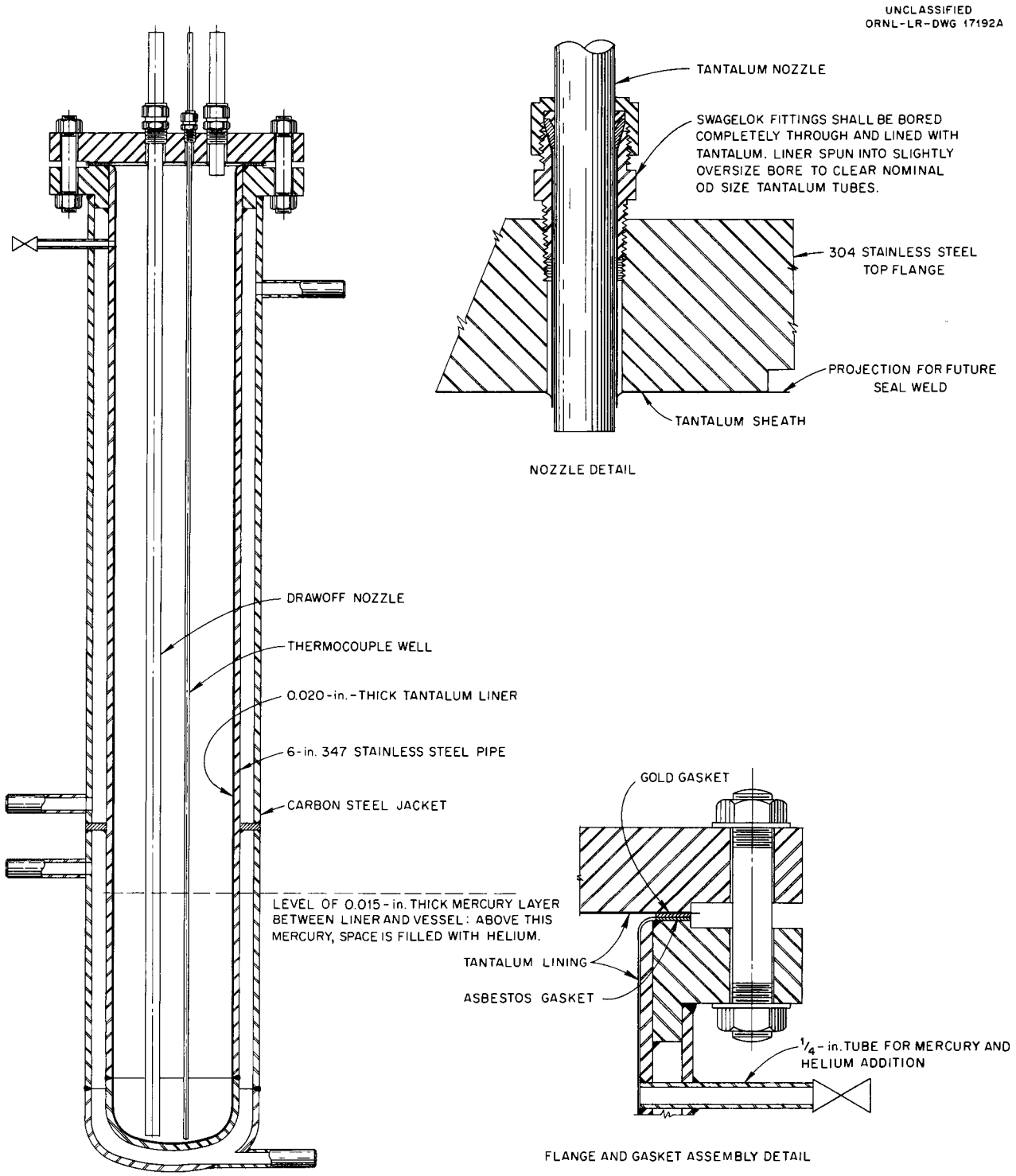

Fig. 6.1. Revised HRT-CP Tantalum Lined Dissolver.

change in the physical properties of either the tantalum or the type 347 stainless steel in either medium. The corrosion of the tantalum was less than 1 mpy. The corrosion of the type 347 stainless steel, perceptible in the liquid phase only, was fairly general. The deepest penetration was estimated to be about 1 mil, corresponding to a corrosion rate of less than 20 mpy.

The tantalum-lined-dissolver flange assembly with its leak-susceptible fitting connections could be replaced with a Carpenter-20 top flange with all-welded connections, provided that corrosion rates are low. A Carpenter-20 specimen inserted just below the top flange corroded at less than 0.1 mpy during the 126 hr of refluxing in the dissolution tests, indicating that Carpenter-20 is suitable for a top flange closure.

6.3.3 Dissolution Tests

A series of five tests in which simulated corrosion products were dissolved in sulfuric acid demonstrated that the procedures developed for this operation are satisfactory (Table 6.1).

Table 6.1. HRT-CP Dissolver Test Results

Run No.	Solids Charged (g)	Number of Cycles*	Excess Acid (%)	Dissolution** (%)
1	365	2	830	99.7
2	368	2	820	99.9
3	365	2	830	99.6
4	368	1	820	99.5
5	534	2	550	91.7

*One cycle consisted of a 4-hr reflux with 10.8 *M* H_2SO_4, dilution to 4 *M* H_2SO_4, and refluxing for four more hours.

**By undissolved-solids determination.

Dissolution was essentially complete in all except the last run, in which 50% more solids were charged, although in development runs this quantity of solids had been dissolved. The quantity normally collected from the reactor for dissolution probably will be 400 g or less.

6.3.4 H_2O-D_2O Separation Tests

Since the solids dissolution is to take place in a light-water medium following recovery of D_2O from the solids, it was imperative to establish that the dissolver could be routinely cycled from a heavy- to a light-water system without contamination of the heavy-water system. The arbitrary goal – no greater than 35 g of H_2O contamination per cycle, which would contaminate the entire D_2O inventory with 0.25% H_2O in one year's operation – was bettered in a three-cycle run. With an ~5% D_2O mixture in the heavy-water system, the dissolver was cycled three times from the D_2O to the H_2O system, with refluxing for 1 hr in each system. Samples withdrawn following each cycle were analyzed for D_2O content by both specific-gravity and mass-spectrographic techniques. Both methods could detect changes of approximately 0.1% in the D_2O content, corresponding to an H_2O pickup of about 15 g in the total system volume. The actual changes were so small that no trend could be established, and therefore the adequacy of the operating procedures was conclusively demonstrated.

6.4 COMPONENT TESTS

6.4.1 Decay-Tank Operation

Boildown of the decay tanks and transfer from the decay tanks to the transfer tank and thence outside the cell were performed without difficulty. Since 4 *M* H_2SO_4 freezes at a temperature below that at which the existing refrigeration system operates, piping revisions are required in the lines between the decay tanks and transfer tank to eliminate dependence on freeze plugs during transfer.

6.4.2 Fuel Charging

A pressurization system was installed for transferring D_2O from the meter tank to the high-pressure system, because air trapped in the drain lines caused the gravity transfer to be inconsistent. Tests with concentrated natural uranium demonstrated that at least 97% of the uranium charged reached the high-pressure system. The remaining 3% was held up in charging lines to be either drained to the dissolver or flushed to the high-pressure system in subsequent charges.

6.4.3 Recombiner Tests

The two types of recombiners installed in the low-pressure system were tested. The natural-convection-circulation (of O_2, no steam diluent)

recombiners on the decay tanks performed satisfactorily at all rates up to maximum expected production rates. Hydrogen concentrations were maintained at 1% or less in the decay-tank vapor space, indicative of complete recombination on each pass through the recombiner. The recombiners in the vapor lines, operated in superheated steam at about 135°C, were only 90 to 95% efficient.

6.4.4 Westinghouse Pump

The Westinghouse A-13-A-1 pump, prototype of the HRT-CP canned-rotor circulating pump, showed no significant wear after 3200 hr of operation in loop A, at the Unit Operations testing laboratory. About 2500 hr of this time was at 250 to 300°C, and 2900 hr was with 80-cycle a-c electrical supply. After inspection the thermal barrier of this pump was Heliarc-welded in place; the pump has since operated for more than 700 hr without incident.

6.5 TEST OF THE LOW-PRESSURE SYSTEM

As the final test of the low-pressure system, a complete operating cycle was performed, from the addition of solids to the high-pressure system, rinsing them, and draining them to the dissolver; through the dissolving procedure, transfer to a decay storage tank, and thence outside the cell. All procedures, except circulation of the solids and rinse water in the high-pressure system, were performed without incident.

While there was no apparent difficulty with plugging of lines during circulation, gas-binding of the pump made circulation difficult. Following this test, gas was easily cleared from the pump by first establishing circulation through the hydroclone-system low-pressure sampler. This procedure will be followed in the future.

6.6 HRT CHARCOAL BEDS

Calculations based on new data being obtained in the Solid State Division indicate that the HRT charcoal beds can have less than the specified capacities for adsorbing rare-gas fission products. For the amount of activity discharged to be kept below the 80 curies/day recommended as a maximum by the Health Physics Division, the flow rate per bed apparently cannot be allowed to exceed 284 cc/min at a 10-Mw power level or 318 cc/min at 5-Mw power level.

The stack discharge of activity at these flow rates could be substantially greater if there is short-circuiting within the charcoal bed. About 30 months after the shutdown of the HRE the concentrations of Y^{90}, Cs^{137}, and Sr^{89} and Sr^{90} were determined at various points in the charcoal beds. These concentrations were used as the basis for calculations of the performance of the HRE charcoal beds during operation.[2] It was concluded that considerable short-circuiting of the xenon and krypton isotopes occurred in both HRE charcoal beds and adversely affected the performance of the beds.

Recent laboratory experiments showed that such short-circuiting occurs in even carefully packed beds, and there is a high probability that some short-circuiting will occur in the HRT charcoal beds. If so, the actual allowable flow rates may be considerably below the values given above. The quantitative effect of short-circuiting is under laboratory study. The HRT charcoal beds will be given breakthrough tests to detect voids that would result in short-circuiting.

---

[2]H. O. Weeren, memo to R. Van Winkle, *Analysis of Performance Data from HRE Carbon Beds*, June 25, 1957.

Part II

REACTOR DESIGN AND ANALYSIS

J. A. Lane

7. HRE-3 DESIGN

W. R. Gall M. I. Lundin
J. C. Bolger E. A. Mason
R. O. Maak[1] R. C. Robertson
J. M. Trummel

7.1 THORIUM BREEDER REACTOR (HRE-3)

A preliminary high-pressure-system flowsheet and a table of preliminary parameters and major component sizes and capacity data for HRE-3 – a 60-Mw two-region solution-core thorium oxide blanket breeder reactor – are presented in Fig. 7.1 and Table 7.1, respectively.

One of the principal design objectives is minimization of letdown from the high-pressure system. By designing for letdown only as necessary for concentration control, it is possible to achieve reactor operation independent of the low-pressure system during normal reactor operation. In view of this objective, the initial studies were based on 100% internal recombination of D_2 and O_2 in both the core and the blanket, with production of condensate in the high-pressure system for purging of valves and pumps and for effecting minor adjustments in concentration. Alternative systems for removal of I^{135} and Xe^{135} from the high-pressure system are being evaluated.

The proposed oxygen pressurizing system is presented as part of the flowsheet, Fig. 7.1. The concentration of radiolytic deuterium in this system is maintained below 1% in the gas phase by contacting the vapor with the liquid phase, this liquid having been held up in the pressurizer system for sufficient time for the catalyst to recombine essentially all the dissolved deuterium. The copper sulfate catalyst will be maintained at concentrations approaching the estimated maximum which can be tolerated without affecting solution stability (~0.03 g-mole of copper per liter). The core and blanket systems operate on small side streams (~20 and 100 gpm for the core and blanket, respectively), each circulating through a pressurizer–surge tank, with the vapor in the upper region of the tank being continuously recirculated through a D_2O condenser. In the core system, vapor recirculation is effected by means of a jet eductor; in the blanket system, either by a blower as indicated in Fig. 7.1, or with a jet, should a slurry-operated eductor prove feasible.

Conceptual studies on reactor-vessel configuration were started. Examples of a cylindrical vessel and a spherical vessel are shown in Figs. 7.2 and 7.3, respectively. These examples assume approximately equal peak power densities at the core wall, although this is not necessarily a governing criterion. Cylindrical rather than spherical core tanks are being considered because they may permit the use of a smaller closure for the pressure vessel if a removable core arrangement is used. Other advantages that may be possible with a cylindrical shape are a slightly better breeding ratio, improved hydrodynamic behavior, and reduced corrosion due to lower power density at the core wall, achieved at the expense of reduced average power density and increased inventory. The influence of the core-vessel shape on the nuclear behavior has been investigated and is reported in Sec. 8.3. Because an estimated 70% of the blanket heat will be generated within 4 in. of the core-vessel wall, a Zircaloy baffle is used to channel the inlet slurry around the core vessel to assure well-developed flow and effective heat removal in that space. Concentric inlet and outlet piping for the fuel solution is provided to simplify the design and to facilitate replacement of the core tank. Sketches have been completed for the construction of small-scale Lucite models to observe the slurry flow behavior in two conceptual designs similar to those shown in Figs. 7.2 and 7.3.

[1] On loan from Foster Wheeler Corp.

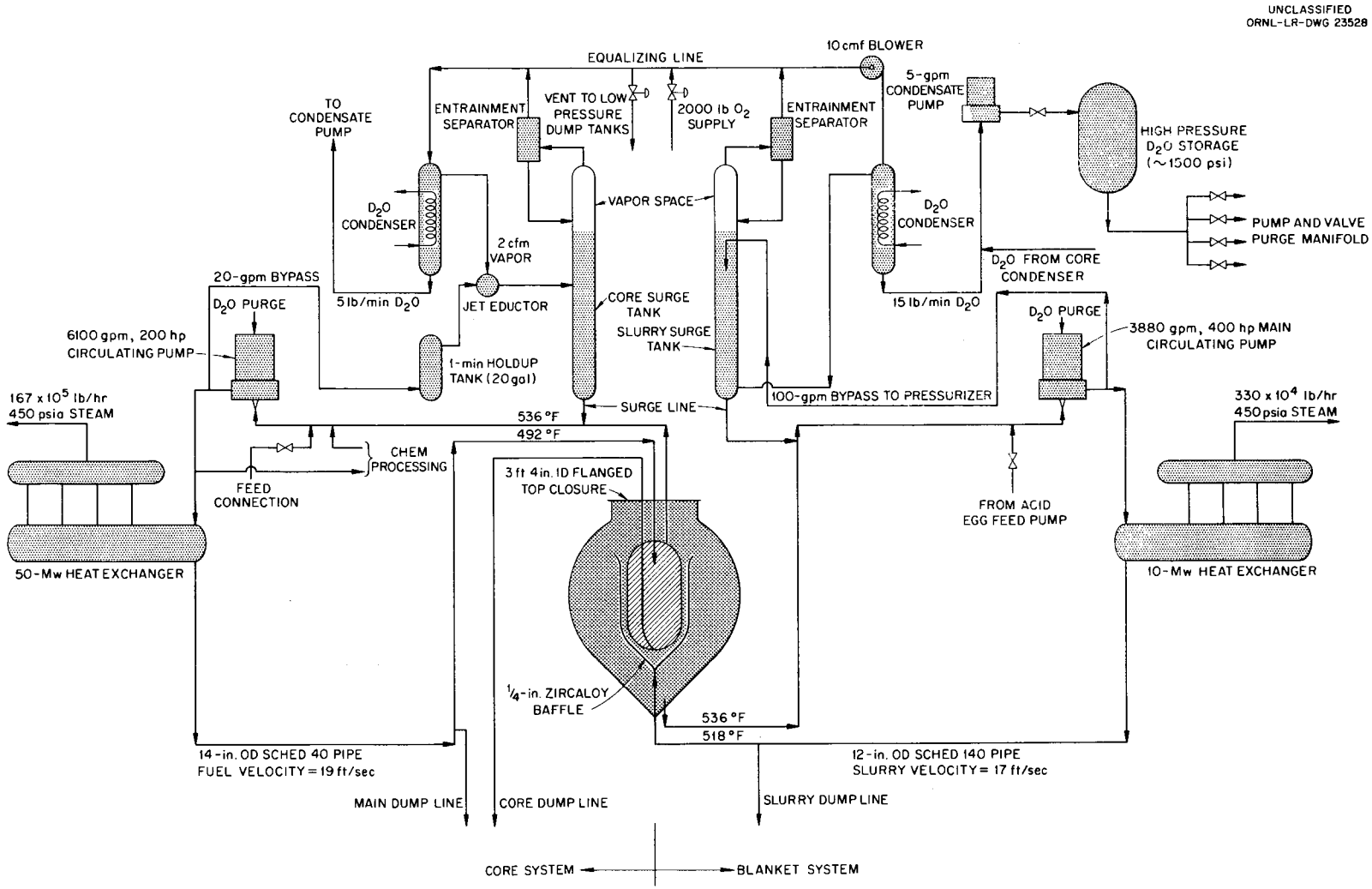

Fig. 7.1. High-Pressure-System Flowsheet – HRE-3.

Table 7.1 Preliminary HRE-3 Design Data

I. General Reactor Data	
1. Reactor	Two region
2. Design power level	
Core	50 Mw
Blanket	10 Mw
3. Core solution	UO_2SO_4-$CuSO_4$·D_2SO_4 in D_2O
4. Blanket composition	1000 g of thorium per liter in D_2O + 3 g of UO_2 (+ MoO_3) per liter
5. Normal operating pressure	1500 psia
6. Reactor dimensions	
Core-tank ID	4-ft sphere or 3-ft-dia × 6-ft cylinder
Pressure-vessel ID	9-ft sphere or 8-ft cylinder (exclusive of thermal shield)
Core-tank thickness	½-in. Zircaloy-2
Core type	Concentric inlet and outlet
Pressure-vessel wall	Type 347 stainless-steel-clad carbon steel
Thermal shield	Requirement undetermined
7. Core volume (approx)	950 liters
Blanket volume (approx)	9600 liters
8. Average power densities (at 60 Mw)	
Core	52.6 kw/liter
Blanket	1.04 kw/liter
9. Power density at Zircaloy wall	23 kw/liter[a]
Estimated corrosion rate	27 mpy[a]
10. Estimated breeding ratio (At equilibrium U^{233} and higher isotopes, with 7% fission-product poisoning. Assumed $\eta^{233} = 2.25$)	1.09
II. Core Data	
1. Critical concentration in core (T_{av} = 270°C), Equilibrium (U^{233} + U^{235})	4.3 g/liter
2. Operating temperatures	
Core power	50 Mw (design)

Table 7.1 (continued)

Inlet temperature	250°C (482°F) design, 240°C (464°F) min
Outlet temperature	280°C (536°F) design, 300°C (572°F) max
Core ΔT	30°C (54°F)
3. Fuel circulation rate	2.547×10^6 lb/hr
	6100 gpm (at pump)
4. Physical properties of fuel solution	
Heat capacity (average from 494–572°F)	1.24 Btu/lb·°F
Density	
At 70°F	69.9 lb/ft^3
At 572°F	50.6 lb/ft^3
At 494°F	55.9 lb/ft^3
Thermal conductivity	
At 70°F	0.35 Btu/hr·ft·°F
At 536°F	0.32 Btu/hr·ft·°F
Viscosity	
At 70°F	3.06 lb/hr/ft
At 572°F	0.24 lb/hr/ft
At 494°F	0.29 lb/hr/ft
5. Decomposition rate of D_2O	1.67 molecules of D_2 per 100 ev
6. Catalyst concentration for 100% internal recombination	0.0181 g-moles of Cu^{++} per liter
7. Fuel heat exchanger	
Heat load	1.707×10^8 Btu/hr
Inlet temperature	536°F
Outlet temperature	482°F
Steam temperature	457°F
Steam pressure	450 psia
Log mean ΔT	47°F
Steam generation rate	1.67×10^5 lb/hr
Estimated total pressure drop across exchanger	18 psi
Velocity of fuel in tubes	12 fps
8. Main fuel loop and components	
Estimated liquid volume of high-pressure fuel system	4000 liters

Table 7.1 (continued)

Design pressure	2000 psi
Design temperature	600°F
Pipe material	347 stainless steel
Size	14 in. IPS, sched 140
Inside diameter and flow area	11.50 in., 0.722 ft^2
Fluid velocity (in 14-in.-OD pipe)	19.4 fps
Pressure drop per 100 ft of 14-in. pipe	2.76 psia
Core pumping requirements	One 6100-gpm pump (536°F)
Estimated total loop pressure drop	35 psia (100 ft of head)
Pump shaft power (hydraulic efficiency = 75%)	167 hp
III. Blanket Data	
1. Slurry composition	1000 g of thorium per liter + UO_2 in D_2O
2. Uranium concentration required (for 10-Mw operation)	3 g of U^{233} per liter
3. Blanket operating temperature	
Power level	10 Mw (design)
Inlet	270°C (518°F) design, 240°C min
Outlet	280°C (536°F) design, 300°C (572°F) max
Blanket ΔT	10°C (18°F)
4. Blanket flow rate	3.69×10^6 lb/hr
5. Physical properties at 270°C (estimated)	
Density[b]	119 lb/ft^3
Specific heat[b]	0.515 Btu/lb·°F
Thermal conductivity[b]	0.444 Btu/ft·hr·°F
τ_y = yield stress[c]	0.5 lb/ft^2
η = coefficient of rigidity[c]	24.2 lb/hr·ft (10 centipoises)
6. Blanket heat exchanger	
Blanket power	10 Mw
Heat load	3.414×10^7 Btu/hr
Inlet temperature	536°F (280°C)
Outlet temperature	518°F (270°C)
Steam temperature	457°F

Table 7.1 (continued)

Steam pressure	450 psia
Log mean ΔT	68.6°F
Steam generation rate	3.33×10^4 lb/hr
Pressure drop across exchanger	60 psia
Velocity of slurry in tubes	15 fps
7. Blanket loop and components	
Total flow rate through blanket	3880 gpm
Estimated total pressure drop	90 psia
Pump shaft power (hydraulic efficiency = 75%)	275 hp
Pipe material	347 stainless steel
Size	12 in. IPS, sched 140
Inside diameter and flow area	10.500 in., 0.602 ft^2
Slurry velocity in main piping	15.2 fps
Pressure drop per 100 ft of pipe	9.5 psi
Design pressure	2000 psia
Design temperature	600°F

[a] If a 5-ft-ID core vessel is used, power density at the wall is 10 kw/liter, with estimated corrosion rate of 18 mpy.
[b] P. N. Haubenreich, *Some Properties of ThO_2-D_2O Slurries*, TBR, Memo No. 10, ORNL CF-55-2-51 (Feb. 10, 1955).
[c] Assumed for design purposes.

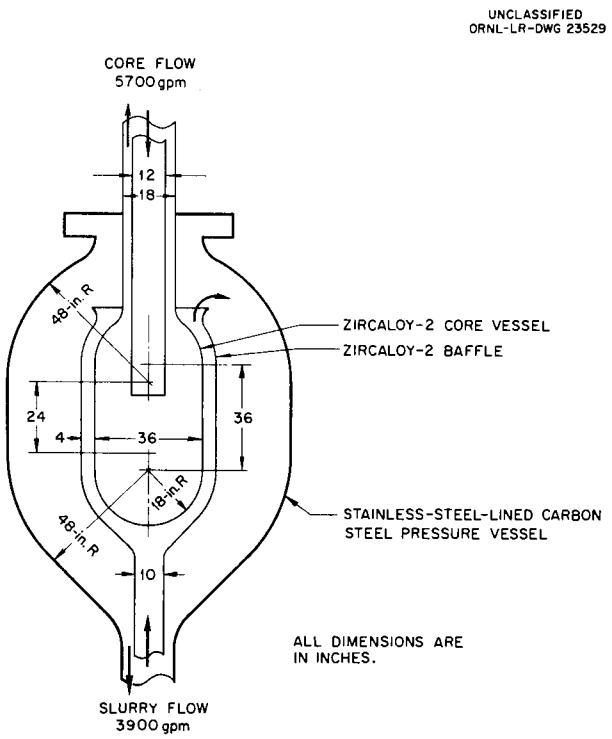

Fig. 7.2. Concept of Cylindrical Core – HRE-3.

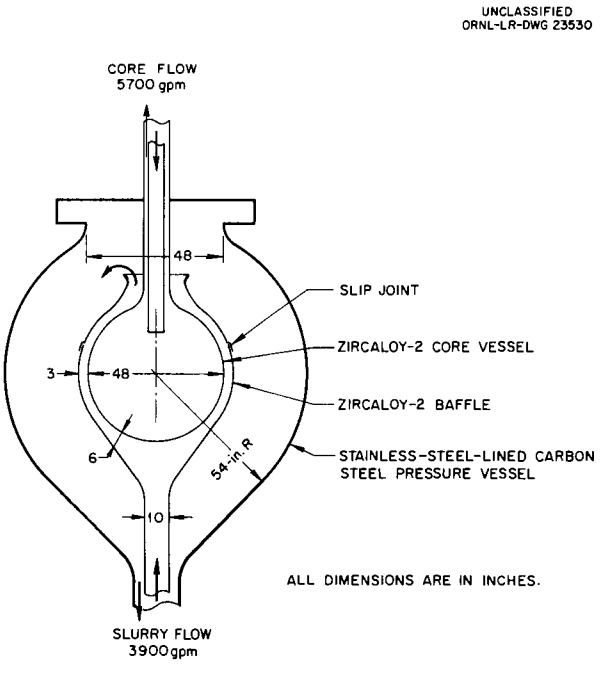

Fig. 7.3. Concept of Spherical Core – HRE-3.

8. REACTOR ANALYSIS

P. R. Kasten

T. B. Fowler C. W. Nestor, Jr.
M. P. Lietzke M. W. Rosenthal
M. Tobias

8.1 EQUILIBRIUM STUDIES FOR HRE-3

Nuclear computations were performed[1] to determine the effects of various design parameters on the characteristics of spherical reactors in the size range likely for HRE-3. In these calculations the conventional two-group model was used to estimate the critical concentration and flux distribution. While useful for survey calculations, this model possibly does not yield very accurate critical concentrations and breeding ratios, particularly for small core sizes (see Sec. 8.2). The following conditions were also specified:

1. The reactor system is at equilibrium with regard to nuclei concentrations.
2. Hydroclone separation of poisons from the core system is employed in addition to Thorex processing.
3. The core Thorex cycle time is a dependent function of the specified total poison fraction; the blanket cycle time is a function of the blanket U^{233} concentration.
4. The poison fraction due to samarium is 0.8%; that due to xenon is 1%.
5. The external core system has 1.0 liter of volume for every 20 kw of core power; the blanket external system has 1.0 liter for every 14 kw of blanket power.
6. The average core and blanket temperatures are 280°C.

Although steady-state conditions were assumed, many years of operation would be required before these conditions would be approached. As a result, the breeding gains given here are lower than would occur in a reactor started "clean," particularly during the first several years.

8.1.1 Breeding Ratio

The breeding ratio (BR) is a quantitative measure of the efficiency of a reactor as a fuel producer and is defined as follows:

$$(1) \qquad BR = \frac{\text{rate of fuel generation}}{\text{rate of fuel consumption}} .$$

The breeding ratio is plotted in Fig. 8.1 as a function of pressure-vessel size for 4- and 5-ft-dia cores with several blanket thorium concentrations. In Fig. 8.2 the effect of core poison fraction on breeding ratio is shown. More extensive results, including neutron balances, are given in Table 8.1 for selected reactors. The neutron balances are normalized to 100 absorptions in U^{233} and U^{235}; therefore the numerical values represent approximately the percentage effects of the various items on the breeding ratio (however, the effect of Pa^{233} losses on breeding ratio would be obtained by doubling the values given).

(a) Reactor Size. – As shown in Fig. 8.1, for a pressure vessel with a given diameter the 4-ft-dia core has a higher breeding ratio than the 5-ft core. Comparison of the neutron balances in Table 8.1 for these two core sizes reveals the higher breeding ratio to be a result of lower neutron absorptions in the core moderator and core vessel and of lower neutron leakage.

(b) Fission-Product Poisons. – The effect of total core poison fraction, f_{pc} (ratio of absorption cross section of poisons to fission cross section of fuel), on breeding ratio is shown in Fig. 8.2. The results indicate that the change in breeding ratio with change in poison fraction can be estimated from the relation

$$(2) \qquad \Delta BR = -0.75\, \Delta f_{pc} .$$

Achievement of a xenon poison fraction of 0.01, as postulated in the computations for Fig. 8.1 and Table 8.1, requires the removal of most of the xenon or its iodine precursor before neutron capture occurs. If there is no fast-cycle system for iodine or xenon removal, the poison fraction resulting from xenon will be about 0.05. According to Eq. 2, the breeding ratio would be reduced by about 0.03 below the values given in Fig. 8.1 if all the xenon were retained in the core system.

[1] M. W. Rosenthal and T. B. Fowler, *Nuclear Computations for HRE-3 Design: Equilibrium Results*, ORNL CF-57-7-23 (July 10, 1957).

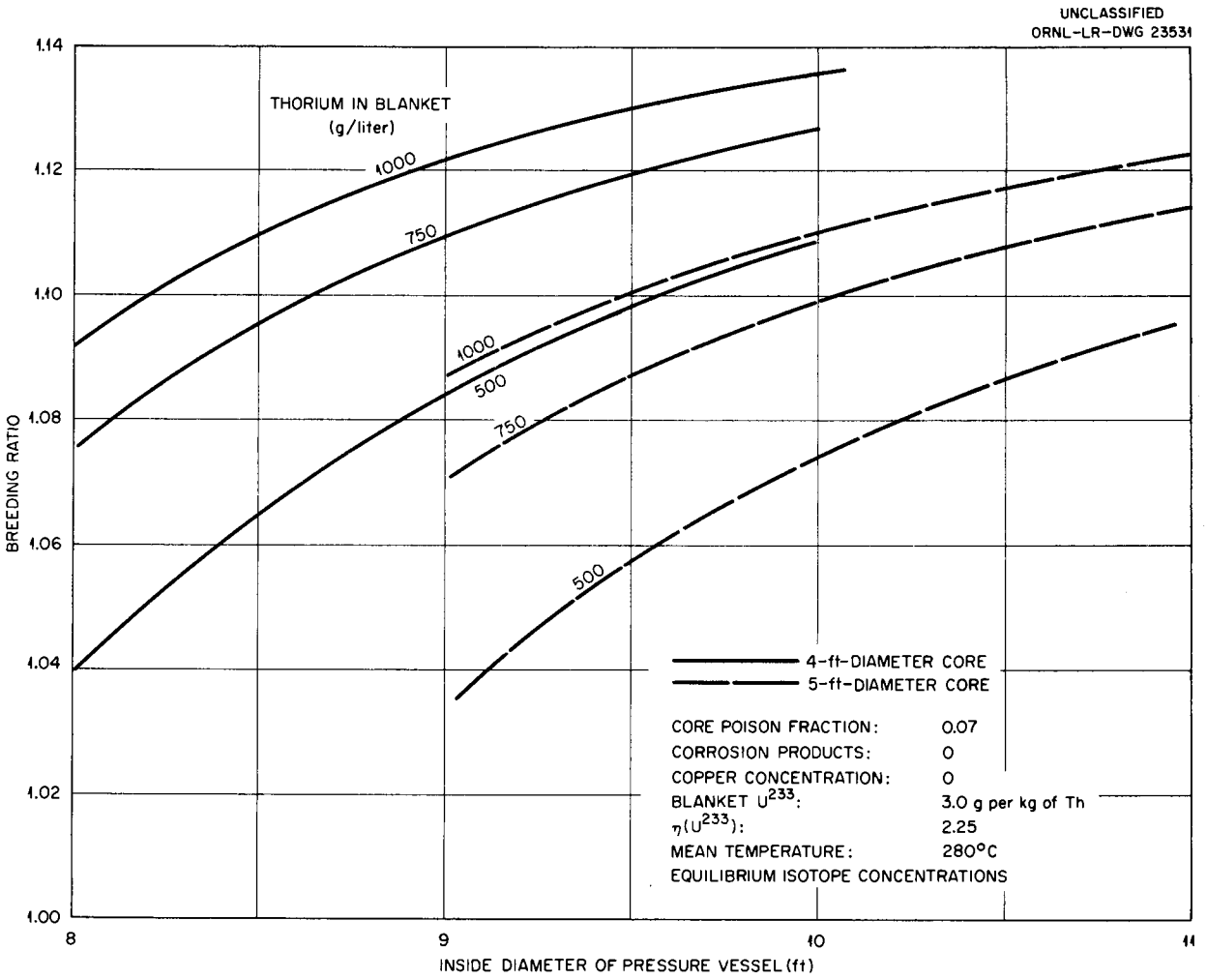

Fig. 8.1. Breeding Ratio as a Function of Pressure-Vessel Size for Various Core Diameters and Blanket Thorium Concentrations.

(c) Core-Tank Absorptions. – The thickness of the Zircaloy core tank was taken as 0.42 in. for the 5-ft core and 0.33 in. for the 4-ft vessel. With these thicknesses, as shown in Table 8.1, neutron captures in zirconium reduce the breeding ratio about 0.02 in the 4-ft core and 0.03 in the 5-ft core. If the core-tank thickness were altered, the losses would be changed proportionately.

(d) Absorptions in Copper. – No allowance for neutron absorptions in the copper recombination catalyst was made in the computations. The poison fraction attributable to copper in various concentrations and the effects on breeding ratio (ΔBR) are given below:

Core Diameter (ft)	Copper Concentration (M)	Poison Fraction	ΔBR
4	0.01	0.004	−0.003
5	0.01	0.008	−0.006

For other copper concentrations the poisoning effects would be proportionate to the values shown above.

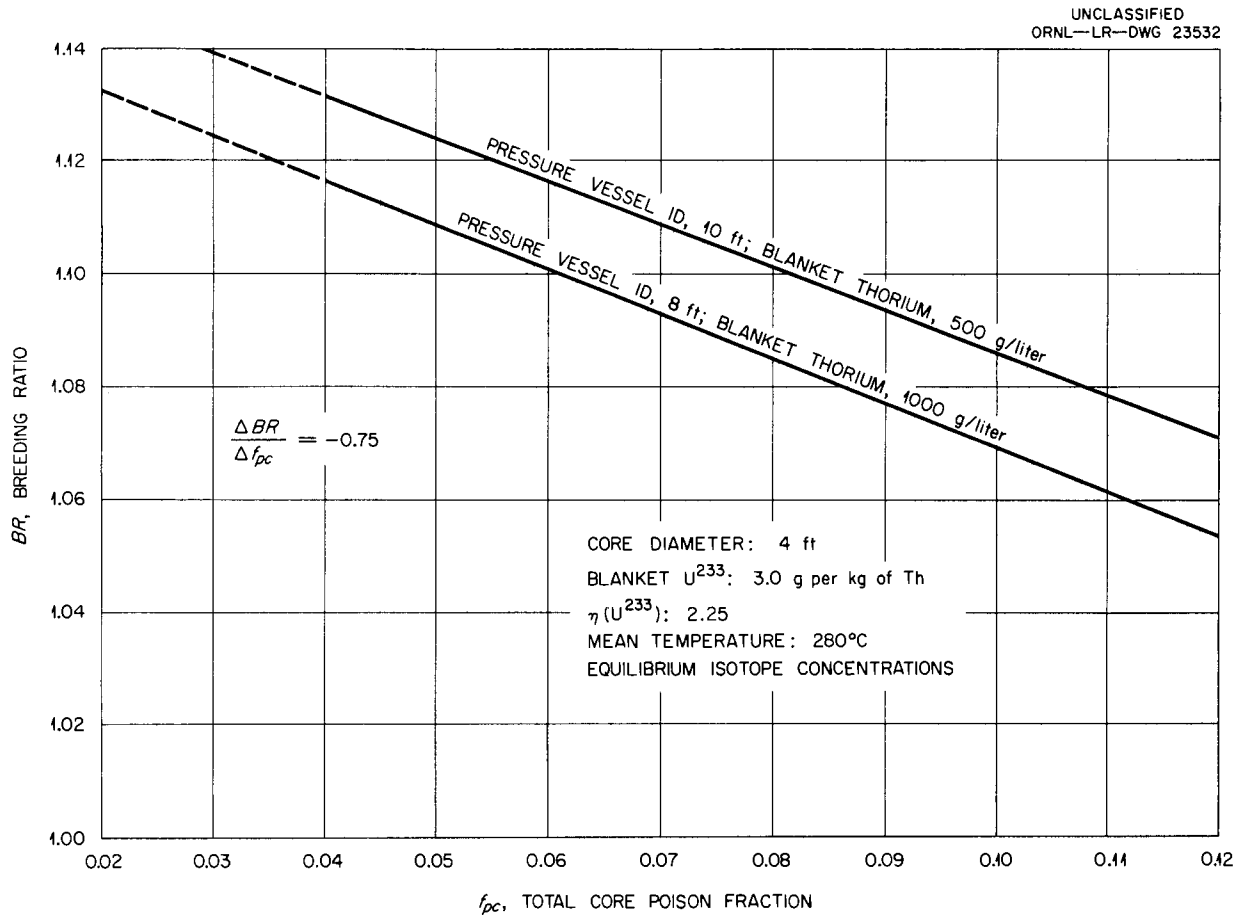

Fig. 8.2. Effect of Core Poison Fraction on Breeding Ratio.

Table 8.1. Characteristics of Selected Reactors (Equilibrium Conditions)

Core diameter, ft	4	4	4	4	5
Pressure vessel ID, ft	8	8	9	9	9
Blanket thorium, g/liter	500	1000	500	1000	1000
Blanket U^{233}, g/kg Th	3.0	3.0	3.0	3.0	3.0
Core poison fraction	0.07	0.07	0.07	0.07	0.07
Concentration of U^{233}, g/liter	3.68	4.04	3.63	4.02	2.19
Concentration of U^{235}, g/liter	0.41	0.39	0.37	0.37	0.21
Breeding ratio	1.041	1.094	1.086	1.123	1.089
Core-wall power density (inside), kw/liter	27	23	27	23	10
Core-wall power density (outside), kw/liter	9	14	9	14	11

Table 8.1 (continued)

Core cycle time, days	833	901	817	893	616
Blanket cycle time, days	220	371	288	504	486
Core inventory of U^{233} and U^{235}, kg	14.4	15.7	14.0	15.5	10.6
Blanket inventory of U^{233} and U^{235}, kg	11.0	21.9	15.9	31.6	28.9
Net U^{233} and U^{235} production, g/day	2.5	5.8	5.3	7.5	5.4
Generation time, days	220	230	210	220	160
Doubling time, days	5760	2710	2640	2050	1950
Core-system volume, liters	3520	3540	3500	3530	4420
Blanket-system volume, liters	7320	7290	10,580	10,520	9610
Mean thermal flux in core system, neutrons/cm^2/sec	1.3×10^{14}	1.3×10^{14}	1.4×10^{14}	1.3×10^{14}	1.8×10^{14}
Core power, Mw (heat)	51.5	51.9	51.0	51.7	51.2
Blanket power, Mw (heat)	10.0	9.6	10.5	9.9	10.3
Absorptions and leakages per 100 absorptions in fuel					
Absorptions in core by:					
U^{233}	74.7	76.4	74.6	76.4	75.3
U^{234}	9.2	8.2	8.4	7.8	8.2
U^{235}	9.1	8.1	8.3	7.6	8.0
U^{236}	0.7	0.4	0.4	0.3	0.4
Poisons	5.2	5.3	5.2	5.3	5.2
Heavy water	0.9	0.8	0.9	0.8	1.6
Absorptions in core tank	2.1	1.6	2.1	1.6	2.4
Absorptions in blanket by:					
U^{233}	16.2	15.5	17.1	16.0	16.0
U^{234}, U^{235}, U^{236}	0.1	0.1	0.1	0.1	0.1
Th	95.8	101.7	100.9	104.8	101.0
Pa^{233}	0.9	0.5	0.7	0.4	0.4
Poisons	0.4	0.4	0.4	0.4	0.4
Heavy water	0.5	0.2	0.5	0.2	0.2
Fast leakage	4.3	3.6	2.2	1.6	3.0
Slow leakage	3.4	0.9	1.7	0.4	0.8

The copper concentration required for 100% recombination in a 4-ft core at 60 Mw has been estimated to be 0.018 *M*. For this core size and copper concentration, the loss of neutrons to copper would reduce the breeding ratio by 0.005.

(e) H_2O Contamination. – Any H_2O contained in the heavy-water moderator will act as a poison and reduce the breeding ratio. The foregoing results are based on the use of heavy water containing 0.25% H_2O. Neutron captures in the moderator in a 4-ft core reactor (see Table 8.1) were found to be about 0.009 per absorption in fuel, of which about 60% were in H_2. Thus, 0.25% H_2O, which is 9 liters in a 3600-liter system, reduced the breeding ratio by 0.005. Other values are given below:

Core Diameter (ft)	H_2O Concentration (%)	ΔBR
4	1.0 (36 liters)	−0.02
5	1.0 (44 liters)	−0.04

Different concentrations of H_2O would cause changes in breeding ratio proportionate to the values given above.

A specified volume of H_2O added to the blanket has much less effect on breeding ratio than the same amount added to the core. This is a result of both the lower flux in the blanket region and the larger volume of the system.

(f) Corrosion Products. – Assuming the surface area of stainless steel in the core high-pressure system to be 6000 ft^2, corrosion to an average depth of 0.001 in. would remove 250 lb of metal. If this were distributed uniformly throughout the fuel solution, the poison fraction resulting from it would be about 0.18 in a 4-ft core and 0.36 in a 5-ft core. However, iron and chromium would precipitate and be removed by hydroclones. If the hydroclones were operated on a fast cycle time (several days), neutron capture in iron and chromium would be unimportant. Nevertheless, the absorption cross sections of the nickel and manganese (which probably remain in solution) amount to about 15 and 9%, respectively, of the total absorption cross section of type 347 stainless steel. Thus, from 0.001 in. of corrosion, the nickel and manganese would yield a poison fraction of about 0.04 (ΔBR = 0.03) in a 4-ft core and 0.08 (ΔBR = 0.06) in a 5-ft core.

The actual value of the poison fraction from corrosion products would depend on the corrosion rate and the chemical processing rate. If the corrosion products are assumed to change to isotopes of the same cross section upon neutron capture, the following relations are obtained under equilibrium conditions:

$$(3)\quad f_p = 0.04 \times R \times (T_c/365) \qquad \text{(core ID = 4 ft)} ;$$

$$(4)\quad f_p = 0.08 \times R \times (T_c/365) \qquad \text{(core ID = 5 ft)} .$$

In Eqs. 3 and 4, f_p is the equilibrium core poison fraction from corrosion products, R the mean corrosion rate in mils per year, and T_c the core cycle time in days.

An additional point of concern resulting from corrosion of stainless steel is the adverse effect of high corrosion-product concentrations on the stability of fuel solution. The concentration of nickel resulting from 0.001 in. of corrosion would be 0.052 *M*; that of manganese would be 0.011 *M*. Unless adjustments were made to the acid concentration, there would probably be formation of a second phase before the above concentration of nickel were attained.

The corrosion products from the Zircaloy core vessel would not appreciably affect the breeding ratio, even if they remained in suspension. Due to the dilution effect associated with the large volume external to the core region, corrosion of the Zircaloy would result in a slight increase in the breeding ratio.

8.1.2 Generation and Doubling Times

The gross rates of fuel generation in the blanket, G, can be estimated by use of the equations below (based on 185 Mev/fission):

$$(5)\quad G = 1.25 \times P_t \times BR \qquad (U^{233} \text{ fuel}) ;$$

$$(6)\quad G = 1.34 \times P_t \times BR \qquad (U^{235} \text{ fuel}) .$$

The generation rate, G, is in grams of U^{233} per day; P_t is the total reactor power in megawatts; and BR is the breeding ratio. The net generation rate in the blanket would be obtained by subtracting the rate at which uranium is consumed in the blanket. For convenience, the generation time of a two-region reactor is defined here as the time required to accumulate an amount of material in the blanket equal to the core-system inventory. This does not at all represent a net production of fuel, since approximately one core inventory would

be consumed in the process. The generation time of the HRE-3 with a 4-ft core would be about 220 days and with a 5-ft core would be about 150 days.

The time required for a breeding demonstration is dependent on the concentration of U^{233} to be attained in the blanket. The times given in Table 8.2 are estimates of the periods required for the U^{233} plus Pa^{233} concentration in the blanket to reach 1 g per kilogram of thorium.

The doubling time, as defined here and as given in Table 8.1, is the period required for the production of a net excess of fuel equal to the core inventory. This time is dependent on the breeding *gain* ($BR - 1.0$), rather than the breeding ratio, and hence varies considerably with the reactor design, ranging from 1400 to 5800 days for the reactors considered.

8.1.3 Core-Wall Power Density

Some values of the power density in the fuel solution at the inside and outside surfaces of the core vessel are given in Table 8.1. For a 4-ft core vessel with 3.0 g of U^{233} per kilogram of thorium in the blanket, the inside core-wall power density would be between 22 and 27 kw/liter; for a 5-ft vessel the range would be 9 to 12 kw/liter. The core-wall power density would be about 15% higher if there were no uranium in the blanket and if the reactor were operated at the same total power.

8.2 COMPARISON OF RESULTS FROM MULTIGROUP AND TWO-GROUP CALCULATIONS

To obtain a comparison of calculational methods, breeding ratios and critical fuel concentrations were obtained for three two-region, D_2O-moderated thorium-blanket breeder reactors by using the Eyewash multigroup, multiregion UNIVAC program[2] and the two-group, two-region Oracle program.[3]

The following characteristics were considered common to all reactors:

1. The cores contained U^{233} and D_2O, with absorptions occurring only in U^{233}.
2. The blankets contained ThO_2 and D_2O, with absorptions occurring only in Th^{232}.
3. A 1-in.-thick zirconium tank separated the core from the blanket.
4. A 6-in.-thick iron pressure vessel contained the reactor.

Microscopic absorption and fission cross sections for U^{233} and Th^{232} were obtained from the Hughes and Harvey and the Hughes and Schwartz compilations of neutron cross sections;[4] a value of 2.52

[2] J. H. Alexander and N. D. Given, *A Machine Multigroup Calculation. The Eyewash Program for UNIVAC*, ORNL-1925 (Sept. 6, 1955).

[3] T. B. Fowler, *Oracle Code for a General Two-Region, Two-Group Spherical Homogeneous Reactor Calculation*, ORNL CF-55-9-133 (Sept. 22, 1955).

[4] D. J. Hughes and J. A. Harvey, *Neutron Cross Sections*, BNL-325 (July 1, 1955) and D. J. Hughes and R. B. Schwartz, *Neutron Cross Sections, Supplement No. 1 to BNL-325* (Jan. 1, 1957).

Table 8.2. Time Required to Attain 1 g (U^{233} + Pa^{233}) per Kilogram of Thorium

Core ID (ft)	Pressure Vessel ID (ft)	Blanket Thorium (g/liter)	Production Time (days)
4	8	500	60
	9	500	80
	10	500	110
5	9	500	70
	10	500	100
4	8	1000	110
	9	1000	150
	10	1000	210
5	9	1000	140
	10	1000	200

was taken for ν^{23}. Data presently on the Eyewash tapes were used for deuterium, oxygen, and zirconium. The thermal cross sections were evaluated at 250°C. The two-group parameters, τ, D_1, and p, given in Table 8.3 were computed from the multigroup cross sections by numerical integration.[5]

In the two-group, two-region calculations a "thin-shell" approximation[6] was used to estimate core-tank absorptions, while the effect of the pressure vessel was simulated by adding an extrapolation distance to the blanket thickness. Basic data for the two-group calculations are listed in Table 8.3.

Preliminary results of the calculations are given in Table 8.4. The fast effect, ϵ, is defined as the ratio of total fissions to thermal fissions, and the quantity η_R/η_T is the ratio of the number of fission neutrons produced per neutron absorbed in fuel material averaged over all the fast groups to the number of fission neutrons produced per thermal neutron absorbed in fuel material. The values obtained for η_R/η_T are significantly lower than those commonly used.

The two-group calculation takes no account of epithermal fissions or captures in fuel material. Because of this the two-group calculation predicts breeding ratios about 5% higher than does the multigroup calculation.

8.3 NUCLEAR CHARACTERISTICS OF SPHERICAL AND CYLINDRICAL HRE-3 REACTORS

Some calculations were made to compare the nuclear characteristics of two-region cylindrical thorium breeder reactors with those of spherical reactors in the range of HRE-3 power and dimensions. The core volume was considered to be the same for the two geometries. It may be possible to obtain improved breeding gains with a cylindrical geometry since a higher critical concentration is required and competition by parasitic captures is

[5] M. Tobias, *An Oracle Code for Calculation of Fermi Ages by Numerical Integration*, ORNL CF-56-4-53 (April 10, 1956).

[6] M. Tobias, *A "Thin-Shell" Approximation for Two-Group, Two-Region Spherical Reactor Calculations*, ORNL CF-54-6-135 (June 16, 1954).

Table 8.3. Values for Two-Group Parameters in D_2O-ThO_2 Mixtures

Thorium Concentration (g/liter)	Fermi Age, τ (cm^2)	Fast Diffusion Constant, D_1 (cm)	Slow Diffusion Constant, D_2 (cm)	Resonance Escape Probability, p	Thermal Absorption Cross Section, Σ_a^T (cm^{-1})
0	183.9	1.567	1.222	1.000	0
500	175.1	1.506	1.181	0.6021	7.334×10^{-3}
1000	185.7	1.436	1.132	0.3467	1.467×10^{-2}

Table 8.4. Comparison of Multigroup and Two-Group Results

Core Diameter (ft)	Pressure-Vessel Diameter (ft)	Blanket Thorium (g/liter)	Breeding Ratio		Critical Fuel Concentration (g/liter)		ϵ	$\frac{\eta_R}{\eta_T}$
			$2G - 2R$	Eyewash	$2G - 2R$	Eyewash		
4	9	500	1.16	1.10	2.28	2.34	1.090	0.7927
4	9	1000	1.20	1.14	2.45	2.58	1.100	0.7924
5	9	500	1.13	1.08	1.38	1.37	1.051	0.7974

thereby reduced; however, the maximum wall power density was lower for the spherical reactors. By increasing the length of the cylindrical reactors, it would be possible to obtain maximum wall power densities lower than those in spherical reactors of the same core diameter.

The properties of the reactors studied and the results obtained are presented in Table 8.5. The cores were assumed to contain 7% poisons; the protactinium level in the blanket was approximately that at equilibrium. The core wall was ½-in. zirconium. In all cases the blankets contained 3 g of U^{233} per liter and 1000 g of ThO_2 per liter in heavy water. The core fuel was U^{233} in heavy water. Except for the poison and protactinium mentioned, the reactors were "clean."

The two-group, two-region model used to obtain the results for the cylindrical reactors did not account for axial reflection; however, the effects that an end reflector would have on neutron leakage were estimated and are included in the results.

The breeding ratio obtained for the cylindrical reactors was on a par with those for the spherical reactors. The required fuel concentrations were higher, as expected, so that the average flux was lower for the cylindrical geometry. Although the maximum core-wall power density decreased with increasing cylinder diameter, it was always higher than the wall power density obtained for the spherical reactors of equal volume.

8.4 MATHEMATICS AND COMPUTATION

An Oracle code was completed for calculating the two-group nuclear characteristics of two-region, time-dependent, thorium breeder reactors, considering the buildup of U^{233}, U^{234}, U^{235},

Table 8.5. Nuclear Characteristics of Some Spherical and Cylindrical Thorium Breeder Reactors*

		Spherical Reactors		Cylindrical Reactors		
Core diameter, ft		4	4	2½	3	3½
Pressure-vessel diameter, ft		8	9	6½	7	7½
Pressure-vessel height, ft				10.8	8.8	7.5
Core height, ft				6.8	4.8	3.5
Breeding ratio		1.11	1.13	1.12	1.11	1.09
Critical concentration, g of U^{233} per liter		3.6	3.6	6.5	4.7	4.1
Core power, Mw		49	49	51	52	53
Maximum core-wall power density, kw/liter		22	22	36	29	27
Neutron balance (absorptions per absorption in U^{233})						
Core:	U^{233}	0.824	0.821	0.834	0.828	0.828
	Poison	0.052	0.052	0.052	0.052	0.052
	Heavy water	0.010	0.010	0.006	0.008	0.009
Core tank		0.028	0.028	0.024	0.028	0.030
Blanket:	U^{233}	0.175	0.178	0.166	0.172	0.172
	Heavy water	0.003	0.003	0.002	0.003	0.003
	Protactinium	0.004	0.004	0.004	0.004	0.004
	Thorium, thermal	0.753	0.766	0.712	0.739	0.740
	Thorium, resonance	0.358	0.370	0.416	0.376	0.351
Leakages:	Fast	0.036	0.016	0.026	0.030	0.045
	Slow	0.009	0.004	0.007	0.009	0.016

*Total power, 60 Mw; core volume, 949 liters; core poison fraction, 7%; blanket thorium concentration, 1000 g/liter; blanket U^{233} concentration, 3 g/liter.

U^{236}, Pa^{233}, and fission-product poisons with respect to time. Breeding ratio, as a function of time, is also computed. The calculation considers either a slurry or a solution core, startup with either U^{233} or U^{235}, and chemical processing for core and/or blanket beginning at times which depend upon core poison level (for core processing) and blanket U^{233} concentration (for blanket processing). The variable parameters include reactor power level (total or core), reactor diameter (core and over-all), thorium concentration (core and blanket), and nuclear values.

Two output routines were prepared for use with the two-group *N*-region Oracle code.[7] The first routine computes and punches on paper tape the fluxes and power densities for a given total reactor power output; the second routine assembles and punches on paper tape the normalized fluxes at each interface, the critical fuel cross section, and the total absorptions in reactor fuel materials.

An extension of the Bessel-function subroutine for the Oracle was completed. This permits evaluation of $Y_0(x)$ and $Y_1(x)$, the zero- and first-order Bessel functions of the second kind.

[7] C. W. Nestor, Jr., *Two-Group Analysis of Thermal, One-Dimensional, Multi-Region Spherical Reactors*, ORNL CF-57-5-14 (May 1, 1957); *Two-Group Analysis of Multi-Region Reactors. Part II. Construction and Use of Oracle Code*, ORNL CF-57-5-49 (May 14, 1957).

Part III

ENGINEERING DEVELOPMENT

J. A. Lane

9. DEVELOPMENT OF FUEL-SYSTEM COMPONENTS

I. Spiewak

J. M. Baker
R. Blumberg
J. S. Culver
B. D. Draper
C. H. Gabbard
P. G. Herndon
E. C. Hise
P. P. Holz
J. C. Moyers
I. K. Namba

9.1 20-cfm CANNED-MOTOR BLOWER

The 20-cfm canned-motor blower was operated for 1462 hr while circulating cold air at atmospheric pressure with water as the bearing fluid. This run will be the basis for comparison of bearing wear when ThO_2 slurry is used as the bearing fluid. No measurable bearing wear was noted following the water run. Final preparation of the loop and blower for a long-term run with ThO_2 slurry as the bearing fluid is being completed.

9.2 4000-gpm LOOP

Repair of the Byron Jackson 4000-gpm pump was completed. This included the replacement of the stator liner and the stator expansion bellows, and the machining of labyrinth grooves in one member of each pair of stainless steel wear rings. Modifications were made to the pump cooling-water system to aid in taking material and heat balances. It is planned to study mixing across the shaft seal and thermal barrier of the pump with varying purge flows.

9.3 OXYGEN COMPRESSORS

The diaphragm oxygen compressor manufactured by Pressure Products Industries was returned to the manufacturer for modifications to eliminate the problems of water leakage into the crankcase, gas binding on the water side, and cracking of the diaphragm at the O-ring seal.

A portion of the compressor manufactured by Harwood Corporation was returned to the manufacturer for revision. This machine has not operated satisfactorily to date.

9.4 10-gpm FEED PUMPS

A multipump test facility is being fabricated and is 75% complete. It contains all piping, valves, and instruments necessary for testing up to six 10-gpm feed pumps simultaneously. Pumps will be connected by flanged suction and discharge lines and plug-in electrical receptacles.

A triplex power end and variable-speed drive capable of driving 10-gpm-pump components was ordered. It will be used to test larger displacement diaphragm heads and also piston or plunger pumps if adequate seals can be procured.

A double-diaphragm pump head was designed and will be fabricated for testing on the multipump loop. This unit has twice the displacement of present diaphragm heads, but by using higher speeds and more of the available stroke it is planned to develop 3.3 gpm per head.

A single-stage Roth turbine pump rated at 14 gpm at 340 psi was ordered. A loop is being designed to test its performance with fuel solution. Depending upon the results of the test, a multistage unit for 2000-psi operation will be considered.

9.5 DIRECT WATER DRIVE FOR DIAPHRAGM HEADS

A test was made of two water-service hydraulic cylinders operated as pulse generators to drive diaphragm heads directly, eliminating the pulsators and the phasing system. After 123 and 302 hr, respectively, the bronze pistons were heavily scored, as if by high-velocity water flow, and most of the rings were stuck. Since the manufacturer indicated that much longer life could be expected, he is being consulted prior to further testing.

9.6 TITANIUM PROGRAM

A titanium-to-stainless-steel transition joint was designed for application to titanium letdown heat exchangers for reactor use. The joint consists of a carbon-steel welding-neck ring-joint flange clad on the process side with stainless steel, a titanium ring-joint stub end and carbon-steel backup flange, and a titanium ring. This type of joint can be integrated into an HRT-type leak-detection system. A sample joint will be fabricated and then installed on the multiple-flange test facility for evaluation.

Crane Company finally received satisfactory titanium liners for the 3½- and 20-in. carbon-steel pipes. Fabrication was started, and completion is expected in two to three months.

The Pfaudler Company had difficulty with a new set of ⅜-in. titanium tubes purchased for the small heat exchanger which they are fabricating. The tubes passed all preliminary inspection but failed when rolled into the tube sheet. Small longitudinal tool marks were blamed for the failure. In order to aid the tube vendor in producing better quality tubes, new tubes will be ½ in. in outside diameter.

9.7 REMOTE MAINTENANCE

A bibliography of reports dealing with reactor maintenance is being prepared. Included also are reports of devices and methods that might be adaptable to maintenance of reactors. A report summarizing this literature survey was issued.[1]

Several types of high-strength stainless steel bolts and screws were purchased; their resistance to galling while in contact with fuel solutions will be evaluated.

9.8 THERMAL-CYCLE TEST FACILITY

The thermal-cycle test facility is being constructed. The Besler boiler (5000 lb of steam per hour), its fuel oil tank, flue gas stack, and utilities were installed. Work is proceeding on the deaerator installation and on steam and water piping.

9.9 HEAT EXCHANGER TEST FACILITY

Preliminary design of a 30-gpm facility for testing small steam generators modeled after advanced homogeneous reactor designs was completed. High-pressure steam, from the Besler boiler of the thermal-cycle facility, will be condensed continuously while heating the 30-gpm stream from 250°C to 300°C. The heat will be removed continuously from multiple steam-generator models. The circulating medium will originally be dilute uranyl sulfate solution and later will be ThO_2 slurry.

Specifications were written and requisitions were sent out for the first heat exchangers to be tested. The heater will be a small replica of the HRT spare heat exchanger.[2] The steam generators will contain the following tube and tube-sheet materials: (1) type 347 stainless steel tubes, type-347-clad carbon-steel tube sheet; (2) type 304 stainless tubes, type-304-clad carbon-steel tube sheet; (3) Croloy 16-1 tubes and tube sheet; and (4) duplex type 347–carbon-steel tubes, type-347-clad carbon-steel tube sheet.

9.10 HEAT EXCHANGER TUBE-JOINT TEST

Testing of the six tube bundles listed in Table 9.1 was completed. All bundles contained type 347 stainless steel tubes (some nickel-plated) and type-347-weld-clad carbon-steel tube sheets.

Table 9.1. Heat Exchanger Tube-Joint Test Bundle

Identification	Exposure (hr)	Tubes	Tube Sheet
A	1000	Unplated	Normal bore
B	1000	Ni plated	Normal bore
C	1000	Ni plated	Counterbored
G	500	Unplated	Normal bore
F	500	Ni plated	Normal bore
H	500	Ni plated	Counterbored

The units were thermally cycled with 250-psi steam in the tubes for 5 min and were off for 4 min. The shells were partially filled with water containing 100 ppm of Cl and 50 ppm of O_2.

Metallographic examination indicates that numerous voids were introduced into the weld-clad during fabrication. There are some indications of intergranular attack (Fig. 9.1) but no confirmed stress-corrosion cracking. The nickel plating separated from the tubes in some cases (Fig. 9.2). No solids were deposited in the tube–tube-sheet crevices; counterboring of the tube sheet produced no significant effect.

9.11 5000-gpm PUMP

Proposals were requested for the development and fabrication of a 5000-gpm top-maintenance circulating pump which would serve as a prototype for use in 50-Mw homogeneous reactors. Replies were received from Allis-Chalmers, Byron Jackson, General Electric, Reliance Electric, and Westinghouse.

[1] B. D. Draper, *Maintenance of Various Reactor Types*, ORNL CF-57-4-92 (April 8, 1957).

[2] I. Spiewak *et al.*, *HRP Quar. Prog. Rep. April 30, 1957*, ORNL-2331, p 28–29.

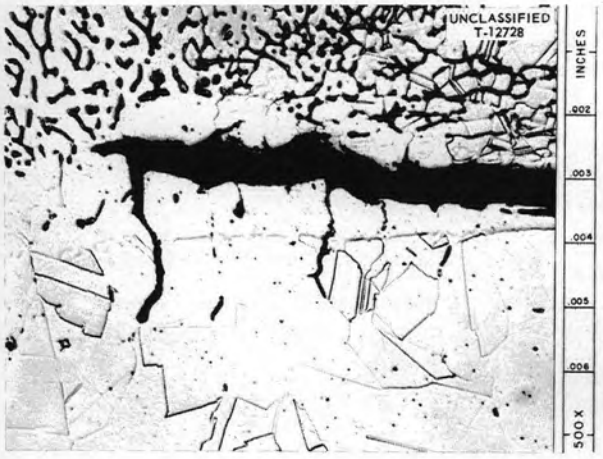

Fig. 9.1. Intergranular Attack Noted in Tube-Joint Test Bundle Exposed for 500 hr (Unit F).

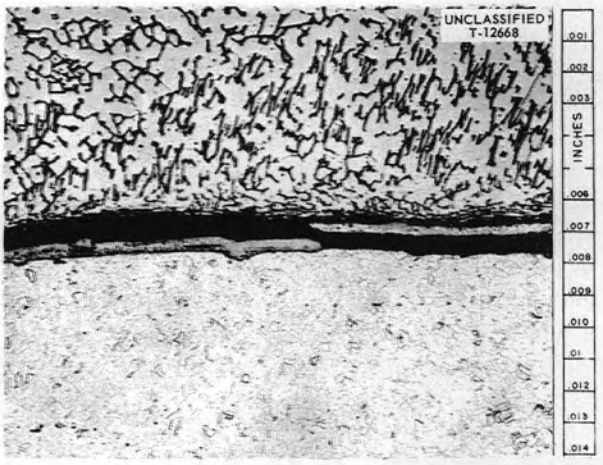

Fig. 9.2. Photomicrograph Showing Nickel Plating Loosened from a Tube of Tube-Joint Test Bundle B.

10. DEVELOPMENT OF REACTOR SLURRY SYSTEMS

R. B. Korsmeyer

D. G. Davis
H. L. Falkenberry[1]
L. D. Felten[2]
R. B. Gallaher
C. H. Gibson
V. L. Kenyon
C. G. Lawson
I. M. Miller
W. R. Mixon
C. S. Morgan
R. H. Nimmo
L. F. Parsly
M. Richardson
A. N. Smith
D. G. Thomas
C. F. VandenBulck[3]
R. P. Wichner
E. H. Wissler[2]

10.1 RHEOLOGY OF THORIUM OXIDE SLURRIES

10.1.1 Turbulent-Flow Pressure-Drop Measurements

Turbulent-flow pressure-drop measurements were made with a thorium oxide slurry over a velocity range of 4 to 47 fps, by using the $\frac{3}{8}$- and $1\frac{1}{8}$-in.-dia copper tubes, 16 ft 10 in. long, of the heat transfer loop,[4] after calibration tests with water had agreed to within ±15% with the Koo equation for smooth tubes[5] over a Reynolds number range of 3.7×10^3 to 9.6×10^5. The slurry concentration was 570 g of thorium per kilogram of H_2O, the yield stress was 0.03 lb/ft^2, and the coefficient of rigidity was 2.2 centipoises. Figure 10.1 is a plot of Fanning friction factor against Reynolds number based on the slurry density and coefficient of rigidity. The slurry friction-factor line is below the Newtonian line for smooth tubes for Reynolds numbers up to 10^5 and appears to connect directly onto the laminar flow line for Newtonian fluids (Hedström number = 0) at a Reynolds number of 2100. The laminar flow line for this slurry is shown at a Hedström number of 3.0×10^4. Similar observations have been made for data on a cement-rock slurry.[6]

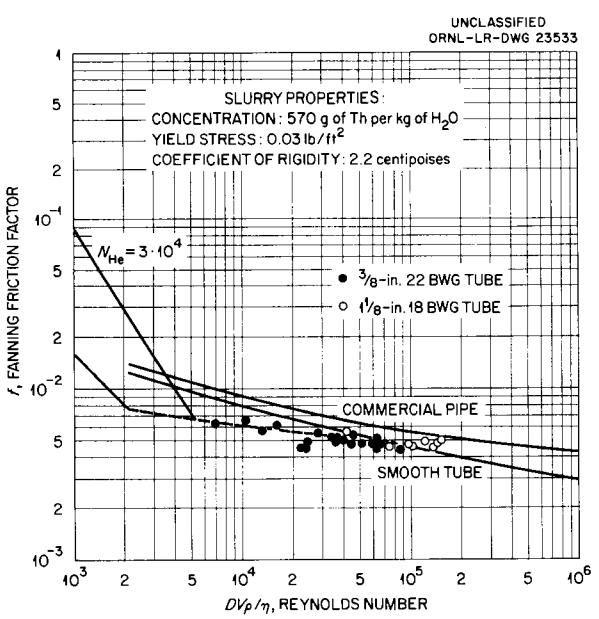

Fig. 10.1. Pressure Drop vs Flow for Thorium Oxide Slurry.

10.1.2 Laminar Flow

The usefulness of the concept proposed by Hedström[7] for the calculation of laminar-flow pressure drop of Bingham plastic materials in circular conduits by using a modified Fanning friction-factor plot has been pointed out previously.[8] The range of Hedström numbers has now been extended[9] by a machine calculation from 10^7 previously reported to 10^{15}. (The computation was made by the K-25 Numerical Analysis Laboratory with their IBM-605 magnetic-drum data

---

[1] On loan from TVA.

[2] Summer participant.

[3] On loan from Union Carbide Nuclear Co., New York Office.

[4] D. G. Thomas, *Proposed System for Atmospheric Pressure Slurry Heat Transfer Studies*, ORNL CF-56-9-131 (Sept. 13, 1956).

[5] T. B. Drew, H. H. Dunkle, and R. P. Genereaux, p 383, Eq. 24 in *Chemical Engineers Handbook*, 3d ed., edited by J. H. Perry, McGraw-Hill, New York, 1950.

[6] H. J. Garber *et al.*, *Pennsylvania Advanced Reactor Project Nov. 30, 1956*, WCAP-400, p 89–92.

[7] B. O. A. Hedström, *Ind. Eng. Chem.* **44**, 651–656 (1952).

[8] C. G. Lawson, *HRP Quar. Prog. Rep. July 31, 1956*, ORNL-2148, p 55–56.

[9] D. G. Thomas, *Hedstrom Plot for the Calculation of Laminar Flow Pressure Drop for Bingham Plastic Materials with Hedstrom Numbers from 0 to 10^{15}*, ORNL CF-57-6-111 (June 20, 1957).

processing machine.) The modified Buckingham equation[10]

$$\frac{1}{N_{Re}} = \frac{f}{16} - \frac{1}{6}\left[\frac{N_{He}}{(N_{Re})^2}\right] + \frac{1}{3}\left[\frac{N_{He}^4}{f^3(N_{Re})^8}\right]$$

was used in the computation, and the results are presented in Fig. 10.2.

10.1.3 Capillary Sampler-Viscometer

A capillary sampler-viscometer is being constructed which can be attached to slurry loops to give pseudo-shear diagrams of the slurry at the loop operating temperature at the same time that samples are taken. The instrument has been designed for use with slurries of yield stress between 0.1 and 3.0 lb/ft^2 at a maximum temperature of 300°C, a maximum static pressure of 2000 psi, and a maximum pressure drop across the capillary tube of 150 psi.

A schematic drawing of the viscometer is shown in Fig. 10.3. The pressure drop across the tube is measured with a differential pressure cell, and the flow rate is measured by timing and weighing the sample flowing out of the letdown valve. Temperature control is accomplished with an electric heater and an electrically heated air jacket. The heater compensates for any heat losses in the sample line before the sample enters the capillary tube, and the jacket is controlled at the temperature of the loop, thus maintaining the temperature of the sample at the desired value throughout the length of the capillary tube. Slurry traps filled with water are used to transmit pressure to the differential pressure cell. The traps have connections for flushing

[10] A. B. Metzner in *Advances in Chemical Engineering*, p 92 (ed. by T. B. Drew and J. W. Hoopes, Jr.), Academic Press, New York, 1956.

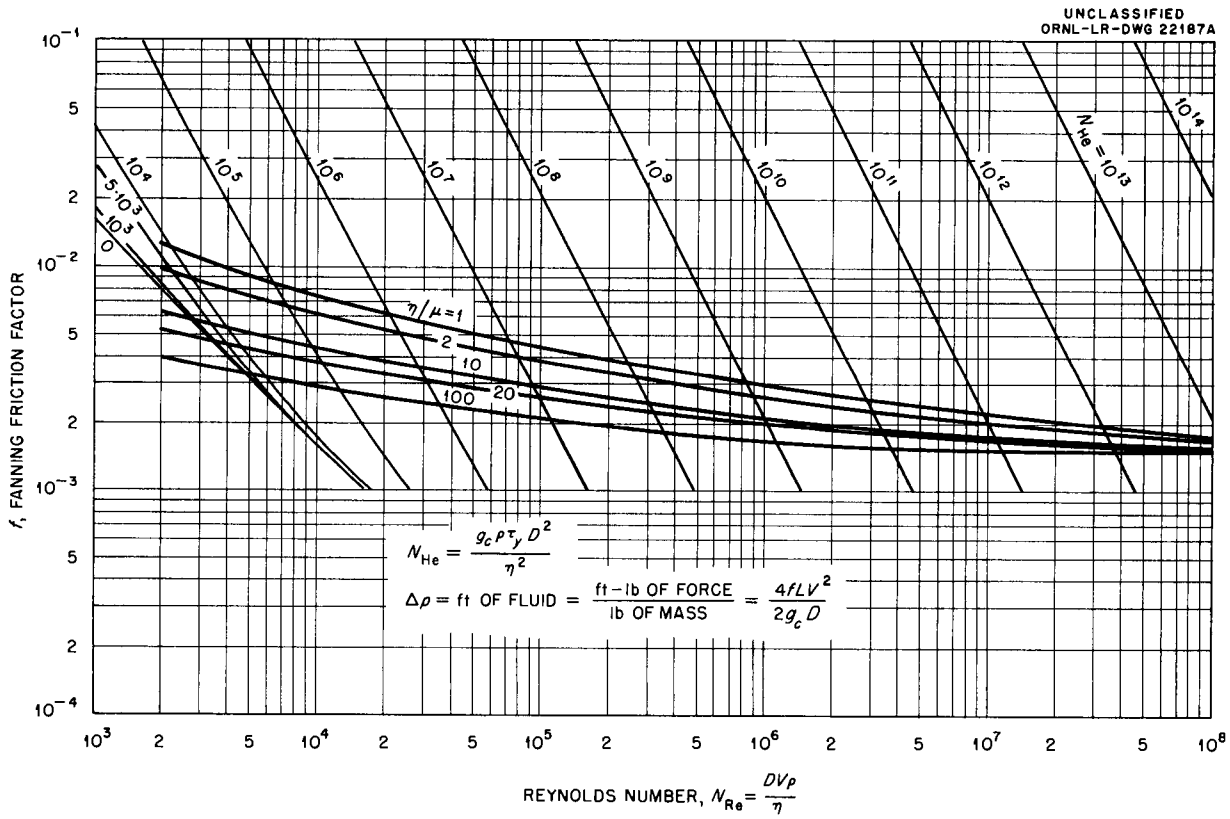

Fig. 10.2. Friction-Factor–Reynolds-Number Diagram for Bingham Plastic Slurries in Smooth Pipes.

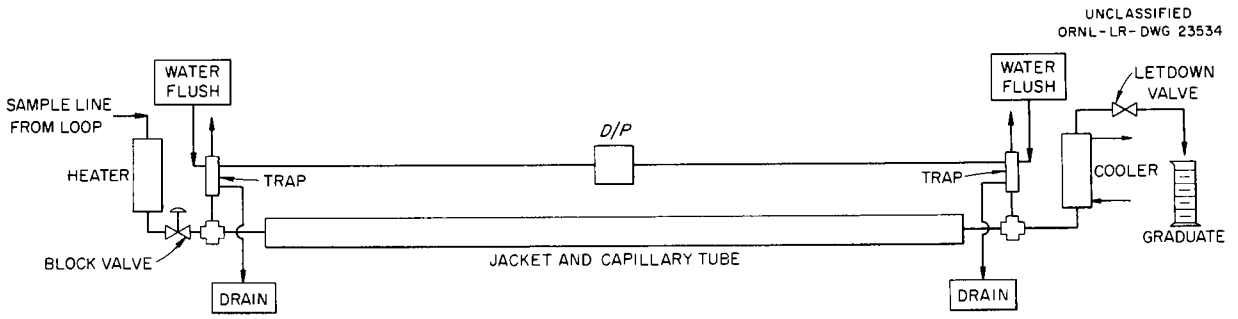

Fig. 10.3. Capillary-Tube Viscometer-Sampler.

the tube or the traps with water and for venting the traps or the differential pressure cell.

10.1.4 Slurry Flow Measurement

A Foxboro electromagnetic flowmeter (described in Foxboro Technical Information Bulletin 27-A-71) was tested in a low-temperature ThO_2 slurry loop for a total of 100 hr with the slurry concentration at approximately 800 g of thorium per kilogram of H_2O. The average per cent deviation between the flow rate as determined by the venturi and the Foxboro was $\pm 2\frac{1}{2}\%$. This uncertainty is within the precision of the venturi, the associated differential pressure cell, and the slurry density determination. The venturi size limited comparison of slurry flow rates to 40% of the range of the electromagnetic flowmeter.

The high ratio of the electrical conductivity of the pipe wall to that of the flowing fluid requires that the electrodes be electrically insulated from the pipe through which they protrude. In addition to this, an insulating sleeve is required to prevent a short circuit between the electrodes via the pipe wall. The insulating material in the model tested is Teflon. A search is being made for ceramic-type materials for high-temperature service.

10.2 EFFECT OF SLURRY PHYSICAL PROPERTIES ON HEAT EXCHANGER AND PUMP CHARACTERISTICS

A parametric study was made[11] for a system consisting of a pump, 100 ft of pipe, and a heat exchanger to remove 1 Mw of heat from various aqueous thorium oxide slurries. The rheological properties of the slurries were varied over a range of yield stresses from 0 to 1.5 lb/ft^2 and of coefficients of rigidity from $\frac{1}{2}$ to 2 centipoises. Two different cases were studied:

1. A heat exchanger having fixed axial and radial ΔT in which the tube length was allowed to vary.
2. A heat exchanger having fixed tube length in which the axial and radial ΔT were allowed to vary.

In both cases the tube velocity was taken as about twice the critical velocity for the onset of turbulence as given by the modified Hedström plot.[9] The slurry film coefficient was calculated by using a version of the Dittus-Boelter equation modified for transition effects in slurry.[12] The over-all heat transfer area for the case 1 heat exchangers was calculated in a manner similar to that described by Lane.[13] Calculations were made for the case 2 heat exchangers by using the same slurry-side coefficients obtained in the case 1 study, but by using a constant steam-side coefficient of 2000 $Btu/hr \cdot ft^2 \cdot °F$. Results of the calculations are summarized in Figs. 10.4, 10.5, and 10.6.

For a yield stress of 1.5 lb/ft^2, the electrical pump horsepower dissipated in the heat exchanger alone corresponds to about 20% of the electrical power produced from the steam generated, and the power for the total system is 30 to 60% of the output, depending on the tube diameter (and consequently on the axial temperature drop). If a

[11] D. G. Thomas, *Effect of Slurry Physical Properties on Heat Exchangers and Pump Characteristics*, ORNL CF-57-6-7 (June 10, 1957).

[12] R. B. Korsmeyer *et al.*, *HRP Quar. Prog. Rep. Oct. 31, 1956*, ORNL-2222, p 59.

[13] S. Glasstone, *Principles of Nuclear Reactor Engineering*, p 698–703, Van Nostrand, New York, 1955.

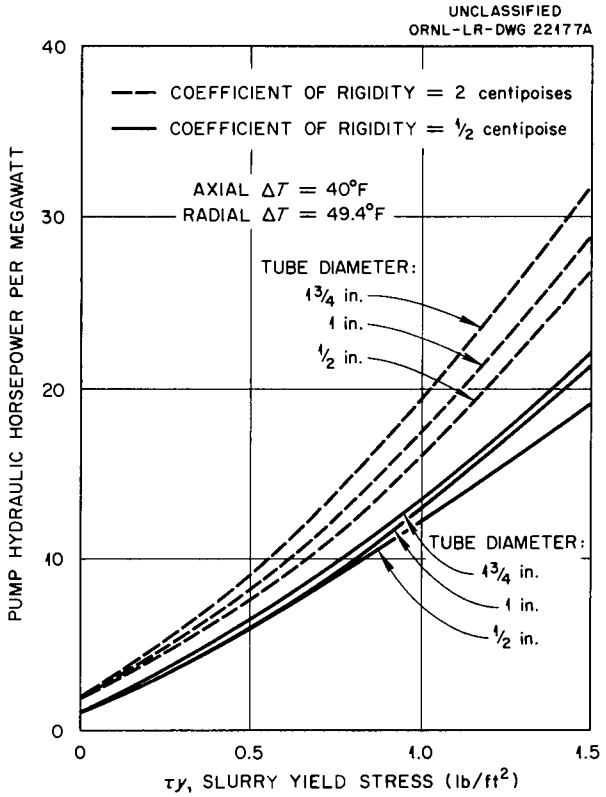

Fig. 10.4. Effect of Slurry Properties on Pump Hydraulic Horsepower per Megawatt for Heat Exchanger (No External Piping).

critical velocity of four times instead of two times the Hedström criterion is used, then about four times as much pump power is required. This situation would be alleviated somewhat, however, by the increase of the slurry heat transfer coefficient to essentially that of a Newtonian fluid of the same viscosity and density. Reduction of the yield stress from 1.5 to less than 0.1 lb/ft^2 gives better than a 20-fold reduction in pump power requirements. The results of the case 2 calculation also showed that, if the heat exchanger tube velocity is maintained at twice that calculated from the critical Hedström number as the slurry properties are changed, the pump power must be increased by a factor of 15 to 30 as the yield stress increases from 0 to 1.5 lb/ft^2, and, in comparison with case 1, a much larger fraction of the pump power is dissipated, at high yield stresses, in parts of the circuit other than the heat exchanger.

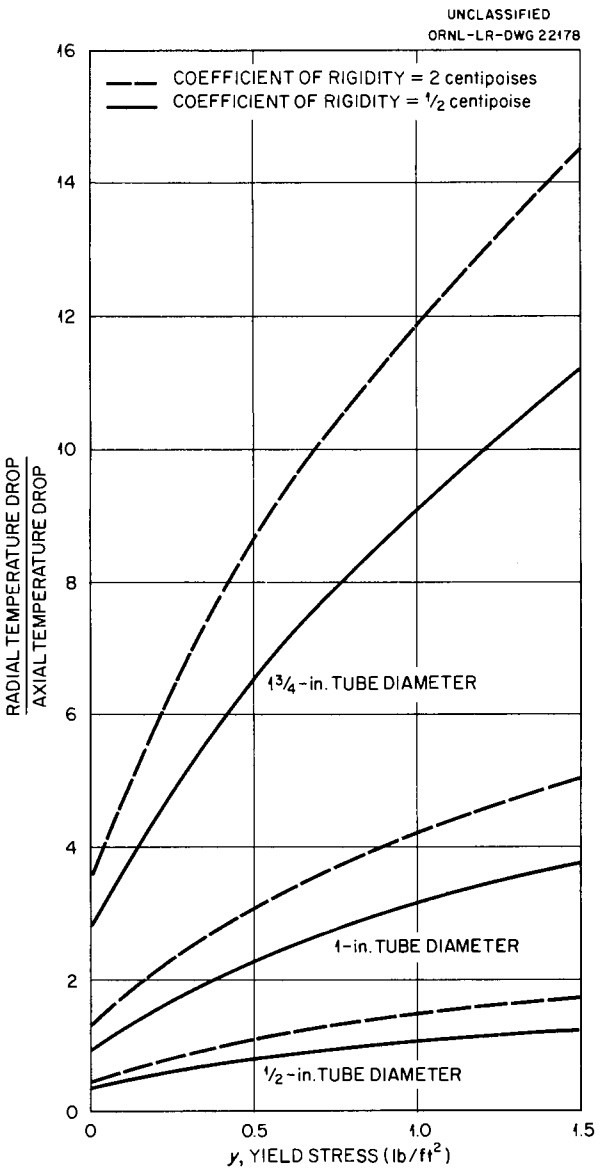

Fig. 10.5. Effect of Slurry Properties on Ratio of Radial to Axial ΔT for Heat Exchangers with 40-ft Tubes.

10.3 THORIUM OXIDE CAKE STUDIES

In particle-size degradation tests the Waring Blendor was used to produce slurries which formed thorium oxide cakes of varying degrees of cohesion when the slurry was allowed to dry in the air. Measurement of the cake resuspension index[14]

[14] R. B. Korsmeyer *et al.*, *HRP Quar. Prog. Rep. April 30, 1957*, ORNL-2331, p 64.

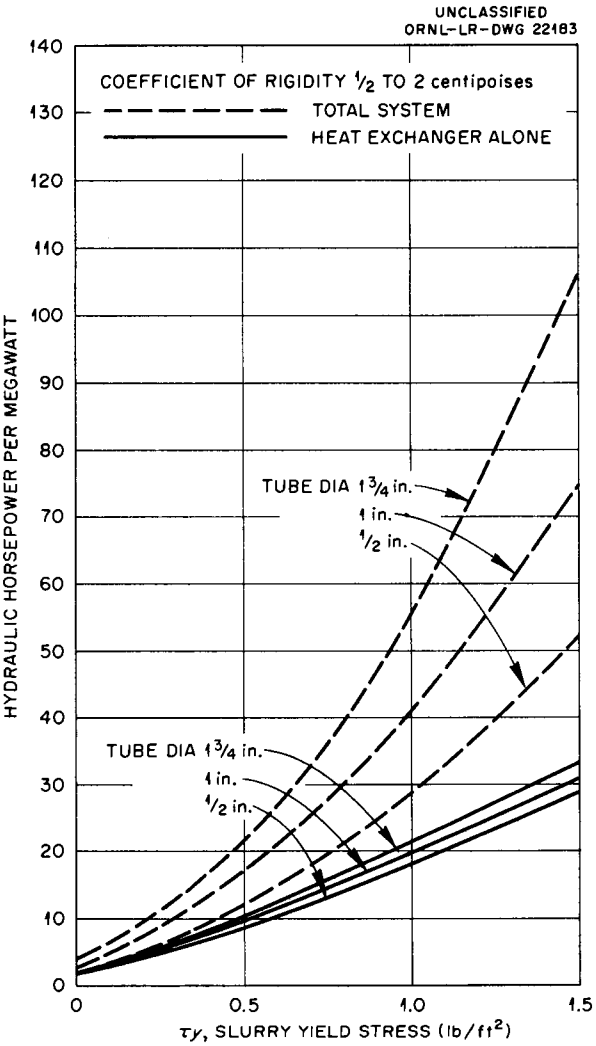

Fig. 10.6. Effect of Slurry Properties on Pump Hydraulic Head per Megawatt for Heat Exchangers with 40-ft Tubes and for Total System (Variable Axial and Radial ΔT).

(CRI) of the various cakes, as well as the particle size of the slurry producing the cake, yields the correlation shown in Fig. 10.7. (The CRI is a measure of the degree of hardness of a cake; the higher the index, the harder the cake.) As can be seen, the CRI increases very rapidly where more than 20 wt % of the particles are less than 1 μ in diameter. These results tend to confirm the hypothesis by Lyon[15] that ThO_2 cakes are

[15]R. N. Lyon, *The Choice in Thorium Oxide Slurries for the Prevention of Caking in Circulating Systems*, ORNL CF-57-4-77 (April 22, 1957).

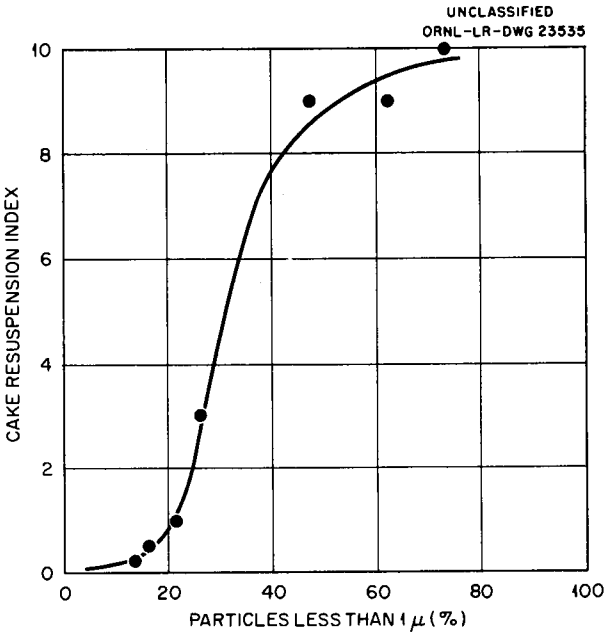

Fig. 10.7. Cake Resuspension Index vs Per Cent of Particles Less Than 1 μ.

formed by the arrangement of small particles into positions of minimum energy, where they are held together by van der Waals forces. Other factors, however, such as particle size distribution over an extremely wide range of sizes, may play an equally important role in cake hardness.

Application of the Waring Blendor particle-size degradation tests in conjunction with the CRI tests may prove useful in determining the sphere-forming tendency of various oxide batches. This is indicated by tests with oxide samples from batches LO-7, LO-20, and LO-23, which were agitated for 5 hr in a Waring Blendor, and then cakes were formed by air-drying the resultant slurries. The CRI of the non-sphere-forming oxide batch (LO-7) was 1, whereas the CRI's of sphere-forming oxide batches (LO-20 and LO-23) were always greater than 9. The usefulness of these tests in screening oxide batches will be more thoroughly explored.

10.4 CIRCULATING-SLURRY BEHAVIOR

Water and slurry were circulated for more than 2200 hr during the quarter in slurry loops S, T, and 200A. These runs are summarized in Table 10.1.

Table 10.1. High-Temperature Slurry Circulation – Run Summary

	Run No.						
	200A-11	200A-12	200A-13	200A-14	S-98	S-99	S-100
Test dates	1/10 to 4/25	6/3 to 6/10	6/17 to 6/21	7/18 to I[a]	4/2 to 4/21	5/17	5/28
Running time, hr	2303	164.3	90.5	I	404.7	10.1	15.4
Objective	Determine handling characteristics of admixed thorium-uranium slurry	Standard slurry production run (ref 14)	Standard slurry production run (ref 14)	Determine handling characteristics of 1600°C-fired ThO_2	Determine handling characteristics of sulfated thorium oxide containing MoO_3	Determine handling characteristics of 1600°C-fired ThO_2	Same as S-99
Charge							
ThO_2, kg	See ref 13	27.8 (LO-20)	32.8 (LO-23)	30 (LO-22)	13.6 (LO-8)	7.2 (LO-22)	7.2 (LO-22)
Water, kg		75	75	71	11.1	11.8	11.8
Additives		75 liters O_2	75 liters O_2	75 liters O_2	80 g $Th(SO_4)_2$ 80 g MoO_3 25 liters O_2	25 liters O_2	25 liters O_2
Temperature, °C	300	200	200	300	290	290	290
Pressure, psig	2000	1000	1000	2000	1600	1600	1600
Average circulating concentration, g Th/kg H_2O	995 in first 890 hr, max 1600 next 900 hr	550	570	I	900	NA[b]	875
Reason for termination	Rattle in pump	Reached equilibrium sphere size	Reached equilibrium sphere size	I	Scheduled shutdown	Noise in pump	Noise in pump
Maximum sphere diameter, μ	None	23	25	I	No spheres	No spheres	No spheres
Cake location	None	Impeller vanes	Impeller vanes	I	No cake	No cake	No cake
Total Fe in slurry, g	59.6	12.8	7.3	I	22.8	2.5	1.26
Total Cr in slurry, g	NA[b]	2.9	1.6	I	4.6	0.7	0.40
Total Ni in slurry, g	NA	2.5	1.0	I	3.7	0.4	0.15
Impeller weight loss, g	(Ti) 19.5	(SS) 7.5 for both 200A-12 and 200A-13		I	(SS) 16	(SS) 1	(SS) 3
Orifice plate weight loss, g	1½ in.: 1.4 1⅛ in.: 8.3	1½ in.: 0.06 for both 200A-12 and 200A-13 1⅛ in.: 0.14 for both 200A-12 and 200A-13		I I	Not measured	1.27 for runs S-99, S-100 and S-101 combined	

[a] I = incomplete (still running)
[b] NA = not availoble

Table 10.1 (continued)

	Run No.							
	S-101	S-102	T-87	T-88	T-89	T-90	T-91	T-92
Test dates	6/10 to 6/27	7/29 to I	4/1 to 4/24	5/14 to 5/27	6/4 to 6/6	6/17 to 6/20	6/25 to 7/6	7/15 to I
Running time, hr	304.5	I	551	304.8	14.9	11.6	115.4	I
Objective	Determine handling characteristics of 800°C-fired micra-pulverized ThO_2	Determine handling characteristics of sulfated slurry containing uranium and MoO_3	Determine the effect of Ti on handling characteristics of thorium oxide slurry	Determine the effect of Al on handling characteristics of thorium oxide slurry	Check operation of pump	Same as S-99	To compare sphere formation ot o particular slurry in 100A and 200A loops; sodium silicate was added to test sphere stability	To determine the effect of concentration on sphere formation
Charge								
ThO_2, kg	7.2 (LO-22)	14.4 (LO-17)	9.1 (LO-8)	8.8 (LO-8)		9.3 (LO-22)	9.2 (LO-23)	16.6 (LO-23)
Water, kg	11.8	11	15.1	15.2	16.0	15.1	15	14.3
Additives,	25 liters O_2	80 g $Th(SO_4)_2$ 87 g MoO_3 184 g $UO_2 \cdot H_2O$ 25 liters O_2	20 g TiO_2 25 liters O_2	7.8 g $Al_2O_3 \cdot H_2O$ 25 liters O_2	25 liters O_2	25 liters O_2	25 liters O_2	25 liters O_2
Temperature, °C	290	290	290	290	200	200	205	200
Pressure, psig	1600	1600	1600	1600	1600	1600	1600	1600
Average circulating concentration, g Th/kg H_2O	660	I	580	1024	0	850	406	I
Reason for termination	Scheduled shutdown	I	Failure of rupture disk	Scheduled shutdown	Pump out of balance	Pump out of balance	Noise in pump	I
Moximum sphere diameter, μ	No spheres	I	No spheres	No spheres	NA	No spheres	20	I
Cake locatian	No cake	I	No cake	No cake	NA	No cake	Impeller vanes	I
Total Fe in slurry, g	31.4	I	34.2	44.2	NA	6.9	34.8	I
Total Cr in slurry, g	7.4	I	6.6	7.5	NA	2.30	5.5	I
Total Ni in slurry, g	5.4	I	NA	NA	NA	1.15	4.9	I
Impeller weight loss, g	(SS) 16.5	I	27	48.5	0	9	33	I
Orifice plate weight loss, g	1.27 for runs S-99, S-100, and S-101 combined	I	1.6		NA		0.024	I

Run 200A-11, which had accumulated 2100 hr at the end of the last quarter,[16] was terminated at the end of 2303 hr because a rattle developed in the pump. The slurry was easily flushed out of the system. There was no evidence of caking or of a buildup of solids in the loop or the pump except for a small, easily removed deposit between the vanes on the rear of the impeller. The titanium impeller and the 1½-in. type 347 stainless steel orifice plate were severely attacked. A protective oxide film coated the loop piping and parts not exposed to high turbulence. The handling characteristics and the generalized attack rate at 300°C for the sulfated thorium–½% uranium oxide slurry were similar to those observed for the sulfated thorium oxide slurry. In regions of high turbulence, such as the orifice plates and impeller, the attack rate appeared greater for the admixed oxides. However, there has been no comparable run with a sulfated thorium oxide slurry in which there were as many additions of fresh oxide during the course of the run. (The initial charge of 61.8 kg of oxide was circulated for 890 hr; during the next 910 hr an additional 55.5 kg of unpumped ThO_2 was added to the system.) The reason for the noise in the pump at the end of the run was not evident, as the clearances between the journals and bearings were within tolerance even though part of the lower radial bearing had been severely attacked, presumably by oxidation brought about by excessive temperature.

The sphere-forming tendencies of two different batches of thorium oxide were compared in the 200A system. The two oxides – batches LO-20 and LO-23, produced by the Chemical Technology pilot plant – were run at 200°C and 1000 psig (in runs 200A-12 and 200A-13, respectively), at approximately 500 g of thorium per kilogram of H_2O, which are the conditions under which spheres were first formed (runs 200A-6 to 8).[17] Both oxides proved to be sphere-formers. In run 200A-12 the larger spheres had grown to 23 μ in diameter by the time the 55-hr sample was taken and remained that size until the run was terminated after a total of 164.3 hr of circulation. In run 200A-13 the larger spheres were 25 μ in diameter when the 21.5-hr sample was taken and remained that size until the run was terminated after a total of 90.5 hr of circulation.

When the loop was examined after each of these runs, the pipe wall was found to be covered with a light film of thorium oxide that could not be removed by a water rinse. To remove this film, the loop was dried over night by drawing warm air through it and was then quickly filled with dilute sulfuric acid, and the circulating pump was turned on. About 75% of the oxide was removed by this process. The remainder of the oxide was easily removed after run 200A-13 with a bristle brush and water. A small deposit of cake was found on the trailing surface of the impeller vanes after each run.

Run T-91 was initiated during this quarter to study the sphere-forming tendencies of an oxide circulated in a 100-gpm system. Batch LO-23 was charged into T-loop to approximately 500 g of thorium per kilogram of H_2O concentration. Spheres of 20 μ in diameter were found in the 13-hr samples, and no further growth was noted. After 47 hr of circulation 0.3 wt % sodium metasilicate was added, with the expectation that the addition of electrolyte would cause the spheres to disappear. No change in the appearance or size of the spheres was observed by microscopic examination during the 68 hr of circulation after the silicate addition. The run was terminated by pump failure. When the loop was examined after the run, the impeller vanes were caked on the trailing surface and the balancing holes were nearly closed with cake. One small piece of cake was in the pump scroll. The walls of the loop pipe appeared clean.

The remainder of the runs during the quarter were of a routine nature in which the handling characteristics of various oxide preparations were studied with and without additives.

10.5 HRT BLANKET-SYSTEM DEVELOPMENT

During the first half of the current quarter the slurry blanket test system was shut down while the alterations outlined in the previous quarterly report were completed. The following major changes were made:

1. The circulating pump was reassembled with new bearings and a 300-gpm stainless steel impeller.
2. The blanket inlet nozzles were redesigned, with the nozzle diameter being reduced from 2.16 in. to 1.50 in.

[16] R. B. Korsmeyer *et al.*, *HRP Quar. Prog. Rep. April 30, 1957*, ORNL-2331, p 70.

[17] R. B. Korsmeyer *et al.*, *HRP Quar. Prog. Rep. Oct. 31, 1956*, ORNL-2222, p 54.

3. A sampling system was installed which permits withdrawing samples at the outer wall, 6 in. into the blanket, and 12 in. into the blanket at each of 12 locations on the pressure vessel.

4. The gamma survey equipment was considerably expanded. In particular, a continuous survey track was installed which covers 180 deg of arc and is positioned on a great circle inclined approximately 17 deg off vertical in order to avoid inspection ports on the vessel. A reversible motor and speed reducer drives the dolly carrying the scintillation head along the track at 8 in./min. The head output is fed through appropriate circuitry to a standard millivoltmeter recorder. This arrangement proved very useful in that it permitted the obtainment of scans of the full height of the vessel.

5. A vent trap was mounted on top of the pump to permit the venting of gas without drawing slurry into the pump.

After completion of the alterations, three weeks were required to check out the system and make it leak-tight. During the leak-testing period, the gasket in the girth joint of the dummy reactor vessel was replaced, and the body-to-bonnet joints of some 40 small bar-stock valves installed during the shutdown were seal welded. Ultimately the loop sustained a hydrostatic test pressure of 500 psi with no visible leaks, and the leak-down rate was less than 2 psi/hr.

The loop was started and was run on water for 276 hr, during which time various systems and sampling facilities were tested and gamma surveys were made at 95, 170, and 200°C. Hydraulic measurements made while running on water indicated that the loop flow was 350 gpm, the pump head was 56 ft, the pressure drop through the blanket was 33 ft, and the loss across the blanket inlet nozzles was 25 ft.

Over the next 150 hr the charged thorium concentration was brought to 238 g of thorium per kilogram of H_2O by the addition of 350 kg of thorium as thorium oxide slurry. The slurry was that used in the previous run, but containing sufficient sulfuric acid to increase the sulfate content from 2700 to 3700 ppm sulfate, based on thorium.

The loop was then run at 170°C for 138 hr. Samples were taken of the material in the blanket, and a number of gamma surveys were taken. The surveys indicated that the distribution of thorium in the blanket was considerably better than in the previous run. No evidence of any slurry deposit was found.

While at 170°C a 26-min pump stoppage occurred when the motor fuses blew. After the fuses were replaced, the pump was restarted with no difficulty, and the original circulating concentration was re-established in approximately 20 sec.

After the desired data were obtained at 170°C, the temperature was raised to 200°C. No sharp changes in instrument readings occurred, in contrast to the previous run when a sudden jump in instrument readings, apparently due to a loss of slurry from the circulating stream, occurred between 180 and 185°C. The loop was run at 200°C for 60 hr with similar data being taken. While at 200°C the pump was stopped for 45 min so that data could be obtained on the rates at which the slurry settled out and was resuspended. The slurry was found to settle within 3 min to approximately 840 g of thorium per liter, as determined both by calculation from the thorium charge and settled bed volume, and by sampling. Complete resuspension was again obtained within 20 sec after starting the pump.

After the data were obtained at 200°C, the temperature was decreased to 170°C and charging operations were started to bring the system to the 500 g of thorium per kilogram of H_2O level.

Typical traces from the gamma scanner are shown in Fig. 10.8, in which the relative transmission of the gamma rays is plotted vs position on the great circle from top to bottom. The odd shape of the traces is due to the presence of the core vessel and particularly to the large girth flanges, which attenuated the beam sufficiently to render the instrument blind to changes in slurry concentration at the equator. A similar blindness occurred close to the poles. The reason why the peaks of the settling test curve lie above the maximum transmission for water has not been established, but it is believed to be due to the radiation from the large mass of thorium (and daughters) lying in the bottom of the blanket.

Figure 10.9 shows the temperature, pump head, pump power, pressure drop across the blanket, pressure drop across the blanket inlet, and loop flow plotted as a function of time for the period from 200 to 700 hr. The four differential-pressure instrument readings have been corrected for density by using the calculated density based on the

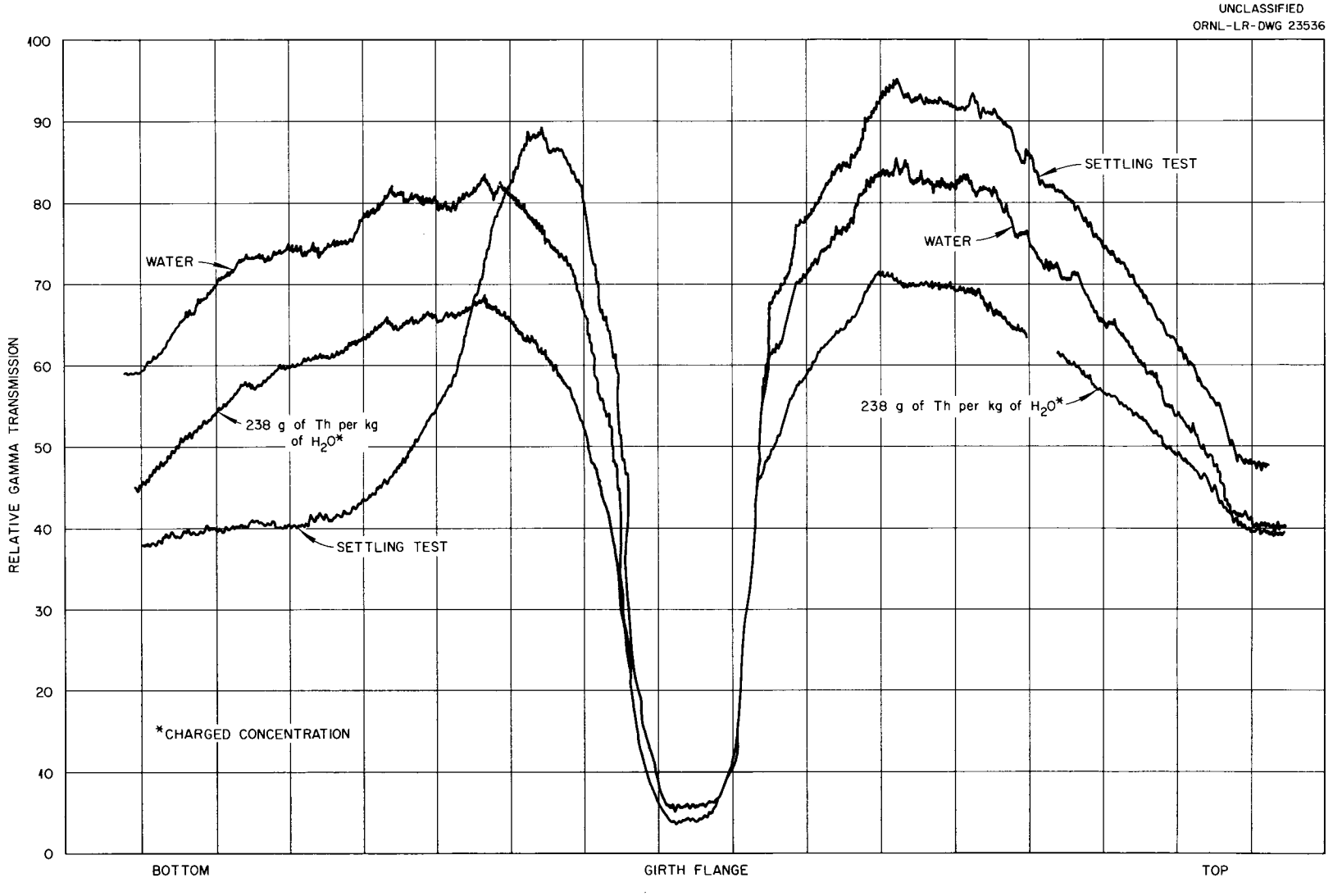

Fig. 10.8. Relative Gamma Transmission Through the Blanket vs Position, at 200°C.

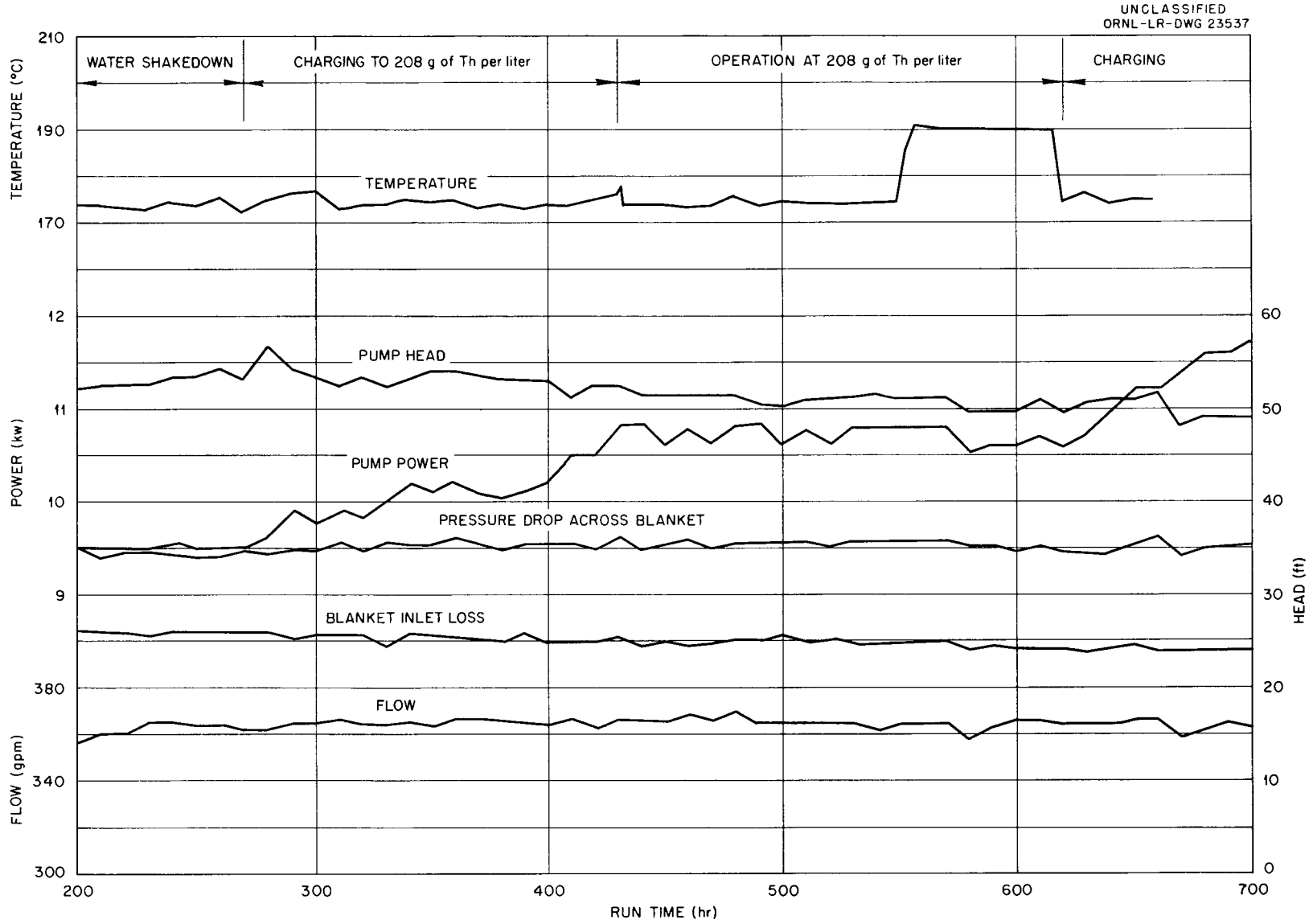

Fig. 10.9. Slurry Blanket Test, Run SM-3.

thorium charge in the system and the operating temperature. As corrected, the loop flow and blanket loss appear to have remained constant, while the blanket inlet loss and pump head appear to have dropped slightly. This behavior is not understood.

The data obtained up to the present time are not adequate to permit an evaluation of the blanket performance with the modified inlet nozzles. So far, the gamma surveys appear to indicate fairly uniform distribution in the blanket, and the displacements of the instrument readings indicate that the circulating concentration is close to the loaded concentration. However, the samples taken from the blanket and the circulating loop are generally of lower concentration than that estimated from the thorium charge. It is believed that continued operation with increasing concentrations will clear up these inconsistencies.

11. INSTRUMENT AND VALVE DEVELOPMENT

D. S. Toomb

A. M. Billings E. H. Bell

11.1 INSTRUMENT DEVELOPMENT

11.1.1 Pressure Transmitters

The pressure transmitter shown in Fig. 11.1 (manufactured by the Callery Chemical Co.) is being evaluated as to suitability for use in HRP systems. The transmitter is designed for operation at temperatures up to 640°F and therefore can be directly connected to process lines. Presently used Bourdon-tube-element transmitters are not suitable for use above 200°F and must be connected through long uninsulated lines to reduce the operating temperature. The new transmitter was found to have a natural frequency of 375 cps and an accuracy of 2%. It should be useful in reactor kinetic experiments, where long connecting lines would limit the response of transmitters of the Bourdon-tube-element type. It is expected that this transmitter will be used in studies to determine the effectiveness of the pressurizer in damping reactivity excursions.

11.2 VALVE DEVELOPMENT

11.2.1 Pneumatic Actuators

A pneumatically-powered-bellows valve actuator capable of developing thrusts to 12,000 lb was received from the Fulton Sylphon Div. This actuator is the most powerful manufactured so far by this vendor and will be evaluated for use on 2-in. valves for 2000-psi service. The actuator, shown in Fig. 11.2, can be reversed so that air pressure opens the valve. The loading-spring location determines the valve action with zero air pressure applied.

11.2.2 Valve Trim

In continuation of the valve-trim-materials evaluation program,[1] two sets of stainless steel plugs capped with Baker & Company, Inc., platinum alloy E-130 (70% Pt, 20% Au, 10% Pd) hardened to R_C 29 were tested with 400 "dump" cycles. Leak rates after testing were approximately 1 cc of H_2O per minute with a 3800-psi ΔP. One plug capped with Baker alloy No. 872 (80% Pt, 10% Au, 10% Pd) was subjected to a 420-dump test, and a slightly greater leak rate after testing was observed. These materials are apparently not so satisfactory for valve trim as the Baker 80% platinum, 20% iridium alloy or the Armco 17-4 PH trims previously tested. Type 347 stainless steel plugs flame-plated with aluminum oxide by Linde have not given satisfactory test results. Flaking of the aluminum oxide in the seating region was so severe as to preclude further investigation.

A type 347 stainless steel plug flame-plated with tungsten carbide by Linde was tested, and the results are comparable to those obtained for the Baker alloys. However, hardness tests are being performed to determine if the plate survives in the seating area.

One plug made from Kennametal K501, a cemented tungsten carbide composition employing a platinum binder, shattered after a few test cycles. This material is extremely hard, and the method of attaching the plug to the stem may be at fault. A second assembly made from K96, a similar material but employing a cobalt binder, shattered after 50 cycles.

---

[1] A. M. Billings, *HRP Experimental Valve Program*, ORNL CF-56-2-42 (Feb. 14, 1956).

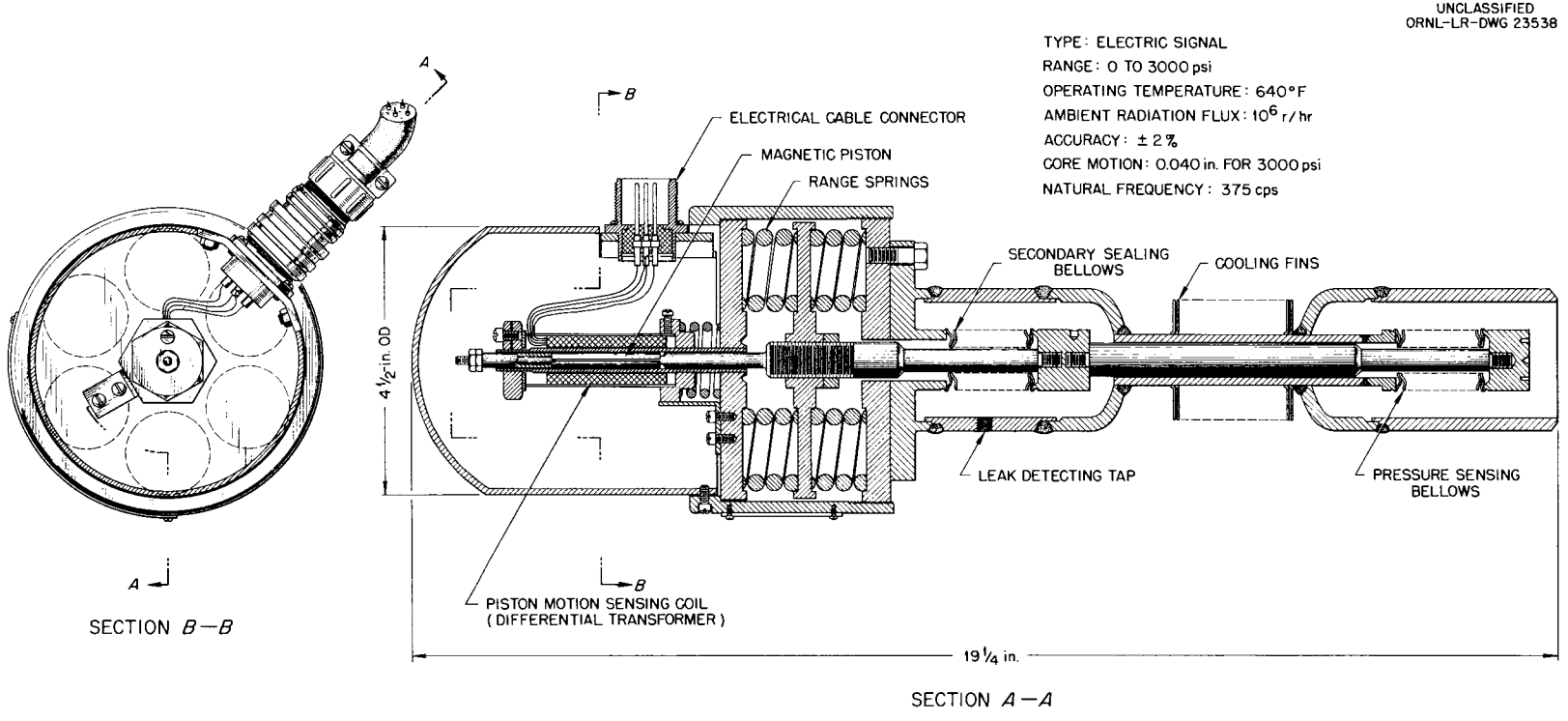

Fig. 11.1. Pressure Transmitter.

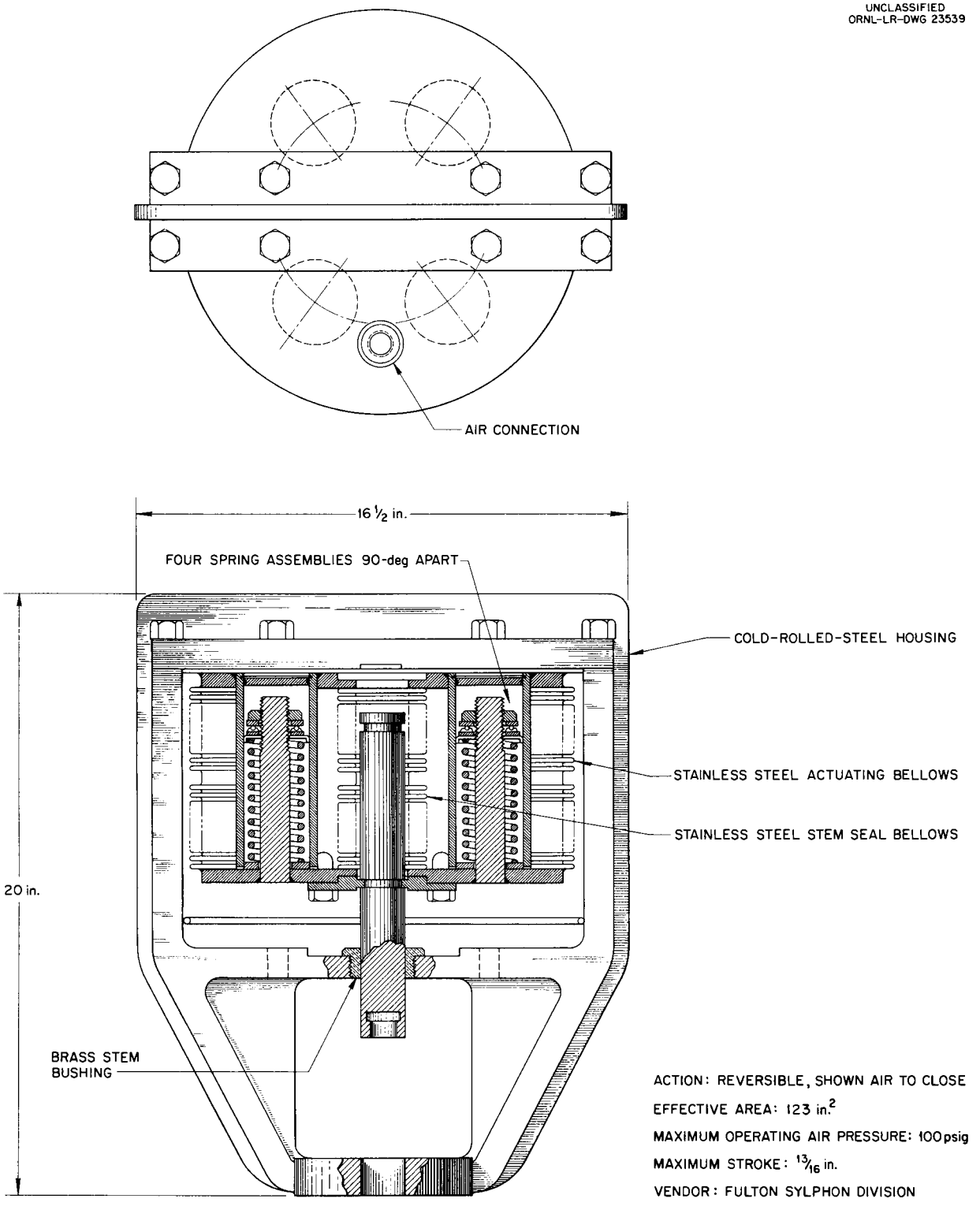

Fig. 11.2. Pneumatic Valve Actuator.

Part IV

REACTOR MATERIALS RESEARCH

E. G. Bohlmann

12. SOLUTION CORROSION[1]

J. C. Griess H. C. Savage
S. R. Buxton D. N. Hess
J. L. English T. H. Mauney
R. S. Greeley P. D. Neumann
W. C. Ulrich

12.1 DYNAMIC CORROSION STUDIES

12.1.1 100A Loop Engineering

(a) 100A Loop H. – The second all-titanium loop, 100A loop H, was placed in operation during the past quarter and has operated satisfactorily for more than 400 hr with uranyl sulfate solution at 250°C and approximately 1000 psi.

Loop H was constructed of titanium for the purpose of eliminating the contamination of circulating solution by corrosion products which originate from type 347 stainless steel loops. This is desirable in studies of the mechanism of corrosion of stainless steels. In addition, solutions that are highly corrosive to stainless steel can be circulated in the titanium loop to determine corrosion resistance of materials other than stainless steels which are of interest to the HR program. The loop consists essentially of a model 100A Westinghouse circulating pump, three horizontal sample barrels, a pressurizer, a pressurizer mixing line, and associated loop piping. Sample barrels can be arranged in any combination as required to expose a number of corrosion specimens to various solution flow rates. Figure 12.1 is a photograph of the completed loop.

The sample barrels and loop piping were constructed from 1.90-in.-OD × 1.34-in.-ID titanium tubing and 1½-in. sched-80 forged titanium welding fittings. The pressurizer was made from 3½-in.-OD × 2¾-in.-ID titanium tubing and has an over-all length of 82 in. The pressurizer mixing line is ⅞-in.-OD × ½-in.-ID titanium tubing. Commercially pure titanium metal (yield strength <55,000 psi; tensile strength <75,000 psi) was used throughout.

(b) 100A Loop I. – Loop I has been modified to provide close control of the oxygen concentration in the circulating solution, particularly at low concentrations (<100 ppm). The system is operated completely full of solution, and overpressure is maintained by a Pulsafeeder feed pump and letdown system. The oxygen addition is made at approximately room temperature and atmospheric pressure by bubbling oxygen through the loop solution in the dump tanks before it is pumped back into the pressurized loop. By varying the temperature and/or oxygen partial pressure in the dump tank where the oxygen addition is made, the concentration of oxygen in the loop can be varied.

The dissolved oxygen in the circulating solution is removed after passing through the letdown valve by maintaining the solution at a temperature higher than that in the dump tank. This reduces the oxygen solubility, and the oxygen that is removed from the loop circulating solution is collected and measured. The measurement of the oxygen removed from the letdown stream provides a check of the dissolved-oxygen concentration actually present in the loop circulating solution. The solution is then cooled, reoxygenated, and pumped back into the loop. The first test run (I-47) of the system is now in progress.

12.1.2 Fourth Operating Test of the HRT Core–Pressure-Vessel Flange and Transition-Joint Mockup

A fourth test of the mockup of the Zircaloy-2–stainless steel transition and expansion joint as used in the HRT reactor vessel has been made in 100A dynamic loop F. The first three tests were described previously,[2–4] and detailed reports were published elsewhere.[5,6]

---

[1] Reported in greater detail by J. C. Griess *et al.*, *Quarterly Report of the Solution Corrosion Group for the Period Ending July 31, 1957*, ORNL CF-57-7-121 (to be issued).

[2] H. C. Savage *et al.*, *HRP Quar. Prog. Rep. Oct. 31, 1956*, ORNL-2222, p 75–76.

[3] J. C. Griess *et al.*, *HRP Quar. Prog. Rep. Jan. 31, 1957*, ORNL-2272, p 77–79.

[4] J. C. Griess *et al.*, *HRP Quar. Prog. Rep. April 30, 1957*, ORNL-2331, p 83.

[5] T. H. Mauney *et al.*, *Operating Test of the HRT Core Vessel Transition Joint and Expansion Bellows Mockup*, ORNL CF-57-1-68 (Jan. 31, 1957).

[6] R. S. Greeley *et al.*, *Second and Third Operating Test of HRT Core Vessel Transition Joint and Expansion Bellows Mockup*, ORNL CF-57-4-44 (April 30, 1957).

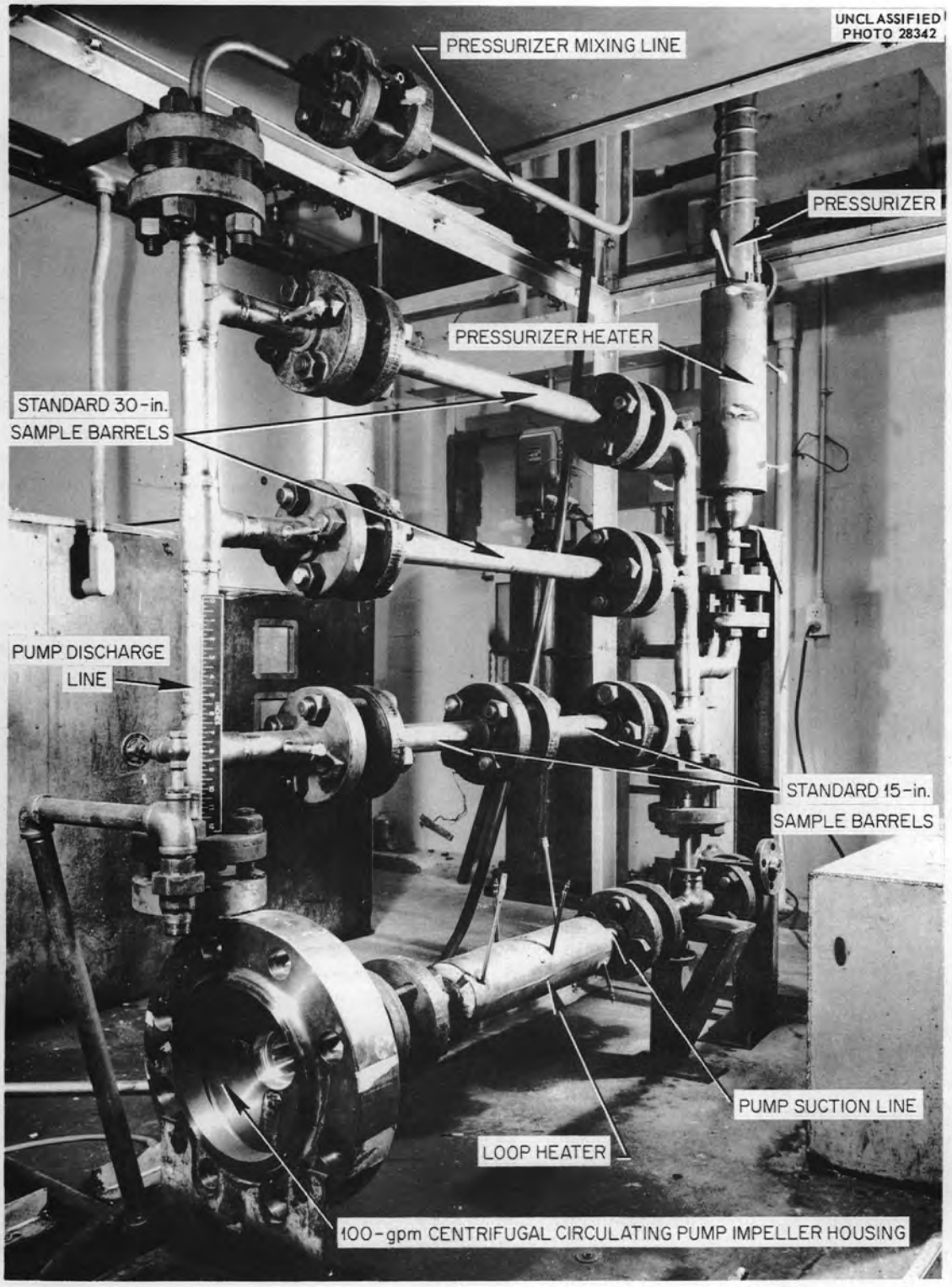

Fig. 12.1. Photograph of 100A Loop H.

This test lasted 1201 hr, 143 hr on water and 1058 hr on fuel solution (0.04 *m* UO_2SO_4, 0.02 *m* H_2SO_4, 0.005 *m* $CuSO_4$). Fifty thermal cycles were made, one per day, between 300 and 100°C. Steady-state operation was at 300°C. No mechanical deflections of the bellows were made, whereas in the first two tests, daily mechanical deflections were made.

Prior to disassembly, the 10-in.-IPS, 1500-lb test-vessel oval-ring joint was leak-tested at 200 psig of helium with a mass-spectrograph-type leak detector. No leakage was observed. After disassembly of the joint and removal of the oval-ring gasket, examination of the flange grooves showed that there had been no leakage of fuel solution into the grooves.

No leakage of fuel solution through the bellows or past the transition joint was detected during the run. After disassembly of the flanged joint, no leakage was detected when the bellows and transition joint were leak-tested with 50 psig of helium and a mass-spectrograph-type leak detector. Therefore, during the four tests, the bellows and transition joint have remained sound and leak-tight for 4118-hr total operating time, 3617-hr exposure to fuel solution, 166 thermal cycles, and 148 mechanical deflections.

The pitted areas on the bellows[7] were examined closely by moving the reinforcing rings to reveal the entire crevice area between the rings and the bellows. A microscope–dial-gage-indicator assembly was used again to measure the pit depths. No significant increase in pit depths was observed. Also, the pitted areas were covered with the adherent, black film observed on other areas of the bellows, in contrast to the loose, red oxide observed in the pits after the previous tests. Therefore, since no mechanical deflections were made during this fourth test, it appears that the pitting attack was, in some unexplained way, caused by the mechanical deflections made during the first and second tests.

The corrosion specimens in the loop were removed, scrubbed, and weighed. They were not defilmed but were replaced in the loop for further testing. The type 304L and 347 stainless steel pins at 17 fps and type 347 stainless steel coupons at 7 to 50 fps exposed in the loop bypass lost small amounts of weight, as did the titanium-alloy pins (Ti–6% Al–4% V; Ti–3% Al–5% Cr; Ti–5% Al–2½% Sn; Ti–4% Al–4% Mn) exposed at 68 fps. The coupon exposed at 50 to 64 fps corroded at a high rate. The Incoloy and type 309 SCb stainless steel pins at 17 fps and the titanium RC-55, crystal-bar zirconium, and Zircaloy-2 pins at both 17 and 68 fps gained small amounts of weight.

The solution remained stable throughout the test. The increase in nickel ion concentration corresponded to a generalized corrosion rate of about 0.1 mpy. This is in good agreement with a previous test made without thermal cycling under similar conditions[8] and is lower than previously observed in this series of tests with mechanical deflection of the bellows. Further testing of the unit is in progress.

12.1.3 Long-Term Runs with 0.04 *m* UO_2SO_4 Containing 0.025 *m* H_2SO_4 and 0.005 *m* $CuSO_4$

Long-term runs with 0.04 *m* UO_2SO_4 containing 0.025 *m* H_2SO_4 and 0.005 *m* $CuSO_4$ at 200, 250, and 300°C were terminated after 3630, 4411, and 3611 hr, respectively. Previous runs made with lower acid concentrations are discussed in Sec. 12.1.4.

The solution in the present series of runs with 0.025 *m* H_2SO_4 was entirely stable at 200 and 250°C. At 300°C, however, during the first 1832 hr, a gradual decrease in cupric ion concentration from 360 ± 20 ppm to 270 ± 20 ppm was observed. After 1832 hr, the run was restarted with fresh solution and continued for 1078 hr. A third part of the run was made for 701 hr, also with fresh solution. Within 20 ppm, no cupric ion was lost from solution during the latter two parts of the run. An examination of the analytical data showed that the only difference between the three parts of the run was the pH. During the first part of the run, the pH of the solution was 1.5 to 1.6, whereas in the last two parts, the pH was consistently 1.4 to 1.5. Although it seems unlikely, this slight difference in acidity may account for the difference in solution stability.

Table 12.1 lists the corrosion rates of the pins exposed in the present runs with 0.025 *m* H_2SO_4

[7] J. C. Griess *et al.*, *HRP Quar. Prog. Rep. Jan. 31, 1957*, ORNL-2272, p 78.

[8] R. S. Greeley, J. C. Griess, and S. R. Buxton, *HRP Dynamic Corrosion Studies: Summary of Run K-17. 0.04 m UO_2SO_4 + 0.02 m H_2SO_4 + 0.005 m $CuSO_4$ at 300°C*, ORNL CF-56-11-104 (Nov. 23, 1956).

Table 12.1. Corrosion Rates in Long-Term Runs with 0.04 *m* UO_2SO_4 + 0.025 *m* H_2SO_4 + 0.005 *m* $CuSO_4$, 500–1500 ppm O_2

Material	Flow Rate (fps)	Over-all Corrosion Rate (mpy)			Continuing Corrosion Rates Based on Scrubbed Weights (mpy)		
		200°C (3630 hr)	250°C (4411 hr)	300°C (3611 hr)	200°C (1081 to 3630 hr)	250°C (1614 to 4411 hr)	300°C (1832 to 3611 hr)
Stainless steels (new pins)*	8	3.3			0		
	12		1.2	0.32		0	0
	20	5.8	2.0	0.38	1.3	0	0
	26		3.0	0.40		0	0
	34	13	6.6	0.40	14	0	0
	42	23			20		
Niobium	8	0.03			0		
	12		0.40	0		0.28	0
	34		1.8	10		1.9	13
	42	12			9.9		

*Includes types 202, 304, 304 cast, 304 sensitized, 304L, 309 SCb, 347, 347 cast, 347 sensitized, 430, and 446 (defilmed).

determined both from the final, defilmed weight loss averaged over the entire run (over-all corrosion rate) and from the difference between the intermediate and final scrubbed weights (continuing corrosion rate). The table shows that there was substantial attack on the stainless steel pins at all velocities at 200 and 250°C, but that only those pins at 20 to 42 fps at 200°C were exposed above their critical velocity and continued to corrode. All other pins developed films during the first exposure period and stopped corroding.

12.1.4 Conclusion of Long-Term Runs with HRT Solution

The series of runs at 200, 250, and 300°C with the solution proposed for use in the HRT, 0.04 *m* UO_2SO_4, containing various amounts of sulfuric acid and 0.005 *m* $CuSO_4$, was concluded. The runs with solution containing 0.006, 0.010, 0.015, and 0.020 *m* H_2SO_4 have been reported previously (see refs 9, 10, 11, and 12, respectively). The present runs with a solution containing 0.025 *m* H_2SO_4 were discussed above. Table 12.2 gives the conditions of all the runs. Pins of a variety of alloys were carried over from run to run throughout the test. Also, in each run, new pins were exposed.

All the pins that had been exposed at 200 and 250°C for 19,342 and 20,657 hr, respectively, were defilmed. The pins that had been exposed at 300°C for 20,143 hr were not defilmed and were carried over to another test. Table 12.3 lists the defilmed weight losses of the stainless steel pins carried over from run to run at 200 and 250°C and compares them with the defilmed weight losses of the pins exposed in the first run only.

The very significant result of the tests is apparent from Table 12.3; namely, weight losses of the pins carried over for roughly 20,000 hr were at most only very slightly greater than weight losses of pins exposed in the first test only. That is, once the oxide film formed on the pins in the

[9] J. C. Griess *et al.*, *Quarterly Report of the Solution Corrosion Group for the Period Ending Jan. 31, 1956*, ORNL CF-56-1-167, p 24–25.

[10] *Ibid.*, p 25–26.

[11] J. C. Griess *et al.*, *HRP Quar. Prog. Rep. July 31, 1956*, ORNL-2148, p 77.

[12] J. C. Griess *et al.*, *HRP Quar. Prog. Rep. Jan. 31, 1957*, ORNL-2272, p 79–80.

Table 12.2. Conditions of Runs with HRT Solution, 0.04 *m* UO_2SO_4 + 0.005 *m* $CuSO_4$ + Various Amounts of H_2SO_4

Acid Concentration (*m*)	Time (hr)		
	L Loop 200°C	M Loop 250°C	K Loop 300°C
0.006	6,799	7,272	8,515
0.010	1,139	1,163	945
0.015	4,093	4,151	3,231
0.020	3,681	3,660	3,841
0.025	3,630	4,411	3,611
Total	19,342	20,657	20,143

first test, very little corrosion occurred in subsequent exposures. Also significant is the fact that the pins exposed at 19 to 42 fps at 200°C were above the critical velocity (measured on new stainless steel pins) during the last two or three runs. In other words, the oxide film formed below the critical velocity in HRT solution containing 0.006 *m* H_2SO_4 was protective for the duration of the tests at flow rates above the critical velocity in HRT solution containing 0.015 to 0.025 *m* H_2SO_4. Various titanium alloys, also carried over from run to run at 200 and 250°C, were defilmed. The commercially pure titanium specimens showed zero corrosion rate, whereas the high-strength titanium alloys corroded at rates between 0.01 to 0.12 mpy.

Although the specimens exposed at 300°C were not defilmed, the scrubbed weight losses and visual appearances of the specimens indicated that very little corrosion occurred after the first run. The high-strength titanium alloys corroded at rates of 0.3 to 0.4 mpy, and the zirconium and Zircaloy-2 specimens showed a slight attack under the Teflon insulation. The attack on the crystal-bar zirconium specimens was greater than on the Zircaloy-2 specimens, but even in the worst case, the average attack rate was less than 0.2 mpy. It appeared that during the approximately 20,000-hr exposure, the Teflon partially decomposed, releasing fluoride ions which corroded the zirconium.

Stress specimens of the following alloys were exposed in vapor and liquid regions during all but the first runs in this series: stainless steel types 309 SCb, 347, 17-4 PH (partially hardened to R_C 37), AM-350 (precipitation hardened to R_C39), and AM-350 (refrigeration hardened to R_C 38) and titanium alloys 110AM and 130AM. The specimens exposed for 12,543 hr at 200°C and for 13,385 hr at 250°C were defilmed and examined microscopically. The specimens exposed for 11,628 hr at 300°C were examined microscopically without defilming. No cracks or significantly greater corrosion due to the applied stress was observed.

The runs were made with increasing amounts of acid at each temperature in order to attain a solution stable with regard to hydrolytic precipitation of copper and uranium. All solutions were stable at 200°C. At 250°C, only the solutions containing 0.020 and 0.025 *m* H_2SO_4 were stable. At 300°C, none of the solutions were entirely stable, but as noted previously,[11] the solution containing 0.020 *m* H_2SO_4 was stable for 2740 hr and as noted in Sec. 12.1.3, the solution containing 0.025 *m* H_2SO_4 was stable for 1779 hr when the room-temperature pH was 1.4 to 1.5.

12.1.5 Effect of Several Variables on the Corrosion of Type 347 Stainless Steel

(a) Effect of Heat Treatment. – The effects of various heat treatments and surface preparations on the corrosion rates and critical velocity of type 347 stainless steel were investigated in five runs. All tests were performed in 0.17 *m* UO_2SO_4 at 250°C. The heat treatments and surface preparations given the specimens are listed in Table 12.4.

Consideration of the weight losses of coupons exposed at 10 to 80 fps and pins exposed at 17 fps leads to the following conclusions:

1. Heat treatment for 1 hr at 1250 to 1950°F had little effect on weight losses or critical velocity. One hour at 1650°F with slow cooling gave slightly lower weight losses up to the critical velocity and 1 hr at 1950°F gave a critical velocity 5 to 10 fps lower than control coupons simultaneously exposed.

2. Heat treatment for 2½ hr at 2200°F followed by 1 hr at 1950°F was deleterious to corrosion resistance in that weight losses below the critical velocity were increased by a factor of 3 to 5, and the critical velocity was decreased about 10 fps.

3. Electropolished surfaces gave lower weight losses below the critical velocity than as-machined or pickled surfaces. No change in critical velocity was observed as a result of the electropolishing.

Table 12.3. Comparison of Weight Losses of Stainless Steel Pins Exposed ~20,000 hr to HRT Solution at 200 and 250°C with Pins Exposed ~7000 hr

6799 hr at 200°C (L-32 Only)			19,342 hr at 200°C (L-32, 33, 34, 35, 36)		
Material	Flow Rate (fps)	Defilmed Weight Loss (mg/cm^2)	Material	Flow Rate (fps)	Defilmed Weight Loss (mg/cm^2)
			304 cast	10	3.7
314L	10	3.4	304L	10	3.9
309 SCb	10	4.9	309 SCb	10	6.2
			347 cast	10	4.4
347	10	3.4	347	10	4.0
			304 cast	19	3.9
304L	19	5.6	304L	19	5.4
309 SCb	19	2.1	309 SCb	19	2.1
347	19	4.2	347	19	5.5
309 SCb	34	1.5	309 SCb	34	3.0
347	34	3.9	347	34	4.0
309 SCb	42	3.1	309 SCb	42	11.0
7272 hr at 250°C (M-26 Only)			20,657 hr at 250°C (M-26, 27, 28, 29, 30)		
Material	Flow Rate (fps)	Defilmed Weight Loss (mg/cm^2)	Material	Flow Rate (fps)	Defilmed Weight Loss (mg/cm^2)
			304 cast	10	1.0
304L	10	1.0	304L	10	1.0
309 SCb	10	1.9	309 SCb	10	5.7
			347 cast	10	0.7
347	10	1.0	347	10	1.0
304L	19	1.1	304L	19	1.1
309 SCb	19	2.2	309 SCb	19	2.9
347	19	1.3	347	19	1.2
			304 cast	38	1.3
304L	38	1.2	304L	38	1.3
309 SCb	35	3.5	309 SCb	35	3.1
347	38	1.6	347	38	1.9

Table 12.4. Heat Treatment and Surface Preparation of Type 347 Stainless Steel Specimens

No.	Heat Treatment			Surface Treatment Prior to Run
	Time (hr)	Temperature (°C)	Cooling Method	
A-109	1	1650	Furnace cool at 50°F per hr to 800°F; air cool	Defilmed
A-110	1	1650	Furnace cool at 40°F per hr to 800°F; air cool	Pickled
A-111	1	1250	Air cool	Electropolished
A-112	1	1950	Air cool	Electropolished
A-113	2½	2200	Furnace cool to 1950°F;	Pickled and buffed to remove
	1	1950	then water quench	scale; electropolished

The above results are relevant to the question of the corrosion resistance of welds, the heat-affected zone adjacent to welds, and other heat-treated areas. It can be seen that areas heated above 1950°F may have somewhat lower critical velocities and may lose more weight during film formation than parent metal. However, as long as the solution velocity is below the critical velocity, the areas will develop protective films, after which corrosion will be negligible.

(b) Effect of Chromic Acid Pretreatment. – It was found previously that pretreatment of type 347 stainless steel specimens at 250°C with a solution containing 100 ppm chromium(VI) as chromium trioxide and 1000 to 2000 ppm oxygen was effective in extending the critical velocity upon subsequent exposure of the specimens to 0.17 and 1.3 *m* UO_2SO_4 at 250°C (ref 13). Further experimentation has been carried out to determine whether the pretreatment film formed at 250°C would be protective during subsequent exposure at lower temperatures.

Pretreatments of 100 hr at 250°C with 100 or 200 ppm chromium(VI) as chromium trioxide and 1000 to 2000 ppm oxygen were used. Exposure in one run was to 1.3 *m* UO_2SO_4 at 200°C. In three other runs, exposure was to 0.04 *m* UO_2SO_4 containing 0.020 *m* H_2SO_4 and 0.005 *m* $CuSO_4$ at 225°C. The latter temperature was used since corrosion is most severe in the solution at 225°C.

The major effect of these pretreatments was to decrease the amount of weight lost by the specimens below the critical velocity. A secondary effect was to delay for several hours the onset of rapid attack above the critical velocity. The critical velocity was affected to only a small extent, 5 to 10 fps, under certain conditions. Increasing the chromium(VI) concentration from 100 to 200 ppm in the pretreatment solution appeared to be beneficial in this regard. It is not known whether higher chromium(VI) concentrations would be more beneficial. It was concluded that pretreatment was in general beneficial in decreasing initial weight loss but could not be depended on to increase the critical velocity.

(c) Effect of Oxygen Exhaustion. – In the previous quarterly progress report, a series of runs was reported in which stress-corrosion cracking of type 347 stainless steel occurred in 0.17 *m* UO_2SO_4 solution containing 50 ppm chloride when oxygen exhaustion occurred.[14] It was of significance to determine whether stress-corrosion cracking would occur in 0.17 *m* UO_2SO_4 in the absence of oxygen if no chloride were present. Therefore, type 347 stainless steel specimens stressed to 26,600 psi (75% of room-temperature yield strength) were exposed at 200, 250, and 280°C to 0.17 *m* UO_2SO_4 containing less than 3 ppm chloride in the absence of oxygen.

Soon after startup of each run, the trace of oxygen remaining in the solution was used up by the corrosion process and then the uranyl ion began to be reduced and precipitated. As the

[13] *Ibid.*, p 80.

[14] J. C. Griess *et al.*, *HRP Quar. Prog. Rep. April 30, 1957*, ORNL-2331, p 89.

uranium precipitated (as U_3O_8) the pH decreased. The runs were stopped when the room-temperature pH had fallen from 2.4 to 1.7. This process took less time for each temperature increase (84 hr at 200°C, 30 hr at 250°C, and 7 hr at 280°C).

The specimens were pitted, particularly at 200°C, but metallographic examination of the stress specimens showed no stress-corrosion cracks. Since the runs had to be terminated after such short times, it is not known whether cracks would have developed at the base of the pits. However, for short periods of time, oxygen exhaustion does not lead to stress-corrosion cracking in the absence (<3 ppm) of chloride.

(d) Effect of Acid Concentration in 0.17 *m* UO_2SO_4. – A series of runs was made to determine the effect of sulfuric acid in uranyl sulfate solutions on the corrosion of type 347 stainless steel. Loop G, the all-titanium loop, was used to minimize interference from corrosion products originating from the loop piping. Two-hundred-hour runs were made at 250°C with 0.17 *m* UO_2SO_4 containing 0, 0.017, 0.025, and 0.040 *m* H_2SO_4. The results of the runs are shown in Fig. 12.2. The results at 70 fps were quite erratic, as indicated by the length of the vertical line at each acid concentration used. It can be seen that corrosion rates increased linearly with acid concentration at 6 and 12 fps, but at 70 fps, corrosion rates increased more sharply with acid concentration. Due to the scatter in the data, no quantitative treatment has been attempted. The extremely high corrosion rates at 70 fps in the runs with solution containing 0.040 *m* H_2SO_4 are more than twice as great as rates observed in similar runs in stainless steel loops.

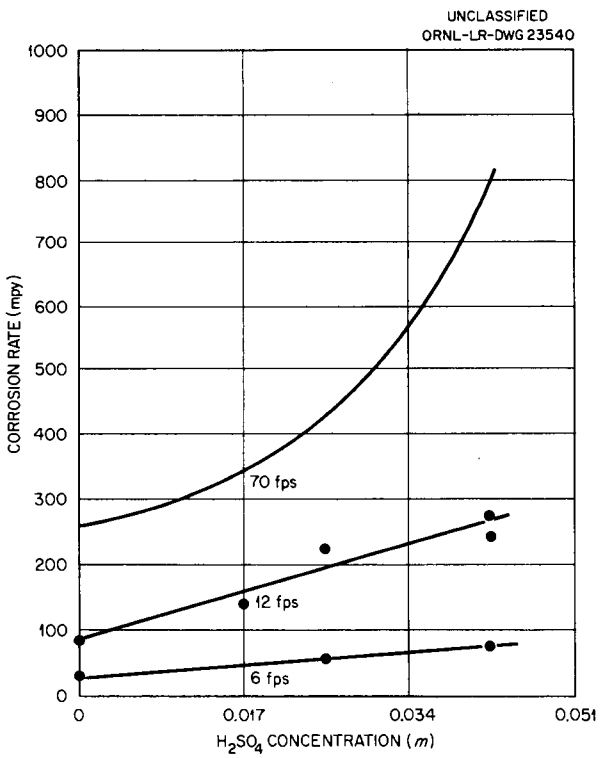

Fig. 12.2. Effect of Sulfuric Acid on Corrosion of Type 347 SS Pins in 0.17 *m* UO_2SO_4 at 250°C.

12.1.6 Failure of a Type 347 Stainless Steel Pipe

In connection with another test, 0.04 *m* UO_2SO_4 containing 0.02 *m* D_2SO_4 and 0.005 *m* $CuSO_4$ in heavy water was circulated in a stainless steel loop at temperatures as high as 335°C. After the solution was circulated for a short time at 330 and 335°C, it was cooled to 300°C, and shortly thereafter, the ½-in. type 347 stainless steel mixing line leaked and terminated the run. The piping was removed and sectioned for detailed examination. The inside of the pipe had corroded severely in several localized areas underneath the cast-on aluminum heater (1500 w).

The cast-on heater had been used in the two previous tests during which time 0.17 *m* UO_2SO_4 had been circulated at 250°C with the pressurizer maintained at 280°C for a total of 400 hr. It is probable that during any or all of the three tests, the mixing-line heater was set so high that the slowly flowing (1-gpm) solution became heated substantially above the second-liquid-phase-separation temperature. The appearance of the interior of the pipe indicated that the heavy liquid phase collected in small areas on the piping wall and caused localized corrosion severe enough to penetrate the wall. The above experience illustrates the necessity for preventing two-liquid-phase separation even in dilute solution.

12.2 LABORATORY CORROSION STUDIES

12.2.1 Stress-Corrosion Cracking

(a) Stress-Corrosion Cracking in Uranyl Sulfate Solutions. – Tests to determine the stress-corrosion cracking behavior of type 347 stainless steel in boiling (~100°C) HRT fuel solution (0.04 *m* UO_2SO_4, 0.02 *m* H_2SO_4, and 0.005 *m* $CuSO_4$) containing halide ions and other additives have continued. It has been shown that chloride

concentrations of 25 to 500 ppm in the HRT core solution are capable of producing stress-corrosion cracks during exposure times varying from 25 to 500 hr, either in the presence or absence of oxygen.[15,16] Anomalous results were obtained at the 100 ppm Cl^- level, and this point is under further investigation. It has also been reported[17] that the addition of platinum ions to the chloride-containing solution accelerated the cracking process; however, recent tests have not confirmed the previous ones, and this point is being checked further.

Experiments have been initiated to determine the effects of the components of the simulated HRT core solution containing chloride ions on the susceptibility of type 347 stainless steel to stress-corrosion cracking. In one test, the uranyl ions were replaced by potassium ions so that the solution contained 0.04 *m* K_2SO_4, 0.02 *m* H_2SO_4, 0.005 *m* $CuSO_4$, and 50 ppm Cl^-. In a similar test, this same solution was used except that the copper sulfate was absent. Two elastically stressed U-bends prepared from type 347 stainless steel 0.019 in. thick were exposed to each solution at its boiling point. To date, the tests have continued for 1500 hr with no evidence of cracking on any of the four specimens. In the normal HRT solution with 50 ppm chloride, cracking has always occurred after exposure of 25 to 400 hr. Even though the results are preliminary, it does appear that uranyl ions conjointly with chloride ions are capable of influencing the susceptibility of type 347 stainless steel to stress-corrosion cracking.

In the last quarterly report,[18] it was indicated that bromide ions in boiling simulated HRT core solution produced stress-corrosion cracks in type 347 stainless steel. With 100 ppm bromide in the solution, one simple beam-type specimen stressed to 15,000 psi developed one apparent crack in the region of maximum applied stress during the exposure period of 2000 to 2500 hr. At the 200 ppm bromide level two specimens, one stressed at 15,000 psi and the other at 30,000 psi, each developed one fine crack at the region of maximum applied stress during the exposure period of 1000 to 1500 hr. Figure 12.3 shows a surface photograph of a typical crack developed in the bromide-containing solution. Figure 12.4 shows

Fig. 12.3. Superficial Cracks on Type 347 SS Stressed at 15,000 psi After 2500 hr in Boiling, Aerated Uranyl Sulfate Solution Containing 100 ppm Bromide. 5X. Reduced 13%.

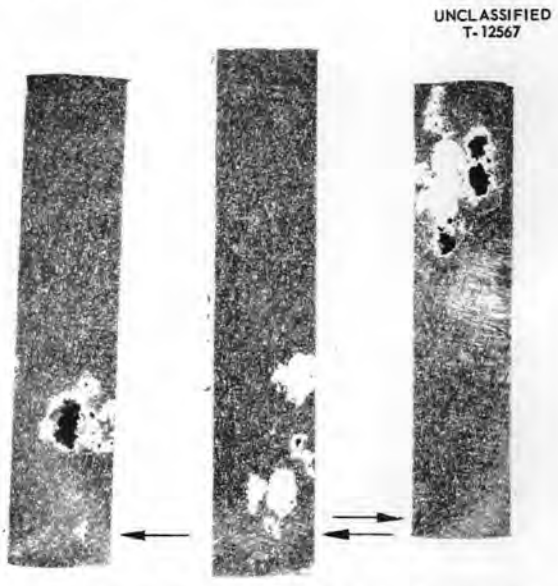

Fig. 12.4. Subsurface Attack on Type 347 SS Stressed at 15,000 psi After 2500 hr in Boiling, Aerated Uranyl Sulfate Solution Containing 100 ppm Bromide. Arrows indicate the tensile side of the specimens. 6X. Reduced 21%.

[15] J. L. English *et al.*, *Quarterly Report of the Solution Corrosion Group for the Period Ending January 31, 1957*, ORNL CF-57-1-144, p 27–30.

[16] J. L. English *et al.*, *Quarterly Report of the Solution Corrosion Group for the Period Ending April 30, 1957*, ORNL CF-57-4-55, p 30–33.

[17] *Ibid.*, p 35–37.

[18] J. C. Griess *et al.*, *HRP Quar. Prog. Rep. April 30, 1957*, ORNL-2331, p 90.

a photomicrograph of sections taken through one crack. Both the black and the white areas within the metal represent large corroded areas. The white areas were those near the surface and were filled with the plastic mounting compound; the black areas were so far below the surface that they remained free of the mounting compound. All three surface cracks that have been observed were similar in both surface and cross-sectional appearance. Thus it seems that the presence of bromide ions in a simulated HRT core solution does not produce stress-corrosion cracking of the stainless steel in the normal sense of the word; the results more nearly suggest a case of stress corrosion by the bromide ion.

(b) Stress-Corrosion Cracking in High-Temperature Water. – Testing of the susceptibility of type 347 stainless steel to stress-corrosion cracking in high-temperature water containing chloride ions has continued during the past quarter. The variables under investigation have included the effects of chloride ion concentration, pH, temperature, and, to a lesser extent, dissolved-oxygen concentration. In each test, duplicate U-bend specimens, the ends of which were pulled together with stainless steel tie bolts, were used, and in all cases, the specimens were totally immersed. The specimens were removed from the autoclaves at 100-hr intervals and examined microscopically. The results are shown in Table 12.5. The "time to cracking" in Table 12.5 refers to the first appearance of a visible crack, not to the time of complete fracture. The pH listed in the table is the starting pH. In nearly all cases,

Table 12.5. Stress-Corrosion Cracking Behavior of Type 347 Stainless Steel U-Bends in High-Temperature, Chloride-Containing Water

Test No.	Chloride (ppm)	O_2 Concentration (ppm)	pH	Temperature (°C)	Time to Cracking (hr)	
					1st	2nd
U-95	100	1200	2.8	300	300	400
V-2	100	10	2.8	300	200	200
V-53	100	10	2.8	300	400	400
V-83	100	1200	6.5	300	200	300
V-84	100	10	6.5	300	>300*	>300*
U-96	100	1200	10.5	300	400	400
V-5	100	10	10.5	300	200	200
U-97	50	1200	2.8	300	600	700
V-3	50	10	2.8	300	200	200
V-85	50	1200	6.5	300	>100*	>100*
V-52	50	10	6.5	300	500	500
V-86	50	10	6.5	300	100	100
U-98	50	1200	10.5	300	400	400
V-6	50	10	10.5	300	700	800
U-99	25	1200	2.8	300	>700*	>700*
V-4	25	10	2.8	300	300	400
V-88	25	10	6.5	300	>400*	>400*
V-1	25	1200	10.5	300	200	700
V-7	25	10	10.5	300	300	300
V-92	100	10	2.8	250	100	100
V-93	100	10	2.8	250	300	300
V-94	100	10	2.8	200	100	100
V-95	100	10	2.8	200	100	100

*Tests still in progress.

the pH changed during a run so that after 200 to 300 hr, the pH was between 4 and 6 regardless of the initial pH.

An inspection of the data shows that all specimens cracked between the time interval from 100 to 800 hr, regardless of the initial pH (2.8 to 10.5), chloride concentration (25 to 100 ppm), and oxygen concentration (either 10 or 1200 ppm).

At 200 and 250°C, cracking appeared to occur in slightly less time and the frequency of cracking seemed to be somewhat greater than at 300°C. In addition to the tests shown in Table 12.5, sixteen specimens have been exposed to boiling aerated water containing 100 ppm chloride at a pH of 2.8 for periods in excess of 1000 hr without a single indication of cracking.

Since the data suggest the existence of a threshold temperature for the rapid initiation and propagation of cracks, tests will be carried out in the temperature range of 100 to 200°C to see if such is the case. Further testing will also include the effect of the absence of oxygen and the effect of certain chemical additives on the susceptibility of type 347 stainless steel to stress-corrosion cracking in high-temperature water.

12.2.2 Corrosion Tests with Cast Zirconium Alloys

The corrosion test program for the evaluation of zirconium-base alloys has continued. The purpose of the program, which is a cooperative effort with the HRP Metallurgy Group, is to determine the corrosion behavior of a number of binary, ternary, and quaternary alloys of zirconium and to supply corrosion specimens for the study of the oxide film structures. As a result, no attempt was made to defilm any of the specimens at the end of the test. Corrosion results from other zirconium alloys tested in this program have been reported previously.[19,20]

The corrosion environment for the present and previously reported zirconium tests consisted of oxygenated 0.04 *m* UO_2SO_4 solution containing 0.02 *m* H_2SO_4 and 0.005 *m* $CuSO_4$ at 300°C. When corrosion attack was not excessive, the tests were run for 1000 hr. Otherwise, the tests were of shorter duration. The present series of tests included zirconium specimens alloyed with platinum, tin, silver, uranium, palladium, iron, niobium, molybdenum, and manganese in various combinations. All the alloys were prepared from high-purity iodide-process zirconium. The specimens were mechanically abraded, before they were tested, on either 80 or 120 grit paper. The results of the corrosion tests are included in Table 12.6.

Three of the alloys (in wt %: 5 Pt–95 Zr, 10 Pt–90 Zr, and 5 Pd–95 Zr) exhibited very good corrosion resistance. In all three cases, the 1000-hr exposure period produced very slight weight increases, not in excess of 0.2 mg/cm^2. The appearance of the specimens was characterized by very thin, adherent, and highly lustrous black films. A single alloy in the same composition series, 10 Pd–90 Zr alloy, was severely attacked; the corrosion rate was 45.7 mpy in 1000 hr.

Other alloys that corroded excessively included: a 2 Sn–7.5 Ag–90.5 Zr alloy, which corroded at rates of 11 and 46 mpy for duplicate specimens, and a 2 Mn–98 Zr alloy, which corroded at rates of 54 and 59 mpy for duplicate specimens after 200 hr. The remaining alloys (10 U–90 Zr, 1 Fe–10 Nb–89 Zr, 5 Mo–95 Zr, 2 Sn–2 Mo–96 Zr, and 2 Sn–7.5 Nb–90.5 Zr) exhibited appreciable weight increases, ranging between 2 and 10 mg/cm^2. In these cases, the corrosion films generally were nonuniform, bulky, and relatively nonadherent.

The effect of high-temperature air-formed films on the corrosion behavior of a number of zirconium alloys will be examined during the next quarter. The films on the specimens were produced by heating in air for 3 to 5 min at a temperature of 1100°C.

12.2.3 Miscellaneous Corrosion Tests

A number of miscellaneous corrosion tests related to the HRP were completed during the past quarter. A brief resumé of the results follows. The chemical compositions of the alloys tested are shown in Table 12.7.

[19] *Ibid.*, p 93.

[20] J. C. Griess *et al.*, *HRP Quar. Prog. Rep. Jan. 31, 1957*, ORNL-2272, p 86–88.

Table 12.6. Corrosion of Cast Zirconium-Base Alloys by Oxygenated 0.04 *m* UO_2SO_4–0.02 *m* H_2SO_4–0.005 *m* $CuSO_4$ Solution at 300°C

Lab No.	Material Identity	Alloy Composition (wt %)	Specimen Treatment	Specimen No.	Total Time (hr)	Corrosion Rate
T-62	Zr-55	5 Pt–95 Zr	Abraded	1	1000	(+0.2 mg/cm^2)
				2	1000	(+0.1 mg/cm^2)
T-62	Zr-56	10 Pt–90 Zr	Abraded	3	1000	(+0.1 mg/cm^2)
				4	1000	Negligible
T-63	Zr-76	2 Sn–7.5 Ag–90.5 Zr	Abraded	1	1000	11.3 mpy
				2	1000	45.8 mpy
T-64	Zr-43	10 U–90 Zr	Abraded	1	1000	(+6.4 mg/cm^2)
				2	1000	(+10.4 mg/cm^2)
T-80	Zr-24	5 Pd–95 Zr	Hot rolled at 500°C; ground to 0.094 in. thick; abraded	1	1000	Negligible
				2	1000	(+0.2 mg/cm^2)
T-81	Zr-31	10 Pd–90 Zr	Hot rolled at 700°C; ground to 0.098 in. thick; abraded	1	1000	45.7 mpy
T-83	Zr-19	1 Fe–10 Nb–89 Zr	Abraded	1	1000	(+22.6 mg/cm^2)
T-84	Zr-23	5 Mo–95 Zr	Abraded	1	1000	(+8.8 mg/cm^2)
				2	1000	(+10.0 mg/cm^2)
T-96	Zr-39	2 Mn–98 Zr	Abraded	1	200	58.7 mpy
				2	200	53.7 mpy
T-98	Zr-78	2 Sn–2 Mo–96 Zr	Abraded	1	1000	(+2.1 mg/cm^2)
				2	1000	(+2.5 mg/cm^2)
T-99	Zr-79	2 Sn–7.5 Nb–90.5 Zr	Abraded	1	1000	(+6.5 mg/cm^2)
				2	1000	(+7.6 mg/cm^2)

(a) Surface-Hardened Type 347 Stainless Steel. – Surface-hardened type 347 stainless steels have possible HRT engineering applications, and as a result, type 347 stainless steel hardened by two different processes was corrosion tested in uranyl sulfate solutions. One hardening process, Malcomizing, was performed by the Lindberg Steel Treating Co. at Melrose Park, Illinois; the second process, designated as Thermospray 16-C, originated from the Metallizing Engineering Co. in Westbury, New York. The depth of the hardened layer on the Malcomized specimen was between 0.006 and 0.007 in.; the measured hardness was 92 on the Rockwell 15-N scale (65 on the Rockwell C scale). The Thermospray 16-C coating was approximately $\frac{1}{16}$ in. thick. The composition of the coating in weight per cent was: 2 Fe, 16 Cr, 4 Si, 4 B, 3 Cu, 3 Mo, and balance, Ni. The measured hardness of the coating varied between R_C 85 and R_C 92.

The specimens were tested at 80°C in aerated 0.04 *m* UO_2SO_4 solution containing 0.02 *m* H_2SO_4 and 0.005 *m* $CuSO_4$. The Malcomized specimen deteriorated appreciably within 3 hr from the start of the test; the corrosion rate was found to be 860 mpy. The Thermospray 16-C specimen corroded at a rate of 60 mpy during the first 150 hr. However, during the next 150-hr exposure, portions of the coating flaked from the surface of the stainless steel and the test was discontinued. The conclusion from the tests was that neither of the surface-hardening treatments for type 347

Table 12.7. Composition of Several Alloys

Alloy	Composition (wt %)						
	Ni	Cr	Fe	C	Mo	Mn	Other
Hastelloy R-235	Bal	14–17	9–11	<0.16	4.5–6.5	<1	Al, 1.75–2.25; Ti, 2.25–2.75
Multimet	19–21	20.0–22.5	Bal	0.08–0.16	2.5–3.5		Co, 18.5–21.0; Nb/Ta, 0.75–1.25; W, 2–3; N, 0.1–0.2
Timken 16-25-6	25	16	Bal	0.08–0.10	6	<2	N, 0.15
202 SS	5.18	18.00	Bal	0.09	0.31	7.85	
347 SS	9–12	17–19	Bal	0.08 (max)		2.00 (max)	Nb/Ta 10 × C (min)
414 SS	1.90	12.06	Bal	0.11	0.11	0.48	
431 SS	2.30	16.24	Bal	0.166	0.06	0.60	
431 SS	1.56	16.00	Bal	0.154	0.06	0.57	
30-14	Bal			0.08	16.5		Al, 2.45; Ti, 1.52
30-21	Bal			0.07	16.4		Nb, 4.71
30-24	Bal	6.19		0.09	17.3	0.27	Al, 0.69
30-45	Bal	7.97	7.15		16.64	0.30	Al, 0.77
420 SS		13.31	Bal	0.37		0.57	
17-4 PH SS	3–5	15.5–17.5	Bal	0.07 (max)		1.0 (max)	Cu, 3–5; Nb/Ta, 0.25–0.45
Stellite No. 6	6 (max)	27.5	3 (max)	1.15			Co, 60; W, 4

stainless steel would be suitable for HRT applications with uranyl sulfate solutions.

(b) Alternate Bolt Materials for Centrifugal Pumps. – Several alloys considered as alternate materials for the PH 17-4 and 17-7 stainless steel alloys presently used for bolting thermal barriers in the Westinghouse canned-rotor centrifugal pumps were corrosion-tested in an oxygenated 0.04 *m* UO_2SO_4–0.02 *m* H_2SO_4–0.005 *m* $CuSO_4$ solution at 300°C. The alloys included Hastelloy R-235, wrought Multimet, and Timken 16-25-6, the compositions of which are shown in Table 12.7.

The Hastelloy R-235 and Multimet alloys were heat-treated, as recommended by the vendors, for 6 hr in air at 871°C (1600°F) to improve their physical properties. The Timken alloy was tested in a hot-swaged condition. A summary of the observed corrosion rates appears in Table 12.8.

The physical condition of the specimens of the three alloys, as well as the relatively low corrosion rates obtained in the high-temperature uranyl sulfate environment, suggested that any or all of the alloys conceivably could be useful in a number of homogeneous-reactor components. The corrosion rates, after 1000 hr, were: Timken 16-25-6, 0.4 mpy; Multimet, 1 mpy; and Hastelloy R-235, 1.5 mpy. Further testing under other conditions is in progress.

Table 12.8. Corrosion Rates of Bolt Materials by Oxygenated 0.04 *m* UO_2SO_4 Solution Containing 0.02 *m* H_2SO_4 and 0.005 *m* $CuSO_4$ at 300°C

Cumulative Time (hr)	Corrosion Rate (mpy)		
	Hastelloy R-235	Multimet	Timken 16-25-6
50	5.6	2.9	1.5
150	3.2	2.3	1.1
310	2.3	1.6	1.1
614	1.6	1.1	0.6
1014	1.5	1.0	0.4

(c) Corrosion of Various Stainless Steels. – Four stainless steel alloys were subjected to a number of HRT-related environments to evaluate their corrosion resistance. The alloys included types 202, 414, and two types of 431 stainless steel; the chemical compositions of the alloys are shown in Table 12.7. The two types of 431 stainless steel were of similar composition with the exception that the nickel content of one was 1.6% and of the other, 2.3%. The corrosion-test environments were: (1) boiling and aerated 5 wt % HNO_3; (2) oxygenated 0.04 *m* UO_2SO_4–0.02 *m* H_2SO_4–0.005 *m* $CuSO_4$ solution at boiling, 200, and 300°C temperatures; and (3) boiling and aerated 1.33 *m* UO_2SO_4 solution. A summary of the corrosion rates determined from defilmed weight losses on the specimens appears in Table 12.9. Frequently, because of unusually severe corrosion attack, the tests were terminated after short periods of time.

Type 202 stainless steel exhibited excellent corrosion resistance in all the environments; the observed corrosion rates after 1000 hr were not in excess of 1 mpy. In fact, in the boiling environments, the corrosion rates were 0.1 mpy and less. The corrosion resistance of type 202 stainless steel was essentially the same as that observed for type 347 stainless steel under the same conditions.

The over-all corrosion behavior of the three 400 series stainless steels was poor in all environments. The magnitude of the reported corrosion rates in Table 12.9 demonstrates the unsuitability of these alloys for applications involving contact with either nitric acid or uranyl sulfate solutions.

(d) Corrosion of In-Pile-Loop Valve-Stem Materials. – Twelve type 420 stainless steel valve stems designed for use in valves to be used with in-pile loops were subjected to acidified uranyl sulfate solutions to determine their corrosion resistance. Universal Cyclops Steel Corporation supplied the valve stems, and they were hardened to R_C 50 to R_C 52 by Autoclave Engineers. The stems were exposed to either 0.17 or 0.04 *m* UO_2SO_4 containing 0.03 *m* $CuSO_4$ and either 0.04 or 0.4 *m* H_2SO_4. The test temperatures were either 25 or 90°C.

At 90°C, all valve stems, except one, corroded at the rate of 1000 to 2300 mpy, regardless of solution composition; with a solution containing 0.04 *m* UO_2SO_4, 0.04 *m* H_2SO_4, and 0.03 *m* $CuSO_4$ at 90°C, one specimen corroded at 187 mpy, whereas its duplicate corroded at 1080 mpy.

At 25°C, corrosion rates were considerably lower. With 0.17 *m* UO_2SO_4 and 0.03 *m* $CuSO_4$ containing either 0.04 or 0.4 *m* H_2SO_4, corrosion rates of 0.5 to 0.6 mpy were observed. With 0.04 *m* UO_2SO_4 and 0.03 *m* $CuSO_4$ containing

Table 12.9. Corrosion of Various Stainless Steels in Several HRT-related Environments

Stainless Type	Cumulative Time (hr)	Corrosion Rate (mpy)				
		5 wt % HNO_3 Boiling	HRT Core Solution			1.33 *m* UO_2SO_4 Boiling
			Boiling	200°C	300°C	
202	100	<0.1	<0.1	3.5	0.3	<0.1
	500	<0.1	<0.1	0.9	0.2	<0.1
	1000	0.1	<0.1	0.9	0.4	<0.1
414	100	1500	700	250	141	480
431 (1.6 Ni)	100	2.0	1.0	Gain*	103	1.4
	500	4.0	2.5			4.4
	1000		3.7			9.1
431 (2.3 Ni)	100	35	2.5	14.0	134	3.7
	500	11	6.8	3.1		9.6
	1000			1.7		

*Specimens continued to show weight increase after two successive cathodic defilming treatments.

0.04 *m* H_2SO_4, the corrosion rate was 0.3 mpy; with the same solution, but containing 0.4 *m* H_2SO_4, the rate was 9.1 mpy.

From the above results, it is obvious that type 420 stainless steel is not sufficiently corrosion resistant to acidified uranyl sulfate solution at 90°C to be practical. At 25°C and lower, type 420 stainless steel has adequate corrosion resistance, provided that the acid concentration does not exceed 0.04 *m* in 0.04 *m* UO_2SO_4 or 0.4 *m* in 0.17 *m* UO_2SO_4.

As a result of the poor corrosion resistance shown by type 420 stainless steel, two type 17-4 PH stainless steel valve stems and four pins of Stellite No. 6 were subjected to the solution which was most corrosive to type 420 stainless steel, namely, 0.04 *m* UO_2SO_4, 0.4 *m* H_2SO_4, and 0.03 *m* $CuSO_4$ at 90°C. The 17-4 PH valve stems corroded at rates of 0.6 and 0.8 mpy, and the corrosion rate of the Stellite No. 6 pins varied between 0 and 0.2 mpy. Thus it is obvious that from only the corrosion standpoint, either Stellite No. 6 or 17-4 PH would be a better choice than type 420 stainless steel in the acidified uranyl sulfate solution.

(e) Corrosion of Nickel-Molybdenum Alloys. – Four nickel-molybdenum alloys designated as 30-14, 30-21, 30-24, and 30-45 (composition shown in Table 12.7) were corrosion tested in a boiling solution containing 0.04 *m* UO_2SO_4, 0.02 *m* H_2SO_4, and 0.005 *m* $CuSO_4$. Tests were continued for only 200 hr because all alloys showed high corrosion rates. The corrosion rates were 146 mpy for 30-14, 81 mpy for 30-21, 121 mpy for 30-24, and 29 mpy for 30-45. Further corrosion testing with these alloys is not anticipated.

13. SLURRY CORROSION

E. L. Compere
S. R. Buxton
H. D. Cole[1]
S. A. Reed
H. C. Savage
J. A. Russell, Jr.
W. C. Ulrich
R. M. Warner

13.1 PUMP LOOPS

13.1.1 Loop Engineering: Venturi Installation and Performance

(a) 100A Loop BS. – Two calibrated venturis were installed in Loop BS (ref 2) as an aid in monitoring the density and/or changes in flow rate of the circulating thorium oxide slurry. One venturi, identical to that previously installed in 100A loop CS (ref 3), was placed in the pump suction line; the other venturi was installed in the ½-in.-pipe pressurizer mixing line. Piping was arranged to permit flushing of the venturi pressure taps with loop condensate water, either directly from the condensate tank through the pressure taps or from the condensate tank via the Pulsafeeder through the pressure taps. The condensate may be adjusted to flow continuously through the pressure taps or to flow through the taps only when it is desired to flush them out. Experience with the venturis already installed and operated in 100A loop CS has shown that an intermittent flushing of the venturi pressure taps is usually sufficient to prevent plugging of the lines during operation.

The addition of these two venturis increased the horizontal length of loop BS by 15 in. At present, the system is undergoing final tests prior to startup on thorium oxide slurry after installation of the venturis.

(b) 100A Loop CS. – Loop CS was operated with the pump-suction-line venturi in place for a total of 827 hr on slurry during runs CS-34 (ref 3) and CS-35. After run CS-35, a second calibrated venturi was installed in the ½-in.-pipe pressurizer mixing line, and the loop was operated with both venturis for 509 additional hours on slurry during runs CS-36, CS-37, and CS-38. Circulating slurry concentrations varied from 456 to 716 g of thorium per kilogram of water during these runs.

The venturis were operated continuously during all runs and performed satisfactorily. Although it is possible to provide continuous flushing-water flow through the pressure taps to prevent their becoming plugged with slurry, they were flushed only once each day. Plugging occurred only once in 1336 hr of operation with slurry. The plugging is believed to have been caused by improper operating procedure, which has since been corrected. The plug was removed by flushing the pressure taps with loop condensate, which was routed through the Pulsafeeder, and the lines were cleared without interrupting the run.

13.1.2 100A Pump Loop Tests: Introduction

During the quarter, seven slurry corrosion test runs were made at 300°C in 100A pump loops BS and CS. In one test, of 579 hr duration, in loop BS, an oxygenated slurry prepared from 550°C-calcined thoria was circulated at an average concentration of 404 g of thorium per kilogram of water. Rapid attrition of the thoria particles occurred early in the test. Corrosion rates and pump wear were moderate. In two other tests in loop BS, one of 100 hr duration and the second of 250 hr duration, slurries prepared from 1600°C-calcined thoria were circulated, with oxygen addition, at average circulating concentrations of 740 and 408 g of thorium per kilogram of water, respectively. The thoria, which had a mean particle size of 1.3 μ, underwent no detectable degradation during the tests. In both runs, attack rates were low.

In loop CS, a 311-hr test employing previously circulated, 800°C-calcined thoria slurry was made at 300°C with hydrogen and hydrazine additions at an average circulating concentration of 583 g of thorium per kilogram of water. Specimen corrosion rates were moderate, but severe localized

[1] At present on National Science Foundation Fellowship, University of Texas.

[2] E. L. Compere *et al.*, *HRP Dynamic Slurry Corrosion Studies: Quarter Ending April 30, 1956*, ORNL CF-56-4-139, Fig. 1.1.2, p 11.

[3] E. L. Compere *et al.*, *HRP Quar. Prog. Rep. April 30, 1957*, ORNL-2331, p 96.

attack of the stainless steel pump and impeller occurred.

Two additional runs in loop CS were made at 300°C with oxygenated slurry prepared from 650°C-calcined thoria. The target concentration for each test was 1000 g of thorium per kilogram of water. In both runs, soft slurry plugs formed in low-velocity sections of the loop system when the loop charge concentration reached 700 to 800 g of thorium per kilogram of water. The tests were stopped after 13 hr and 196 hr, respectively.

Circulated in a fourth test in loop CS was an oxygenated slurry prepared from 800°C-calcined thoria which had been passed twice through a Mikro-pulverizer to provide a mean particle size of 1 μ. Attack rates of specimens exposed during the 300-hr test were in good agreement with rates observed in previous tests with 800°C-calcined thorium oxide slurries; however, the front hub of the pump impeller and the associated seal rings, which were fabricated of stainless steel, were badly abraded.

In loop BS, tests have been continued to study the effect of thorium oxide calcination temperature and particle size on attack rates and handling properties of circulating aqueous thoria slurries.

It has been shown in pilot tests in toroids that metal attack rates decrease with diminishing size of the thoria particles in a circulating aqueous slurry.[4,5] Further, the calcination temperature of the thorium oxide appeared to have little effect on the corrosivity of a slurry when small-particle-size thoria was used.[4,5] Tests in pump loops have shown that a rapid decrease in the rate of attack by slurries occurs after the thoria particles are degraded during circulation and that the degradation rate of the thoria particles is dependent, at least in part, on the calcination temperature of the thorium oxide.[6]

A systematic study of these variables, as well as the effect of slurry concentration and slurry flow velocity, is now being made in the 100A pump loops.

[4] E. L. Compere *et al.*, *Dynamic Slurry Corrosion Studies: Quarter Ending January 31, 1956*, ORNL CF-56-1-168, p 33.

[5] E. L. Compere *et al.*, *HRP Quar. Prog. Rep. Oct. 31, 1956*, ORNL-2222, p 81.

[6] E. L. Compere *et al.*, *HRP Dynamic Slurry Corrosion Studies: Quarter Ending April 30, 1957*, ORNL CF-57-4-139 (to be issued).

13.1.3 Circulation of 550°C-Calcined Thoria Slurry

Slurry prepared from 550°C-calcined thoria was circulated at an average concentration of 404 g of thorium per kilogram of water at 300°C with oxygen addition for 579 hr in run BS-14. The ORNL-produced thorium oxide, batch LO-17, was made by precipitating thorium nitrate with oxalic acid at 70°C and firing for 24 hr at 550°C. The mean particle size of the material was 4.7 μ.

Three sets of pin corrosion specimens were exposed during the test at relative flow velocities, measured on water at room temperature, of 10, 21, and 31 fps. Slurry was charged to the loop while it was operating on water at 300°C.

Major degradation of the thoria particles occurred during the first 2 hr of the test. After 2.1 hr of circulation, the mean particle size, measured by sedimentation analysis, had diminished from 4.7 μ to 1 μ, and after 18 hr of circulation, to 0.4 μ. No further detectable attrition occurred. System attack rates during these periods, calculated from chemical analyses of the slurry samples and the circulating inventory at run hours 2.1 and 18, were 13.6 and 4.9 mpy, respectively. Thereafter, the differential attack rates dropped gradually to a final 0.8 mpy.

Corrosion rates of the 42 pin specimens exposed during this test were low. Values are shown in Table 13.1.

Wear of pump components during the 579-hr test was minor.

13.1.4 Circulation Tests with 650°C-Calcined Thoria Slurry

Two tests, runs CS-36 and CS-37, were made during the quarter in an attempt to circulate a 650°C-calcined thoria slurry at a concentration of 1000 g of thorium per kilogram of water.

In several earlier runs[7] with slurries of 650°C-calcined thoria, soft plugs and/or heavy deposits of thoria were formed in the test loop before a concentration of 1000 g of thorium per kilogram of water was attained. Since that time, major modifications in loop CS geometry have been made and a different slurry loading technique

[7] J. C. Griess *et al.*, *HRP Quar. Prog. Rep. July 31, 1955*, ORNL-1943, p 64.

Table 13.1. Corrosion by Circulating Thorium Oxide Slurries in Loop Tests at 300°C

	Run Number						
	BS-14	CS-36	CS-37	CS-35	CS-38	BS-15	BS-16
Hours	579	13	196	311	300	100	250
Concentration, g Th/kg H_2O							
Load	462	1046	795	531	590	408	593
Average	404	716	456	583	591	740	408
Calcination temperature, °C	550	650	650	800	800 micro-pulverized	1600	1600
Thoria batch No.	LO-17	LO-18	LO-18 from CS-36	LO-2A from CS-32-34	LO-27	TO-10-1600	TO-10-1600
Additives	None	None	None	0.02 m N_2H_4	None	None	None
Atmosphere	O_2 + A	O_2 + A	O_2 + A	H_2 + A	O_2 + A	O_2 + A	O_2 + A
Average particle size, μ							
Prerun	4.7	3.3	0.6	0.6	1.0	1.3	1.3
Postrun	0.4	0.6	0.5	0.9	0.5	1.3	1.3
Impeller weight loss, g	5	1.5	19	55 (pits)	31 (hub pits)	1	0
Loop corrosion rate, mpy	0.8	1	4	18	4.5	1.0	1.2
Range of pin attack rates, mpy, at given flow velocity							
Velocity,* fps						*	*
Austenitic Stainless Steels							
10–15	2–4			0.1–0.3		0.9–1	0.8
18–25	3–5		2–3**	Coupon 0–0.1	1–2	3–4	3
30–35	4–9			0.2–0.3		3–6	3
40–50			6–12**	16–39	3–11		
Carbon Steels							
10–15				5–7			
20–25			13–22**	Coupon 3–4	13–16		
30–35				4–7			
40–50			29–44**	11–24	13–18		
Titanium Alloys							
10–15	1–2					0.6–1	0.7
20–25	2–3		0 (coupon)**	0.1 (coupon)	0 (coupon)	5–6	4
30–35	2–4					5–6	5
40–50							

Table 13.1 (continued)

	Run Number						
	BS-14	CS-36	CS-37	CS-35	CS-38	BS-15	BS-16
				Zirconium Alloys			
10–15	0.7–0.8			0		0	0
20–25	1		1**	0	0.7	0.7	0.3
30–35	2			0		1	0.5
40–50			4–6**	2	3		
				Gold and Platinum			
10–15	0.1–0.2			0–0.2		0.5	0.3–0.4
20–25	0.2–0.4		0–0.3**		0.3–0.4	3–5	3–5
30–35	0.3–0.6			0		4–7	4–6
40–50			2–3**	0.1–0.7	1–2		

*Velocities for runs BS-15 and BS-16 higher by factor of 2 for approximately last half of the run.

**Total specimen exposure, 209 hr: runs CS-36 and CS-37.

has been developed.[8,9] Therefore it was of interest again to test such a slurry.

Batch LO-18 thoria was used. It was prepared at ORNL in the usual manner by precipitating thorium nitrate at 70°C with oxalic acid and then firing at 650°C for 24 hr. One successful run had been made previously with this material in loop BS (ref 8) at an average circulating concentration of 478 g of thorium per kilogram of water.

For run CS-36, flow velocities in loop CS were maintained at normal levels. In the three headers to the parallel sample barrels the velocities, measured with water at room temperature, were: header to barrel No. 1, 4 fps (23 gpm); header to barrel No. 2, 10 fps (53 gpm); and header to barrel No. 3, 1 fps (6 gpm). Flow through the bypass mixing line was 19 fps (14 gpm). All flow measurements were made with the circulating pump operated at 3600 rpm on 60-cycle current.

After a 43.6-hr checkout period at 300°C with oxygenated water, slurry charging was begun. Thoria was added in three increments. The first charge contained 6.4 kg of thoria, the second 6.4 kg, and the third 6.7 kg. The additions were made without difficulty over a period of 8.5 hr. Net system inventory after the final addition was 19.5 kg of thorium oxide (17.2 kg of thorium) and 16.4 kg of water, which provided a charge concentration of 1046 g of thorium per kilogram of water.

Characteristic increases in pump power demand and venturi differential pressure were noted during the first two additions. The calculated slurry concentration after the second addition was 680 g of thorium per kilogram of water. Corresponding increases did not occur during the third addition.

A sample withdrawn from the loop main stream 8.9 hr after the final addition contained, by chemical analysis, 783 g of thorium per kilogram of water. At that time, readings of thermocouples attached to barrels No. 1 and 3 and the mixing line had dropped from 300°C to 295, 272, and 296°C, respectively, which indicated reduced flow and probable deposition of thoria in these lines.

A second sample, taken after 12.8 hr of slurry circulation, contained only 648 g of thorium per kilogram. During the 4-hr period between samples, the temperature of the mixing line had dropped to 184°C and that of No. 3 barrel to 214°C. System

[8] E. L. Compere *et al.*, *HRP Quar. Prog. Rep. April 30, 1957*, ORNL-2331, p 96.

[9] E. L. Compere *et al.*, *HRP Quar. Prog. Rep. April 30, 1956*, ORNL-2096, p 87.

pressure declined from 1545 to 1300 psig. Consequently, the run was terminated at slurry circulation hour 13.

When the system had cooled to room temperature, the loop was drained and was rinsed with 60 gal of water, by using the pump. The system was then disassembled for routine inspection.

A heavy thoria sludge was found in the No. 1 and No. 3 barrels and in the adjoining headers upstream of the specimens holders. Neither line was completely blocked. The No. 2 barrel was relatively clean, except for a thin film of pasty slurry which adhered to the pipe walls. There was no slurry in the lower half of the mixing line, which extended from the loop main stream to the metering orifice. Downstream of the metering orifice, the entire length of pipe which extended to the pressurizer was completely filled with a damp chalky deposit of solids. No other deposits were found.

Because of the short slurry circulation period, corrosion specimens were not removed from the system. They were exposed for an additional 196.2 hr in run CS-37 which is described below.

The system corrosion rate, calculated from the loop inventory and corrosion ions detected in the two samples taken during the 13-hr test, was 1.0 mpy.

System flow velocities were readjusted for run CS-37 in an effort to relieve plugging problems. In the header to barrel No. 1, the velocity remained at 4 fps; in the header to barrel No. 2, it was reduced from 10 fps to 9 fps; and in the header to barrel No. 3, it was increased from 1 fps to 4 fps. The mixing-line velocity was changed from 19 fps to 23 fps.

An 85-hr checkout run at 300°C with oxygenated water was made before slurry charging was begun. Batch LO-18 slurry which had been removed from run CS-36 was recharged to the loop. As a possible preventative to sudden deposition of solids in the system, six slurry charges were made over a period of 194 hr to afford a gradual increase in thoria concentration.

The results of this procedure are presented graphically in Fig. 13.1, in which is shown a comparison of pump power and venturi differential pressure with slurry concentration.

The concentration of samples withdrawn from the system agreed reasonably well with the calculated charge concentration, until the fifth slurry addition. After that time, sample concentrations were about 25% below the calculated load concentration. Corresponding decreases in venturi readings were also observed.

At slurry circulation hour 193, charging of the sixth slurry addition was begun, to increase the charge concentration to 1000 g of thorium per kilogram of water. Within 10 min after charging was started, readings of thermocouples attached to the No. 1 and No. 3 sample barrels and the bypass mixing line dropped markedly, which indicated that thoria deposition probably had occurred in these components. During the following 30-min period, system operation became so erratic that it was necessary to terminate the run. The final load concentration reached 795 g of thorium per kilogram of water. The total slurry circulation time was 196.2 hr.

After the loop was drained and rinsed, slurry deposits were found in the same sections of the system as in the previous test, run CS-36. The lines, none of them completely blocked, contained heavy soft sludges, which adhered tenaciously to the pipe walls.

Attack rates of the specimens exposed in runs CS-36 and CS-37 were mild. Values are shown in Table 13.1.

Average corrosion rates of the austenitic stainless steels were from 2 to 4 mpy over the velocity range of 10 to 30 fps and 6 to 12 mpy over the velocity range of 39 to 46 fps. Mild steels exposed at the same velocities displayed rates from 13 to 32 mpy and from 29 to 44 mpy, respectively. Corresponding rates for Zircaloy-2 were 1 to 2 mpy and 4 to 6 mpy, respectively.

The average corrosion rate of the loop, calculated from corrosion products detected in slurry samples and system inventory, was 4 mpy. The type 347 stainless steel impeller used in the tests lost 19 g.

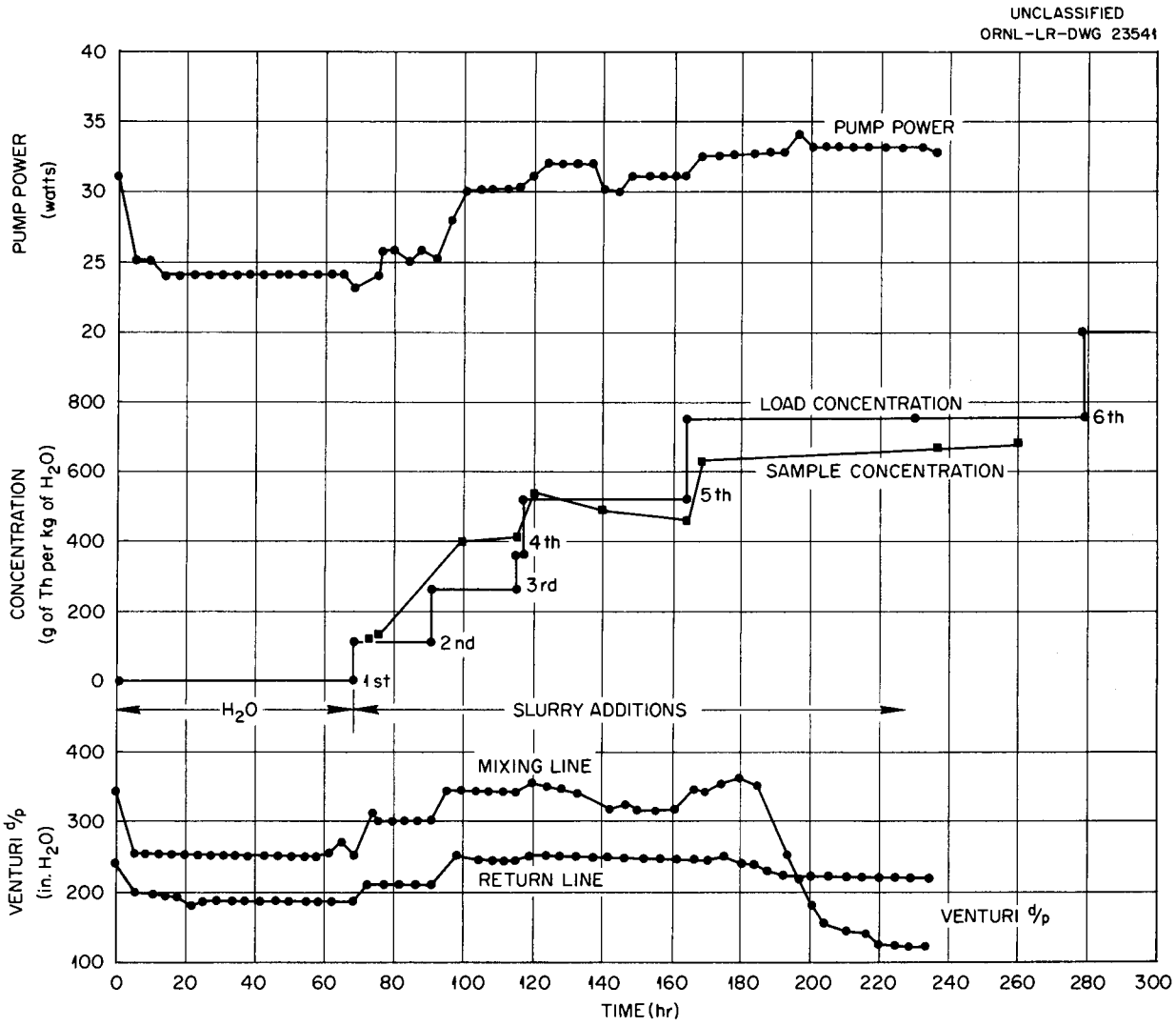

Fig. 13.1. Comparison of Pump Power and Venturi *d/p* with Slurry Concentration for Run CS-37.

13.1.5 Attack by Circulating Slurries in Hydrogen Atmosphere

The results of three previous runs with hydrogenated slurries have been reported.[10,11] During the report period, a fourth circulation test, run CS-35, was completed. Slurry which had been pumped previously (runs CS-32, -34) for 566 hr in a test loop was recirculated at 300°C in run CS-35 for 311.4 hr at an average concentration of 583 g of thorium per kilogram of water. The previous circulation had degraded the 800°C-calcined thoria, batch LO-2A, to a mean particle size of 0.6 μ.

Initially, the loop was charged with the appropriate volume of water and then alternately evacuated and purged with argon to remove residual air in the system. Ten milliliters of 85% hydrazine hydrate was then injected into the loop to destroy traces of oxygen dissolved in the water. The quantity of hydrazine added, approximately 400 ppm, was a twentyfold excess over the calculated quantity needed to react with dissolved and residual gaseous oxygen. Then 120 psig of hydrogen

[10] E. L. Compere *et al.*, *HRP Dynamic Slurry Corrosion Studies: Quarter Ending April 30, 1957*, ORNL CF-57-4-139 (to be issued).

[11] E. L. Compere *et al.*, *HRP Quar. Prog. Rep. April 30, 1957*, ORNL-2331, p 96.

and 80 psig of argon were charged to the system at room temperature.

After a 23-hr checkout period at 300°C on hydrogenated water, two batch additions of previously pumped LO-2A slurry were charged to the loop. With each charge, an additional 5 ml of hydrazine hydrate was added.

The test was scheduled to run 1000 hr; however, it was shut down after a total of 311.4 hr of slurry circulation because of a sharp increase in pump power demand.

The average circulating slurry concentration during the test, determined by chemical analysis of samples withdrawn from the loop, was 583 g of thorium per kilogram of water. Room-temperature pH values of the slurry samples ranged from 9.8 to 10.0. Hydrogen concentration, based on slurry, averaged 59 μg/ml.

Sixty-four pin corrosion specimens and 20 coupon specimens were exposed in the test at relative velocities of 10 to 52 fps. Corrosion rates of representative groups of specimens are shown in Table 13.1.

Moderate corrosion rates were observed with pin specimens exposed at 10 and 30 fps and with coupon specimens exposed at 18 fps.

Corrosion rates of stainless steel pin specimens exposed at 40 fps were about twofold higher with the hydrogenated slurry than with oxygenated slurry in the otherwise comparable test, run CS-34 (ref 10). Carbon-steel specimens exposed in the hydrogenated slurry corroded about 10% less than duplicate specimens in oxygenated slurry.[10]

Armco iron coupon specimens exposed in a variable-velocity holder displayed rates from 4.5 to 7.0 mpy over the velocity range 6 to 33 fps. The trailing coupon, with a velocity profile of 41 to 52 fps, corroded at the rate of 140 mpy. Entrance effects were marked on the first two coupons in the specimen holder.

The slurry attack rates of stainless steels and carbon steels (or iron) under a hydrogen atmosphere are indicated to become accentuated and similar above a threshold at about 40 fps in this run.

In addition to the above materials, specimens, each stressed to approximately 80% of yield stress at 300°C, of types 347 and 350 AM stainless steels, titanium–6A1–4V alloy, and Zircaloy-2 were exposed in the vapor space of the loop pressurizer. By microscopic examination, no pits or cracks were detected in the four stressed specimens.

The average system attack rate, calculated from corrosion products in slurry samples and circulating slurry inventory, during run CS-35 was 18 mpy. From chemical analytical data, a total of 128 g of iron, chromium, and nickel was calculated to be in the circulating slurry. The corrosion ions were largely due to the excessive localized attack which occurred in the circulating pump. The front seal rings were badly attacked, and the impeller housing was deeply pitted. Each was fabricated from type 347 stainless steel. Attack of the type 347 stainless steel impeller was mainly localized at the periphery of the intake port, adjacent to the front wear rings. The impeller lost 55 g during the test.

The eroded areas of the pump head and pump suction line are shown in Figs. 13.2 and 13.3, respectively. Pit depths ranged from 0.13 to 0.18 in.

Circulation properties of the slurry were quite satisfactory during the run. After the system was drained and rinsed, no deposits were found. The particle distribution, measured by sedimentation analysis, was changed little during circulation, and no attrition was observed.

Fig. 13.2. Erosion in Pump Head; Slurry Run CS-35.

Fig. 13.3. Attack on Pump Suction Line; Slurry Run CS-35.

13.1.6 Attack by Micropulverized Thoria Slurry

One test was completed during the quarter in which slurry prepared from batch LO-27 thorium oxide was used. This oxide was prepared at ORNL by precipitating thorium nitrate with oxalic acid at 70°C and calcining at 800°C for 4 hr. The dry powder was then passed twice through a Mikro-pulverizer; after pulverization, the thoria had a mean particle size of 1 μ. It was hoped that such a treatment would eliminate the particle-size reduction, with its attendant corrosion, that is ordinarily encountered in the initial period of loop runs.

An aqueous oxygenated slurry of this thoria was circulated in run CS-38 at 300°C for 299.8 hr at an average circulating concentration of 591 g of thorium per kilogram of water. Slurry concentration during the course of the run was relatively constant; variation in circulating slurry concentration, determined by chemical analysis of 14 samples taken during the test, was less than 10%.

To attain the desired concentration, two charges of thoria were injected into the loop during operation at 300°C. Operational performance during the entire test was satisfactory.

It was of interest to follow the change in particle size of the thoria during circulation, especially during the first 10 hr of the test. For this purpose, samples were withdrawn from the loop at 30-min intervals, beginning with the first addition of slurry. Eleven such samples were taken, and these, along with 13 subsequent samples taken during the remainder of the run, were submitted for particle-size analysis.

Little detectable attrition was observed until circulation hour 71, 65 hr after the final addition of thoria to the loop. At that time, the mean particle size had diminished to approximately 0.9 μ. The mean particle size of the thoria in the final sample, withdrawn from the loop after 299.7 hr of circulation, was 0.5 μ.

No notable differences in specimen attack rates were observed with the thoria slurry ground in a Mikro-pulverizer as compared with unground thoria prepared in the same way. Rates obtained over a velocity range of 22 to 77 fps with both pin and coupon specimens of the austenitic stainless steels, mild steels, Zircaloy-2, titanium alloys, and noble metals closely paralleled rates observed in previous tests with oxygenated slurries of 800°C-calcined thoria at this concentration. Values for run CS-38 are shown in Table 13.1.

Differential loop attack rates, based on corrosion products detected in slurry samples and circulating inventory, ranged from 20 to 3.7 mpy during the first 22.5-hr period of the run, mostly being 15 to 20 mpy. After that time, a gradual downward trend to a final rate of 1.8 mpy was observed. The average loop attack rate for the 299.8-hr test was 4.5 mpy.

Pump component wear was not excessive with the exception that the type 347 stainless steel impeller lost 31 g during the test. Attack was mainly localized along the front hub of the impeller adjacent to the wear rings in the pump head. Wear of the front and rear Graphitar bearings and 98M2 Stellite journals was negligible. The type 347 stainless steel front and rear seal rings wore 0.0015 and 0.0075 in., respectively.

13.1.7 Circulation of 1600°C-Calcined Thoria Slurry

A 100-hr test, run BS-15, and a 250-hr test, run BS-16, were made at 300°C with slurry prepared from a special pilot lot of thorium oxide which had been calcined at 1600°C. The oxide was made at ORNL by precipitation of thorium nitrate with oxalic acid at 10°C in small laboratory batches, with initial calcination for 4 hr at 1000°C. The 10°C precipitation step in the preparation of the thorium oxalate produced an oxide with a mean particle size of 1.3 μ.

Before loop tests were made, portions of this preparation were recalcined at 1200, 1400, and 1600°C, respectively, for an additional 4 hr. Slurries of the original material and of the recalcined oxides were then circulated in toroids[12] to evaluate the most suitable temperature at which to recalcine the entire batch for loop circulation studies. Approximately equal attack rates were observed in all tests, although slightly lower rates resulted with the 1600°C-calcined thoria slurry. Consequently, the batch was recalcined for 4 hr at 1600°C.

Moderate sintering occurred when the thoria was recalcined. Therefore the concentrated slurry prepared for loop loading was homogeneized in a laboratory Waring Blendor for 2 hr before charging.

For run BS-15, the loop was charged to a concentration of 408 g of thorium per kilogram of water while the system was operated on water at 300°C. No difficulty was encountered while charging the loop.

Operation proceeded normally for the first 63-hr period of the test, with little variation in circulating concentration. However, an erratic period of operation followed which was attributed to leakage of steam from the system. During this time, the circulating concentration, determined by chemical analysis of samples withdrawn from the loop, reached 1288 g of thorium per kilogram of water. The test was terminated after 100 hr of slurry circulation, at which time the liquid level in the loop had decreased, because of leakage, to a point where system operation could not be controlled. After the run had been stopped, the slurry resuspended easily when water was added and the pump was started. The slurry was then readily removed from loop.

Three sets of pin corrosion specimens were used in the test. During the 63-hr period of normal operation, the centrifugal pump was operated at about half-speed (1825 rpm) on 35-cycle current provided by a motor-generator set. Relative flow rates over the specimens during this period of operation were, respectively, 10, 21, and 31 fps. After operation became erratic, the rotational speed of the pump was changed to increase the bulk flow of slurry throughout the system. For an 8-hr period, the pump was run on 45-cycle current, during which time flow velocities across the specimens were 15, 30, and 40 fps, respectively. There was an additional 28-hr period, with pump operation on 60-cycle current, when the slurry velocity over the specimens was 24, 48, and 68 fps, respectively.

There was no evidence of erosive attack by the slurry. All specimens, the loop system, and the pump were covered with a thin, adherent protective corrosion film. The type 347 stainless steel impeller in the circulating pump lost 1 g. There was no detectable wear of the Graphitar bearings, Stellite journals, or type 347 stainless steel seal rings used in the pump. The system differential corrosion rate, calculated from corrosion products detected in slurry samples and circulating inventory, showed a gradual downward trend in the course of the run from 3.5 to 1.0 mpy.

Attack of all specimens was mild. Values are shown in Table 13.1.

By sedimentation analysis, no detectable attrition of the thoria particles occurred during the run.

The same slurry was recirculated in run BS-16. In this test, the system was charged to a concentration of 593 g of thorium per kilogram of water. The average circulating concentration for the 250-hr test was 408 g of thorium per kilogram of water.

As in run BS-15, erratic loop operation prevailed during much of the test and was attributed to a recurring leak apparently in the vapor region of the loop. Thus wide variations in the circulating concentration resulted.

For the first 21-hr circulation period, when operation was normal, the concentration of samples withdrawn from the system was quite constant.

[12] E. L. Compere *et al.*, *HRP Dynamic Slurry Corrosion Studies: Quarter Ending April 30, 1957*, ORNL CF-57-4-139 (to be issued).

After approximately 80 hr of circulation, system operation became very unsteady. In the run, the average circulating concentration of slurry from hour 81 through hour 98, at which time the system was temporarily shut down, was 938 g of thorium per kilogram of water.

The system was cooled to room temperature and pressurized with helium for leak checking. After no leaks were located with a helium leak detector, the liquid volume of the loop was estimated by injecting water into the system until the liquid level reach a calibrated section of the pressurizer. The estimated volume loss was 4.5 liters.

Because no leaks could be located in the system at room temperature, it appeared probable that leakage occurred only at operating temperatures and pressures. Based on the estimated volume loss, the liquid level in the system was adjusted to the initial charge volume. The test was then continued.

The slurry, which had remained quiescent in the system for 50 hr, was readily resuspended. A sample withdrawn from the loop after a 4-hr circulation period, during which time the system was being heated to 300°C, contained by chemical analysis 503 g of thorium per kilogram of water. This agreed well with calculated values based on the assumption that no thoria had been lost in the leak. The test was continued for an additional 149 hr in an effort to locate the leak. Operation was on manual control during most of the period. When it was no longer possible to keep the thoria in suspension, the run was stopped. The total slurry circulation period was 250 hr.

After the system was cooled to room temperature, make-up water was again added. The pump was then run for an additional 10 min at room temperature to check the resuspension characteristics of the slurry. The sample withdrawn from the loop mainstream valve after 10 min of circulation contained 523 g of thorium per kilogram of water, in good agreement with the calculated value, indicating essentially complete resuspension.

Attack rates were low in run BS-16, as shown in Table 13.1, and in good agreement with rates obtained in the previous test. Again, in run BS-16, pump rotational speed was changed during periods of operational instability. Specimen flow rates varied accordingly. The pump was operated on 35-cycle current for 107 hr, during which time flow velocities across the pin specimens were 10, 21, and 31 fps, respectively. The pump was operated on 60-cycle current for a total of 143 hr; corresponding velocities then were 24, 48, and 68 fps.

The average system attack rate for the 250-hr period was 1.2 mpy. There was no detectable attack of pump components other than the front type 347 stainless steel seal rings, which wore 0.007 in.

No detectable attrition of the thorium oxide was noted. The slurry, samples of which were quite fluid, appeared to be more nearly Newtonian than do slurries prepared from oxides fired at lower temperatures. The slurry appeared to settle rapidly at room temperature to a fairly loose bed, which then settled only very slowly and was easily resuspended after an extended period of settling.

Generally, despite system operational difficulties, the handling properties of the slurry of 1600°C-calcined thoria were good. Unlike lower-calcined preparations which have been tested, the slurry did not adhere to the walls of the loop piping or the cavity of the circulating pump. No cakes or deposits of any sort were found in the system. In both runs, over 95% recovery of slurry from the system was effected by five water rinses at room temperature by using the pump. In addition, in the three cases noted above, resuspension was found to be very easy.

13.2 TOROIDS

During the quarter, a series of tests was made to determine the effect of the addition of sodium silicate on the corrosiveness and circulation properties of aqueous thorium oxide slurries. With slurries prepared of 1600°C-calcined thoria, increased corrosion of type 347 stainless steel and 75A titanium resulted with oxygenated slurries containing 1000 to 15,000 ppm SiO_2 (based on thoria) added as sodium metasilicate. Slightly-higher-than-usual rates were observed for Zircaloy-2. Except in one test, corrosion of SA-212 B mild steel was lessened by the addition of silicate.

Low attack rates were observed in tests in which were circulated slurries of special preparations of thoria spheres of 5 μ and 85 μ mean diameter. The larger material was degraded during circulation in toroids, whereas the integrity of the 5-μ spheres was quite good.

Attack rates of hydrogenated and oxygenated slurries of a special ORNL preparation of thorium-uranium oxide were low. In the tests involving the incorporation of 0.005 *M* MoO_3, a proposed recombination catalyst, this substance appeared to be a mild corrosion inhibitor.

In a toroid test of 1026 hr total duration with an oxygenated, previously circulated slurry, corrosion rates of selected alloys decreased with increasing exposure. Some specimens were removed after 308 hr of exposure and replaced by new specimens subsequently exposed 718 hr; others in another toroid remained in test for the entire 1026 hr. Each material was compared with similar specimens exposed in duplicate tests using oxygenated water.

13.2.1 Corrosion by Thoria Slurries with Silicate Additives

A series of tests has been initiated to make a systematic study of the addition of silicate on the corrosiveness and circulation properties of aqueous slurries in toroids. Variables to be investigated are thorium oxide calcination temperature, silicate concentration, Na/Si ratio, pH, and gaseous atmosphere.

One series of tests has been made to determine the effect of silicate concentration on the corrosion of selected materials by slurries of 1600°C-calcined thoria. The results of these tests are shown in Table 13.2. Each 300-hr test was made at the standard conditions: 250°C, 26 fps, 50 psi oxygen (at room temperature), with slurries which contained 1000 g of thorium per kilogram of water. Silicate was added as sodium metasilicate, $Na_2SiO_3 \cdot 9H_2O$.

Generally, with the exception of SA-212 B mild steel, attack increased with the addition of sodium silicate. In particular, attack rates of 75A titanium specimens were excessive when silicate levels were 5000 ppm and above. With SA-212 B steel, lower attack rates were observed with silicate-treated slurries containing 1000 to 5000 ppm and 15,000 ppm SiO_2; however, excessive attack was noted with 10,000 ppm SiO_2. It is probable that the effect of pH and gaseous atmosphere, which are to be investigated, may considerably alter the corrosion pattern with these materials.

Interesting changes in slurry properties were observed in these tests. In the runs without silicate additive, slurry was readily poured from the toroids after 300-hr circulation. Ninety-four to 100% of the slurry was recovered in this manner. Recovery of slurries with 1000 and 5000 ppm SiO_2 added as sodium metasilicate was 96 and 88%, respectively. Both were fluid after circulation.

Table 13.2. Attack by Slurries with Silicate Additives

Test conditions: 300 hr, 26 fps, 250°C, 90 psig O_2 at 250°C, batch TO-10-1600°C calcined ThO_2, av dia 1.3 μ

Concentration of SiO_2 (ppm)[a]	pH of Slurry[b]	Corrosion Rate[c] (mpy)				
		347 SS	Zircaloy-3A	SA-212-B Steel	TI-75A	Toroid
0	6	3	<1	113	2	0.5
1,000	6	23	<1	3	7	1
2,000	7	17	<1	4	19	1
5,000	12	21	1	76	[d]	
10,000	12	33	1	[d]	[d]	
15,000	12	11	3	[d]	[d]	2

[a] SiO_2 based on thorium oxide; added as Na_2SiO_3.
[b] After circulation.
[c] Pins defilmed; uncorrected for slug flow; 45% fill at 250°C.
[d] Specimen consumed during test.

A few slurry spheroids, 5 to 60 μ, formed during each test.

Lower recoveries, only 34 and 50%, respectively, were obtained from the toroids which circulated slurries with 10,000 and 15,000 ppm SiO_2. The consistency of each was like that of thick cream. No spheroids were found in these runs.

13.2.2 Pilot Tests with Special Preparations of Thoria

Several pilot tests were made during the quarter, in cooperation with the Chemical Technology Division, to ascertain the corrosivity and circulation behavior of slurries prepared from special thorium oxide preparations. Nine tests were made with aqueous slurries of thorium oxide spheres furnished as experimental samples by Houdry Process Corporation and Davison Chemical Company. Eight toroid runs were made with slurries prepared of a thorium-uranium mixed oxide. The latter material was made at ORNL by coprecipitation of thorium and uranium oxalates at 10°C and subsequent firing at 650, 1000, 1200, 1400, and 1600°C.

The corrosion results obtained in those tests in which thoria spheres were circulated are given in Table 13.3.

The mean particle size, measured by gravitational sedimentation, of the 650°C-calcined spheres from Davison Chemical Company (batch RD-4995) was 5 μ. The mean particle size of Houdry spheres, calcined at 2600°F (1420°C), was 85 μ. By chemical analysis, no significant impurities were detected in the latter material. The Davison spheres contained 300 ppm chloride and 1200 ppm silicon. Photographs of those materials are shown in Figs. 13.4 and 13.5.

Oxygenated slurries of 500 g of thorium per kilogram concentration prepared from the Houdry

Table 13.3. Attack by Slurries of Experimental Preporations

Test conditions: 300 hr, 26 fps, 250°C

	Davison Chemical Co. Spheres;[a] Av Dia, 5 μ			Houdry Process Co. Spheres;[a] Av Dia, 85 μ[b]		MSO-10, Th–0.5% U Oxide; Av Dia, 0.7 μ					
Thorium oxide calcination temperature, °C	650	650	1600	1427	1600	650	650	1000	1200	1400	1600
Slurry concentration, g Th/kg H_2O	500	1000	1000	500	500	500	500	500	500	500	500
Additives	O_2	O_2	O_2	O_2	O_2	O_2	O_2; 0.005 *M* MoO_3	O_2	O_2	O_2	O_2
Corrosion rate,[c] mpy											
347 SS	3	13	1	1	2	2	0.7	0.6	1	2	2
SA-212 B steel	48	102	3	3	5	2	3	3	2	2	2
Ti-75A	ND[d]	ND[d]	1	1	3	3	0.1	2	2	2	1
Zircaloy-2	1	1	2	7	6	0.7	0.5	0.1	ND[d]	ND[d]	0.2
347 SS toroid	1	2	0.3	0.4	1	0.2	0.1	0.2	0.1	0.2	0.2

[a]From experimental sample received by Chemical Technology Division.

[b]Degraded to 0.7-μ av dia during circulation.

[c]Defilmed, uncorrected for slug flow, 45% fill at 250°C.

[d]None detected.

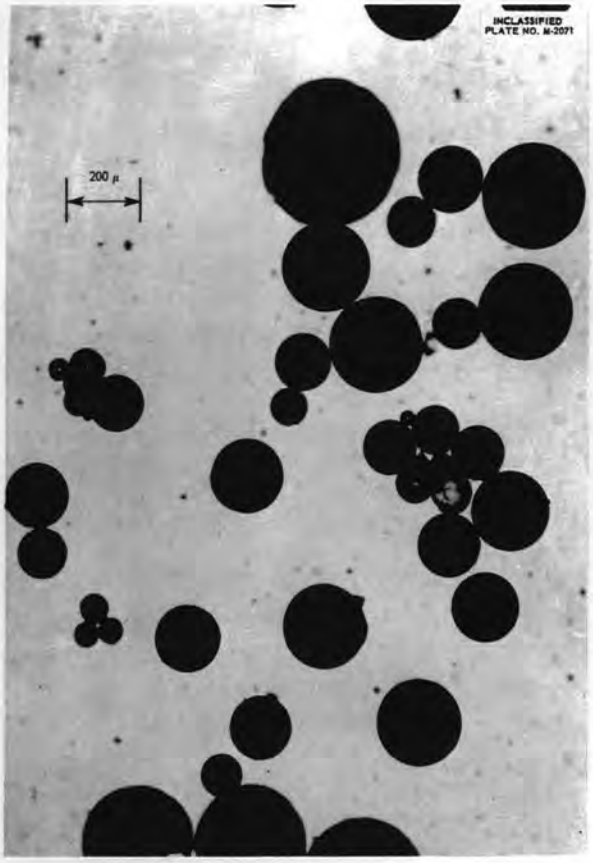

Fig. 13.4. Thorium Oxide Spheres from Houdry Process Company, Before Circulation in Toroids. 100X. Reduced 51%.

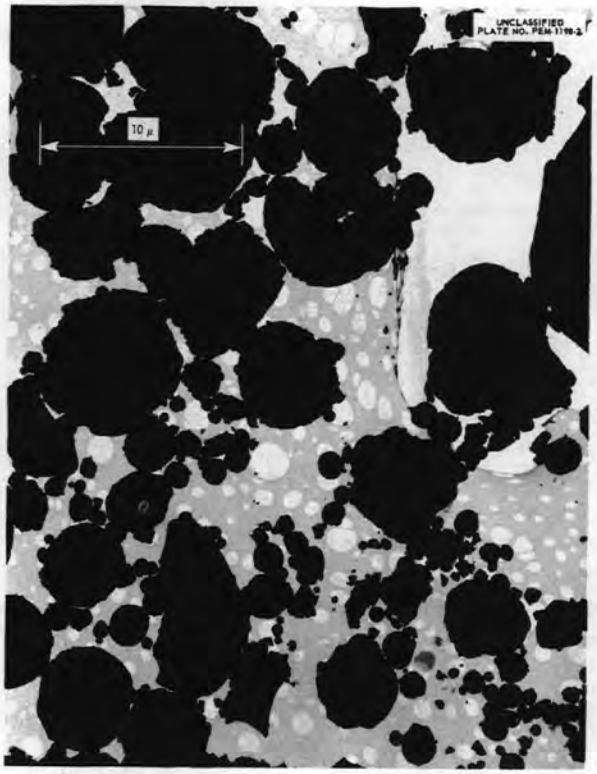

Fig. 13.5. Thorium Oxide Spheres from Davison Chemical Company Before Circulation in Toroids. 6000X. Reduced 54.5%.

thoria circulated satisfactorily with moderate corrosion; however, both the 1420°C-calcined and the 1600°C-recalcined spheres were degraded during 300 hr of circulation at 250°C and 26 fps to a mean particle size of 0.7 μ.

Slurries of the Davison thoria spheres, tested at concentrations of both 500 and 1000 g of thorium per kilogram of water, also circulated satisfactorily. By microscopic examination some of these spheres were fractured but in general the integrity of the material was good.

In eight toroid tests made with slurries prepared from mixed thorium-uranium oxides, corrosion was mild in both hydrogenated and oxygenated runs at 500 g of thorium per kilogram of water concentration, 250°C, and 26 fps. Results of the tests are given in Table 13.3. In one test, a proposed recombination catalyst, 0.005 M MoO_3, was added. Except for the SA-212 B steel, a moderate reduction in attack was observed on all specimens. Slurries of the higher-calcined mixed oxides appeared no more aggressive than those of the 650°C-fired material.

The mean particle size of the thorium-uranium oxide was 0.7 μ. By sedimentation analysis, no detectable changes in particle size resulted from subsequent recalcination or circulation.

13.2.3 Effect of Time on Corrosion by Circulating Slurries

Slurry prepared from 800°C-calcined thoria, which had been circulated previously in a 100A pump loop, was circulated at 250°C and 26 fps to study the rate of attack as a function of time. Two toroids contained oxygenated slurry at 1000 g of thorium per kilogram of water concentration. Two duplicate toroids contained oxygenated water.

In two toroids, specimens of type 347 stainless steel, Zircaloy-2, titanium 75A, and SA-212 B steel were exposed for a total of 1026 hr. In the other two toroids, specimens of the same materials

were exposed for 308 hr and then removed and replaced with new specimens which were exposed for the final 718 hr of the 1026-hr test. Each toroid contained 90 psig oxygen overpressure (at 250°C), provided by the addition of the appropriate volume of hydrogen peroxide. Corrosion results from the tests are given in Table 13.4. In each test, data indicate a generally lower corrosion rate with longer exposure time. A single Zircaloy-2 pin showed a higher corrosion rate, 1.6 mpy, for the 1026-hr period, while the 718-hr value for another pin of this material was 0.2 mpy.

Room-temperature pH values of the slurries ranged from 7.2 to 7.5 after circulation, whereas those of the water were 5.0 to 6.3. The initial mean particle size, calculated from sedimentation analyses, was 1.0 μ. No detectable further degradation occurred during the circulation in toroids.

13.3 IN-PILE SLURRY TOROID DEVELOPMENT

Test evaluation of the two present models of the experimental in-pile toroid rotators[13] was continued during the past quarter. Dependable mechanical performance has been attained with the first, or "gear train" model,[14] using double-row angular-contact ball bearings and case-hardened gears. At present, this rotator has operated for approximately 250 hr at 350 rpm and a toroid temperature of 250°C with no bearing failures and only slight evidence of gear wear. With the toroids heated to 250°C, the operating temperature of the bearings and gears approaches 150°C. The gears will not perform satisfactorily at this temperature without lubrication, and powdered graphite has been found to be superior to standard lubricating oil for this application. Performance of the air motor has been very satisfactory to date. The rotator is capable of attaining rotational speeds up to approximately 1500 rpm (slurry velocities up to 40 fps).

The second model[13] utilizes two gimbals and rotated arms, and a universal joint to obtain circular motion. Continued efforts have been made to reduce operational vibrations in this machine. Design revisions to the original model

[13] E. L. Compere *et al.*, *HRP Quar. Prog. Rep. April 30, 1957*, ORNL-2331, p 110.

[14] E. L. Compere *et al.*, *HRP Quar. Prog. Rep. Jan. 31, 1957*, ORNL-2272, p 100–101.

Table 13.4. Effect of Time on Attack by Circulating Slurries

Toroids: titanium
Temperature: 250°C; O_2 atmosphere
Velocity: 26 fps
Thoria: batch LO-2A, 800°C, circulated 566 hr in runs CS-28-29, washed, and dried

Concentration, g Th/kg H_2O	1000			None; Pure Water		
Hours	308	718	1026	308	718	1026
Particle size, μ						
Prerun		1.0	1.0			
Postrun		0.95	1.35			
pH		7.2	7.5		5.0	6.3
Pin corrosion rate,* mpy						
347 stainless steel	2.0	1.5	0.7	0.1	0.2	WG**
SA-212 B steel	1.9	2.6	1.0	3.2	0.8	1.7
SA-212 B steel			0.7			1.5
Titanium 75A	0.8	0.2		WG	0.02	
Zircaloy-2	0.2	0.2	0.1	0.1	0.2	1.6

*Defilmed; uncorrected for slug flow; 27% fill at 250°C.

**WG = weight gain.

include changing the configuration of the rotator-arm block, to eliminate the bearing reaction at this point, and the enclosure of the frames of both gimbals within a cylindrical retaining structure, which also supports the drive-shaft shoulder block and the air motor. A rotator incorporating these design changes and fulfilling the dimensional requirements for in-pile operation is being fabricated.

Tests are still in progress to obtain the information necessary for the design of a suitable heating and cooling system for temperature control of the toroids during in-pile operation. The initial tests have been conducted by using the first model rotator with approximately 26 ft of No. 20 gauge Nichrome resistance wire wrapped around a toroid bundle of two rings to provide heat, and approximately 8 ft of $\frac{1}{8}$-in. × 0.010-in.-wall stainless steel tubing wound around the rings as cooling coils. The cooling coil was wrapped to form two separate parallel circuits with approximately 1-in. spacing between the turns. Air-water mixtures flowing countercurrently in the parallel circuits were used as the coolant medium. By varying the water content of the air-water mixtures, while maintaining a toroid control temperature of 250°C, cooling rates ranging from 550 w with air and water flows of 0.8 scfm and 22 cc/min, respectively, to 1600 w (~ 1.5 w/g) with air and water flows of 1.1 scfm and 173 cc/min, respectively, were obtained at a rotational speed of 350 rpm. Attempts to perform tests at higher rotational speeds with the gear-train model rotator resulted in severe flexing and frequent failure of the thermocouple and heater leads and the coolant lines.

The gamma heat load anticipated for in-pile operation with the ORR at a 20-Mw power level is approximately 2 w per gram or 2200 w for the above two-ring toroid bundle. The test results to date indicate that the operational range of the heating and cooling system can be increased to include this in-pile gamma heat load by improving the contact bond between the coolant tubing and the metal wall of the toroid.

14. RADIATION CORROSION

G. H. Jenks H. C. Savage

A. L. Bacarella
J. E. Baker
S. E. Bolt
J. W. Brown
R. J. Davis
V. A. DeCarlo
B. O. Heston
D. T. Jones
R. A. Lorenz
T. H. Mauney
J. R. McWherter
A. R. Olsen
J. A. Russell
M. D. Silverman
F. J. Walter
K. S. Warren
A. Weitzberg
S. H. Wheeler
L. F. Woo
W. C. Yee

14.1 IN-PILE LOOPS

14.1.1 Development and Construction

(a) HB-2 Loop Package. – The operation of loop L-2-17 (ref 1) in beam hole HB-2 of the LITR was completed during the past quarter.

Loop L-2-19, a type 347 stainless steel loop containing coupon-type corrosion specimens and stressed specimens, is being constructed. Zircaloy-2 tapered-channel coupon holders in the core and line contain Zircaloy-2, titanium-110AT, and type 347 stainless steel samples. Stress specimens of titanium-110AT are installed in the core, the in-line holder, and in the pressurizer. A low-velocity coupon holder has been designed to expose the maximum surface area of the coupon specimens to the fuel solution in the core annulus. The coupon specimens also have been modified for this purpose. Figure 14.1 is a photograph of the assembled coupon holder containing modified coupon specimens. Three low-velocity coupon holders in the core and two in the line of loop L-2-19 contain modified coupon specimens of Zircaloy-2, Zircaloy-2 weldments, crystal-bar zirconium, type 430L stainless steel (Croloy 16-1), type 304 stainless steel (sensitized), Incoloy, and titanium oxide. One type 347 stainless steel specimen, one Zircaloy-2 specimen, and one zirconium oxide specimen are mounted in the forward section of the core, where the neutron flux is the highest. A cobalt flux monitor encased in type 347 stainless steel is located in the core.

(b) HB-4 Loop Package. – The fabrication and testing of loop L-4-18 (ref 2) were completed, and the loop is now in operation in beam hole HB-4 of the LITR.

Components for loop L-4-21 are being fabricated. This will be the first loop to incorporate the Byron-

[1] G. H. Jenks *et al.*, *HRP Quar. Prog. Rep. Jan. 31, 1957*, ORNL-2272, p 102.

[2] G. H. Jenks *et al.*, *HRP Quar. Prog. Rep. April 30, 1957*, ORNL-2331, p 112.

UNCLASSIFIED
PHOTO 29217

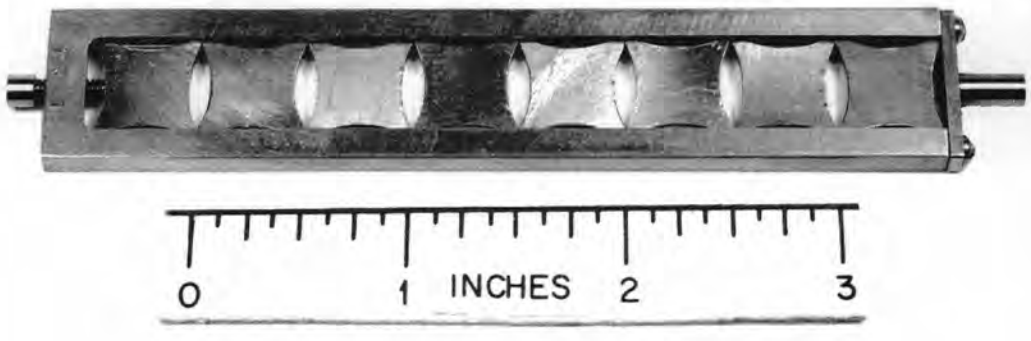

Fig. 14.1. Low-Velocity Coupon Holder with Modified Coupons.

Jackson 5-gpm pump[3] (Fig. 14.2). The combination heater-cooler unit[4] as designed for use in the ORR loop will be utilized in loop L-4-21, instead of separate heater and cooler units as used in all previous loops, to provide space for the Byron-Jackson pump and to allow a test of the heater-cooler unit.

(c) ORR Loop Package. – All components of the ORR in-pile loop, except the core section, are now fabricated and ready for final assembly. Tests on the core[4] were continued to determine flow patterns and pressure drop. The tapered-channel coupon corrosion specimen holders[5] were redesigned to reduce the fluid velocity and thus the pressure drop through the holder, since two holders in series will be used in the ORR loop core (Fig. 14.3). Flow tests in a clear plastic model of the core with baffles and two sample holders indicated no stagnant areas.

(d) Byron-Jackson 5-gpm Pump. – Tests at room temperature of the hydraulic and electrical operating characteristics of the ten Byron-Jackson pumps[3] were completed. Performance curves of the individual pumps vary considerably. All pump

[3] G. H. Jenks *et al.*, *HRP Quar. Prog. Rep. July 31, 1956*, ORNL-2148, p 92.

[4] G. H. Jenks *et al.*, *HRP Quar. Prog. Rep. April 30, 1957*, ORNL-2331, p 112–113.

[5] G. H. Jenks *et al.*, *HRP Quar. Prog. Rep. April 30, 1954*, ORNL-1753, p 83.

UNCLASSIFIED
ORNL-LR-DWG 23542

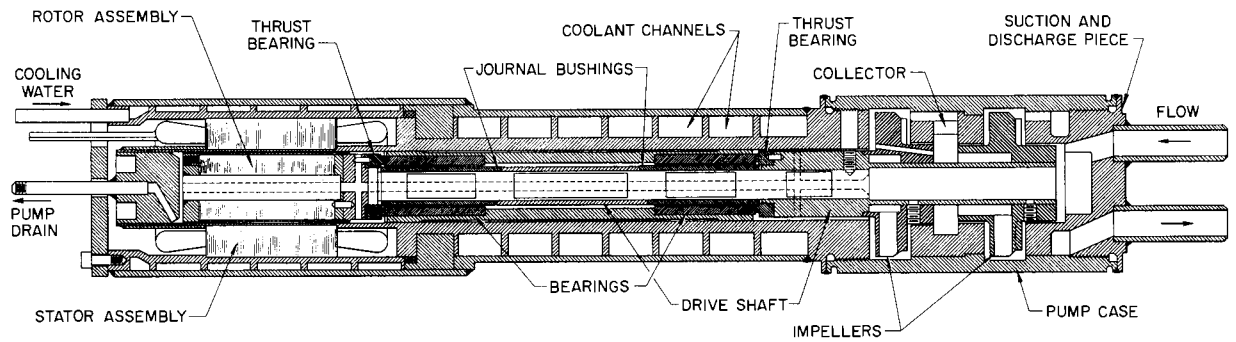

Fig. 14.2. Byron-Jackson 5-gpm In-Pile Loop Pump.

UNCLASSIFIED
ORNL-LR-DWG 23543

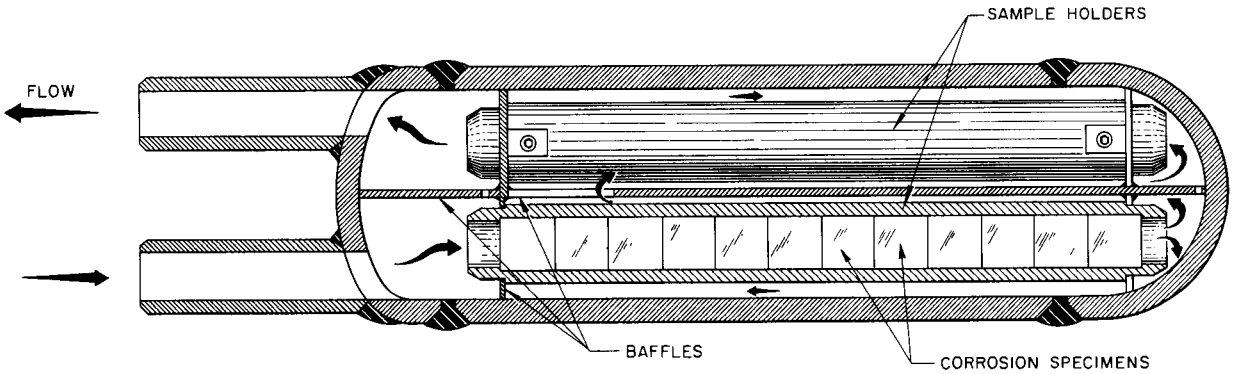

Fig. 14.3. Core for ORR In-Pile Loop.

outputs are below the design specifications of 40 ft of head at 5-gpm flow. However, some of the pumps have sufficient head and capacity for use with in-pile loops. All pumps were found to be acceptable with respect to electrical circuitry. One pump satisfactorily circulated a uranyl sulfate solution at 250°C for about 1200 hr.

(e) ORNL 5-gpm Pump. – An electrical failure of the ORNL 5-gpm pump in in-pile loop L-2-17 after approximately 1000 hr of operation in the LITR has prompted a redesign of the pump stator. A 220-v 3-phase stator to replace the present single-phase 110-v stator is being tested. With the 3-phase stator at 560 w of electrical power, the pump developed 40 ft of head at 5-gpm flow; with the single-phase stator, 1300 w of electrical power is required when the pump develops 36 ft of head at 5-gpm flow. The improved efficiency of the 3-phase 220-v stator resulted in a lower operating temperature of the stator windings, which should prolong the life of the stator. In addition, the class-A Formvar electrical insulation in the present stator will be replaced with the more heat resistant class-H type of insulation in order to prolong the operating life of the pumps.

14.1.2 General Description of In-Pile Loop Experiments L-2-15 and L-4-16

(a) Introduction. – At the time the final plans were made for loop experiments L-2-15 and L-4-16, eight loop experiments had been irradiated and a ninth was being irradiated. Eight of these previous experiments had been conducted in beam hole HB-4 at the LITR; the other had been exposed in beam hole HB-2, where the unperturbed thermal-neutron flux is about 3×10^{13} neutrons/cm^2/sec. This is about 3 times the unperturbed flux in HB-4. The eight HB-4 experiments contained 0.17 *m* UO_2SO_4 solution at 250°C, and the HB-2 loop experiment,[6] L-2-10, contained 0.04 *m* UO_2SO_4 solution at 280°C. In order to obtain data at higher power densities and to provide a basis for direct comparison between experiments in the two holes, loops L-2-15 and L-4-16 were inserted in HB-2 and HB-4, respectively, and operated with 0.17 *m* UO_2SO_4 solution at about 280°C. With the exception of metallographic examination of specimens from L-4-16, these experiments have been completed. A summary of the experiments is given below.

(b) Loop L-2-15. – Loop L-2-15 was constructed from type 347 stainless steel. Identical sets of corrosion coupons (24 each) in Zircaloy-2 tapered-channel coupon holders were installed in the core and in-line positions. These coupons were of type 347 stainless steel, Zircaloy-2, and titanium-55A. The core and in-line positions each contained a ladder[7] coupon assembly, which held identical coupon arrays (14 coupons each). These ladder specimens were made of Zircaloy-2 (some of which were plated with nickel and platinum), types 347 and 309 SCb stainless steel, platinum, and titanium-110AT. This was the first loop experiment to contain Zircaloy-2 specimens plated with nickel and platinum. Nickel was plated on the Zircaloy-2 to a depth of about 1 mil and platinum on the nickel to a depth of about 0.2 mil. Since the specimens were cut from a plated bar, all three metals were exposed on at least one edge of each coupon. Each specimen contained about 80 mg of nickel and about 40 mg of platinum. Two of these plated coupons were contained in the core-ladder assembly and two in the in-line ladder assembly. Two tensile and two impact specimens of crystal-bar zirconium were placed in the core, and one tensile and two impact specimens in the in-line position. Two Zircaloy-2 impact specimens were placed in the core, and one was in the in-line position. One stress assembly of titanium-110AT was placed in the core and one in the in-line position.

The structure of the loop was essentially the same as for the previous experiments. The circulating pump was an ORNL 5-gpm pump of the outboard-bearing type with pure sintered aluminum oxide bearings and journal bushings.

The solution charged to the loop was 0.17 *m* UO_2SO_4 (enriched), 0.015 *m* $CuSO_4$, and 0.03 *m* H_2SO_4. In an effort to better control the acidity of the loop solution during the run, both the original solution and a solution 0.07 *m* in H_2SO_4 were used as makeup to replace solution withdrawn in sampling. In both cases 100 ppm Cr was added to the makeup solution in an effort to protect valve stems during addition. The excess acid in the loop ranged between 0.027 and 0.03 *m*, with a calculated mean concentration of 0.028 *m*.

[6] G. H. Jenks *et al.*, *HRP Quar. Prog. Rep. Jan. 31, 1957*, ORNL-2272, p 104–108.

[7] G. H. Jenks *et al.*, *HRP Quar. Prog. Rep. Oct. 31, 1956*, ORNL-2222, p 100.

The main-stream loop temperature was controlled at 278°C at the core inlet. The estimated temperature rise of the solution in the core based on fission and gamma heat measurements was 2°C. The pressurizer temperature was 298°C.

Enriched solution was circulated for about 75 hr in the loop before irradiation commenced. After 470 hr of circulation time the loop was drained in order to replace valve 30, which failed during solution makeup addition following the eighth sample. The loop was then recharged with fresh solution, and operation was resumed. The experiment was terminated when the loop circulating pump failed after 792 hr of circulation time with enriched solution. The energy output of the LITR during the inserted time was 1632 Mwhr, essentially all of which was accumulated with the reactor at 3 Mw.

The average fission power during operation of the loop, which was determined from Cs^{137} analyses, was 1838 w. The average total fission and gamma heat was 2764 w as determined from the difference in electric-heater power requirements with the reactor down and at full power.

The thermal-neutron flux at a given position in the core was determined from measurements of the induced activities of representative Zircaloy-2 core-holder coupons. These values were in agreement with the thermal fluxes calculated from the activities of three pieces cut from the type 347 stainless steel core body, indicating the absence of a radial neutron-flux gradient in the core of this experiment. The fission power density at a given position in the core was determined from the thermal-neutron flux calculated for the Zircaloy-2 core-holder coupons. The solution power density at a given position was corrected to include the estimated power density associated with moderation of the fast neutrons at the position. The power densities determined in this manner ranged, for this experiment, from 20.2 w/ml for the leading core coupon to 4.7 w/ml for the rear core coupon. These included estimated contributions from fast-neutron moderation of 0.5 and 0.1 w/ml, respectively. The estimated solution power density at the nose of the core was 27.2 w/ml.

No evidence of solution instability was observed during this experiment. The over-all stainless steel corrosion rate was 1.5 mpy based on oxygen data and 0.5 mpy based on nickel in solution. If the oxygen data are corrected for the amount consumed in zirconium oxidation, the over-all steel corrosion rate, based on the corrected data, is 1.3 mpy.

(c) Loop L-4-16. – Loop L-4-16, constructed of type 347 stainless steel, contained identical sets of corrosion coupons (24 each) in type 347 stainless steel tapered-channel coupon holders in the core and in-line positions. These coupons were of type 347 stainless steel, Zircaloy-2, and titanium-55A. Two ladder[7] coupon assemblies were contained in the core position and one ladder assembly in the in-line position. All ladder holders were fabricated of type 347 stainless steel. Each ladder assembly contained 15 coupons, fabricated from 11 different alloys, including type 347 stainless steel, Zircaloy-2, and alloys of zirconium with niobium, palladium, or platinum. These zirconium alloys other than Zircaloy-2 were submitted by the HRP Metallurgy Group. Specimens of the zirconium alloys were subjected to one of two heat treatments prior to installation in the loop. The heat treatment used was either (1) at 900°C for 3 hr, followed by a water quench, or (2) at 900°C for 3 hr, followed by a water quench, and at 600°C for 48 hr, followed by air cooling. There were five impact specimens and one tensile specimen located in the core, and three impact specimens and one tensile specimen in the in-line position. The core impact specimens were fabricated from titanium-110AT, titanium-55A, Zircaloy-2, zirconium–15% niobium with heat treatment No. 1 above, and zirconium–15% niobium with heat treatment No. 2 above. The in-line impact specimens were fabricated from titanium-110AT, Zircaloy-2, and zirconium–15% niobium with heat treatment No. 1. Both the core and in-line tensile specimens were fabricated from titanium-110AT.

The structure of the loop was essentially the same as for the previous experiments. The circulating pump was an ORNL 5-gpm pump of the outboard-bearing type with pure sintered aluminum oxide bearings and journal bushings. In-pile loops L-2-10 (ref 6) and L-4-13 (ref 8) were the only previous experiments with steel coupon holders. The other experiments, with one exception, had Zircaloy-2 holders. The exception was L-4-12 (ref 9), which had titanium holders.

Enriched solution was circulated for 134 hr in the loop before irradiation commenced. After a

[8] G. H. Jenks *et al.*, *HRP Quar. Prog. Rep. April 30, 1957*, ORNL-2331, p 113–118.

[9] G. H. Jenks *et al.*, *HRP Quar. Prog. Rep. Oct. 31, 1956*, ORNL-2222, p 101–106.

total of 1032 hr of circulation time with enriched solution, the experiment was terminated as a result of failure of the loop circulating pump. The energy output of the LITR during the inserted time was 2325 Mwhr, essentially all of which was accumulated with the reactor at 3 Mw.

The average fission power density during operation as determined from cesium analyses was 620 w. This is in reasonably good agreement with values observed in previous HB-4 experiments.[10] The power density at a given position in the core was determined from measurements of the induced activities of Zircaloy-2 core coupons and Zircaloy-2, zirconium–33% niobium, and zirconium–15% niobium core ladder coupons. As has been noted previously in loops containing stainless steel core coupon holders,[6,8] a pronounced radial neutron flux was observed in this experiment. The log mean value of the thermal-neutron flux calculated from the core-ladder coupons was found to be 24% greater than the corresponding value calculated from the Zircaloy-2 core-holder coupons. Neutron fluxes calculated from the activities of three pieces cut from the type 347 stainless steel core body were in agreement with the fluxes calculated from the ladder coupons. The power densities determined from induced activities ranged from 5.3 w/ml for the leading core-holder coupon to 1.3 w/ml for the rear core-holder coupon and from 5.7 w/ml for the leading core-ladder coupons to 2.7 w/ml for the rear core-ladder coupons. The power density in solution at the nose of the core, calculated from induced activities, was 7.5 w/ml.

The average over-all corrosion rate of stainless steel as calculated from the oxygen data for the total period of operation was 0.51 mpy, with little change during the run. The over-all corrosion rate for the same period based on the amount of nickel in solution was 0.50 mpy.

14.1.3 Qualitative Results of Inspection and Evaluation of Loops L-2-15 and L-4-16

No unforeseen difficulties were encountered during the dismantling of loops L-2-15 and L-4-16. Components cut from the loops were the cores, the in-line sample holders, the pressurizers, two sections from the pressurizer heater of each loop, a section of piping adjacent to each loop pump outlet, and the pumps. The loop coolers jacketed with type 347 stainless steel were cut from loop L-2-15. Other portions of the loop packages were buried.

The impact and tensile specimens from the loops were transferred to the HRP Metallurgy Group for testing and evaluation.

Several coupons of each material from the core and in-line coupon arrays, together with sections from the core cap, pressurizer, pressurizer heater, and main loop piping from each loop, were sent to the Solid State Division for metallographic examination. In addition, sections from the L-2-15 loop-cooler annulus regions were also sent for examination.

(a) L-2-15. – An air-water mixture was used to remove heat from the loop cooler in loop L-2-15. Air alone or water alone had been employed previously. Although water in the mixture was demineralized, the type 347 stainless steel materials in the cooling jacket were examined for cracking or other damage which might have occurred during the in-pile operation. Visual and metallographic[11] examination of the cooler annuli showed no evidence of cracking. There was some staining of the metal and accumulation of light-colored scale near the inlet and outlet parts of both coolers.

In an attempt to determine the cause of the pump failure, the volute, stator, and rotor were removed from the pump. Examination of the volute and impeller showed no evidence of the impeller having dragged on any of the surfaces. The impeller appeared to have adequate end-play; it would turn, but would not spin freely. Examination of the rotor, bearings, and journals also failed to produce evidence of the cause of the pump failure. Journal and bearing diameters were the same as when installed except for the front bearing, which showed a slight increase (0.003 in.) in inside diameter, probably a result of normal wear. A small chip of Al_2O_3 was missing from near the outer edge of the rear journal thrust surface, but there was no evidence of damage to the mating surface on the bearing.

As with previous loops, all the components outside the core region were covered with a brown

[10] J. E. Baker *et al.*, *HRP Radiation Corrosion Studies, In-Pile Loop L-4-8*, ORNL-2042 (Aug. 8, 1956).

[11] J. O. Stiegler, *Metallographic Examination of Components, Coupons and Stress Specimens from HRP In-Pile Loop L-2-15*, ORNL CF-57-5-103 (May 22, 1957).

rustlike scale. This scale was heavy on all surfaces that had been wetted by solution, but the scale was thin on the pressurizer surface that had been exposed to vapor only. There was no evidence of localized attack on any of the loop components.

All specimens from the in-line positions were uniformly covered with a brown rustlike scale. As with previous loops the standard cathodic defilming technique was only partially effective on the Zircaloy-2 coupons, and all in-line holder coupons and ladder coupons of Zircaloy-2 exhibited weight increases following defilming.

The inside surface of the type 347 stainless steel core body was generally covered with a thin, dark-brown, rustlike scale, the thickness of which increased from the high- to the low-flux end of the core. Along a line oriented with the ladder-coupon assembly included in the annulus region of the core, the scale was slightly discolored. A similar discoloration was noted in the same general region in loop L-2-10 (ref 6), although the color range in L-2-10 was more pronounced than in this loop.

All the stainless steel components and coupons in the core array were covered with a thin rustlike scale similar to that found on the core body. The titanium stress specimens and coupons were covered with the typical thin brass-colored film. The Zircaloy-2 coupons, impact samples, and coupon holder were covered with a very thin iridescent film. The crystal-bar zirconium impact and tensile specimens were covered with a similar thin film, which was darker in color, ranging from light gray to black. All the zirconium and Zircaloy-2 surfaces in the core had a lightly etched appearance.

(b) Loop L-4-16. – In an effort to locate the source of the pump failure, the L-4-16 pump was carefully sectioned and examined. Figure 14.4 is a sketch of the pump showing the cutting sequence and approximate location of various cuts. As with all previous pumps the seal weld was first cut so that the volute could be removed. Visual examination of the interior of the volute and of the impeller surfaces showed no indications of scoring or other signs of mechanical damage. The pump rotation was then tested by using a long-handled screwdriver inserted into the impeller. The impeller did not spin freely, but there was no evidence of mechanical locking. The amount of end-play appeared to be normal. A second cut was then made at B-B′ through the cooling jacket, front-bearing spacer, and the shaft. This permitted the removal of the thermal barrier and the impeller, with that section of the shaft in the area of the seal rings still attached to the impeller. Some scoring of the shaft adjacent to the rear seal rings was apparent, but this damage was quite shallow.

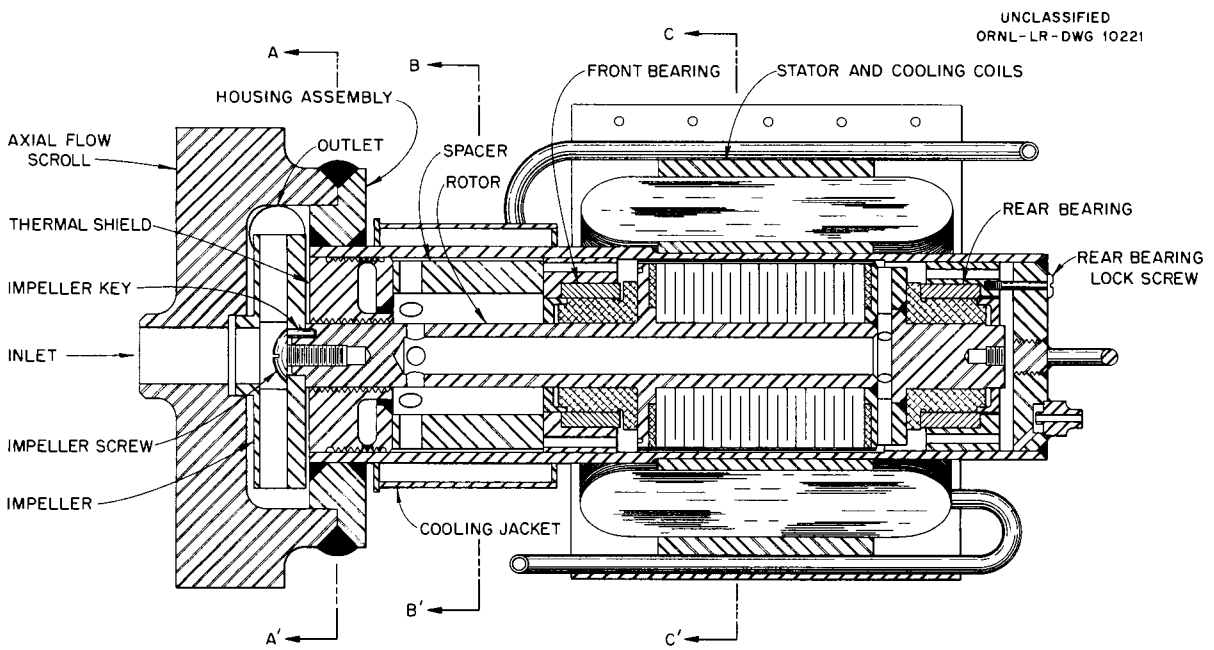

Fig. 14.4. In-Pile Loop Pump.

The stator was then removed, and the seal can was cut at C-C'; this permitted the removal of the rotor assembly. Very careful visual examination of the rotor can, bearings, and journals showed no indications of wear or other damage. No dimensional measurements were made.

From this examination it was concluded that there was no evidence of any mechanical failure which could have caused the pump failure. An attempt will be made on future pumps to remove the stator in such a way as to permit careful electrical checks of the various individual windings. Pre-exposure measurements are being initiated to provide the necessary control information.

As with previous loops all the components outside the core region were covered with a uniform dark-brown rustlike scale which was thin only in the vapor region of the pressurizer.

The tensile specimens, impact specimens, ladder coupons from the special in-line holder, and coupons from the in-line tapered-channel holder were uniformly covered with a brown rustlike scale. Several coupons from the ladder array were held on one end only, as removed from the loop. There was no apparent evidence to indicate that these coupons were dislodged during removal of the assembly from the loop. They did not fall out during subsequent handling. This indicates that they may have been dislodged while the loop was in operation.

As with previous loops the standard cathodic defilming technique was only partially effective on the zirconium-alloy coupons.

The interior surface of the type 347 stainless steel core body was covered with a relatively thin rustlike film, ranging from a deep red-black color at the core cap to a red-brown color at the outlet or low-flux end. As with previous loops this film gradually increased in thickness with decreasing neutron-flux exposure. This graduated scale thickness was also observed on the stainless steel spiders, coupons, and core coupon holder. Machine marks on the interior surface of the core holder were found to decrease in distinctness in the direction of increasing neutron flux, and were completely absent at the high-flux end.

Titanium specimens and coupons in the core were covered with the typical thin brass-colored film. The Zircaloy-2 coupons and impact specimens were covered with a thin iridescent film predominantly gray. The remaining zirconium alloys were, in general, covered with an apparently heavier film which was much darker and in some places was a distinct shiny black.

In an effort to determine the distribution of corrosion products throughout the loop, specimens of scale were scraped from the metal at the rear of the core, from the special in-line holder, from the pressurizer, and from the pump volute. These samples, along with a portion of the front and rear aluminum oxide journals from the pump, were analyzed for uranium and copper and for the corrosion products (chromium, nickel, iron, and zirconium). The results of these analyses are listed in Table 14.1.

Table 14.1. Chemical Analysis of Loop Scale and Bearing Material

Position	Weight (g)	Gross Activity	Analysis (wt %)					
			U	Cu	Cr	Ni	Fe	Zr
Scale								
Rear of core	0.0136	40 mr	0.029	0	7.03	5.98	50.74	5.15
Special in-line holder	0.0127	600 mr	0.039	0	4.53	7.39	43.94	10.71
Pressurizer	0.0177	500 mr	0.025	0.23	6.64	9.32	41.36	7.68
Pump volute	0.0144	1 r	0.18	0	4.94	4.06	35.28	10.42
Al_2O_3 Journals								
Front	25.12	4 r	0.0068	0.0007	0	0.0003	0.0019	0.0017
Rear	10.04	700 mr	0.0134	0.0006	0	0	0.0025	0.0011

14.1.4 Quantitative Results of Inspection and Evaluation of Loop L-2-15

All corrosion-rate values reported below were calculated from weight-loss data, with the exposed specimen area and total radiation time (equivalent to 543 hr of LITR operation at 3 Mw) used as the bases for the calculations. Average solution velocities across the coupons contained in the tapered Zircaloy-2 core and in-line holders were from 9.2 to 43.6 fps. Power-density values for the core specimens include the estimated contribution from fast neutrons at the specimen position.

(a) Zircaloy-2. – The corrosion rate of Zircaloy-2 based on the eight core-holder coupons and three core-ladder coupons was found, as in previous experiments, to be power-density dependent. Observed rates were from 5.9 mpy at 4.9 w/ml to 15.4 mpy at 19.2 w/ml for the holder coupons, and from 15.7 mpy at 9.2 w/ml to 21.4 mpy at 15.7 w/ml for the ladder coupons. If the total specimen area and total radiation time are used as bases for calculation of the corrosion rates of the core-ladder coupons, the resulting rates vary from 10.0 to 13.6 mpy. Following defilming, the eight in-line holder coupons showed weight gains of from 1.2 to 5.1 mg, and the three in-line ladder coupons showed gains of 0.4 to 0.5 mg. The two core coupons plated with the combination of nickel and platinum exhibited weight losses of 123 and 100 mg at 16.5 and 6.9 w/ml, respectively. The corresponding in-line coupons exhibited weight losses of 60 and 69 mg, respectively.

(b) Type 347 Stainless Steel. – Eight type 347 stainless steel coupons were contained in the core coupon holder. Corrosion rates for these specimens varied from 0.6 mpy at 4.7 w/ml to 15.9 mpy at 16.0 w/ml. The eight in-line holder coupons exhibited corrosion rates of 0.2 to 1.2 mpy, with an average of 0.7 mpy. The solution velocity across the specimens varied from 9.7 to 39.4 fps and produced no apparent effect on the relative corrosion rates in either the core or in-line holders.

The three core-ladder coupons exhibited corrosion rates of 44.6 mpy at 14.7 w/ml, 55.4 mpy at 12.0 w/ml, and 55.7 mpy at 8.7 w/ml, while the three corresponding specimens in the in-line ladder coupon array exhibited corrosion rates of 0.5 to 0.8 mpy and averaged 0.7 mpy.

(c) Type 309 SCb Stainless Steel. – Specimens of type 309 SCb stainless steel in the core-ladder coupon assembly exhibited corrosion rates of 39.3 mpy at 9.9 w/ml and 115.0 mpy at 7.6 w/ml. The specimens in corresponding positions in the in-line ladder coupon array exhibited rates of 0.2 and 0.8 mpy.

(d) Titanium-55A. – Eight titanium-55A coupons were contained in the core coupon holder. Corrosion rates for these specimens varied from 1.9 mpy at 5.2 w/ml to 2.1 mpy at 20.2 w/ml. The specimens in the in-line holder exhibited, in general, weight increases following defilming, varying from 0.7 to 4.3 mg for seven of the coupons and averaging 2.2 mg. The eighth specimen showed no weight change following defilming.

(e) Titanium-110AT. – Specimens of titanium-110AT in the core-ladder coupon assembly exhibited corrosion rates of 2.4 mpy at 12.9 w/ml and 3.1 mpy at 10.5 w/ml. The specimens in corresponding positions in the in-line ladder coupon array exhibited rates of 1.9 and 1.4 mpy, respectively.

Two titanium-110AT stress specimens in the core at 10.1 w/ml exhibited corrosion rates of 1.3 and 1.6 mpy. Two similar specimens in the in-line position both corroded at 0.3 mpy. All specimens were stressed to approximately 60,000 psi.

(f) Platinum. – This was the third loop experiment to contain platinum specimens. The previous loops with platinum specimens were L-4-11 (ref 12) (which contained one core-holder coupon, three core rod coupons, one in-line holder coupon, and one in-line rod coupon of this material) and L-2-10 (ref 13) (which contained four platinum core rod coupons). The present experiment contained two platinum specimens in the core-ladder array and two in the in-line ladder array. One core coupon at 11.2 w/ml showed a weight increase following defilming. The other core coupon and both in-line coupons exhibited slight weight losses following defilming. This latter core-ladder coupon exhibited a corrosion rate of 0.1 mpy at 8.1 w/ml; the in-line ladder coupons exhibited rates of 0.2 and 0.1 mpy. As reported,[12,13] corrosion rates for the platinum

[12] J. R. McWherter *et al.*, *HRP Quar. Prog. Rep. July 31, 1956*, ORNL-2148, p 93–97.

[13] G. H. Jenks *et al.*, *HRP Quar. Prog. Rep. Jan. 31, 1957*, ORNL-2272, p 104–108.

specimens in the core positions in both previous loops ranged between 0 and 0.4 mpy.

14.1.5 Quantitative Results of Inspection and Evaluation of Loop L-4-16

All corrosion-rate values reported below were calculated from weight-loss data, with the exposed specimen area and total radiation time (equivalent to 775 hr of LITR operation at 3 Mw) used as the bases for the calculations. Average solution velocities across the coupons contained in the tapered type 347 stainless steel core and in-line holders were from 9.4 to 44.4 fps. As mentioned previously, power-density values were calculated on the basis of the thermal-neutron flux at the coupon location.

(a) Zirconium Alloys. – Corrosion rates observed on the eight Zircaloy-2 core-holder coupons varied from 1.9 mpy at 1.3 w/ml to 4.5 mpy at 5.0 w/ml. The solution velocity across these specimens varied from 10.2 to 44.4 fps and produced no apparent effect on the relative corrosion rates.

The eight Zircaloy-2 in-line holder coupons all showed weight increases, ranging from 0.8 to 2.1 mg (av 1.5 mg), following defilming.

The four Zircaloy-2 core-ladder coupons exhibited corrosion rates varying from 3.6 mpy at 2.8 w/ml to 6.6 mpy at 5.7 w/ml. The two Zircaloy-2 coupons contained in the in-line ladder coupon array showed weight increases of 0.2 and 0.4 mg.

Some of the other zirconium alloys tested in the core-ladder arrays corroded at appreciably different rates than Zircaloy-2 in the core region at the same power density. Corrosion rates exhibited by these alloys, and power densities to which they were exposed, are summarized in Table 14.2. Also shown for comparison are the Zircaloy-2 core coupon data. Specimens of each of the zirconium alloys contained in the core-ladder arrays were also contained in the single ladder coupon assembly in the in-line position. All these coupons showed weight increases following defilming, varying from 0.2 to 3.7 mg and averaging 1.3 mg.

(b) Type 347 Stainless Steel. – Eight type 347 stainless steel coupons were contained in the core coupon holder. Corrosion rates for these specimens varied from 0.3 mpy at 1.3 w/ml to 2.6 mpy at 4.4 w/ml. An identical in-line holder coupon array exhibited corrosion rates from 0.2 to 0.8 mpy, averaging 0.5 mpy. The solution velocity across the specimens varied from 9.9 to 40.1 fps and produced no apparent effect on the relative corrosion rates.

The two core-ladder coupons, both at 2.7 w/ml, but in separate ladder assemblies, exhibited corrosion rates of 0.16 and 0.24 mpy.

(c) Titanium-55A. – Eight titanium-55A coupons were contained in the core coupon holder. With one exception corrosion rates for these specimens varied from 0.1 mpy at 1.4 w/ml to 0.4 mpy at 5.3 w/ml. The exception, a specimen at 2.7 w/ml, exhibited a corrosion rate of 0.6 mpy. The solution velocity across the specimens varied from 9.4 to 37 fps. The specimen with the highest velocity was also the specimen with the highest corrosion rate.

With one exception the in-line coupons exhibited corrosion rates which varied from 0.1 to 0.8 mpy. The exception, a specimen exposed to a solution velocity of 15 fps, showed a weight increase of 0.1 mg. The coupon exposed to a solution velocity of 37 fps showed a corrosion rate of only 0.3 mpy. The average corrosion rate for the in-line coupons which lost weight was 0.3 mpy.

14.1.6 Discussion of Results from Loops L-2-15 and L-4-16

(a) Zircaloy-2. – In a previous discussion of Zircaloy-2 in-pile corrosion data,[14] the relationship of corrosion rate to power density over the range studied was shown to be expressed by

$$R = AP\left(1 - e^{-B/R^{1.5}}\right),$$

where

R = corrosion rate, mpy,
P = power density, w/ml,
A = constant dependent on solution composition and temperature,
B = constant primarily dependent on temperature.

For the in-pile experiments containing 0.17 m UO_2SO_4 with excess acid at 250°C, the values for constants A and B as determined from the data are 1.25 and 6.5, respectively.[15] For the same solution in-pile at 280°C, the values as determined from the core coupon data from L-2-15 and L-4-16, are 1.04 and 95, respectively. These 280°C data, with the curve represented by the above equation

[14] G. H. Jenks *et al.*, *HRP Quar. Prog. Rep. Oct. 31, 1956*, ORNL-2222, p 111–112.

[15] G. H. Jenks *et al.*, *HRP Quar. Prog. Rep. April 30, 1957*, ORNL-2331, p 113–118.

Table 14.2. Corrosion Data for Zirconium Alloys in Experiment L-4-16

	Power Density (w/ml)	Corrosion Rate (mpy)	
		Observed	Observed / Calculated
Core-holder coupons			
Zircaloy-2	1.3	1.9	1.4
	1.6	2.0	1.2
	2.0	2.4	1.2
	2.3	2.5	1.0
	2.8	2.9	1.0
	3.4	3.4	0.9
	4.7	4.5	0.9
	5.0	4.5	0.9
Core-ladder coupons			
Zircaloy-2	2.8	3.6	1.2
	3.9	5.3	1.3
	5.7	7.3	1.2
	5.7	6.6	1.1
85% Zr sponge, 15% Nb*	3.3	2.6	0.7
	5.3	4.8	0.9
85% Zr sponge, 15% Nb**	5.0	9.1	1.8
85% crystal-bar Zr, 15% Nb*	3.3	2.6	0.7
	4.3	4.0	0.9
85% crystal-bar Zr, 15% Nb**	4.1	6.9	1.6
83% crystal-bar Zr, 15% Nb, 2% Pd*	3.2	1.2	0.4
	4.7	2.8	0.6
83% crystal-bar Zr, 15% Nb, 2% Pd**	4.9	5.0	1.0
83% crystal-bar Zr, 15% Nb, 2% Pt*	3.1	1.6	0.5
	4.3	2.9	0.6
83% crystal-bar Zr, 15% Nb, 2% Pt**	4.1	7.2	1.7
80% crystal-bar Zr, 15% Nb, 5% Pt*	3.1	1.7	0.5
	5.3	2.9	0.5
80% crystal-bar Zr, 15% Nb, 5% Pt**	5.0	5.5	1.0
95% crystal-bar Zr, 5% Pd*	3.5	3.6	1.0
	3.5	3.9	1.1
95% crystal-bar Zr, 5% Pt*	3.9	3.3	0.8
	3.2	3.4	1.0
75% crystal-bar Zr, 20% Nb, 5% Pd*	3.8	2.7	0.7
	3.8	3.0	0.8
67% crystal-bar Zr, 33% Nb*	4.7	5.1	1.0
	2.8	3.3	1.0
67% crystal-bar Zr, 33% Nb**	4.7	13.2	2.7

*Heat Treatment: Held at 900°C for 3 hr, water quenched.

**Heat Treatment: Held at 900°C for 3 hr, water quenched; then held at 600°C for 48 hr, air cooled.

and the latter constants, are shown in Fig. 14.5. The curve representing the 250°C data is shown as the broken line in Fig. 14.5.

It can be seen in Fig. 14.5 that the core rod coupon data are not in very good agreement with the core coupon data from the holder. All these data are based on the exposed specimen area, not including the area in contact with other metal surfaces. Loops L-2-15 and L-4-16 were the first loop experiments in which the rod or annulus coupons were mounted in ladder holders.[16] There is evidence that the area normally considered unexposed on these ladder coupons was attacked. Metallographic examination[17] of one of the L-2-15 ladder coupons showed that the penetration had been uniform over the entire surface. If the total area of the ladder coupons is employed, the calculated Zircaloy-2 corrosion rates for L-2-15 are in near agreement with the curve plotted in Fig. 14.5. The rates calculated for L-4-16 fall below the line.

The values for constants A and B for 0.04 m UO_2SO_4 solution at 280°C had been previously established from L-2-10 data as 3.2 and 40, respectively.[13] As defined, the constant B for L-2-10 data should be the same as that for the other 280°C loops, L-2-15 and L-4-16 (i.e., equal to 95). Assuming this value for B, the L-2-10 data are expressed reasonably well by the above equation with A equal to 2.45, as shown in Fig. 14.5. In this case, the line with A equal to 2.45 is a rough average of all the points, although, as for L-2-15 and L-4-16, it appears that, at a given power density, the annulus coupons corroded at a higher rate than those in the core. It is possible that in this experiment, also, differences in the specimen area exposed to attack may account for some of the difference in calculated rates. However, since no Zircaloy-2 specimens from this loop have been examined metallographically to date, there is no evidence to support this thesis. The results of autoclave experiment Z-12 (ref 18), which, with the exception of velocity, was carried out under similar conditions, are also expressed by the equation for the L-2-10 data.

Metallographic examination[17] of the Zircaloy-2 specimens plated with nickel and then platinum and exposed in the L-2-15 experiment showed the nickel layer to be missing from all coupons. The platinum appeared to remain in place. As mentioned previously, the nickel was exposed to the solution on one or more edges as a result of the method of fabrication. If it is assumed that the platinum on these specimens underwent no corrosive attack and that the weight losses were attributable to the loss of all the nickel and part of the Zircaloy-2, then the Zircaloy-2 corrosion rates would have been about 28 mpy at 16.5 w/ml and 14 mpy at 6.9 w/ml, and the in-line coupons would have exhibited weight increases following defilming of 20 and 11 mg, respectively. These rates are somewhat higher than those of the Zircaloy-2 core-holder coupons in L-2-15.

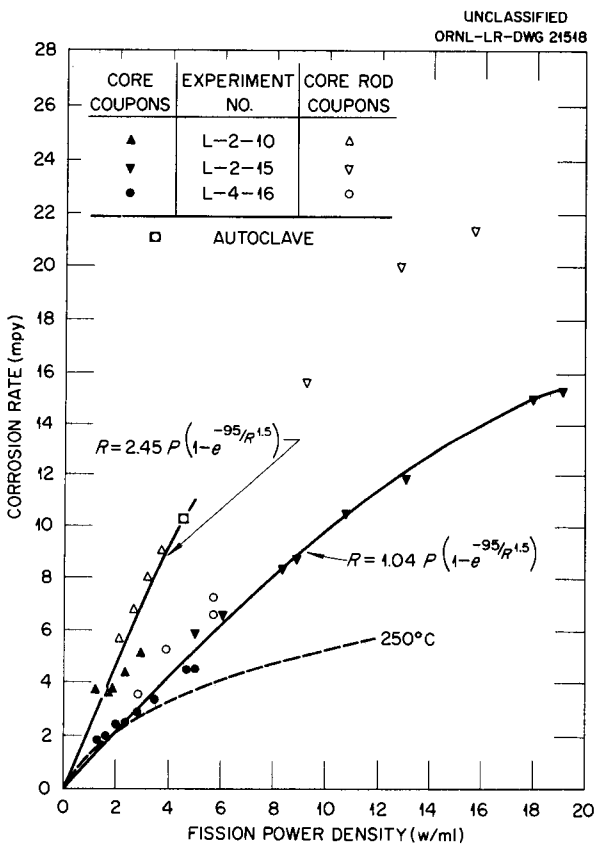

Fig. 14.5. Radiation Corrosion of Zircaloy-2; Loop Results at 280°C.

[16] G. H. Jenks *et al.*, *HRP Quar. Prog. Rep. Oct. 31, 1956*, ORNL-2222, p 100.

[17] J. O. Stiegler, *Metallographic Examination of Components, Coupons and Stress Specimens from HRP In-Pile Loop L-2-15*, ORNL CF-57-5-103 (May 22, 1957).

[18] G. H. Jenks *et al.*, *HRP Quar. Prog. Rep. July 31, 1955*, ORNL-1943, p 129.

The corrosion rates of the L-4-16 ladder coupons of zirconium alloys are compared with Zircaloy-2 corrosion rates in Table 14.2. The ratio of the observed corrosion rate to the rate calculated from the above equation by using 1.04 and 95 for the constants A and B, respectively, is also given. These data are also compared in Fig. 14.6. In general, the alloys that contained 15% niobium and that had been heat treated at 900°C and then water quenched exhibited corrosion rates about 30% lower than Zircaloy-2 ladder coupons at similar power densities. Similar alloys containing 2% platinum or palladium in addition to 15% niobium exhibited rates about 50% lower than Zircaloy-2 coupons. Heat treatment at 600°C for 48 hr following the water quench from 900°C appears to lower the corrosion resistance of the alloys. The scatter of the data is such that the lack in some instances of effect of a small increase in power density on the corrosion rate is not considered significant.

(b) Stainless Steel. – The corrosion data for the steel specimens which were located in the L-2-15 and L-4-16 core holders are shown in Fig. 14.7. The logarithm of the corrosion rate is plotted against the fission power density which prevailed in the solution adjacent to the specimen. Steel data from previous experiments[13,15,19–21] are also shown in Fig. 14.7. The data for each of the 280°C experiments, L-2-10, L-4-16, and L-2-15, appear to be very regular when plotted in this manner. Also, it appears that the effect of power density on the corrosion rate was less in L-2-15 than in either L-4-16 or L-2-10. There were two obvious differences between experimental conditions for L-2-15 and L-4-16. Loop L-2-15 operated at a radiolytic-gas pressure in the main stream of slightly more than 100 psi, whereas the radiolytic-gas pressure in L-4-16 was about 30 psi. The core-holder material for experiment L-2-15 was Zircaloy-2; that in L-4-16 was type 347 stainless steel. Either or both of these differences may be responsible for the difference in the observed radiation effect. However, it must be mentioned that these apparent differences in corrosion rates may be subject to revision when metallographic examination is complete. The report of the metallographic examination of a steel core-holder specimen from the high-flux region of L-2-14 (ref 17) indicates that all surfaces of the specimen were attacked, including the clamped areas which are normally considered protected and which were excluded in the calculation of the corrosion rates shown in Fig. 14.7. Incidentally, the attack was of the pitting nature frequently observed with stainless steel under irradiation. In this type of attack, shallow pits (usually 1 mil or less) form and then spread out until adjacent pits coalesce. No pitting was observed with another steel core specimen which was in the lowest flux region of L-2-15. Some attack of the clamped areas was also observed in examination of L-2-10 (ref 22) steel specimens. The examination of L-4-16 specimens has not been completed.

Metallographic examination[17] of the type 309 SCb stainless steel core-ladder coupon in L-2-15, which corroded at 115 mpy, showed that the coupon had been heavily attacked in the clamping region. A similar metallographic examination of the type 347 stainless steel core-ladder coupon in L-2-15, which corroded at 55 mpy, also showed attack on all surfaces, although in this case it was more severe in the exposed portion than at the edges. It seems likely that some attack of these steel ladder coupons was a result of fretting due to a loose fit in the holders.

(c) Titanium. – As mentioned, the corrosion rates of titanium-55A coupons in L-2-15 varied from 1.9 mpy at 5.2 w/ml to 2.1 mpy at 20.2 w/ml, and those in L-4-16 varied from 0.1 mpy at 1.4 w/ml to 0.4 mpy at 5.3 w/ml. The in-line rates in L-4-16 averaged 0.3 mpy; the in-line coupons in L-2-15 showed weight gains. From these data, it appears that the radiation-induced corrosion of titanium is not directly dependent upon the fission power density in solution adjacent to a specimen. There is a suggestion that the attack depends also on the average power density in solution.

(d) Scale Analyses in L-4-16. – A material balance (based on scale analyses and corrosion data) for several elements in experiment L-4-16 is shown in Table 14.3. The values listed in column 2 for the ratio of mass of the given element to the mass

[19] G. H. Jenks *et al.*, *HRP Quar. Prog. Rep. Oct. 31, 1956*, ORNL-2222, p 101–106.

[20] J. E. Baker *et al.*, *HRP Radiation Corrosion Studies, In-Pile Loop L-4-8*, ORNL-2042 (Aug. 8, 1956).

[21] J. R. McWherter *et al.*, *HRP Quar. Prog. Rep. July 31, 1956*, ORNL-2148, p 93–97.

[22] J. O. Stiegler, *Metallographic Examination of Components and Coupons from HRP In-Pile Loop L-2-10*, ORNL CF-57-3-42 (March 9, 1957).

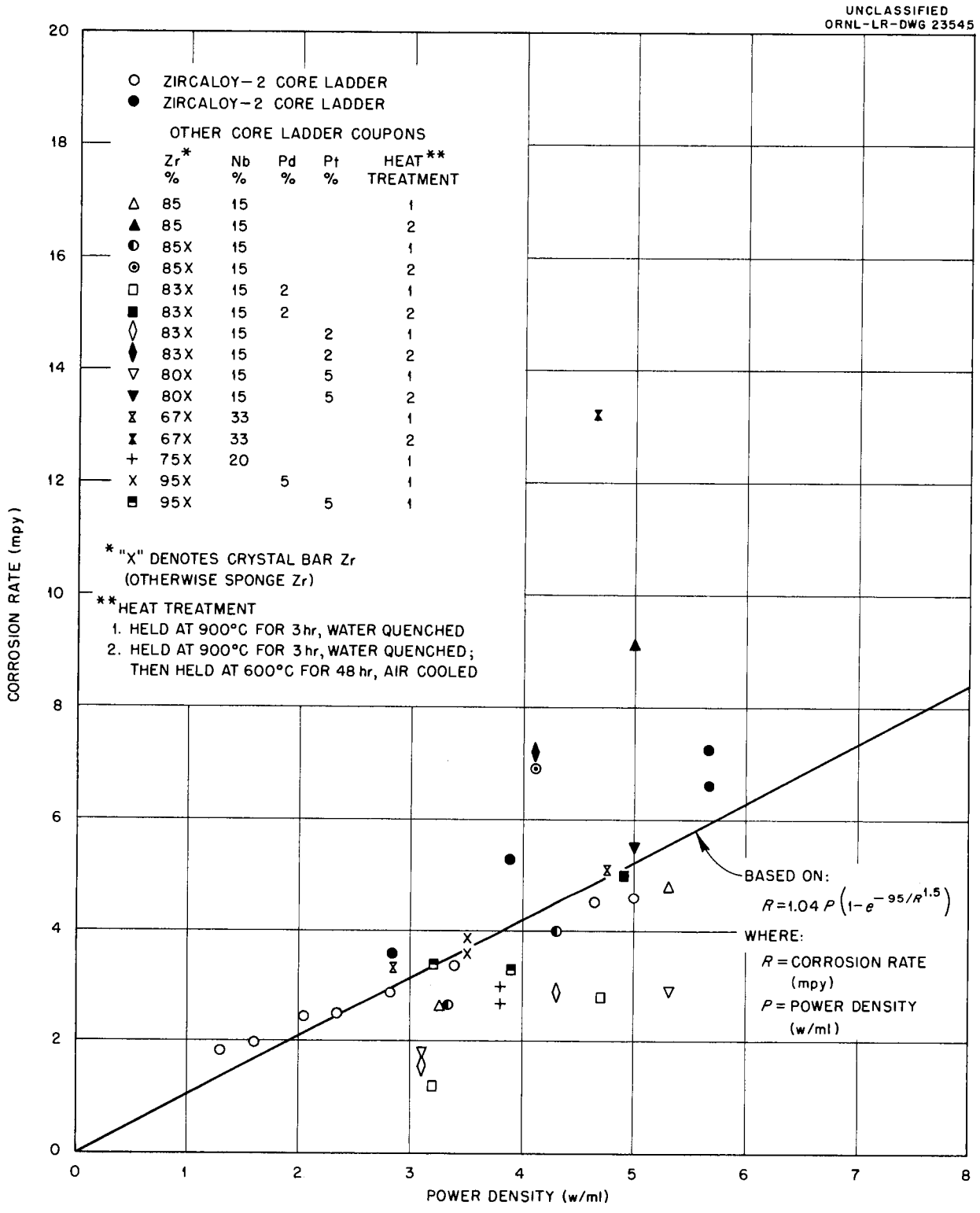

Fig. 14.6. Loop L-4-16 Zirconium-Alloy Corrosion.

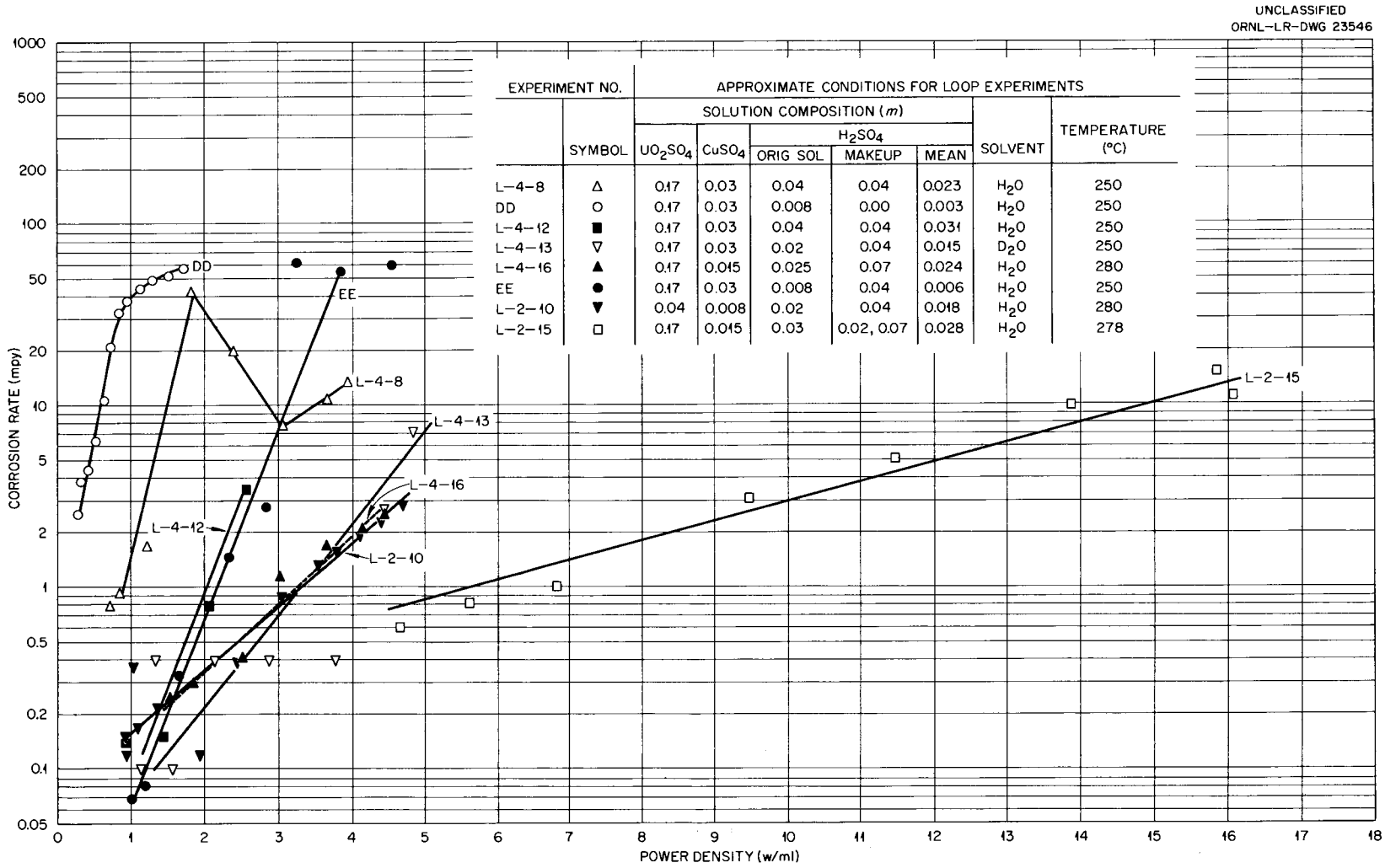

EXPERIMENT NO.	SYMBOL	APPROXIMATE CONDITIONS FOR LOOP EXPERIMENTS						
		SOLUTION COMPOSITION (*m*)						
		UO_2SO_4	$CuSO_4$	H_2SO_4			SOLVENT	TEMPERATURE (°C)
				ORIG SOL	MAKEUP	MEAN		
L-4-8	△	0.17	0.03	0.04	0.04	0.023	H_2O	250
DD	○	0.17	0.03	0.008	0.00	0.003	H_2O	250
L-4-12	■	0.17	0.03	0.04	0.04	0.031	H_2O	250
L-4-13	▽	0.17	0.03	0.02	0.04	0.015	D_2O	250
L-4-16	▲	0.17	0.015	0.025	0.07	0.024	H_2O	280
EE	●	0.17	0.03	0.008	0.04	0.006	H_2O	250
L-2-10	▼	0.04	0.008	0.02	0.04	0.018	H_2O	280
L-2-15	□	0.17	0.015	0.03	0.02, 0.07	0.028	H_2O	278

Fig. 14.7. Radiation Corrosion of Stainless Steel; Loop Results.

Table 14.3. L-4-16 Material Balance of Scale Constituents

Element	Mass Ratio of Element to Iron in Scale	Mass Ratio of Element to Iron in Stainless Steel	Element Oxidized During In-Pile Exposure (g)	Element in Scale Based on Iron (g)	Excess of Element in Scale over Amount Calculated from Corrosion Data (g)
Zr	0.2		0.62*	0.66	0.04
Cr	0.14	0.26	0.83**	0.46	–0.37
Ni	0.16	0.15	0.46**	0.53	0.53
Fe	(1)	(1)	3.3**	(3.3)	(0)

Stainless Steel Oxidized During In-Pile Exposure	
Based on Oxygen Data (g)	Based on Nickel Data (g)
4.64	4.50

*Based on weight-loss data.

**Based on oxygen-consumption data.

of iron in the scale were calculated from the average of the analytical results reported in Table 14.1. The value in column 4 for the weight of zirconium oxidized during exposure is the sum of the measured weight loss for all zirconium specimens in the core. It is assumed that no selective oxidation of any constituent of a zirconium alloy took place. The values in this column for the elements chromium, nickel, and iron were obtained from the value for the total corrosion of steel during in-pile exposure as determined from oxygen data. Again it is assumed that there was no preferential attack of any constituent of the steel.

Values for the amount of a given element contained in the total loop scale are listed in column 5. Several assumptions were made in obtaining these values as discussed below. The value of 3.3 g for the amount of iron oxidized is the total amount of iron in that portion of the loop scale which contains zirconium. An appreciable amount of corrosion occurred during the preparatory operations which preceded the in-pile operation. However, the scale formed during these preparatory operations probably contained no zirconium. In addition, the scale sampling method was such that a given sample is probably more representative of scale formed during latter portions of the operation than of the average composition of the total scale. Some iron was in solution at the end of the in-pile operation. This iron has been neglected in the calculations since the amount was small and since some zirconium was also in the solution. Consideration of these solution components would not change appreciably the conclusions regarding zirconium in the scale. Using the value of 3.3 g for iron, the amounts of zirconium, chromium, and nickel were calculated from the values in column 2 for the ratio of the given element to iron in the scale.

As shown in the final column, the value for the amount of zirconium in the scale obtained in the above manner is in near agreement with the value for the amount of zirconium oxidized during the experiment. This is regarded as evidence that zirconium oxide is indeed removed from the corroding surface during irradiation in the loop and deposited elsewhere in the loop. It has been mentioned previously that the appearance of the Zircaloy-2 specimens when removed from a loop experiment is indicative of such behavior. In general, a core specimen appears to be free of heavy scale and to have only a thin adherent film.

The value for chromium shown in the final column is the difference between the values in columns 4 and 5. This difference shows that the amount of chromium found in the scale is about one-half that expected if the ratio of iron to chromium in the scale samples were the same as that in the metal. The value for nickel in the final column is the same as the value listed in column 5 since it is expected that essentially all the nickel which is oxidized is in solution. This value of 0.53 g indicates that the amount of nickel in the scale is greater than the amount which went into solution. No explanation is offered for these apparent discrepancies in the nickel and chromium material balances. However, these results appear significant and more data of this type will be obtained.

14.1.7 In-Pile Loop L-2-17

Irradiation of stainless steel loop L-2-17 was completed in beam hole HB-2 at the LITR. Total circulation time with enriched solution was 1147 hr, of which 57 hr was accumulated outside the reactor. The energy output of the LITR during insertion was 2625 Mwhr. Almost all this energy was liberated at the 3-Mw level. After 610 hr of circulation the loop was drained to permit replacement of a plugged valve. A fresh solution was charged to the loop before operation resumed.

Operating conditions and contents were reported previously.[23] The solution originally charged to the loop for both periods of operation was 0.04 *m* UO_2SO_4 (enriched), 0.005 *m* $CuSO_4$, and 0.025 *m* H_2SO_4 in a light-water solvent. The calculated free-acid concentration was maintained reasonably constant during the run. The main-stream operating temperature was 300°C; the pressurizer temperature was 315°C. No evidence of solution instability was observed at these operating conditions. The over-all stainless steel corrosion rate was 0.8 mpy based on oxygen consumption and 0.6 mpy based on the nickel in solution.

14.1.8 In-Pile Loop L-4-18

Stainless steel loop L-4-18 is now being exposed in beam hole HB-4 at the LITR. Coupon specimens in tapered-channel type 347 stainless steel holders are located in both the core and line positions. These holders contain coupon specimens of type 347 stainless steel, type 430L stainless steel, and Zircaloy-2. Two ladder coupon assemblies and one stress-specimen assembly are also contained in both the core and in-line locations. The ladder-type coupons are fabricated from Zircaloy-2, zirconium–15% niobium, titanium 55A, titanium–3% aluminum, type 347 stainless steel, and type 430L stainless steel. The zirconium- and titanium-alloy ladder specimens are mounted in a titanium 75A holder. The steel ladder specimens are held in a type 347 stainless steel holder. Both stress-specimen assemblies were fabricated entirely from Zircaloy-2.

The solution composition for L-4-18 is 0.17 *m* UO_2SO_4 (enriched), 0.07 *m* $CuSO_4$, and 0.02 *m* H_2SO_4 in a heavy-water solvent. Loop L-4-13 is the only previous experiment in which heavy water was used.

The makeup solution used to replace samples withdrawn from the loop is the same as above except that it contains 0.05 *m* H_2SO_4 to replace acid consumed in corrosion and 100 ppm of chromium to protect the valve stems during solution addition.

Operating temperatures for this loop are 235°C in the main stream and 265°C in the pressurizer.

14.2 IN-PILE AUTOCLAVE TESTS – LITR

14.2.1 Development and Construction

The assembly and testing of static autoclaves for radiation-corrosion studies in beam holes HB-5 and HB-6 of the LITR continued during the past quarter. Two experiments, L52Z-107 and L53Z-108, fabricated from Zircaloy-2 and containing Zircaloy-2 coupon-type corrosion specimens were prepared for in-pile operation in HB-5. Experiments L6Z-106 and L6Z-112, fabricated from Zircaloy-2 and containing zirconium-alloy and type 347 stainless steel pin-type corrosion specimens, were prepared for the HB-6 facility. Figure 14.8 is a photograph of the HB-6 type autoclave.

A transparent Lucite model of the new HB-5 type rocking autoclave[24] was constructed so that the degree of agitation of the fuel solution could be observed during rocking. It was found that the coupon-rack assembly, which consisted of a nine-coupon arrangement, prevented smooth flow of the fuel solution above and below the coupon-rack assembly. In trying several other arrangements it was observed that six coupons, equally spaced,

[23] G. H. Jenks *et al.*, *HRP Quar. Prog. Rep. April 30, 1957*, ORNL-2331, p 113–118.

[24] G. H. Jenks *et al.*, *HRP Quar. Prog. Rep. Jan. 31, 1957*, ORNL-2272, p 112, Fig. 13.2.

allowed the fuel solution to circulate more freely. Figure 14.9 is a photograph of the new coupon-rack assembly with six coupons which will be incorporated into future experiments.

14.2.2 Analyses for Hydrogen Absorption in Zircaloy-2 in In-Pile Autoclave Tests

(a) Introduction. – No autoclave tests were completed during this quarter. An attempt was made to analyze a few irradiated Zircaloy-2 specimens for hydrogen content and to analyze the pressure and weight data from the numerous Zircaloy-2 experiments for evidence of hydrogen absorption in the metal. These hydrogen analyses are reported here.

(b) Method of Analysis for Hydrogen in Specimens. – The Analytical Chemistry Division recently completed and placed in operation a system for determining hydrogen in radioactive zirconium and titanium specimens. With this system, the specimen is hot fused. In normal operation, with zirconium specimens, a small sample is placed in a quartz tube, out-gassed at room temperature, heated rapidly to 1200°C, held there for 10 min, and then cooled to room temperature. The equilibrium pressure of gas at 1200°C is noted. This pressure is assumed to be caused by hydrogen evolution from the metal, and the hydrogen content is determined from the observed value of the equilibrium pressure. Normally, the evolved gas is reabsorbed during cooling so that the final pressure is only slightly greater than the initial pressure.

The results of attempts to apply this method to analysis for hydrogen in Zircaloy-2 specimens from in-pile bomb tests indicated that some revision of the normal method is necessary. A sharp and significant increase in pressure occurred as the quartz tube containing an irradiated specimen was heated. The pressure decreased from the peak pressure to some equilibrium pressure, but an appreciable fraction of this gas remained in the system after cooling.

A possible interpretation of this behavior is that water and/or other gas adsorbed on scale and film remaining on the irradiated specimens[25] is released at high temperature and is responsible for the pressure behavior. The specimens were not pickled to remove all oxide and scale prior to hydrogen

[25] G. H. Jenks *et al.*, *HRP Quar. Prog. Rep. July 31, 1955*, ORNL-1943, p 129.

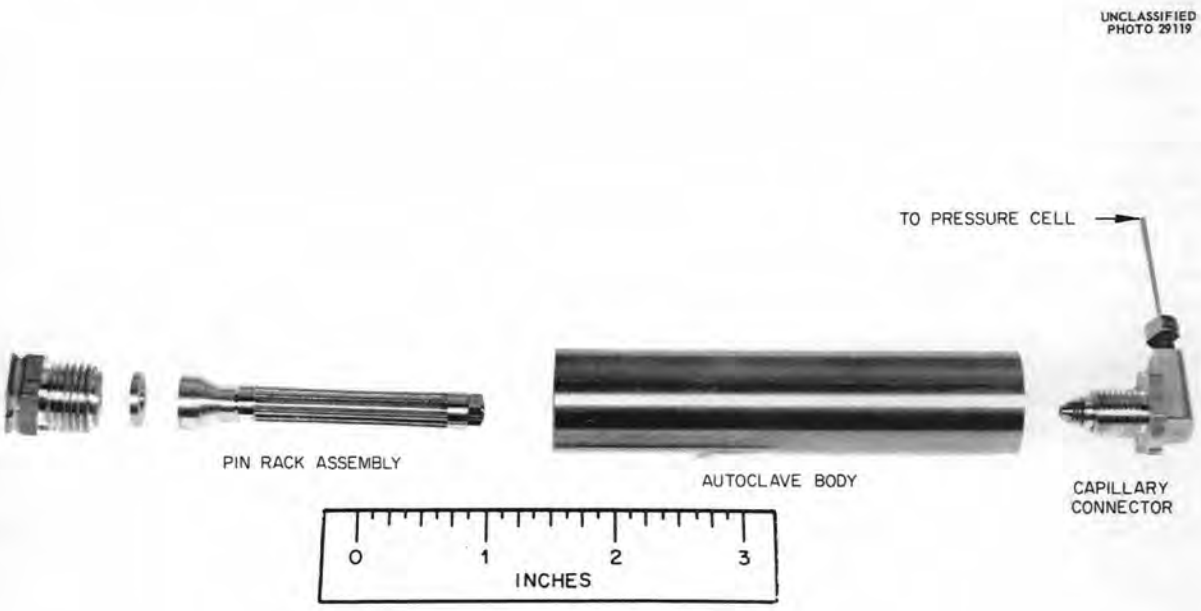

Fig. 14.8. LITR HB-6 Type Autoclave.

UNCLASSIFIED
PHOTO 29265

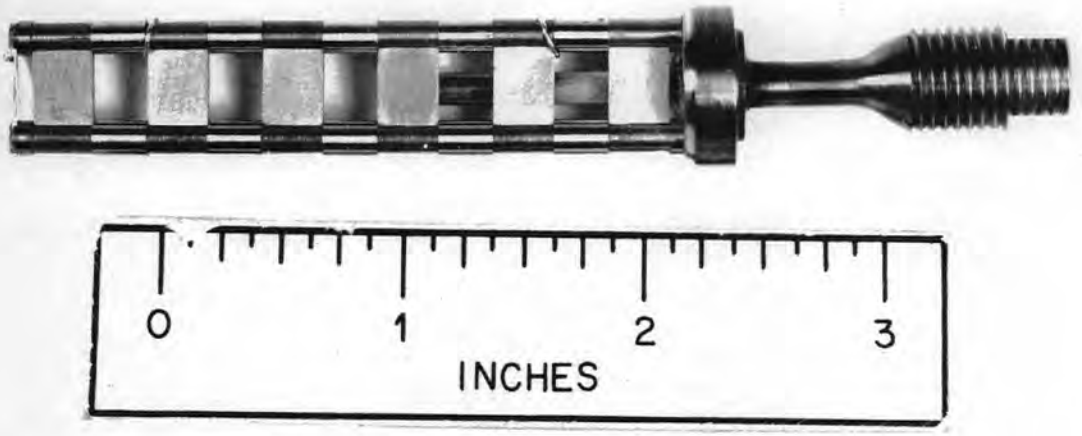

Fig. 14.9. Coupon-Rack Assembly for In-Pile Autoclave; HB-5, LITR.

analysis, because it is believed likely that the hydrogen content of the Zircaloy-2 would be altered during pickling. The specimens were immersed in acetone and then air-dried at 110°C before analysis. This is the usual method of removing a large portion of the scale from irradiated specimens.

To obtain some quantitative measure of the effect of scale in these hydrogen determinations, a series of experiments (Table 14.4) was carried out in cooperation with the Analytical Chemistry Division. Specimens of as-machined Zircaloy-2 from the same stock were used in each measurement. For some experiments, a small quantity of hydrous ZrO_2 was placed in the system along with the specimens. This hydrous oxide (obtained from H. O. Phillips of the Chemistry Division) had been precipitated, washed, and air-dried at 100°C and, prior to use in a measurement, had been treated in various ways to simulate various treatments of irradiated specimens. In the analysis system, out-gassing was carried out at several temperatures. The experimental conditions, specimen dimension, and results of pressure measurements are shown in Table 14.4. Specimens for which the pin designation includes the same number were cut from the same original larger specimen. Two measurements were made on each of the first seven specimens. Between measurements, the given sample was out-gassed overnight at room temperature.

When oxide was present, the peak pressure for the first measurement exceeded the equilibrium pressure in each case except experiment 7, in which the system was off-gassed at 500°C. No value for peak pressure is listed for those cases in which the pressure did not exceed equilibrium pressure. Residual pressures in appreciable amounts were noted for all experiments which included oxide.

The full interpretation of these results is unknown, although several general comments can be made. The results indicate that the burst of pressure observed with the irradiated specimen is caused by off-gassing of the oxide at the high temperature. Spuriously high equilibrium pressures are found when the temperature of off-gassing of the added oxide is 150°C or less. The presence of a high residual pressure in experiment 7 which included off-gassing at 500°C indicates that adsorbed gases are not completely removed from the oxide at this high temperature. However, the 500°C treatment eliminates the burst of pressure observed at the lower off-gassing temperature. It appears that the probability of obtaining a valid result with

Table 14.4. Pressure Behavior of Zircaloy-2 with Oxide in Hydrogen Analytical System

Experiment No.	Pin No.	Conditions	Length (in.)	Diameter (in.)	Area (cm^2)	Weight (g)	Weight of Oxide Added (mg)	First Measurement				Second Measurement		
								Maximum Pressure (mm)	Equilibrium Pressure (mm)	Hydrogen Content of Specimen (ppm)	Residual Pressure (mm)	Equilibrium Pressure (mm)	Hydrogen Content of Specimen (ppm)	Residual Pressure (mm)
1	1A	Control	0.886	0.062	1.15	0.2791	0		0.12	81	0.02	0.11	77	0.02
2	6A	Control	0.852	0.062	1.11	0.2735	0		0.12	82	0.02	0.11	78	0.02
3[a]	1B	Oxide dried for 2 hr at 110°C	0.890	0.062	1.16	0.2729	3.9	0.65	0.20	120	0.17	0.11	78	0.07
4[b]	2A	Oxide submerged in acetone, then air-dried at 110°C for 2 hr	0.907	0.062	1.18	0.2771	3.9	0.8	0.25	140	0.18	0.17	110	0.08
5[c]	2B	Oxide-dried at 110°C for 2 hr. System off-gassed at 150°C	0.867	0.062	1.13	0.2717	3.7	0.5	0.17	110	0.14	0.10	73	0.06
6[d]	6B	Oxide submerged in acetone, then air-dried at 110°C for 2 hr. System off-gassed at 150°C	0.855	0.062	1.11	0.2686	3.4	0.7	0.18	110	0.15	0.12	82	0.04
7[e]	3A	Oxide submerged in acetone, then air-dried at 110°C for 2 hr. System off-gassed at 500°C	0.901	0.062	1.17	0.2848	3.8		0.14	90	0.17	0.10	70	0.05
8	3B	Off-gassed at 500°C	0.892	0.062	1.15	0.2796	0		0.16	97	Not available			
9	4A	Off-gassed at 500°C	0.892	0.062	1.15	0.2876	0		0.15	94	Not available			
10	4B	Vacuum fusion	0.883	0.062	1.14	0.2916	0		Not available	92	Not available			

[a] Immediate surge of pressure upon raising temperature; pressure reached 0.65 mm, then return to equilibrium began immediately; oxide and sample were darkened.

[b] Immediate surge of pressure, reoched 0.8 mm; return to equilibrium began immediately; oxide and sample were black in color.

[c] Some gas evolved during out-gassing at 150°C; no change in sample or oxide; immediate surge of pressure upon heating to 1200°C; return to equilibrium from the peak pressure of 0.5 mm began immediately; sample and oxide were black.

[d] Some gas evolved during out-gassing at 150°C; no change in sample or oxide; immediate surge of pressure upon heating to 1200°C; return to equilibrium from the peak pressure of 0.7 mm began immediately; sample and oxide were black.

[e] Considerable quantity of gas evolved during out-gassing at 500°C; sample turned dark; no surge of pressure upon heating to 1200°C; sample and oxide were dark.

irradiated specimens is increased by out-gassing at 500°C prior to heating to 1200°C. Comparison of the results of experiments 1, 2, 8, 9, and 10 indicates that the hydrogen content of a specimen is not changed appreciably by this treatment. However, further tests will be necessary to establish the reliability of results of measurements with irradiated specimens.

An estimate of the reliability based on the few measurements reported here is that the indicated hydrogen content of a given irradiated specimen can be expected to differ from that of a control specimen by as much as 20 to 30 ppm when there has been no change in the actual hydrogen content of the irradiated specimen.

(c) Results of Measurements of Hydrogen in Irradiated Specimens. – Determinations were made of the hydrogen in one specimen from each of three in-pile autoclave experiments. The general analytical method described above was employed in each. Data concerning these measurements are recorded in Table 14.5. Two of these experiments were with solutions which contained no uranium. The solution for the other contained depleted uranium. Hence the fast neutrons and reactor gamma rays were the principal sources of absorbed radiation energy in each. The analytical procedure employed with specimens 15-7 and 15-8 included out-gassing at 500°C. Specimens A and B were controls for these specimens. For 15-7, the experiment with 0.02 *m* H_2SO_4 solution with an oxygen overpressure, the results indicate that within the experimental uncertainty of 20 to 30 ppm, no hydrogen entered the metal during exposure. The results of experiment 15-8, the experiment with water and a hydrogen overpressure, indicate a significant pickup of hydrogen. The values listed in the final column were calculated by making the following assumptions: (1) the difference between the listed values for hydrogen content in the control and in the given specimen represents the actual amount of hydrogen picked up by the specimen during exposure, and (2) this additional hydrogen is concentrated in a layer of metal at the specimen surface which is 1 mil in thickness. Any hydrogen initially present in the 1-mil layer is neglected.

The analytical procedure for the specimen from Z-22 did not include out-gassing at 500°C. In fact, this specimen was the first one in which an analysis was attempted and the one with which the phenomenon of the burst of pressure was first noted. Controls for this specimen are experiments 1, 2, 8, 9, and 10 in Table 14.4.

Table 14.5. Hydrogen Determinations in Zircaloy-2 Specimens Exposed In-Pile in Solution Free of Appreciable Fissioning

Experiment No.	Solution	Equilibrium Pressure (mm)	Residual Pressure (mm)	Hydrogen Concentration (ppm)	Hydrogen Concentration in Control (ppm)	Change in Hydrogen Concentration	Calculated Hydrogen Concentration in a 1-mil Layer (ppm)
Z-22 (LITR)	0.17 *m* UO_2SO_4 (depleted), O_2 atmosphere	Not available	Not available	98	80–100	No significant change	
15-7 (MTR)	0.02 *m* H_2SO_4, 740 ppm N_2, O_2 atmosphere	0.045	0.015	73	46	No significant change	120
15-8 (MTR)	Water, H_2 atmosphere	0.115	0.05	108	46	Significant increase	430
Control A		0.025	0.020	46			
Control B		0.023	0.015	46			

As discussed previously, experiments Z-22 and the similar experiment Z-13 demonstrated an anomalous pressure excursion during exposure. The possibility that this phenomenon was caused by absorption of hydrogen by the Zircaloy-2 surfaces was suggested.[26] The quantity of absorbed hydrogen necessary to free enough oxygen to exert the increased pressure observed is unreasonably large. For instance, if the hydrogen-rich layer was ZrH_2, about 0.5 mil of metal in Z-22, or 0.3 mil in Z-13, must have reacted to consume the indicated amount of hydrogen. The total corrosion penetration during the entire experiments was far less than 0.3 or 0.5 mil. This would indicate the unlikely situation that the hydrogen was absorbed and later desorbed without noticeably affecting the reactivity of the metal.

Another possible explanation of these pressure excursions during experiments with depleted UO_2SO_4 is that, due to precipitation or some other phenomenon, the copper concentration dropped from 0.04 *m* (initial) to about 10^{-5} *m*, and pressure caused by radiolytic gas built up. Cupric ion catalyzes the recombination of hydrogen and oxygen but it would probably also inhibit the recombination due to the gamma field, even at low concentrations, by reacting with the radical products presumed to be intermediates in the recombination by gamma rays.[27] The later solution of this precipitated copper could then account for the return of the pressure to the normal value.

(d) Hydrogen Absorption in Experiments in Which Fissioning in Solution Is the Major Source of Radiation. – No specimens which have been exposed in in-pile autoclave experiments at appreciable fission power densities have been analyzed for hydrogen. However, possible hydrogen absorption in the relatively large number of Zircaloy-2 autoclaves exposed to significant fission power density can be estimated from the average agreement of corrosion penetrations from oxygen consumption and from specimen weight losses. Absorption of hydrogen would be accompanied by a buildup of oxygen, which, in turn, would contribute a negative error to the corrosion penetration calculated from oxygen consumption.

Table 14.6 shows a summary of such a comparison. Those autoclaves which were free of nitrogen during exposure were averaged separately, and the average difference between penetration from weight losses and from oxygen consumption is very small and in the direction of a negative amount of hydrogen absorption. The comparison of those tests which included some atmospheric nitrogen is not so direct, since nitrogen appears to at least partially oxidize during the exposure.[28]

If no correction for oxygen consumed in nitrogen oxidation is made, then the penetration from oxygen consumption is higher than that from pin weight losses. This agrees qualitatively with the presumption that nitrogen is oxidized. If all the nitrogen is presumed to have been completely oxidized to nitrate and the appropriate correction for consumed oxygen is made, then the corrosion penetration from corrected oxygen consumption is sufficiently smaller than penetrations calculated from specimen weight losses which indicate 140 ppm of hydrogen in a 1-mil surface layer. The 140-ppm value is a maximum value corresponding to a correction for oxygen used to oxidize nitrogen to its maximum valence state.

In summary, those tests which included nitrogen indicate 0 to 140 ppm of hydrogen in a 1-mil surface layer, and those tests without nitrogen indicate no hydrogen absorption.

14.3 IN-PILE AUTOCLAVE TESTS – MTR

Three Zircaloy-2 rocking-bomb experiments, containing no uranium in solution, were exposed in the HB-3 beam-hole facility of the MTR about a year ago. One of these, ORNL-15-5, has been discussed.[29] The other two, ORNL-15-7 and ORNL-15-8, were not discussed previously because the examination of the irradiated specimens was incomplete. They are discussed in this report since the results of measurements of several different types are now available. However, the examination is still incomplete.

---

[26] G. H. Jenks *et al.*, *HRP Quar. Prog. Rep. April 30, 1957*, ORNL-2331, p 120.

[27] J. W. Boyle, personal communication.

[28] G. H. Jenks *et al.*, *HRP Quar. Prog. Rep. Jan. 31, 1957*, ORNL-2272, p 114.

[29] G. H. Jenks *et al.*, *HRP Quar. Prog. Rep. April 30, 1956*, ORNL-2096, p 95.

Table 14.6. Comparison of Zircaloy-2 Corrosion Penetrations Calculated from Oxygen Consumption and from Specimen Weight-Loss Data

	Corrosion Penetration from Weight Losses Minus Corrosion Penetration from Oxygen Consumption (mil)	Calculated Hydrogen Concentration in a 1-mil Surface Layer (ppm)
Autoclaves free of nitrogen (6 experiments)		
Mean	−0.003	Negative
High	0.043	
Low	−0.049	
Autoclaves with about 660 ppm N_2, uncorrected for nitrogen oxidation (20 experiments)		
Mean	−0.018	Negative
High	0.025	
Low	−0.066	
Autoclaves with N_2, corrected by assuming oxidation of N_2 to NO_3^- (20 experiments)		
Mean	0.031	140
High	0.085	
Low	−0.030	

The experimental conditions and some of the results are summarized in Table 14.7. The results of hydrogen analyses are discussed in Sec. 14.2.2. The solution power densities in these experiments is limited to energy dissipated from fast neutrons (about 4 w/ml) and from gamma rays (also about 4 w/ml). Examination of the 15-7 solution indicated that about 80% of the nitrogen included as atmospheric nitrogen was oxidized to nitrate during exposure. Since the oxidation of nitrogen would have consumed considerable oxygen, the corrosion penetration indicated by the pressure measurements was corrected for this N_2 oxidation. It was assumed in applying this correction that N_2 was completely oxidized to NO_3^-. A similar correction for nitrogen oxidation was also applied to the 15-5 pressure data. This correction is very significant; for instance, the uncorrected penetration in 15-5 was 0.084 mil; corrected, 0.051 mil. No correction for nitrogen was made to the 15-8 data since the manner in which the bomb was filled excluded nitrogen.

A comparison of values for corrosion penetrations from pin weight gain and from pressure data is given in Table 14.7. The agreement indicates that the corrosion rates reported are probably correct to about ±30%.

X-ray diffraction patterns of the corrosion film *in situ* in 15-7 and 15-8 show monoclinic ZrO_2.

Table 14.7. MTR In-Pile Zircaloy-2 Bomb Data

Experiment No.	Solution	Corrosion Penetration		Nominal Solution Temperature (°C)	Operating Time Inserted (hr)	Corrosion Rate (O_2 Consumption)[a] (mpy)
		From Weight Gains (mil)	From O_2 Consumed[a] (mil)			
15-5	H_2O,	0.054				
	740 ppm N_2,	0.054	0.051	300	104	4
	O_2 atmosphere	0.083				
15-7	0.017 *m* H_2SO_4,	0.069	0.051	250	95	0.8
	740 ppm N_2,	0.036		280	109	3
	O_2 atmosphere	0.024[b]				
15-8	H_2O,	0.000[b]	0.023[c]	290	357	0.3
	H_2 atmosphere	0.052				
		0.027				

[a]Corrected for oxidation of N_2 to NO_3^-.

[b]These samples analyzed for hydrogen.

[c]Penetration estimated from H_2 production as indicated by pressure increase plus hydrogen absorbed as indicated by specimen analysis.

15. METALLURGY

G. M. Adamson

R. G. Berggren
J. P. Hammond
W. J. Leonard
M. L. Picklesimer
J. J. Prislinger
P. L. Rittenhouse
R. L. Stephenson
J. K. White
J. C. Wilson
O. Zmeskal

15.1 PHYSICAL METALLURGY

15.1.1 Zirconium-Alloy Development

Zirconium-niobium alloys have shown promise in having an in-pile corrosion resistance superior to that of Zircaloy-2. An alloy development program has been under way, with the objectives of improving the corrosion resistance of the Zr-Nb alloys and of determining the transformation kinetics and mechanisms of the alloys. Most of the work has been concentrated on Zr–15% Nb alloys containing minor additions of ternary elements. The earlier work has been reported in three prior reports,[1–3] where micrographs and age-hardening curves were presented in interpretation of the transformation kinetics and products of the system.

During the quarter, studies of the transformation kinetics and products of the Zr-Nb-*X* alloys and Zr-Nb alloys showed that, while the data of the prior reports were correct, although incomplete, some of the interpretation of that data was incorrect. For example, in the last report,[3] the statement was made that the hardening constituent for the retained-beta specimens was thought to be quite similar to the "omega" phase found in the beta-titanium alloys. Very recent x-ray diffraction results have shown, however, that the hardening constituent is actually a niobium phase, supersaturated with zirconium, whose composition changes to lower zirconium contents as aging proceeds.

Age-hardening curves for Zr–15% Nb, sponge Zr–15% Nb, Zr–15% Nb–2% Pd, and Zr–15% Nb–1% Fe at 600, 550, 500, 450, 400, and 350°C for times up to 1 hr were completed, and the data are presented in Figs. 15.1 through 15.4. Numerous hardness points, including the 350°C curve for the Zr–15% Nb alloy, which had been questioned, were rechecked by testing new specimens, and the majority were found to be correct. Each point on the 350°C curve represents a separate specimen tested at a different time. Thus the presence of two aging peaks was verified. (It may be possible that there are three aging peaks; this will be investigated by testing specimens at 1- or 2-min intervals.)

An x-ray diffraction technique using 0.010- to 0.015-in.-dia wire specimens in a Debye-Scherrer camera gave excellent results in the identification of the phases that were present during the aging at 400°C of the Zr–15% Nb alloy. (This x-ray

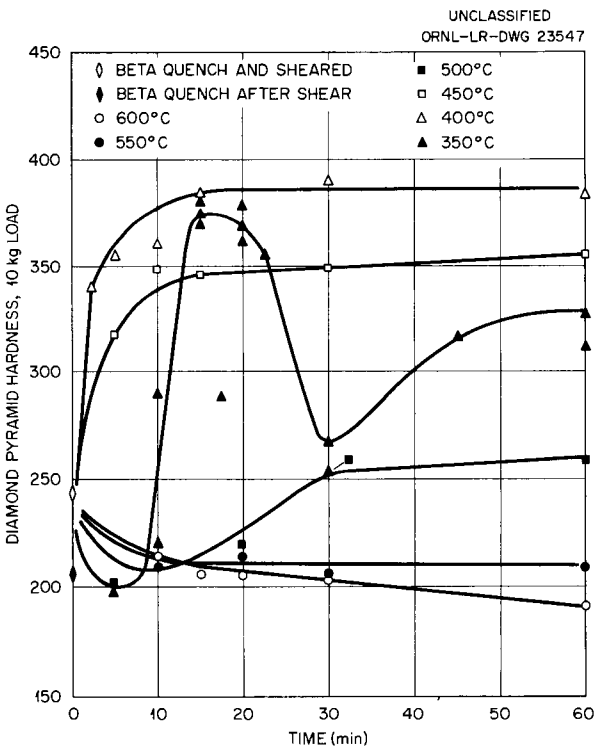

Fig. 15.1. Hardness Curves for Beta-Quenched and Reheated Zr–15% Nb Alloy.

[1] G. M. Adamson *et al.*, *HRP Quar. Prog. Rep. Oct. 31, 1956*, ORNL-2222, p 114–116.

[2] G. M. Adamson *et al.*, *HRP Quar. Prog. Rep. Jan. 31, 1957*, ORNL-2272, p 119–123.

[3] G. M. Adamson *et al.*, *HRP Quar. Prog. Rep. April 30, 1957*, ORNL-2331, p 124.

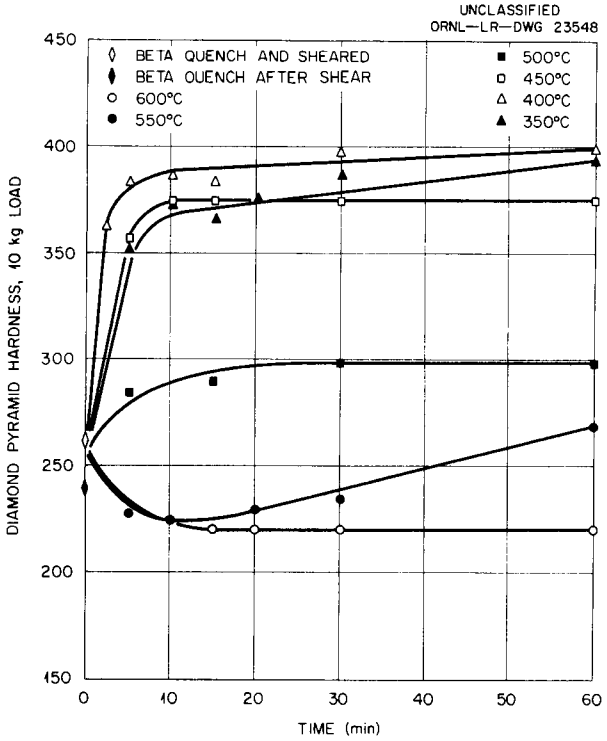

Fig. 15.2. Hardness Curves for Beta-Quenched and Reheated Sponge Zr–15% Nb Alloy.

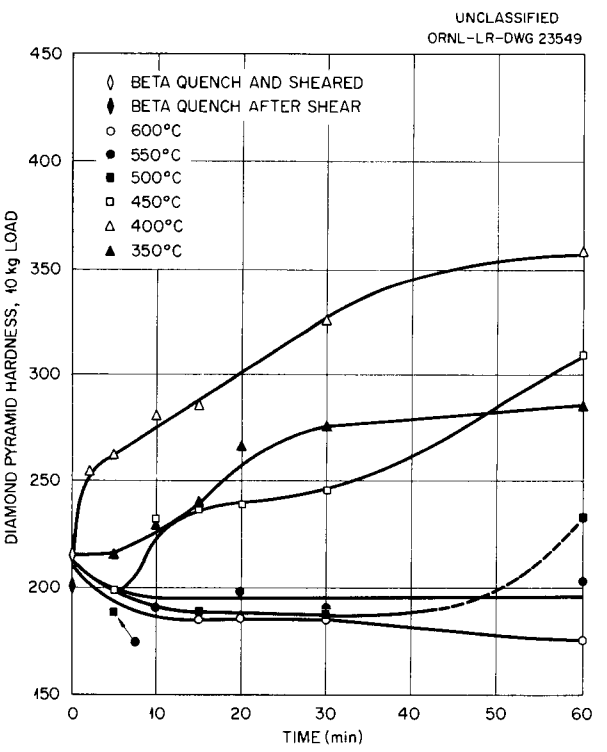

Fig. 15.3. Hardness Curves for Beta-Quenched and Reheated Zr–15% Nb–2% Pd Alloy.

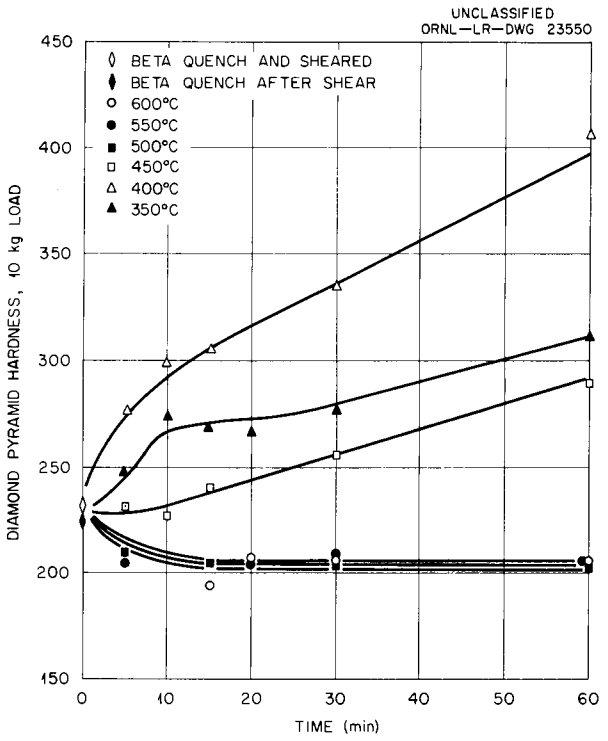

Fig. 15.4. Hardness Curves for Beta-Quenched and Reheated Zr–15% Nb–1% Fe Alloy.

work was done by R. M. Steele of the x-ray diffraction group of the Metallurgy Division.) Wire specimens 0.040 in. in diameter and 1 in. long were capsulated and heat treated. The wires were then cut in half; one half was mounted for metallographic examination, and the other half was chemically polished to 0.010 in. in diameter for x-ray diffraction specimens. Analysis of the x-ray films is not quite complete, but the results to date show that the beta-quenched specimen contained two phases, one phase being beta zirconium, body centered cubic with an a_0 of 3.5437, and the other having a set of lines which index with that of a phase reported for the Zr–7.5% Mo alloy to be "omega."[4] Examination of the quenched specimens after aging at 400°C shows that for 3-hr aging, the specimen consisted of three phases, one body centered cubic with an a_0 of 3.56, one body centered cubic with an a_0 of 3.51, and the third, lines which index with the "omega" phase (see above) but with less intensity. After 24-hr aging, the specimen consisted of only two phases, both body centered cubic, one with an a_0 of 3.57

[4] H. A. Robinson *et al.*, *J. Metals* **8**, 1544 (1956).

and the other with an a_0 of 3.48, and with no "omega" lines whatever. The disappearance of the "omega" lines in the x-ray pattern coincides with the disappearance of the Widmanstätten platelet phase from the microstructure (see Fig. 14.3, ref 3), and thus the "omega" designation is believed to be an incorrect identification since hardening occurs with the disappearance of the phase and not with its appearance in the x-ray patterns. Estimated a_0 values for the phases, pure body-centered-cubic zirconium, pure niobium, and Nb–10% Zr, are, respectively, 3.58 to 3.59, 3.304, and 3.355. Thus it can be seen that, during aging, a niobium phase containing excess zirconium precipitates out of the beta Zr–15% Nb matrix and, as aging time increases, changes its composition toward the equilibrium content of 10% zirconium, while the matrix composition changes toward pure zirconium (beta).

Examination of Zr–5% Nb, Zr–7.5% Nb, and Zr–10% Nb beta-quenched alloys by the above-described wire technique showed that, as-quenched, the 5% Nb alloy is all alpha, while the 7.5% Nb and 10% Nb alloys are retained-beta zirconium with the Widmanstätten platelet phase. Microstructural examination of the specimens revealed that the 5% Nb alloy is fully martensitic with typical martensite needles, while the 7.5% Nb and 10% Nb specimens clearly show the Widmanstätten platelet phase in a retained-beta matrix, leading to the speculation that the Widmanstätten platelet phase may be a very restricted type of martensitic transformation. This possibility will be investigated by quenching alloys of 6, 6.5, and 7% Nb and examining them.

Some of the ternary alloys were investigated by the wire technique described above, but the results are confusing in that some lines cannot be identified. New specimens are being tested in an attempt to elucidate the results.

Age-hardening data at a few temperatures were determined with several ternary alloys; the results are presented in Table 15.1. The addition of 2% Mo to the Zr–15% Nb alloy suppressed the formation of the hardening constituent for more than 2 hr at 400 and 450°C, while the addition of 5% Mo prevented the formation for at least two weeks at temperatures from 300 to 600°C. X-ray diffraction results are being redetermined; they were inconclusive and somewhat confusing in that lines fitting the ZrO_2 pattern were found. The addition of 1% Al, ½% Cu, or 2% Th suppressed the formation of the hardening constituent for at

Table 15.1. Hardnesses of Several Beta-Quenched and Aged Zr–15% Nb–X* Alloys

Aging Temperature (°C)	Aging Time	Diamond Pyramid Hardness, 10-kg Load					
		1% Cr	1% Al	½% Cu	2% Th	2% Mo	5% Mo
400	0	187	196	196	187	193	235
	30 min	193	193	191	186		
	60 min	221	201	196	191	193	230
	120 min	266	206	198	196	191	243
	24 hr					279	224
	48 hr					299	230
	2 wk						215**
450	1 hr					192	222
	2 hr					193	224
	24 hr					274	221
	48 hr					260	232
500	2 wk						216**
300	2 wk						206**
600	2 wk						216**

*X = Weight per cent alloying element.

**Second ingot.

least 2 hr at 400°C, while the addition of 1% Cr did not prevent but did delay the formation.

Specimens of Zr–15% Nb were beta quenched, aged at 400°C for 2 hr, heated in place in the furnace to 600°C, held at 600°C for 5 min, 30 min, and 2 hr, and water quenched. These tests required, respectively, 25 min, 15 min, and 15 min for the furnace to reach 600°C. All specimens were examined by hardness measurements and metallographically, and the 600°C 2-hr specimen was examined by x-ray diffraction. The results indicate that the age-hardening constituent (after being aged at 400°C for 2 hr, the DPH was 395) redissolved at 600°C. The results are given in Table 15.2. Since the times required to heat to 600°C were somewhat long, the phase may actually have started to dissolve at an intermediate temperature; new specimens will therefore be run in the isothermal transformation machine.

Table 15.2. Diamond Pyramid Hardnesses of Double-Aged Zr–15% Nb Specimens*

Temperature (°C)	Time at Temperature			
	0	5 min	30 min	2 hr**
600	395	202	197	177
			199	179

*Specimens beta quenched and aged at 400°C for 2 hr before 600°C treatment.

**2-hr specimen shows 30% αZr, 70% βZr ($a_0 = 3.534$).

The data obtained to date on the Zr-Nb and Zr-Nb-*X* alloys permit the following general conclusions as to their transformation characteristics to be drawn with some confidence.

1. The decomposition of beta alloys, on quenching and reheating, is somewhat sluggish above 550°C, with the first transformation products being alpha Zr plus Nb-enriched beta Zr, which then precipitates the high-Nb phase (90% Nb–10% Zr), with the Nb enrichment of the beta Zr decreasing with time at temperature after precipitation of Nb begins. The sluggishness of the decomposition is increased by increasing the Nb content, and decreased by the addition of ternary elements of Fe, Pd, and Pt and by the use of sponge Zr with its high oxygen content. Other ternary additions studied at lower temperatures have not, as yet, been sufficiently investigated at the higher temperature.

2. At temperatures below 550°C, the transformation of the retained-beta Zr, quenched and reheated, is relatively rapid to transition products whose compositions change with time at temperature and with the temperature of transformation. All transformations below 550°C are characterized by an age-hardening phenomenon caused by the precipitation of a high-Nb-content body-centered cubic phase, which is supersaturated in Zr and which precipitates Zr as the reaction proceeds. This high-Nb phase forms by a volume decrease, which results in hardening through the resultant compressive stress in the matrix.

The maximum rate of hardening apparently occurs at about 400°C, since specimens being aged at 350 or 450°C take more time to reach a given hardness, with the maximum hardening occurring at or below 400°C. The addition of all ternary elements studied, except oxygen, slows down the rate of hardening at all temperatures, with some additions of 1 at. % or less delaying the formation of the hardening constituent (or, actually, the hardening) for at least 1 hr at 400°C. The addition of 2% Mo delays the formation for more than 2 hr at 400 and 450°C, while 5% Mo prevents the formation for at least two weeks at any temperature.

Over-aging does not occur at 400°C in two weeks but does at 500°C (intermediate temperatures are being investigated). Over-aging occurs with the formation of alpha Zr and the Nb-rich phase (90% Nb–10% Zr) and with retained-beta Zr showing a continually decreasing Nb content. Complete decomposition did not occur in two weeks at any temperature investigated.

3. Widmanstätten platelets form when alloys containing from 7.5 to 33% Nb are quenched from the beta field. The crystal structure of the platelets is not known, although it fits with the lines indexed for the so-called "omega" phase identified in a Zr–7.5% Mo alloy.[4] The platelets redissolve in a short time on heating to temperatures of 300 to 600°C. The platelets disappear from the microstructure as their lines disappear from the x-ray diffraction pattern. Neither the temperature nor the mechanism of formation of the platelets is known. Several possibilities for the mechanism will be investigated soon. The quantity and the thickness of the platelets are

only slightly affected by composition, ternary alloying additions, and heat treatment. In no case can the platelet thickness be resolved accurately in an optical microscope. Electron microscopy is being used in the study, but accurate replication of the surface structure is difficult and has, as yet, not been proved.

The aging transformation of the Zr-Nb-*X* and Zr-Nb alloys can be studied only by x-ray diffraction and hardness measurements at the present time. A machine for studying the transformation by resistance changes was designed and is now being assembled for preliminary tests.

15.1.2 Oxide Films on Zirconium-Base Alloys

Zirconium-niobium alloys were initially exposed in in-pile corrosion tests to investigate a postulated mechanism for radiation corrosion. While the postulated mechanism does not appear to be correct, the in-pile corrosion tests did show that the Zr–15% Nb alloy was considerably more corrosion resistant than Zircaloy-2. Studies were then initiated to determine the differences in the structures of the oxide films on these alloys and how these structures might affect the corrosion resistance. In initial studies, with oxides formed by oxidation in air,[5–7] it was concluded that, even with the Zr-Nb alloys at the low temperature (300°C) of interest to the Project, very little, if any, orthorhombic oxide was formed; the oxide consisted primarily of monoclinic zirconia. Since that date, a wide variety of zirconium-base alloys have been oxidized in out-of-pile loops in uranyl sulfate. These specimens are now being examined by x-ray and electron diffraction for phase composition of the oxide.

The results to date are presented in Table 15.3. The oxides on the silicon and chromium alloys were monoclinic and thin, and the diffraction pattern contained both oxide and metal peaks. The film on the 2% Si alloy was thicker than that on the others, and the film on the 1% Cr alloy was very thin. The films on the remainder of the alloys, all of which contained niobium, were adherent, highly oriented, and appeared to show the underlying metal grain structure. Considerable variation in film thickness and appearance could be noted on the various grains. Lighter colored portions of the films were loose and could be readily scraped from the underlying black, hard,

[5] O. Zmeskal, *HRP Quar. Prog. Rep. July 31, 1956*, ORNL-2148, p 112–114.

[6] G. M. Adamson *et al.*, *HRP Quar. Prog. Rep. Oct. 31, 1956*, ORNL-2222, p 118–119.

[7] M. L. Picklesimer, G. B. Wadsworth, and O. Zmeskal, *Met. Semiann. Prog. Rep. Oct. 10, 1956*, ORNL-2217, p 156–160 (Classified).

Table 15.3. Oxides on Zirconium-Base Alloys Exposed 1000 hr in Uranyl Sulfate Solution at 300°C

Specimen No.	Composition (wt %)	Type of Oxide	Corrosion Rate
Zr-59	Sponge Zr–0.5 Si	White, easily removed, monoclinic	0.3 mpy
Zr-60	Sponge Zr–2.0 Si	Tan, easily removed, monoclinic	10.1 mpy
Zr-61	Zr–0.5 Si	White, easily removed, monoclinic	0.6 mpy
Zr-62	Zr–2.0 Si	Tan, easily removed, monoclinic	3.1 mpy
Zr-65	Zr–0.7 Cr	Black, very thin, adherent, monoclinic	0.1 mpy
Zr-12	Zr–10 Nb–5 Mo	Lustrous, black and tan, monoclinic, orthorhombic	1.5 mpy
Zr-14	Zr–10 Nb–5 Mo–5 Ta	Dull black, monoclinic, orthorhombic	0.9 mpy
Zr-17	Zr–15 Nb–5 Mo	Dull black, monoclinic, orthorhombic	0.9 mpy
Zr-42	Zr–33 Nb	Dull gray, orthorhombic, some monoclinic	0.5 mg/cm^2
Zr-48	Zr–20 Nb–1 Ni	Lustrous black, monoclinic, orthorhombic	0.8 mg/cm^2
Zr-67	Zr–15 Nb–3 Sn	Black, gray, and tan, monoclinic, orthorhombic	0.8 mg/cm^2
Zr-68	Zr–15 Nb–3 V	Lustrous, black and tan, monoclinic, orthorhombic	1.1 mg/cm^2

and adherent oxide. The diffractometer patterns made on the films in place were highly distorted and contained both monoclinic and orthorhombic peaks. The oxide on the 33% Nb alloy (Zr-42) was predominantly orthorhombic.

Electron diffraction patterns were made on a sample of the loose oxide on the Zr–5% Mo–10% Nb alloy (Zr-12). Lines of both the orthohombic and monoclinic oxides were found, but the orthorhombic lines were the stronger and were more positive than was the case for the x-ray pattern.

The tan loose oxide on the Zr–15% Nb–3% V alloy (Zr-68) was scraped free from the hard black oxide with the blade of a knife and was examined in a Debye-Scherrer camera. In addition to the monoclinic and orthorhombic lines, strong lines of a hydrated V_2O_5 phase were present. The monoclinic and orthorhombic phases were present in about equal amounts.

The low-temperature air-oxidation tests of these alloys[7] were of short duration, and the resultant oxides were not well crystallized. The x-ray diffraction patterns were correspondingly poor for identification purposes. The oxides produced by the 1000-hr corrosion test in uranyl sulfate solution, however, were much more crystalline and contained a larger amount of orthorhombic phase (for the niobium alloys) than did similar alloys oxidized in air at a higher temperature (400 to 600°C). The niobium alloys yielded oxides that were mixtures of both the orthorhombic and the monoclinic phases, but it was not clear which phase predominated, other than for the 33% Nb, which was mostly orthorhombic.

15.1.3 Effect of Alloying Elements on the Alpha-Zirconium Solubility for Hydrogen

The effect of several alloying elements on the alpha-zirconium solubility for hydrogen at temperatures above 450°C is being studied, under research contract, at the University of Florida by O. Zmeskal. A modified Sievert type of apparatus is being used to determine the equilibrium hydrogen overpressure as a function of the temperature, hydrogen content, and alloying element. Results to date on the high-purity zirconium specimens used to test the apparatus and procedures have agreed quite well with published data. Considerable difficulty has been encountered in reaching equilibrium conditions for the alloys, in that the time required for equilibrium is so long that the virtual leak rate of the apparatus begins to interfere with the pressure measurements. Several experiments involving various means of speeding up the rate of approach to equilibrium have been tried without success. An attempt at cathodic defilming of the specimen in its hydrogen atmosphere failed to show any significant results. Successive treatments at 900°C and cooling to the lower temperatures of test gave partial success but involved the solution of the oxide film formed on the surface and consequent changes in the composition of the specimen at the surface.

The research contract is being terminated, and a final report is expected at the end of the summer.

15.2 MECHANICAL METALLURGY

15.2.1 Tensile Properties of Irradiated Zircaloy-2

Subsize multiple-break tensile specimens of Zircaloy-2 were irradiated in in-pile corrosion loop L-2-10 to determine whether any change occurred in mechanical properties as a result of irradiation and/or hydrogen pickup from the loop environment. This loop was operated for 1456 hr with the reactor at power (a total of 3765 Mwhr) with a core temperature of 280°C and with 0.04 m UO_2SO_4 as the circulating solution. The exposure to fast flux (>1 Mev) varied from 1.7 to 3.2 $\times$ 10^{19} nvt. Specimens were exposed to the circulating solution in both the high-flux (core) and low-flux (in-line) regions. Duplicate control specimens were also available.

A black surface scale was present on the irradiated specimens, but when the specimens were pulled in the tensile test, the black scale separated from the specimens and a clean, glossy, blue-gray surface could be seen. The gross activity of the core samples was about 5 r/hr (contact), and that of the line specimens was about 2 r/hr (contact).

The mechanical-property data from the various samples are listed in Table 15.4 and illustrated in Figs. 15.5 and 15.6. These data do not reveal any changes in the tensile properties of Zircaloy-2 under the limited conditions of exposure in this loop. The data for tensile strength and proportional limit (Fig. 15.5) show slight increases, at room temperature and at 300°C, with increasing strain rate; however, the increase is the same for

Table 15.4. Tensile Properties of Subsize Zircaloy-2 Specimens Irradiated in Loop L-2-10

Specimen No.	Description	Temperature (°C)	Strain Rate (in./in./min)	Tensile Strength (psi)	Proportional Limit (psi)	Reduction in Area (%)
17	Core	RT*	2.0	89,225	72,550	44.7
21	Line	RT	2.0	88,225	63,725	33.9
23	Control	RT	2.0	88,225	60,800	44.3
19	Control	RT	2.0	87,450	60,400	40.0
1	Core	RT	0.05	77,650	62,350	48.0
5	Line	RT	0.05	79,600	53,925	40.0
3	Control	RT	0.05	80,000	55,875	42.7
7	Control	RT	0.05	79,200	62,750	46.1
13	Core	RT	0.002	72,950	47,050	44.0
9	Line	RT	0.002	74,125	47,050	45.9
11	Control	RT	0.002	68,625	41,175	43.1
15	Control	RT	0.002	63,725	35,300	45.1
18	Core	300	2.0	48,400	33,725	73.0
22	Line	300	2.0	47,550	30,600	74.9
24	Control	300	2.0	43,375	29,400	73.1
20	Control	300	2.0	42,750	27,050	68.9
2	Core	300	0.05	38,825	21,575	71.2
6	Line	300	0.05	41,175	28,625	70.7
4	Control	300	0.05	42,600	25,500	69.4
8	Control	300	0.05	42,500	25,100	66.2
14	Core	300	0.002	36,475	21,950	79.5
10	Line	300	0.002	34,500	23,525	69.9
12	Control	300	0.002	36,850	25,500	61.2
16	Control	300	0.002	28,475	21,575	73.8

*RT = room temperature.

core, in-line, and control specimens, which indicates that irradiation was not a factor.

Figure 15.6 demonstrates the effect of strain rate on the ductility, as measured by reduction in area, of core, in-line, and control specimens at room temperature and at 300°C. There was no obvious impairment of ductility due to exposure to the loop environment.

15.2.2 Titanium Alloys

A Charpy V-notch impact curve for high-purity commercial titanium presented in the last report showed a trough in the curve at about 230°C. The usual tensile curves for this material are smooth with no break in this temperature range. To determine whether this material was typical of the grade of commercial titanium, tensile

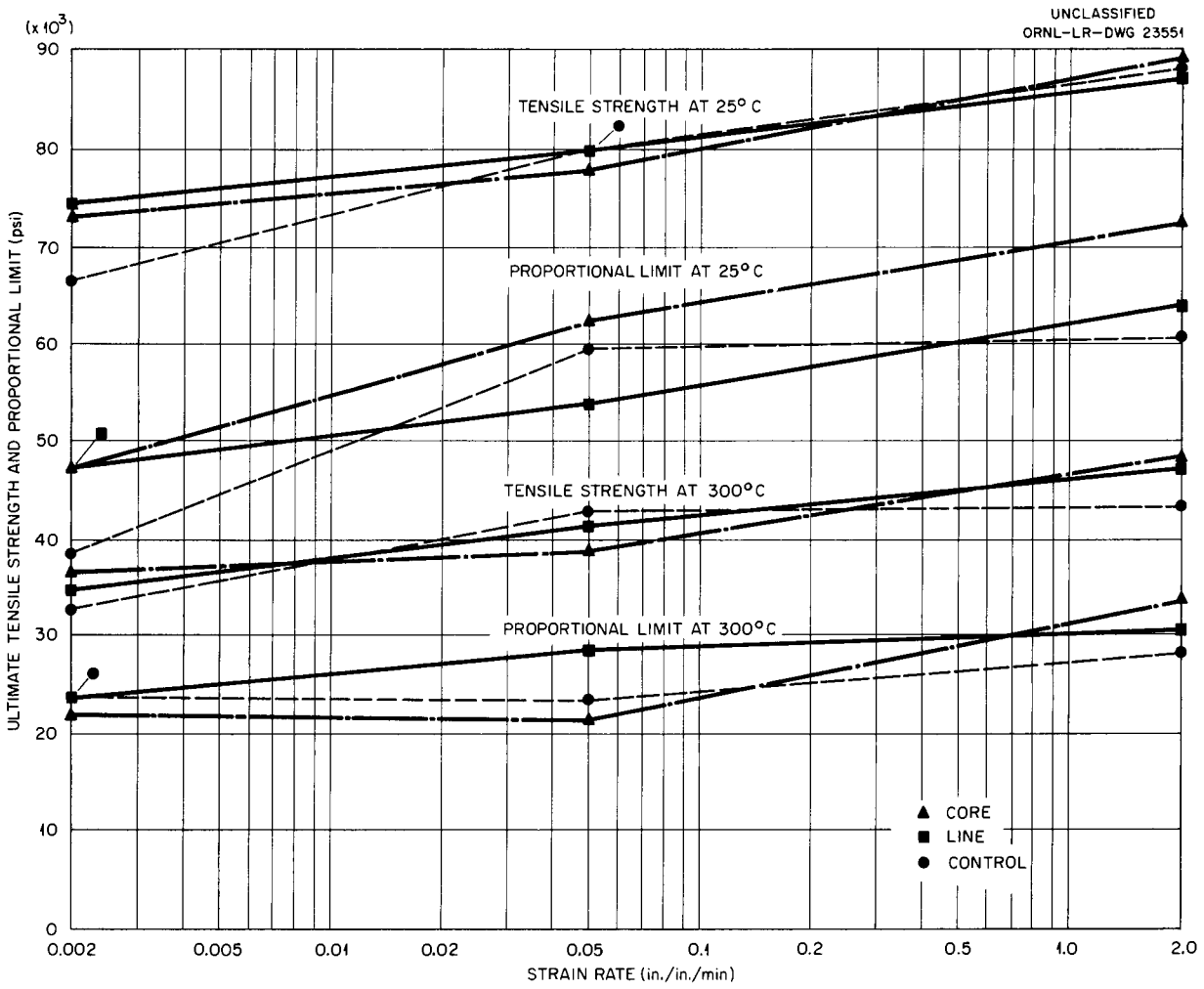

Fig. 15.5. Tensile Properties of Zircaloy-2 Specimens Irradiated in Loop L-2-10.

specimens were broken at room temperature and at 230°C. The data are reported below:

	Temperature	
	25°C	230°C
Elongation, %	37.0	42.0
Tensile strength, psi	56,225	30,560
Yield strength, 0.2% offset, psi	42,790	17,370

The values at these two temperatures do correspond with published values for A-40 titanium.

15.2.3 Effect of Hydrogen on the Embrittlement of Titanium at 300°C

As a possible explanation for some failures in titanium corrosion-specimen holders, a study was made of the effect of aging time on the impact energy for titanium. Samples of A-55 titanium to which various quantities of hydrogen had been added were aged at 300°C and then broken immediately after they had been cooled to room temperature. The data (Fig. 15.7) confirm the previous data and show that the impact energy increased slightly with aging time rather than decreased as would have been the case if embrittlement had occurred.

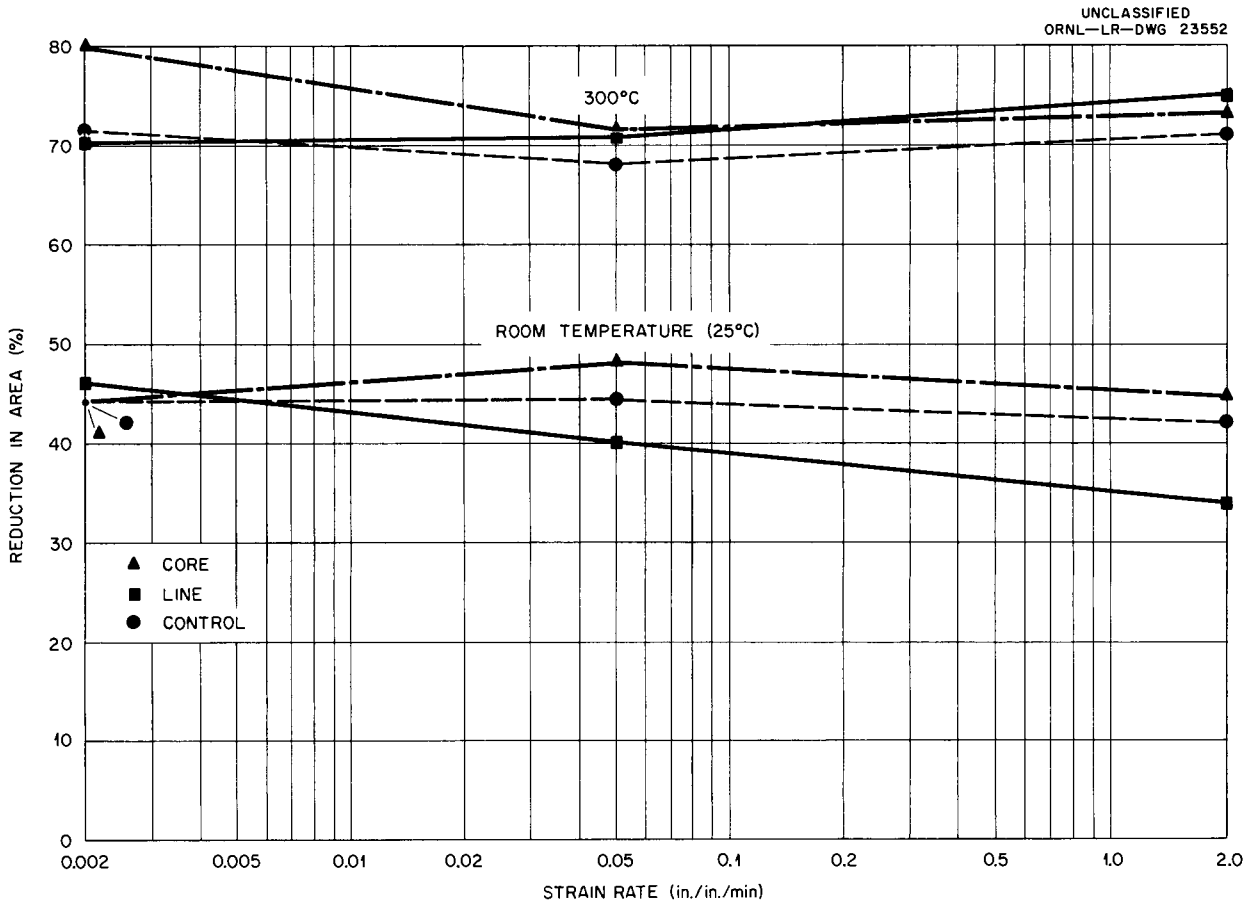

Fig. 15.6. Ductility of Irradiated Zircaloy-2 Tensile Specimens.

15.2.4 Brittle-Fracture Study

Sudden and unexpected brittle failures have occurred in pressure vessels, ships, and other structures which were fabricated with steels that were ductile in conventional room-temperature tests. A general investigation is being conducted to better understand the mechanism of brittle fracture, to develop methods for determining when it will occur, and to obtain information concerning the ductile-to-brittle transition temperature for specific reactor metals.

The drop-weight test, developed by W. S. Pellini and P. P. Puzak of NRL, has been used to study the temperature-dependent crack-propagating properties of Zircaloy-2, titanium-base metals, and steels. Drop-weight testing reveals the temperature at which the metal being tested loses its ability to deform in the presence of a sharp crack. This particular temperature is known as the nil-ductility transition (NDT) temperature.

In conjunction with the Solid State Division, drop-weight tests were conducted on three different grades of pressure-vessel steels in order to determine the NDT temperature of each. The expended drop-weight specimens will be used for additional mechanical-property tests, including a study of the effects of irradiation.

(a) A212B. – Drop-weight tests indicate an NDT temperature of about –100°F for as-received A212B steel and –80°F for the normalized material. Both the as-received and normalized material appeared to undergo a gradual embrittlement (with decreasing testing temperature) starting at about 30°F above the NDT temperature. It was interesting to note that the NDT temperature for the as-received material was lower than for the normalized material.

(b) A285A. – The NDT temperatures were 0°F and –10°F, respectively, for as-received A285A steel and for the normalized material. Some embrittlement was noted at 15°F above the NDT

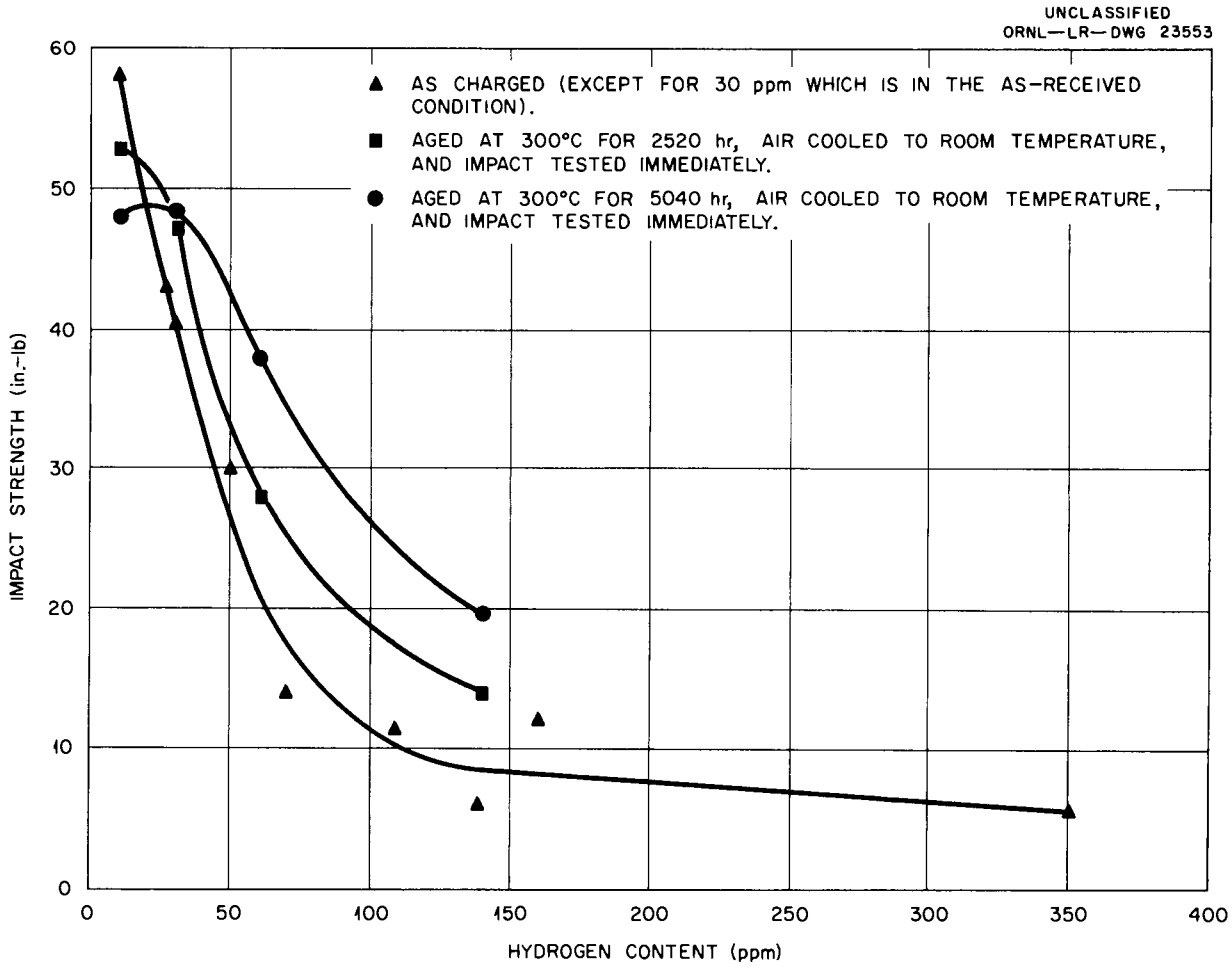

Fig. 15.7. Effect of Aging Time and Hydrogen Content on the Impact Strength of A-55 Titanium.

temperature for the as-received material and as high as 30°F (above NDT) for the normalized material.

(c) A301B. – This steel was held at 1660°F for 1½ hr, furnace cooled to 1100°F, and air cooled to room temperature. The NDT temperature was −10°F, but some embrittlement was noted as high as 20°F above the NDT temperature, where the crack ran 2 in. (within the 3½-in. plate) before stopping.

15.3 WELDING DEVELOPMENT

15.3.1 Titanium Welding

A series of titanium pipe welds was made in the 2G (horizontal) position and 5G (all-position) position with RC-70A, 2½-in. sched-40 pipe. Both RC-40A and RS-55A filler metals were used. The procedure outlined in HRP-7 titanium welding specification for air welding was followed, except that a round wire insert was used in making the root pass. All weldments were radiographed, and bend and metallographic specimens were prepared. In addition, tensile specimens were made from the welds containing RC-40A filler metal.

All specimens passed radiographic standards. Bend specimens were bent 180 deg in a guided bend jig on a 2T radius. No cracking or splits occurred in the weld metal. Some small surface splits were observed in the RC-70A base metal in the heat-affected zone and in the unaffected base metal of all specimens.

The metallographic examination indicated sound full-penetration welds, and, as indicated by microhardness measurements, the welds were without

serious contamination. The RC-70A base metal appeared to have many inclusions, possibly oxides and nitrides, indicating a base metal of dubious quality. After welding, the hardness of the base metal averaged about 225 DPH; the RC-40 filler metal, 226 DPH; and RS-55 filler metal, 272 DPH (10-kg load).

The tensile properties are given in Table 15.5 for welds made in RC-70A base metal with RC-40 filler metal. These results indicate a pickup of oxygen and nitrogen by the filler metal from the base metal and air to produce a weld metal with mechanical properties approximately equivalent to RC-55 weld metal.

15.4 METALLURGICAL DEVELOPMENT AND SERVICE

15.4.1 Cadmium-Embrittled Bolts, Ferrules, and Nuts

In the previous quarterly report, information was given on the nature and extent of the widespread failures which had occurred in the flange bolts, ferrules, and nuts that had been in operation in the HRP flange test loop. The service conditions producing the failures and recommendations for replacement parts were given. While the investigation had not been completed, it seemed likely from the detection of cadmium within fracture interfaces that the failures had resulted from the intergranular diffusion of cadmium within the microstructure, thus embrittling the part.

Since April, other possible causes for the failures have been investigated, and, in addition, tests were made to reproduce cadmium embrittlement in the bolt material in the laboratory. With regard to other possible causes for the failures, tests and deliberations on the available facts produced negative results in each case:

1. Tests designed to show any effects of "blue embrittlement" (strain-aging of nitrides) failed to do so. Moreover, 4140 steel is almost invariably produced by aluminum killing, and its susceptibility to "blue embrittlement" consequently is unlikely.
2. The delayed-failure phenomenon as caused by hydrogen cannot account for the failures because steels become immune to this type of embrittlement at service temperatures in excess of about 150°C. Furthermore, steels do not become afflicted when heat treated to the low hardnesses involved in the present case (below R_C 38 for 4140 steel).
3. Charpy impact tests conducted on samples cut from representative bolts of the same lots involved in the failures gave normal values, indicating that the materials had not been temper-embrittled during the heat treating or affected in any other way such as to influence their toughness.
4. Micro-quench-cracks, which conceivably could act as stress risers and produce premature mechanical failure, were not found at the location of the failures, even for bolts which contained severe macro-quench-cracks at the head-shank interface.

Laboratory attempts to produce cadmium embrittlement in stressed 4140 bolt material proved to be surprisingly difficult. The difficulties stem primarily from the difficulty in getting cadmium to wet the surface of the steel at temperatures only slightly above the melting point of the cadmium. At least in one case, however, cracks were produced in the laboratory. A standard bend-deflection 4140 specimen was zinc plated, stressed beyond the yield point, and immersed in cadmium for 24 hr at 340°C. Visible cracks were present when it was removed from the liquid. A similar specimen, only cadmium plated, did not contain visible cracks.

From the above data, it appears that cadmium was responsible for the test-loop failures. The

Table 15.5. Tensile Properties of Titanium Welds

Weld	Position	Ultimate Tensile Strength (psi)	Elongation, 1 in. (%)	Location of Fracture
1	5G	91,285	18	Weld metal
1	5G	87,500	20	Weld metal
4	2G	89,055	15	Weld metal
4	2G	90,145	10	Weld metal

failures are increased when cadmium and zinc are both present, but since cracks were found in nuts and ferrules the zinc does not appear to be necessary.

Although 186 bolts were removed from the HRT and inspected by Magnaflux, none showed the characteristic cadmium failure which was produced in the flange test loop. A number of defects of lesser importance were reported. The reactor bolts operated at a temperature slightly lower than those in the test loop, which can indicate a narrow temperature range in which this cracking occurs. However, it is believed that a large portion of the bolts inspected are not of the Detroit Bolt & Nut Co. group, which were zinc plated and involved in the loop failures. Of eight ferrules which were examined some six months ago, four had cracks that are believed to have been cadmium induced.

An investigation was conducted to determine whether the HRT stainless steel flanges which had been in contact with cadmium-plated nuts and ferrules had been embrittled. No deleterious effects of any kind were found. The tests consisted in metallographic observations and microspark spectrographic analyses along planes within several mils of where the plated parts had contacted.

15.4.2 Active Metal Reactions

Two programs pertaining to hazardous metal reactions are being carried out on subcontracts. The first, concerned with chemical reactions between zirconium and aqueous uranyl sulfate, was prompted out of concern for possible incidents involving reactions between the HRT core tank and the fuel solution. This program is being conducted by the Aerojet General Corp. Since extensive work has been done on reactions between zirconium and water, including the development of basic data as well as the calculation of effects of reactor accidents, the essential objective of the present work will be only to compare the reactions of zirconium and water with those of zirconium and aqueous uranyl sulfate.

The second program is concerned with reactions of titanium with aqueous uranyl sulfate and with water and was prompted by the titanium valve-trim failures in the HRP dump-valve test loop. These failures involved a rapid and sustained burning of the metal.[8] The primary objective of this program will be to determine the limiting conditions for sustaining titanium-water and titanium–aqueous uranyl sulfate reactions. This program is being conducted by the Stanford Research Institute. The experimental techniques are as follows:

1. Titanium disks are ruptured in an autoclave under dynamic conditions of variable temperature, pressure (velocity), and environment.
2. Tests similar to procedure 1 will be performed, but ignition will be achieved, if possible, by rupturing tensile specimens under *static*, variable environmental conditions.

Using test procedure 1 above, Stanford has initiated and sustained a reaction by rupturing 3- to 12-mil commercial unalloyed titanium foil under pure oxygen at a pressure of 1100 to 1800 psi and 30 to 320°C. An experiment under the same conditions with water being used instead of oxygen failed to ignite the titanium. Also, tests conducted with water containing oxygen up to 200 psi, at 1500 psi total pressure, and 315°C failed to give ignition. However, when the bomb was inverted so that the gas above the liquid passed through the titanium diaphragm first, combustion was obtained.

15.5 EFFECTS OF RADIATION ON STRUCTURAL METALS AND ALLOYS

15.5.1 Equipment and Facilities

Engineering of future experiments, MTR irradiations, and specimen machining occupied most of the effort during the quarter.

Irradiation of ORNL-10-5 in HB-3 of the MTR (steels at a series of elevated temperatures) was completed, and the specimens were returned to ORNL for testing.

ORNL-10-6 (stainless steels and titanium) is presently being irradiated in the MTR lattice.

ORNL-10-8 (carbon steels) is presently being irradiated in the MTR (HB-3) for five cycles. A total of approximately 320 specimens were irradiated or were being irradiated during the quarter.

ORNL-10-9 for HB-3 of the MTR is under construction for irradiation of subsize and Charpy test specimens. ORNL-10-10 for irradiation of zirconium and titanium alloys at elevated temperatures has been completely designed following

[8] G. M. Adamson *et al.*, *HRP Quar. Prog. Rep. Oct. 31, 1956*, ORNL-2222, p 121.

extensive heat transfer tests on a mockup. This apparatus will contain 433 specimens in a volume of less than 300 $in.^3$.

Engineering is in progress on ETR and ORR irradiation facilities, and lattice irradiation units for the ORR are under construction.

Heat treatment and drop-weight testing (see Sec. 15.2.4) were conducted on three steels selected for future irradiations, in which specimen size effects will be investigated with both subsize Izod and Charpy specimens. Specimen blanks were cut, and 800 Charpy specimens are being machined by an outside contractor. These specimens are intended for elevated-temperature irradiation in the ORNL Graphite Reactor, LITR, and ORR.

The new subsize impact machine, and accompanying remote-control system for hot-cell use, is complete, and installation of parts of the unit in the hot cell has begun.

During the quarter a cooperative program with the Naval Research Laboratory (NRL) was begun. A man from NRL was sent to ORNL for training in hot-cell techniques and in the use of the ORNL subsize impact machine to conduct tests of casualty steels (steels that have failed in service) for comparison with other test data. The NRL is starting to study the effects of irradiation on brittle fracture in steels. This work should be a valuable supplement to the ORNL work.

Part V

CHEMICAL ENGINEERING DEVELOPMENT

D. E. Ferguson

16. URANYL SULFATE FUEL PROCESSING

R. A. McNees
R. E. Adams
W. E. Browning
D. E. Guss
R. W. Horton
P. A. Haas
J. F. Krause
E. O. Nurmi
S. Peterson
J. W. Snider

16.1 ADSORPTION OF FISSION GASES BY ACTIVATED CHARCOAL

The exploratory study of the adsorption of krypton on HRT charcoal at temperatures ranging from 25 to 100°C was completed, and it was found that (1) the adsorptive capacity of HRT charcoal in this temperature range was significantly less than had been predicted by extrapolation of lower temperature data; (2) charcoal containing 5 to 6% water, the amount present in a sample of HRT charcoal, had only about 75% of the adsorptive capacity of dry charcoal; (3) any deviation from complete filling which resulted in even a very small channel in a horizontally placed bed decreased the holdup time of the bed significantly.

The adsorption data were obtained from a charcoal trap fabricated from 24 ft of $\frac{3}{4}$-in.-OD copper tubing wound in a helix and filled with 782 g of Columbia grade-G activated charcoal, 8 to 14 mesh. The trap was placed in a small drying oven for studies above room temperature, and oxygen was passed through the trap until equilibrium was attained. A pulse of Kr^{85} was then injected into the flowing oxygen stream, and the passage of activity from the trap was noted as a function of time by use of suitable counting devices.[1] The data obtained at the four temperatures, normalized to a uniform tracer content, are shown in Fig. 16.1. The number of theoretical plates in the trap, N, calculated by methods developed earlier,[2] are shown below:

Temperature (°C)	N
24–27	18.3
50 ± 9	15.0
75 ± 12	14.5
100 ± 18	12.8

These N values are much lower than the predicted values and suggest that the trap was not completely packed.

Analysis of HRT charcoal showed it to contain 5.5 to 6.0% H_2O as received. Data taken with this charcoal and with the same material dried by passing oxygen through the bed at 100°C for 18 hr show that trap holdup time may be increased 25% by drying (Fig. 16.2). Passage of moisture into dry HRT beds resulted in the expulsion of a surge of short-decayed rare-gas activity.

The effect of a small channel in a horizontal trap was studied with a 6-ft length of $\frac{3}{4}$-in.-ID Pyrex pipe. The trap was filled with 249 g of Columbia grade-G charcoal, 8 to 14 mesh, while

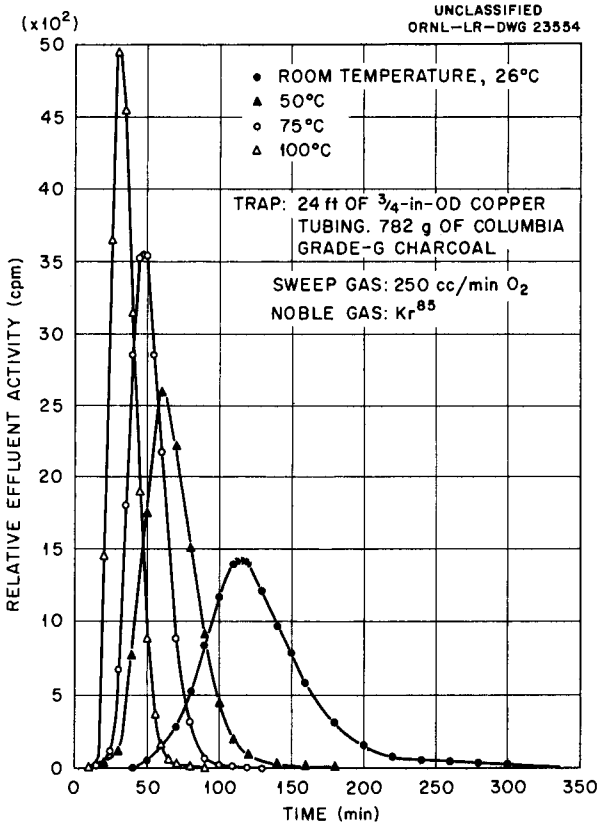

Fig. 16.1. Effect of Charcoal-Bed Temperature.

[1] *Chem. Tech. Monthly Prog. Rep. May 1957*, ORNL-2361 (in press) (Classified).

[2] W. E. Browning and C. C. Bolta, *Measurement and Analysis of the Holdup of Gas Mixtures by Charcoal Adsorption Traps*, ORNL-2116 (Aug. 10, 1956).

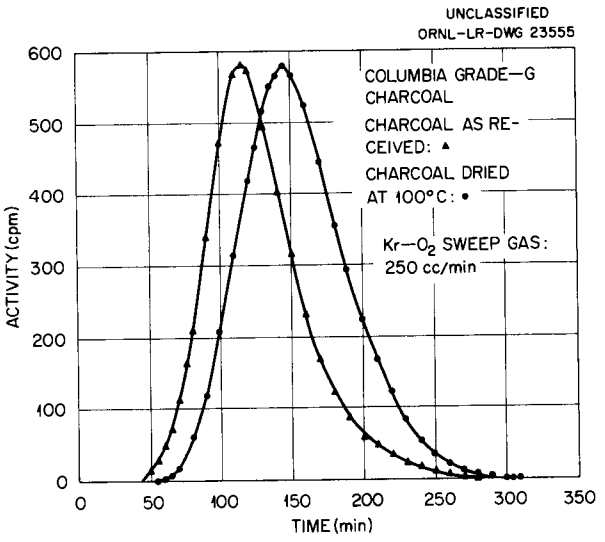

Fig. 16.2. Effect of Moisture on Krypton Adsorption by Charcoal at Room Temperature.

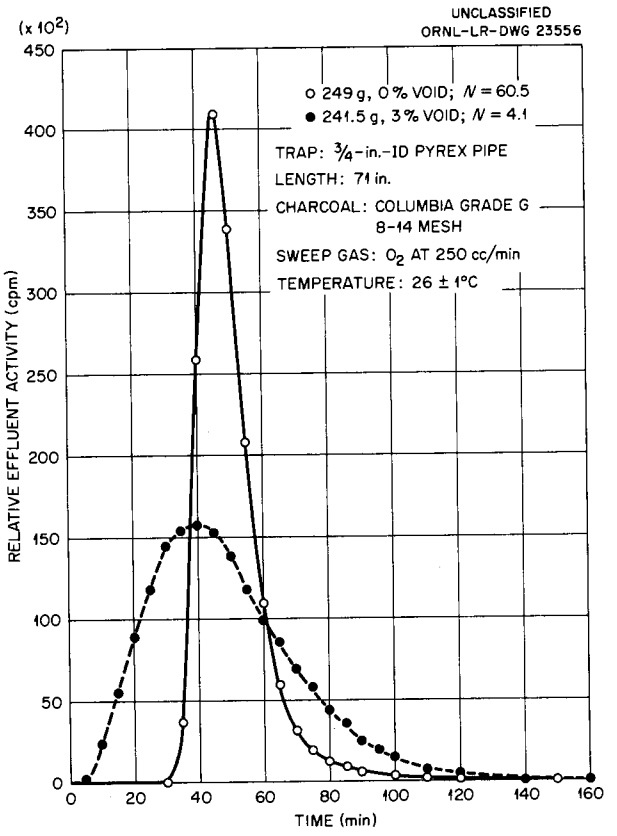

Fig. 16.3. Effect of Channeling in Packed, Horizontal Bed on Krypton Adsorption.

in a vertical position. After the trap was lowered carefully to a horizontal position, the characteristics of the bed were determined in the same way as those for the helical trap. Three per cent of the charcoal was then removed; the remainder was distributed uniformly over the same length of Pyrex pipe; and the characteristics of the trap were again determined. It is important to note that although holdup time (t_{max}) was reduced only from 46 min to 40 min, 93% of the theoretical plates in the fully packed bed were destroyed, and the time to initial breakthrough on the channelized bed was 10% of the time for breakthrough on the fully packed bed (Fig. 16.3).

16.2 IODINE CHEMISTRY

Increasing the amount of sulfuric acid in 0.04 *m* UO_2SO_4 solutions from 0.01 *m* to 0.02 *m* decreased the stability of iodate by about 50% at 100°C in the presence of Co^{60} radiation. The effects of variations in the H_2/O_2 ratio of the gas phase were minimized by increasing the amount of acid in the solution (Fig. 16.4).

Experiments in the HRT mockup loop at Y-12 (see Sec. 3.4.3) confirmed laboratory data on the chemistry of iodine reported in previous quarterly

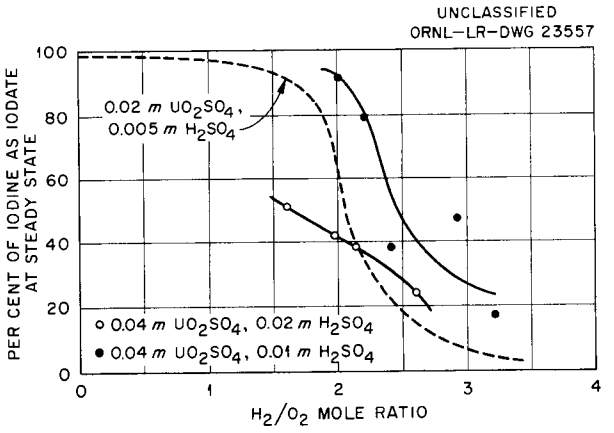

Fig. 16.4. Steady-State Iodate Content for Three Fuel Solutions at 100°C and 2 w/liter.

reports. When iodine was added to the high-pressure portion of the loop, which was operating at 280°C, it was rapidly removed from the high-pressure system via the letdown stream. Analysis of samples taken from the high-pressure system indicated that the iodine concentration in that system dropped by a factor of 10 in 2 hr, 50 in 4 hr, and 100 in 6 hr. After several hours of operation; the only iodine found in the high-pressure system was that being returned in various liquid streams pumped up from the low-pressure system.

In the low-pressure system, iodine collected on the platinum recombiner when it was operating at 420°C and reduced its efficiency. However, when the recombiner was operated at 650°C its reactivity was restored because of the instability of the platinum-iodine complex at that temperature. When a silver absorber was installed ahead of the recombiner, most of the iodine was trapped, and the recombiner operated efficiently at 420°C. Inasmuch as the HRT operation will not be sufficiently uniform to assure recombiner operation at 650°C at all times, installation of an iodine trap, in the form of a silvered-alundum absorption bed, ahead of the platinum recombiner is probably warranted.

16.3 SOLIDS BEHAVIOR

Laboratory tests have shown that the disappearance of simulated HRT corrosion-product solids from dilute suspensions in uranyl sulfate solutions at 275°C is easily reversed by lowering the temperature. The disappearance appears to be due to agglomeration of small particles into larger masses, which settle rapidly and resist breaking up by moderate forces.

In one set of experiments uranyl sulfate solutions containing simulated HRT corrosion-product solids in concentrations of 0.4 to 120 mg per kilogram of H_2O were sealed in stainless steel tubes and heated to 275°C for 33 to 154 hr in a pressure vessel containing water. After cooling over a 6-hr period to room temperature, the tubes were opened and the contents gently flushed from the tube. The solids were collected, washed, dried, and weighed. In most cases more solids were recovered than were charged into the container tubes, and for all the 46 individual tests included in this series, 6.5% more solids were recovered than were charged.

The series was repeated with HRT simulated solids traced with Fe^{55}-Fe^{59} to allow for the use of more dilute suspensions. The solids concentrations ranged from 17 to 670 mg per kilogram of H_2O, and the experimental methods were the same as before except that the amount of solids removed from the steel tubes was determined by counting techniques instead of weighing. In 22 tests, no solids were lost during the experiment; the average solids removal was 114% of the solids charged to the tube. Results of two other tests were obviously in error.

In another set of experiments a slurry of solids in uranyl sulfate solution was charged to a 200-ml steel vessel contained within a rocking pressure vessel partially filled with water. After heating to 275°C, samples of the slurry were periodically withdrawn while at 275°C and analyzed for solids content. At 275°C the solids content was about 10% of the initial concentration. After cooling to room temperature, samples withdrawn from the slurry vessel showed that the solids were again fully suspended.

In solids deposition tests in loops, made with ZrO_2 suspended in 0.04 *m* UO_2SO_4 solution, the solids concentration decreased rapidly immediately after addition to a relatively clean system. Successive additions of solids to the system resulted in decreasing deposition rates and increasing final concentration (Fig. 16.5). These effects can be explained as a result of segregation of solids in certain portions of the equipment (particularly in canned-rotor pumps), which eventually become saturated and will accept no more solids. These segregated solids can be resuspended by flushing through the pump rotor cans.

16.4 HRT SOLIDS DISSOLUTION

Simulation in the laboratory of the geometry and heating methods of the HRT chemical plant dissolver showed that the unsatisfactory performance of the dissolver in preliminary tests was due to lack of agitation of solids during heating. The heating jacket of the glass-lined dissolver was segmented to restrict the heating surface to the lower portion and thereby obtain more agitation in the bottom. The first dissolution was 97% complete after this modification.

The dissolution procedure consists of two heating cycles of 4 hr each, one with 10.8 *M* H_2SO_4 and the other with 4 *M* H_2SO_4. Acid-concentration determination by boiling-temperature measurement

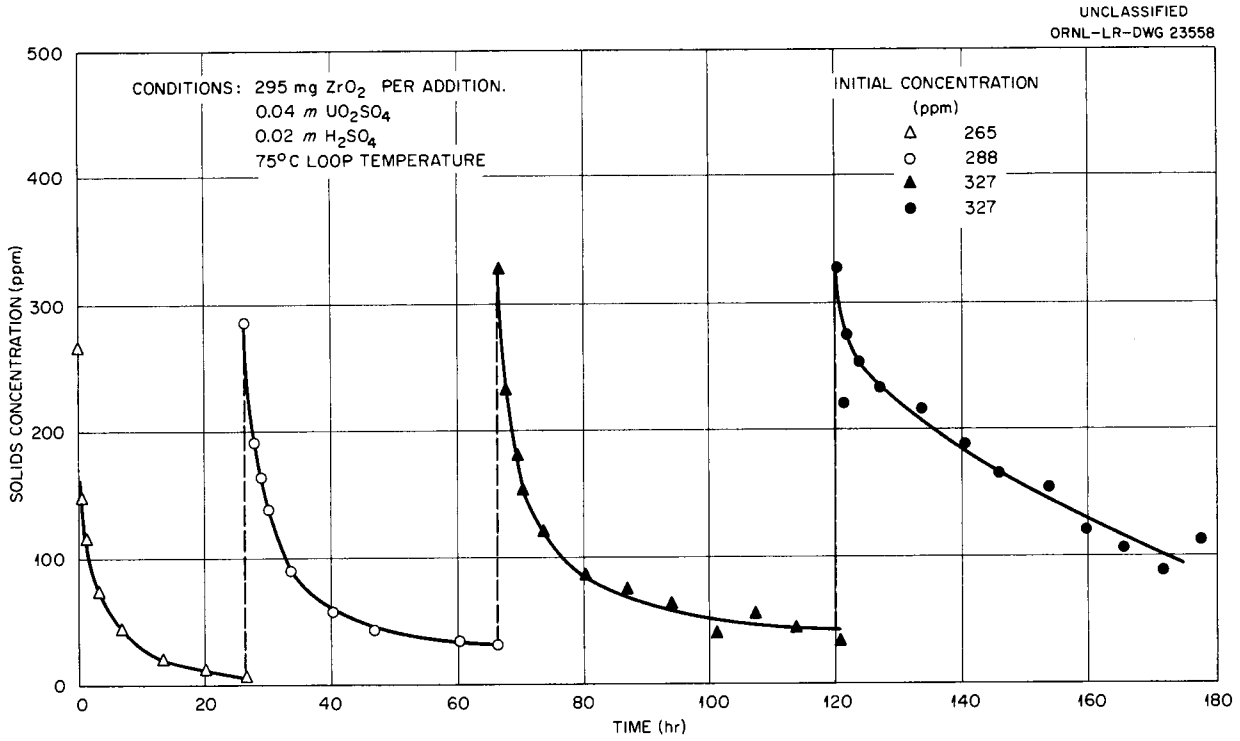

Fig. 16.5. Suspended Solids vs Time for Successive Additions of Solids to A-Loop.

was found to be more accurate than by volume measurement. The thermal well was lengthened to keep the thermocouple immersed during the 10.8 *M* H_2SO_4 cycle. The dissolver had a tendency to boil over at the beginning of the 4 *M* H_2SO_4 cycle. This tendency was prevented by adding the water for dilution through the dip leg and sparging air through the solution while heating. Dissolution was more than 99.5% complete for three runs made after these modifications.

Corrosion rates for Carpenter 20 coupons suspended in the dissolver vapor space were 28 to 51 mpy during these final dissolution tests.

16.5 KRYPTON SOLUBILITY[3]

The study of the solubility of krypton in uranyl sulfate solutions in the temperature range of 100 to 300°C was extended to 0.04 *m* UO_2SO_4, and the Henry's law constants for water and 0.02 *m* UO_2SO_4 were recalculated.[3] The plots of Henry's law constant for krypton vs temperature for the two uranyl sulfate solutions are shown in Figs. 16.6 and 16.7. The data show a linear dependence of Henry's law constant on temperature for water and 0.02 *m* UO_2SO_4 solutions. However, for 0.04 *m* UO_2SO_4 solutions a departure from such a linear relationship is observed. The water solubility data fall within the 95% confidence limits of the 0.02 *m* UO_2SO_4 solution data and are represented by the following equation:

$$K = (9.126 - 0.0263T) \times 10^5 ,$$

$$\text{95\% confidence limits} = K \pm 0.471 \sqrt{\frac{1}{15} + \frac{(T - 202)^2}{75{,}300}} \times 10^5 ,$$

[3] This work was done by Vitro Laboratories; for greater detail, see R. A. Keeler *et al.*, *Homogeneous Reactor Fuel Reprocessing (Monthly Report April 1957, Vitro Job 1087)*, V-87-91-0.

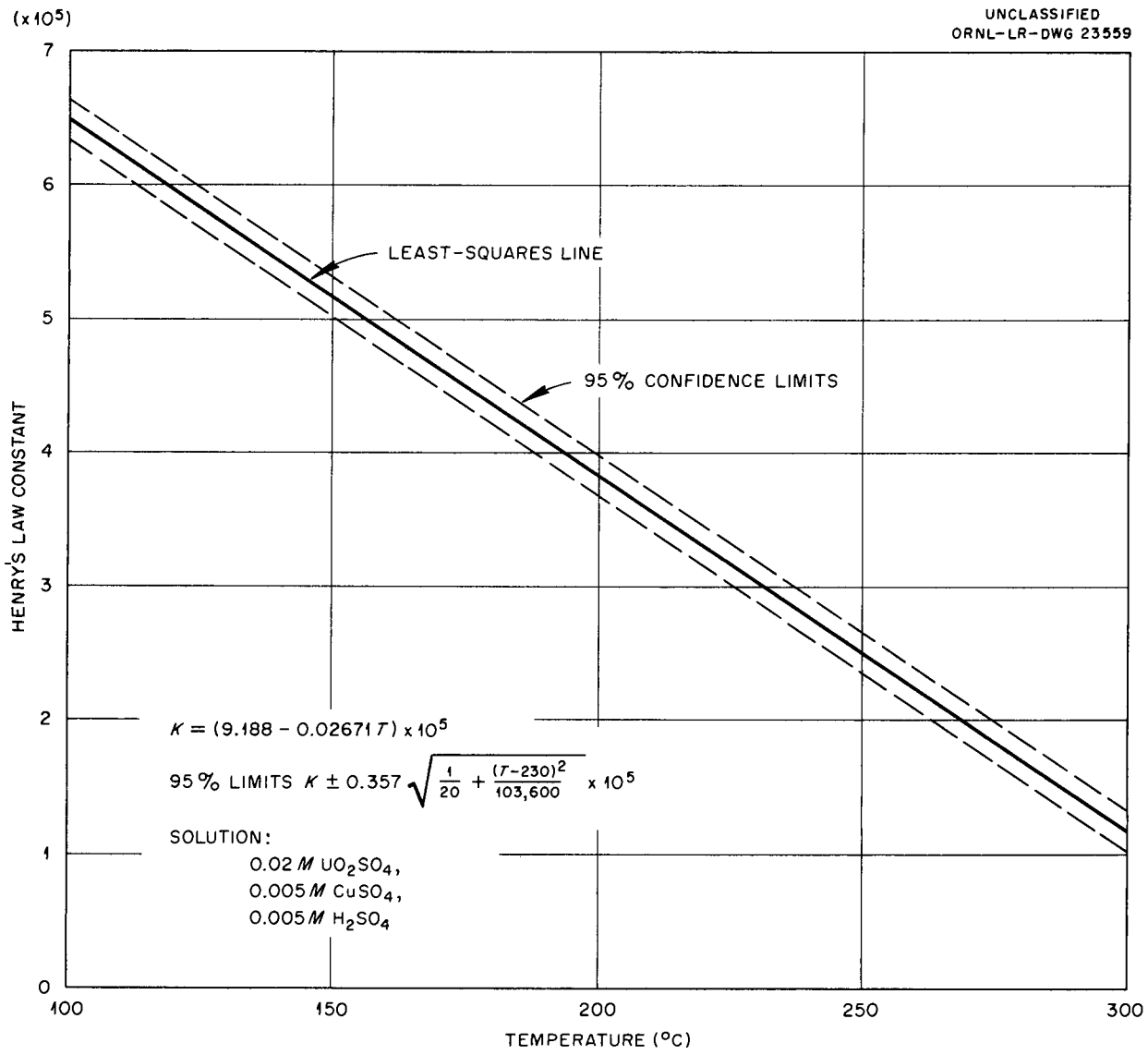

Fig. 16.6. Henry's Law Constant for Krypton in 0.02 *m* UO_2SO_4.

where K is the Henry's law constant and T is temperature in °C.

During the krypton studies the solubility of oxygen in the three solutions was also measured. It was found that the presence of uranium in solution up to 10 g of uranium per liter had no apparent effect on the solubility of oxygen. The data agree well with those obtained by Battelle[4] and are shown in Fig. 16.8.

[4]E. S. Stephan *et al.*, *Solubility of Gases in Uranyl Sulfate Solutions*, BMI-1067 (Jan. 23, 1956).

16.6 URANIUM PROCESSING[3]

Studies of adsorption of uranium on simulated HRT chemical-plant solids have shown that although uranium is adsorbed to some degree by such solids they can be easily washed free of uranium by either water or dilute sulfuric acid. The uranium content of such simulated solids precipitated from and autoclaved in 0.02 *m* UO_2SO_4 solution by hydrolysis at 300°C was 2 mg of uranium per gram of solids after washing.

Some of the factors influencing uranium losses during uranyl peroxide precipitation, separation,

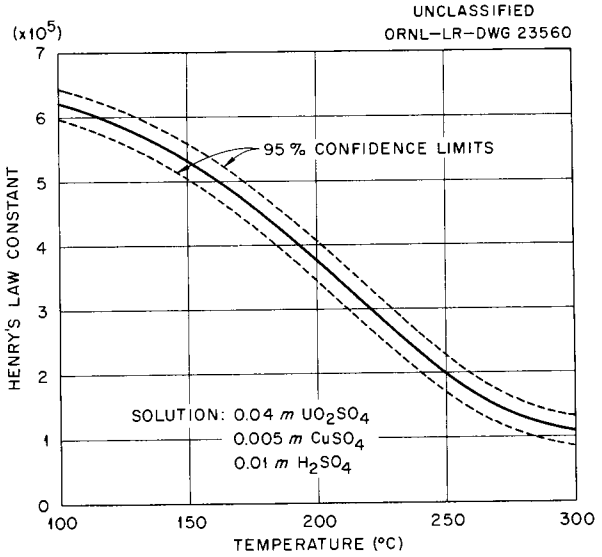

Fig. 16.7. Henry's Law Constant for Krypton in 0.04 *m* UO_2SO_4.

and washing have also been studied. With the use of a 2% sodium peroxide solution as the source of peroxide it was found that adjustment of the pH of such a solution to about 5 was necessary to minimize uranium losses and produce a precipitate with acceptable handling characteristics. Addition of uranium solution to peroxide solution appeared to produce a precipitate with better settling properties than did the reverse method of addition. Washing such precipitates with either unadjusted sodium peroxide solution or water partially solubilized precipitated uranium and adversely affected the nature of the precipitate. Decomposition of peroxide, catalyzed by the presence of simulated fission and corrosion products, resulted in increasing uranium losses as the peroxide concentration decreased. When all the precipitation, settling, and washing operations were done at low temperatures (2 to 6°C), the uranium losses were lower than when the same operations were made at 25 or 40°C. The precipitates obtained at the lower temperature were denser and settled more rapidly. Tests showed that uranium losses through the

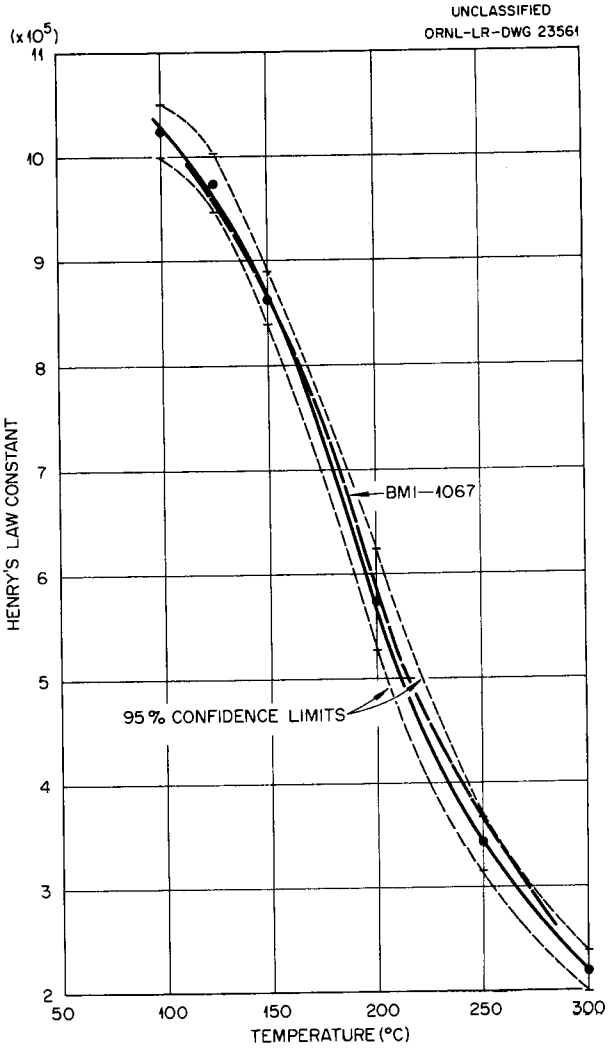

Fig. 16.8. Henry's Law Constant for Oxygen vs Temperature.

precipitation and washing steps (two washes using 3.5 volumes of wash solution per volume of wet solids) amounted to 0.6% at 6°C and 0.23% at 2°C when proper pH control and settling time were used. At room temperature and allowing overnight settling, which resulted in loss of peroxide and uranium solubilization, similar tests showed a 5.9% uranium loss.

17. URANYL SULFATE BLANKET PROCESSING

R. E. Leuze P. A. Haas
S. S. Kirslis S. D. Clinton

17.1 IN-PILE EXPERIMENTS

Two additional[1] in-pile experiments were carried out to determine the behavior of plutonium and neptunium produced in a uranium solution under reactor conditions. A 2.5- to 4.5-ml volume of 1.4 *m* UO_2SO_4 solution was irradiated in the LITR in titanium bombs at 250°C under 200 psi of oxygen. The principal result of the first run was confirmed; namely, less than 4% of the plutonium appeared as loose precipitate, the form desired for hydroclone processing of a uranyl sulfate blanket. Most of the plutonium was deposited on the bomb wall in a form difficult to recover.

The results of this series of runs are summarized in Table 17.1. Data for run 1 differ slightly from those previously reported[1] since additional plutonium was adsorbed on the bomb wall.

The most consistent feature of the plutonium distribution data is that the plutonium in the loose precipitate centrifuged from the bomb solution and from a water wash of the bomb was a small fraction of the total formed. The amount of plutonium in solution varied between 11.6 and 51 mg per kilogram of H_2O. Such wide variations have been observed in similar out-of-pile experiments in which plutonium was added incrementally to uranyl sulfate solution at 250°C. In each in-pile run, a large quantity of plutonium was strongly attached to the bomb wall. The original descaling by four successive treatments with ceric–nitric acid solutions at 85°C for 4 to 16 hr did not remove all the plutonium. For complete plutonium removal it was necessary to repeatedly descale with concentrated sulfuric acid followed by water and with nitric acid–hydrofluoric acid mixtures followed by $Al(NO_3)_3$-HCl solutions, which badly corroded the base metal. Although these results are discouraging, they do not eliminate the possibility of processing a uranyl sulfate blanket by removing precipitated PuO_2 with a hydroclone. The problem of plutonium adsorption is a real one and must be considered; however, it may be much less important in an actual reactor in which the surface-area/solution-volume ratio is only about 0.4 cm^2/ml, compared to 5 cm^2/ml in these experiments.

Most of the neptunium in runs 2 and 3 remained in solution, small amounts were adsorbed on the titanium, and very little appeared in the precipitate. These results are consistent with out-of-pile tests, in which the neptunium stayed in solution. The reason for the larger neptunium adsorption in run 1 is not known. The ceric–nitric acid descaling effectively removed neptunium from the bomb walls. Neptunium was not detected in subsequent descaling solutions.

The last two columns in Table 17.1 provide a means of checking the accuracy of the results, since the theoretical Pu/Np ratio depends only on the irradiation time and the Np^{239} half life. The observed ratio was 7 to 17% low. This means that

[1] For earlier experiments, see R. E. Leuze *et al.*, *HRP Quar. Prog. Rep. April 30, 1957*, ORNL-2331, p 151.

Table 17.1. Plutonium and Neptunium Distribution* in Irradiated Uranyl Sulfate Solution

1.4 *m* UO_2SO_4 in titanium bomb irradiated in the LITR at a flux of 2.7×10^{13} neutrons/cm^2/sec under 200 psi O_2 at 250°C

Run	Irradiation Time (days)	Cu^{++} (*m*)	Solution Volume (ml)	Plutonium				Neptunium				Total Pu/Total Np Ratio	
				In Solution		In Loose Precipitate (%)	On Bomb Wall (%)	In Solution		In Loose Precipitate (%)	On Bomb Wall (%)	Observed	Theoretical
				(mg/kg H_2O)	(%)			(mg/kg H_2O)	(%)				
1	10.89	0.002	4.5	25.8	40.2	0.7	59.1	18.2	56.5	1.0	42.5	1.90	2.34
2	12.44	0.002	4.5	11.6	12.2	0.2	87.5	34.4	95.1	0.9	4.0	2.57	2.78
3	16.57	0.0002	2.5	51.0	49.4	3.3	47.3	28.2	88.5	0.3	11.3	3.28	3.95

*The quantities of plutonium and neptunium are recorded for time of removal from reactor.

either all the plutonium was not recovered or the analytical results are in error by this amount. However, these errors are not large enough to appreciably change the over-all results.

The capture cross-section of U^{238} in 1.4 *m* UO_2SO_4 for the C-44 lattice position of the LITR calculated from neptunium analyses was 13 barns.

17.2 LOOP OPERATION

Loop P-1 is now ready for the preliminary studies on plutonium behavior in a circulating system. Six runs were completed with uranyl sulfate solution (10 to 225 g of uranium per kilogram of H_2O), extending the cumulative loop operating time to 265 hr. Difficulties were encountered during removal of the retainer plug from the coupon holder, installation of the third cell, and resealing of the thermal-probe octagonal-ring gasket. After these runs, a visual inspection of the pressurizer with the thermal probe removed showed considerable amounts of iron oxide around the Raschig-rings retainer tube. Several attempts to reseal the thermal-probe octagonal-ring gasket were unsuccessful. A satisfactory seal was finally obtained after the ring surface had been plated with 3 mils of gold.

Since these preliminary runs, the loop was operated for 180 hr with uranyl sulfate solution (330 g of uranium per kilogram of H_2O) at 255°C and 950 psi with oxygen overpressure. A sample was taken through the high-pressure generator every 4 hr until the rubber O-rings failed, after 86 hr, allowing leakage around the generator shaft. The rubber O-rings were replaced with Teflon, which failed after 8 hr of operation. The generator was again assembled with rubber O-rings. The bomb-type sampler system was used for 70 hr and operated satisfactorily.

During the first 50 hr of operation with concentrated solution, a calculated corrosion rate of 8 mpy was observed. The rate dropped to 2.5 mpy during the last 100 hr. This corrosion rate was based on the soluble nickel content of the solution and on the loop area, including the Raschig rings contained in the pressurizer (the Raschig-ring area is 75% of the total loop area).

18. THORIUM OXIDE SLURRY DEVELOPMENT

J. P. McBride P. A. Haas

W. J. Clossey N. A. Krohn C. E. Schilling
C. C. Haws L. E. Morse J. W. Snider
E. V. Jones R. L. Pearson W. M. Woods

18.1 SLURRY IRRADIATION STUDIES

18.1.1 Slurry Irradiations in the LITR

The long-term irradiation of a settled slurry of 800°C-fired micropulverized thorium oxide was continued; the slurry has now been irradiated for more than 2000 hr at full reactor power.

A slurry of 800°C-fired coprecipitated oxide containing 20,000 ppm MoO_3 and 3000 ppm sulfate, added as $Th(SO_4)_2$, was irradiated for 247 hr in the vertical LITR facility. Oxygen pressure dropped from an initial 316 psi to 187 psi during the run. Stirrer operation stopped after one day in-pile but restarted spontaneously after four days and continued until the end of the run, 12 days later. In all, the bomb contents were stirred for 264 of the 383 hr. The control experiment was stirred at temperature for 226 hr, but the stirrer then stopped and, although it was restarted several times, stirring could not be sustained.

The recovered slurry appeared to be visually unaffected by the irradiation, and recovery was essentially 100%. Most of the fission products were associated with the slurry solids, only cesium and strontium appearing in the supernatant in significant amounts.

18.1.2 Slurry Viscosity Measurements

Out-of-pile measurements of slurry viscosity were made in the dash-pot bomb on slurries of thorium-uranium oxide (U/Th mole ratio = 0.005/1) prepared from the coprecipitated oxalates by calcination at temperatures from 650 to 1600°C. At thorium concentrations of 250 and 500 g per kilogram of H_2O, the viscosity was essentially independent of both calcination and slurry temperature (Table 18.1). When the thorium concentration was increased to 750 g per kilogram of H_2O, however, the apparent viscosity increased markedly with slurry temperature, the relative effect becoming less as the calcination temperature was increased. Only in the case of the 1600°C-fired material was it possible to stir a slurry with a thorium concentration of 1000 g per kilogram of H_2O.

18.1.3 Corrosion Studies

The stirrer for the in-pile autoclave was redesigned in an attempt to accommodate a small corrosion specimen. Out-of-pile tests with the new stirrer were unsuccessful in that the support for the corrosion specimen broke during operation. Efforts to include a corrosion specimen in the in-pile autoclave will continue.

18.2 GAS RECOMBINATION STUDIES

The study of the effect of oxide calcination temperature and time on the catalysis of hydrogen-oxygen combination by thorium-uranium oxide slurries (U/Th mole ratio = 0.005/1; thorium, 500 g per kilogram of H_2O) containing 0.05 *m* MoO_3 has continued. Slurries of thorium-uranium oxides calcined at 1000°C for 16 and 24 hr and at 1600°C for 24 hr showed high catalytic activities (>>10 moles of H_2 per hour per liter). Slurries of the mixed oxides calcined at 800°C for 24 hr and 1000°C for 4 hr showed low catalytic activities even after activation with hydrogen.

The studies were carried out as a result of the interest in the use of slurries of high-fired oxides and in support of a projected gas-recombination experiment to be carried out in one of the corrosion loops at Y-12. The mixed oxide was prepared by calcining the thorium-uranium oxalates coprecipitated at 10°C. The slurries were prepared by tumbling the dry powders for 1 hr and then heating the mixture in water at 280°C for 3 hr with a small oxygen overpressure (300 psi at room temperature). The slurries were activated by heating for 2 hr at 270°C with a hydrogen overpressure (250 psi at room temperature).

The slurry prepared from the material calcined at 1000°C for 24 hr, both as prepared and after activation, gave hydrogen-oxygen combination rates at 250°C and a hydrogen partial pressure of 500 psi greater than 40 moles of hydrogen per haur per liter of slurry. That prepared from the 16-hr firing at 1000°C showed a low activity as prepared but gave very high combination rates after activation. The

slurry of oxide calcined for only 4 hr at 1000°C had negligible activity both as prepared and after activation (Table 18.2). The decreased activity of the material fired for only 4 hr is rather surprising, since measurements of surface area and x-ray crystallite size have demonstrated that these properties are not changed appreciably by heating longer than 4 hr at a given temperature. Hence the result must be associated with some change in the surface chemistry, possibly a diffusion of

Table 18.1. Effect of Calcination Temperature on the Viscosities of ThO_2–0.5% U Slurries

Prepared from coprecipitated oxalates

Calcination Temperature (°C)	Slurry Temperature (°C)	Viscosity (centistokes)			
		250 g Th/kg H_2O	500 g Th/kg H_2O	750 g Th/kg H_2O	1000 g Th/kg H_2O
650	100	4	6	7	*
	200	4	7	14	*
	300	3	8	*	*
800	100	6	7	8	*
	200	5	7	14	*
	300	4	7	*	*
1000	100	6	6	7	*
	200	6	7	12	*
	300	5	8	*	*
1170	100	6	6	6	*
	200	5	6	9	*
	300	6	5	*	*
1400	100	5	7	5	*
	200	4	5	7	*
	300	4	4	9	*
1600	100	6	6	6	5
	200	5	5	6	6
	300	4	5	5	8

*Could not be stirred.

Table 18.2. Reaction Rates of Stoichiometric H_2-O_2 Mixtures in 1000°C-Calcined Thorium-Uranium Oxide Slurries

Slurry preparation: 500 g Th/kg H_2O, 2.5 g U/kg H_2O, 0.05 *m* MoO_3, heated 3 hr at 280°C under O_2 (300 psi at room temperature)

Calcination Time (hr)	Combination Rate at Indicated Temperature, P_{H_2} = 500 psi (moles H_2/hr·liter)	
	Slurry as Prepared	Activated Slurry*
4	0.08 (295°C)	0.08 (288°C)
16	0.1 (284°C)	91.2 (250°C)
24	58.7 (250°C)	41.0 (250°C)

*Slurry heated with H_2 (250 psi at room temperature) for 2 hr at 270°C.

the uranium atoms away from the surface, permitting more interaction of the MoO_3 with the thoria.

Slurries of the mixed oxide calcined at 800°C for 24 hr had very low activity as prepared. After activation the rate was 3.7 moles of hydrogen per hour per liter at 240°C and a hydrogen partial pressure of 500 psi, lower than required for reactor use (Table 18.3).

The initial rate with a slurry of the mixed oxide fired at 1600°C for 24 hr as prepared was 11.9 moles of hydrogen per hour per liter of slurry at 271°C and a hydrogen partial pressure of 500 psi.

18.3 SLURRY IRRADIATION STUDIES

Projected dynamic studies of ThO_2 slurry systems require some means of measuring slurry flow rate. Two sizes of elbow flowmeters, $\frac{3}{8}$ in. and $\frac{1}{4}$ in. ID (Fig. 18.1), were built of glass and calibrated with water. The $\frac{1}{4}$-in.-ID flowmeter was also calibrated with slurry at specific gravities of 1.8 and 1.5. The calibration of velocity vs ΔH in terms of head of fluid flowing was log-log linear in all cases (Fig. 18.2).

For the water calibration the flowmeters were simply attached to the faucet. Flows were measured by catching a measured volume of the discharge

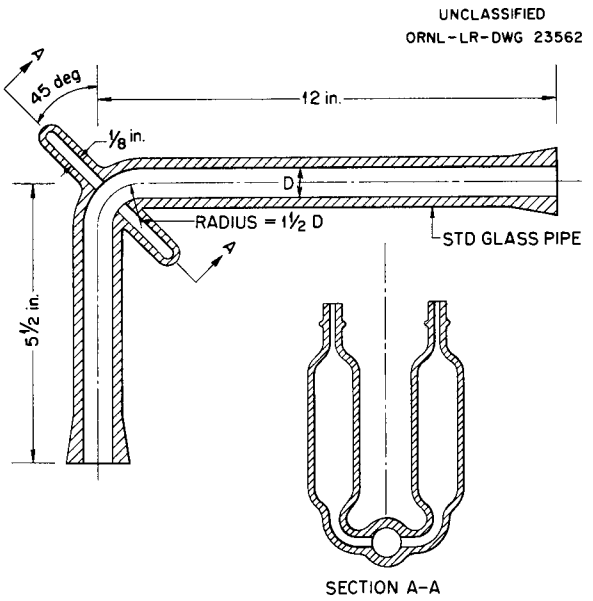

Fig. 18.1. Glass Elbow Flowmeter.

Table 18.3. Reaction Rates of Stoichiometric H_2-O_2 Mixtures in 800°C, 24-hr Calcined Thorium-Uranium Oxide Slurries

Slurry preparation: 500 g Th/kg H_2O, 2.5 g U/kg H_2O, 0.05 *m* MoO_3, heated 3 hr at 280°C under O_2 (300 psi at room temperature)

Reaction Temperature (°C)	Slurry Treatment	Combination Rate, P_{H_2} = 500 psi (moles H_2/hr·liter)
280	As prepared	0.07
210	Activated*	2.4
240		3.7
255		0.7
268		1.7
231	Reactivated**	1.3

*Slurry heated with H_2 (250 psi at 25°C) for 2 hr at 270°C.

**Reheated with H_2.

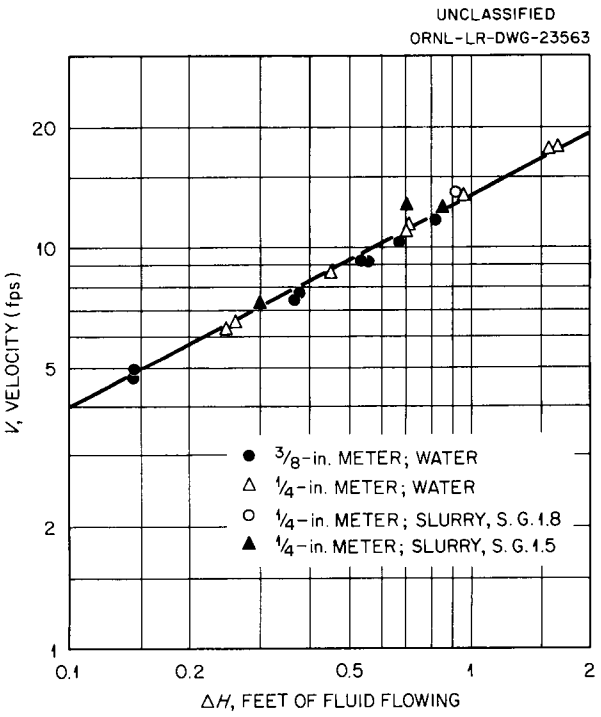

Fig. 18.2. Calibration of $\frac{1}{4}$-in. and $\frac{3}{8}$-in. Elbow Flowmeters with Water and $\frac{1}{4}$-in. Flowmeter with ThO_2 Slurry. Reduced to feet of fluid flowing in the elbow.

in a graduate and measuring the time. The differential head across the elbow was measured with a water–carbon tetrachloride manometer. For the slurry calibration a simple loop, consisting of an agitated tank, an Eastern Industries pump, the flowmeter, and appropriate stopcocks, was used. The slurry was cycled until well mixed, after which a three-way stopcock was quickly turned to direct the discharge into a graduate. The time for flow of a known volume was measured by a stop watch, the differential head was read on the water–carbon tetrachloride manometer, and a sample was caught in a tared container for determination of the specific gravity. The manometer lines and glass settling chambers in the elbow taps were kept clear of slurry by purging intermittently with water in such a way as to return any slurry to the system, with care being taken to purge before each manometer reading.

When the flow rate changed, slurry entered one or the other of the glass settling chambers in the elbow taps. The presence of settled slurry in these chambers had no effect on the differential pressure; the effect of slurry head in the chamber on manometer reading appeared to be restricted to the hindered-settling region, any effect vanishing as the slurry went into compaction.

The pipe elbow meter, properly arranged for purging taps, appears to be an entirely practical device for measuring the flow in ThO_2 slurry systems.

18.4 HIGH-TEMPERATURE SETTLING STUDIES

18.4.1 Effect of Particle Size

The effect of particle size on the high-temperature settling rates of thorium oxide slurries (thorium, 250 g per kilogram of H_2O) was investigated with 800°C-fired oxide prepared in the ORNL pilot plant, the same material after micronizing, and an oxide prepared by the hydrothermal decomposition of thorium oxalate and subsequent firing at 900°C (PO-10-900). The average particle sizes of these materials were 2.6, 1.0, and 0.7 μ, respectively. Data were also obtained for an oxide prepared by Davison Chemical Company (5 μ). The hindered-settling rates decreased with decreasing particle size (Fig. 18.3). Included also in Fig. 18.3 are the data obtained with the "standard slurry" (average particle size, 11 μ).

The settling rates for all the slurries at all temperatures were very much faster than those

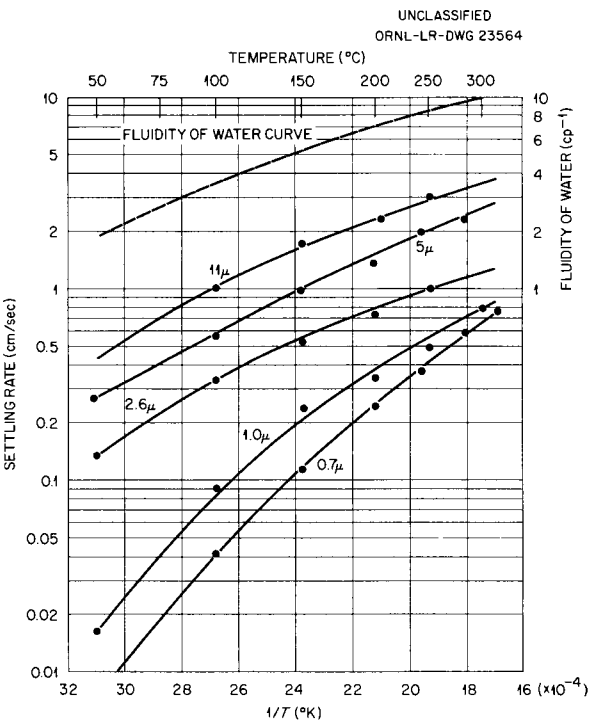

Fig. 18.3. Effect of Particle Size on the Settling Rate of Thorium Oxide Slurries: 250 g of Thorium per Kilogram of H_2O.

predicted by a simple application of Stokes' law, indicating that the slurries were flocculated. The settling-rate–reciprocal-temperature curves for the slurries of the 11-, 5-, and 2.6-μ materials closely parallel the water-fluidity curve (Fig. 18.3), indicating no appreciable change in the agglomeration characteristic of the oxide with increasing slurry temperature. However, with decreasing particle size the slope of the settling-rate curve increases, indicating that, particularly with the small-particle material, the increase in settling rate with increasing temperature is the result of changes in the slurry other than a simple decrease in the water viscosity.

18.4.2 Effect of Firing Temperature

The settling rates of slurries (thorium, 250 g per kilogram of H_2O) of oxides (TO-10) fired for 12 hr at 1000, 1200, 1400, and 1600°C were determined at temperatures from room temperature to 300°C. The temperature-dependence curves (reciprocal of the absolute temperature) of the settling rates all paralleled the curve for the increase in water

fluidity with increasing temperature (Fig. 18.4). The settling rate was highest at all temperatures for the slurry of the 1200°C-fired material. The settling rates of slurries of the 1400 and 1600°C materials were both less than those of the lower fired materials. An average floc size calculated from the observed settling rates, assuming Stokes' law to apply and a floc density of 5, for the 1000, 1200, 1400, and 1600°C material were 34, 38, 28, and 24 μ, respectively.

18.4.3 Settling Rates of a Pumped Slurry of 1600°C-Fired Thorium Oxide

Hindered-settling rates at temperatures from room temperature to 320°C were obtained on a sample of TO-10-1600-4 (d_g = 1.3 μ) that had been circulated for 268 hr at 300°C in loop 100A (runs BS-15 and -16). As taken from the loop, the oxide was highly flocculated and settled into a bed with a low bulk density (thorium, 835 g per kilogram of H_2O) and was readily redispersed. The settling rate at room temperature was 0.24 cm/sec and at 320°C was 2.15 cm/sec. The slope of the 1600°C-fired material paralleled the water-fluidity curve closely, indicating little change in floc size as the temperature increased.

18.4.4 Effect of Silicate Additions

Figure 18.5 illustrates the effect of the addition of 10,000 ppm SiO_2 (added as $Na_2O{\cdot}SiO_2$), based on ThO_2, on the settling rates of the 250 g of thorium per kilogram of H_2O slurries of oxides with average particle sizes of 2.6, 1.0, and 0.7 μ (Sec. 18.4.1). The addition of silicate slowed the settling rates markedly, compared with those of the pure slurries (Fig. 18.3), and had a relatively greater effect on the smaller particle material, particularly above 200°C (Fig. 18.5). In the pure slurries, containing no additive, there was a twofold decrease in settling rate at 300°C for a decrease in average particle size from 2.6 to 0.7 μ. With 10,000 ppm SiO_2, based on ThO_2 added, there was a fivefold decrease in the settling rate at 300°C. In the presence of silicate the temperature

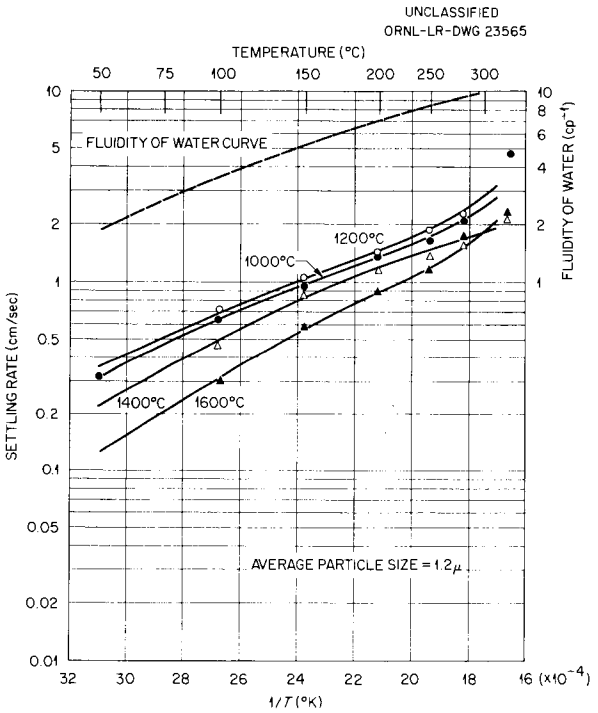

Fig. 18.4. Effect of Firing Temperature on Settling Rates of Thorium Oxide Slurries: 250 g of Thorium per Kilogram of H_2O. Oxide prepared from 10°C-precipitated oxalate.

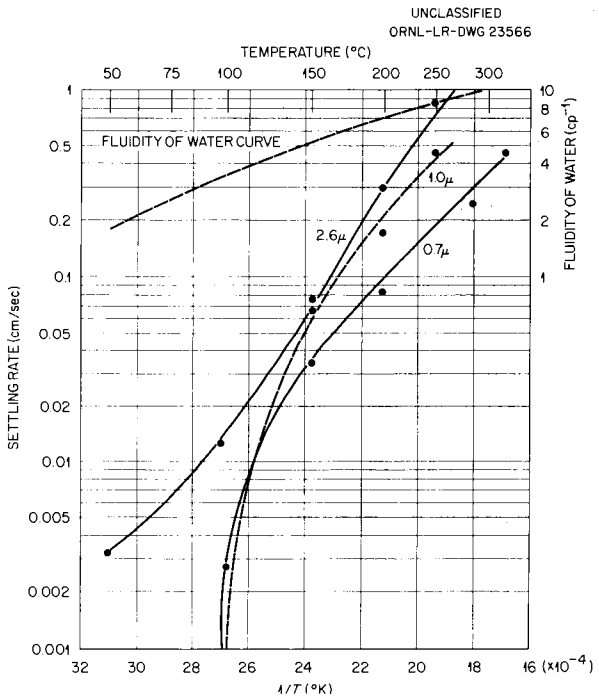

Fig. 18.5. Effect of Average Particle Size on the Settling Rates of Thorium Oxide Slurries Containing 10,000 ppm SiO_2, Based on ThO_2: 250 g of Thorium per Kilogram of H_2O.

dependence of the settling rate was more complex than in the pure slurry, and the relative effect of the silicate depended on both temperature and particle size. Even more than with the pure slurry, in the slurries containing silicate the increase in settling rate with increasing temperature depends on factors other than a simple decrease in water viscosity.

18.5 PROPERTIES OF HIGH-FIRED THORIUM OXIDE

Preliminary dynamic tests with slurries of high-fired thorium oxide have been encouraging. Hence data were obtained on the effect of high firing (1000 to 1600°C) on the characteristic properties of thorium oxide, its resistance to particle degradation, and its abrasive characteristics.

18.5.1 Characteristic Properties

The effect of firing temperature from 1000 to 1600°C, for 6- to 12-hr firings, on the characteristic properties of two thorium oxides prepared from 10°C-precipitated oxalate by multistage firing ending at 650°C (SO-B10) and at 1000°C (TO-10) are shown in Table 18.4. No increase in average particle size was observed with increasing firing temperature. Also, no significant differences in the characteristic properties appeared to result from the use of a 650°C-fired oxide, as opposed to a higher fired oxide, as the starting material for final firing at 1200 to 1600°C.

18.5.2 Mechanical Handling of High-Fired Oxides

Several tests were carried out on the high-fired oxides to determine the effect of mechanical handling on their average particle sizes. The tests consisted in blending a 500 g of thorium per kilogram of H_2O slurry for 1 hr in a Waring Blendor, grinding for 1 hr in a mechanical grinder, and treating for 1 hr as a slurry in an ultrasonic disperser in both the absence and the presence of a dispersing agent (0.005 *M* $Na_4P_2O_7$). None of the conditions significantly lowered the average particle size of the oxides (see Table 18.5).

18.5.3 Abrasive Characteristics of High-Fired Thorium Oxides

Slurries (250 g of thorium per kilogram of H_2O) of the TO-10 oxides fired at 1000, 1200, 1400, and 1600°C were tested in the jet-impingement slurry abrasion tester, in which 1-ml-thick spring-tempered type 302 stainless steel shim stock was used. The 1600°C material was ground before the test in order to minimize particle-size effects. Results were reproducible within ±1.5%. Penetration times decreased with increasing firing temperature (Table 18.6). Each slurry was impinged a second time on a fresh target. Only the 1000°C material showed an appreciable increase in penetration time on the second pass, presumably the result of particle degradation.

Figure 18.6 shows the linear dependence of the log of the penetration time on the reciprocal of the

Table 18.4. Characteristic Properties of High-Fired Thorium Oxide

Starting Material*	Final Firing Temperature (°C)	Average Particle Size (μ)	Average X-Ray Crystallite Size (Å)	Specific Surface Area (m^2/g)
SO-B10-650	1200	0.98	1300	2.2
	1400	1.00		2.2
	1600	1.22	2700	0.9
TO-10-1000	1000	1.2	803	4.3
	1200	1.13	1100	3.0
	1400	1.25	2900	2.4
	1600	1.22	2900	1.0

*Last figure in sample designation indicates firing temperature in °C; prepared from 10°C-precipitated thorium oxalate.

Table 18.5. Degradation of High-Fired Thorium Oxides

Oxide*	Average Particle Size (μ)				
	Original Oxide	After Blending** for 1 hr	After Grinding for 1 hr	After Ultrasonic Treatment for 1 hr	
				In Water	In 0.005 M $Na_4P_2O_7$
SO-B10-1200	1.0	1.0	0.8	1.0	0.8
-1400	1.0	1.0	1.0	0.8	0.8
-1600	1.2	1.2	1.2	0.9	0.8
TO-10-1000	1.2	1.2	0.8	1.3	1.0
-1200	1.1	1.1	0.9	1.2	0.8
-1400	1.2	1.2	1.0	1.2	1.2
-1600	1.2	1.2	0.9	1.1	1.2

*Last figure in sample designation indicates firing temperature in °C; prepared from 100°C-precipitated thorium oxalate.

**In Waring Blendor; 500 g Th/kg H_2O concentration.

Table 18.6. Abrasive Characteristics of High-Fired Thorium Oxide

Conditions: impinged against 1-mil-thick type 302 stainless steel shim stock; 250 g Th/kg H_2O

Oxide*	Average Particle Size (μ)	Penetration Time (sec)	
		1st Pass	2nd Pass
TO-10-1000	1.2	346	440
-1200	1.1	138	140
-1400	1.2	44	44
-1600	1.2	29	29

*Last figure in sample designation indicates firing temperature in °C; prepared from 10°C-precipitated oxalate.

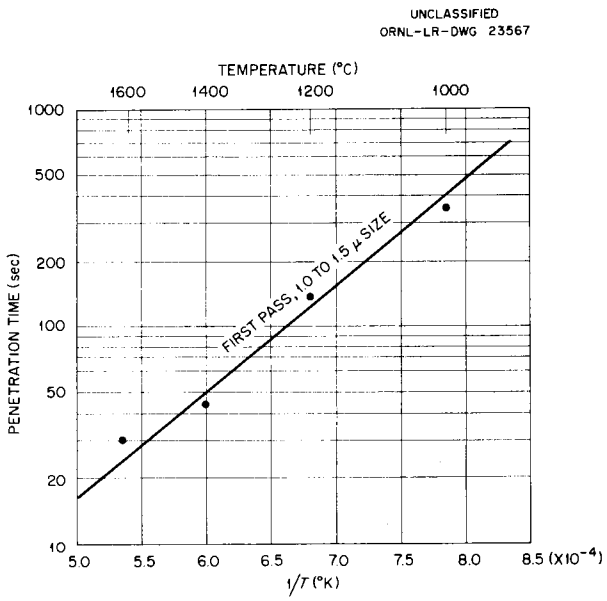

Fig. 18.6. Dependence of Slurry Penetration Rate on Oxide Firing Temperature: 250 g of Thorium per Kilogram of H_2O; 302 SS Target.

absolute temperature at which the material was fired. It has been shown that the crystallite-growth characteristic has a linear logarithmic dependence on the reciprocal of the absolute temperature. This may indicate that the increase in crystallite size with increasing firing temperature is the main factor contributing to the higher abrasive characteristics of the higher fired materials.

In further tests with slurries of the 1400- and 1600°C-fired materials, penetration rates were measured as the slurry accumulated up to 1000 sec of impingement against a steel target. The oxide fired at 1400°C for 12 hr was degraded, as indicated by a steadily decreasing penetration rate with time of impingement. The oxide fired at 1400°C for 64 hr was not degraded during 1000 sec of impingement. Oxide fired at 1600°C for 2 hr started to be degraded after 500 sec; that fired for 12 hr was not degraded during 1000 sec.

18.6 PREPARATION OF THORIA SOLS AND MICROSPHERES[1]

Two liters of a nitrate-stabilized thoria sol, unstable at temperatures above 100°C, were prepared for laboratory testing. This completes the work on thoria sol preparation.

Thoria microspheres of less than 10-μ diameter (wet) were prepared by a technique in which thoria sol was jet-mixed with hexamethylenetetramine solution and collected in oil. Problems in aging, washing, drying, and calcining are under investigation.

Initial tests with a transducer built by Sperry Products, Inc., for slurry settling studies by a pulse-echo technique were unsuccessful in that the gold plating on the crystal and ceramic support flaked off. A metalized ceramic body is being obtained. Studies of alternate transducers have shown that crystal silver-soldered to a $\frac{3}{4}$-in.-dia bar welded in a container wall could be used. The future course of development will be determined when Sperry submits a report on their work.

18.7 PREPARATION OF THORIUM OXALATE

Preliminary tests of precipitation, filtration, and washing techniques for preparing $Th(C_2O_4)_2$ for firing to ThO_2 showed that a jet-mixer precipitator gave the small particle sizes required and that varying conditions gave varying particle sizes. The ThO_2 fired from the jet-mixer product had mean sizes of 0.61 to 1.50 μ, with standard deviations of 0.28 to 2.7 μ. In small-scale filtration tests, losses were 0.2% or less, and filtration and wash rates with commercial filter cloths were low but still practical. A jet mixer and continuous rotary filter are being set up for semi-production-scale tests.

The small jet mixer, for room temperature tests, had as inlet jets for the thorium nitrate and oxalic acid solutions approximately 4-in. lengths of 0.033-in.-ID stainless steel tubing. The solutions were introduced from glass-pipe reservoir tanks pressurized with air. Flows were indicated by rotameters and controlled manually with throttling valves. Thorium oxalate samples were collected during steady-state operation and were filtered, washed, and fired to ThO_2.

The conditions and the ThO_2 particle-size distributions (Table 18.7) showed that the amount of energy dissipated in the mixing is a major variable. The amount of excess oxalic acid had less effect, although smaller excesses of oxalic acid gave smaller particle sizes. Further studies will be required to determine the effects of inlet-stream temperatures and of excess nitric acid in the thorium nitrate solution.

The filtration tests were made with two types of material: (1) thorium oxalate prepared by batch precipitation, at 10°C, with mechanical agitation, and (2) thorium oxalate precipitated in the jet mixer. With the batch-precipitated material, rates and losses during filtration and washing with several commercial filter cloths were determined. The best of these filter cloths were used to determine filtration and washing rates and losses of the jet-mixer material. The test apparatus used a controlled vacuum and a graduated filtrate receiver. The first series of tests was made with the filter suspended in a beaker of gently agitated thorium oxalate slurry. The second series was with a funnel-type filter into which a 100-ml sample of slurry was poured. Water washes were made by substituting a beaker of water for the slurry or by pouring measured volumes of water into the filter funnel. In the first set of tests the filter cake provided the controlling resistance for all cloths tested. Therefore the main criteria for cloth selection would be low losses, durability, and perhaps free cake discharge without progressive blinding. Each cake formed well, drained dry without cracking, and discharged (when $\frac{1}{4}$ in. thick) by its own weight when the vacuum was cut off. Losses for the three filter cloths tested averaged 0.2, 0.1, and 0.05%. High vacuum increased the initial losses and only slightly increased the filtration rates. Therefore some intermediate vacuum ($\sim$20 cm Hg) is probably suitable. Wash volumes of three times the filtrate volume adequately removed nitrate. Acceptable rates for the thorium oxalate filtrations would be 8 gal/ft^2·hr form rate and 5 gal/ft^2·hr wash rate. In tests with the jet-mixer precipitates and the most satisfactory cloth used above, the filtration rate, wash rate, and settling rate decreased as the particle size of the thorium oxalate decreased. The wash nitrate concentration was reduced to below 0.01 and 0.001% of the filtrate nitrate concentration by wash volumes of one and two times the filtrate volume.

[1]Work done by Houdry Process Corp.

Table 18.7. Statistical Constants[a] for ThO_2 Size Distribution

Temperature (°C)	$Th(NO_3)_4$ Concentration (M)	$H_2C_2O_4$ Concentration (M)	$H_2C_2O_4$ Excess (%)	Average Jet Pressure[b] (psig)	Particle Size (μ) Mean[c]	Particle Size (μ) Standard Deviation[d]	Weight Per Cent 0.3–1.0 μ	Weight Per Cent 1.0–3.0 μ	Weight Per Cent >3.0 μ
Batch Laboratory Experiments, Mechanical Agitation									
10	~1.0	0.8	~10		0.78	0.30	70	28	<1
10					0.82	0.30	68	30	<1
Continuous Jet-Mixer Experiments									
24	1.00	0.88	0	9.1	0.61	0.38	67	13	9
			32	16.0	0.86	0.52	55	29	10
			32	2.2	1.50	2.7	32	31	34
			75	16.5	0.98	0.49	50	37	11

[a]Basis: size distributions of apparent Stokes' diameters as determined for a weight basis by neutron-activation analyses. Normal distribution was assumed.

[b]Average pressure calculated from $\frac{V_{H_2C_2O_4} P_{H_2C_2O_4} + V_{Th} P_{Th}}{V_{total}}$.

[c]Size for 50 wt % values from plotted size distributions.

[d]Size change for 30 to 70% is σ; these values were read from plotted size distribution.

19. IN-PILE SLURRY LOOP

W. E. Unger

T. A. Arehart W. F. Schaffer

The in-pile slurry loop program is presently a joint effort of the Pennsylvania Advanced Reactor Project and ORNL. Westinghouse will design and fabricate the loops (10 ft in length, major diameter of 27 in.). ORNL will install and operate the loops in the ORR, together with control instrumentation and auxiliaries such as gas holdup equipment, loop cooling system, sampler and slurry dump equipment; and ORNL will dismantle the loops after irradiation.

Preliminary room-temperature water tests of a mockup of a proposed loop design constructed at Westinghouse were initiated. Mockup operation at temperature and pressure will be demonstrated with ThO_2 slurry concentrations of at least 500 g per kilogram of H_2O.

A special shielding plug for the ORR was designed to accommodate this large loop. Shielded cubicles at the face of the reactor are being designed to house the external equipment associated with the in-pile loop. The loop, after irradiation, will be withdrawn from the reactor into a specially designed 25-ton lead-shielded cask and transferred to cells in Building 3026 for dismantling and segmenting. The cells (formerly used for Rala processing) are being remodeled to provide viewing windows, access plug, remotely operated saws, manipulators, and decontamination equipment.

Westinghouse expects to complete the first in-pile loop by January 1958. An estimated three months will be required for installation and checkout before operation at design power densities, anticipated in March 1958. Building 3026 modifications are scheduled for completion in June 1958.

Part VI

SUPPORTING CHEMICAL RESEARCH

E. H. Taylor

20. AQUEOUS SYSTEMS AT ELEVATED TEMPERATURES

C. H. Secoy H. F. McDuffie

F. E. Clark
J. S. Gill
G. M. Hebert
R. Slusher
H. H. Stone
J. E. Stuckey

20.1 CRITICAL PHENOMENON IN BINARY AQUEOUS SOLUTIONS; THE SYSTEM SO_3-H_2O (ref 1)

A background study of the general field of critical phenomena reveals that the knowledge of critical data concerning aqueous solutions is limited. The high temperatures and pressures developed in the critical region and the highly corrosive nature of many aqueous solutions make ordinary experimental techniques useless.

In this work experimental techniques and apparatus were designed for obtaining data on the SO_3-H_2O system. No satisfactory apparatus was conceived whereby direct simultaneous measurements of pressure, temperature, volume, and composition could be made; therefore measurements were made in two separate experiments and data were correlated by means of a parameter, the ratio of liquid volume to vapor volume.

The first series of experiments was designed to correlate temperature, composition, and the fraction of a fixed volume occupied by the liquid phase. The phase-study apparatus developed by Marshall, Wright, and Secoy[2] for semimicroexperimentation was modified for use in the experiments. The original apparatus was satisfactory to temperatures near 550°C, but higher temperatures required a furnace machined from graphite.

Sample tubes were constructed from 4-in. lengths of 1-mm-ID, 3-mm-OD quartz tubing. Solutions of known concentrations were sealed in the tubes, and a Gaertner micrometer slide comparator was used to measure the liquid fraction filling of each tube. The center of each tube was marked as a reference point, and the tube was placed inside the furnace at a temperature near critical. The tube was agitated by a rod connected to a Vibra-tool. The temperature at which the meniscus disappeared and reappeared was determined by potentiometric readings of voltage output from calibrated iron-constantan thermocouples. The position, relative to the center of the tube, at which the meniscus vanished was determined by observation of the tube through a telemicroscope. This permitted calculation of the relative volumes of each phase at the temperature at which the meniscus vanished.

This semimicroapparatus required a small solution sample in tubes which could be easily prepared. The tubes could withstand high temperatures and pressures without special apparatus and techniques. The use of a telemicroscope gave increased visual perception of phase changes within a sample tube while it was held inside the furnace in a constant-temperature region. The apparatus was inexpensive and readily assembled. The chief limitations were imposed by delays during frequent calibrations of thermocouples and by their limit of accuracy. Too, the corrosion of the quartz tubes, particularly by lower sulfur trioxide concentrations, had to be carefully evaluated.

The critical temperature of the binary solution was arbitrarily defined as the temperature at which the meniscus disappeared and reappeared at the center of the experimental sample tube. Data appear in Table 20.1 and are plotted in Fig. 20.1. Since the pressure was unknown but specific for each point, the plot is a projection of the critical curve on a constant pressure plane in the three-dimensional pressure-temperature-composition diagram.

Data on the SO_3-rich side were limited by the experimental techniques involved and the extreme difficulty of handling highly volatile and corrosive SO_3. Further study in this region will require construction of special equipment to handle sulfur trioxide.

[1] J. E. Stuckey, *Critical Phenomena in Binary Aqueous Solutions; The System SO_3-H_2O*, Doctoral Dissertation, University of Oklahoma, 1957.

[2] W. L. Marshall, H. W. Wright, and C. H. Secoy, *J. Chem. Educ.* 31, 34 (1954).

The second series of experiments involved the design and construction of apparatus capable of measuring pressures of the highly corrosive solutions at elevated temperatures. The principle developed by D. M. Richardson[3] of measuring the pressure of an enclosed system by the displacement of a restrained diaphragm was the basis of design for a special pressure-measuring apparatus suited to high temperatures, relatively high pressures, and highly corrosive solutions.

[3]D. M. Richardson, *Pressure Measurement by Displacement of a Restrained Diaphragm*, ORNL CF-56-2-168 (Feb. 15, 1956).

Table 20.1. Summary of Critical Temperatures

Mole Fraction SO_3	Room-Temperature Fraction Filling of Sample Tube	Critical Temperature (°C)
0.0000	0.32	374.2*
0.0193	0.393	404.2 ± 1.0
0.0419	0.396	447.4 ± 1.0
0.0654	0.376	482.8 ± 1.0
0.0938	0.353	526.1 ± 1.0
0.1251	0.336	562.0 ± 1.0
0.1643	0.333	592.2 ± 1.0
0.2084	0.314	621.0 ± 1.0
0.2664	0.293	646.8 ± 1.0
0.3368	0.283	665.4 ± 1.0
0.4353	0.280	666.4 ± 1.0
0.5591	0.331	637.2 ± 1.0
1.0000	0.336	218.3**

*K. A. Kobe and E. Lynn, Jr., *Chem. Revs.* 52, 117–236 (1953).

**A. Berthoud, *J. chim. phys.* 20, 77–86 (1923).

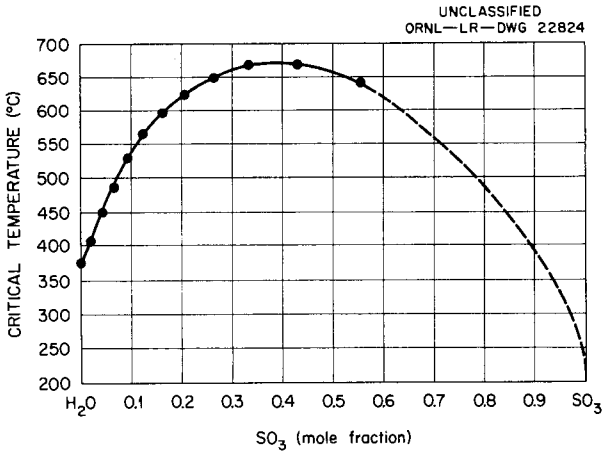

Fig. 20.1. Critical Temperature, System SO_3-H_2O.

Figure 20.2 shows a schematic diagram of the platinum-lined stainless steel pressure vessel. The distinctive feature of the apparatus was the bimetallic diaphragm in the bomb head, which was limited in displacement by a platinum-iridium retainer plate and the concave bomb head. The diaphragm was constructed of two 5-mil well-bonded sheets of stainless steel type 347 and platinum. It was stamped in a concave press corresponding to the bomb head with three concentric corrugations to ensure even displacement with no "cricket" snapping.

The diaphragm was backed up with a mercury system connected to a high-pressure piston-type pressure generator. Volume reduction of the slightly compressible mercury system increased the external pressure on the diaphragm. When the external pressure became slightly greater than the internal pressure of the acid solution, the diaphragm was displaced from the bomb head toward the retainer plate. Further rotation of the pressure piston handle moved the diaphragm but resulted in only a slight increase in pressure of the mercury system. This pressure plateau (Fig. 20.3) was used to determine the internal pressure on the bomb.

Figure 20.4 shows the experimentally determined vapor pressures of pure water compared with the values of Keenan and Keyes.[4] Most of the experimental values are within 0.5% of the standard values.

Further exploratory work is being carried out with the apparatus before pressures of the SO_3-H_2O system are measured. An absolute calibration of the bimetallic diaphragm, as well as the effects of continued mechanical working, is under study. The effect of repeated temperature cycling on various bomb parts is also being noted.

[4]J. H. Keenan and F. G. Keyes, *Thermodynamic Properties of Steam*, p 33, Wiley, New York, 1936.

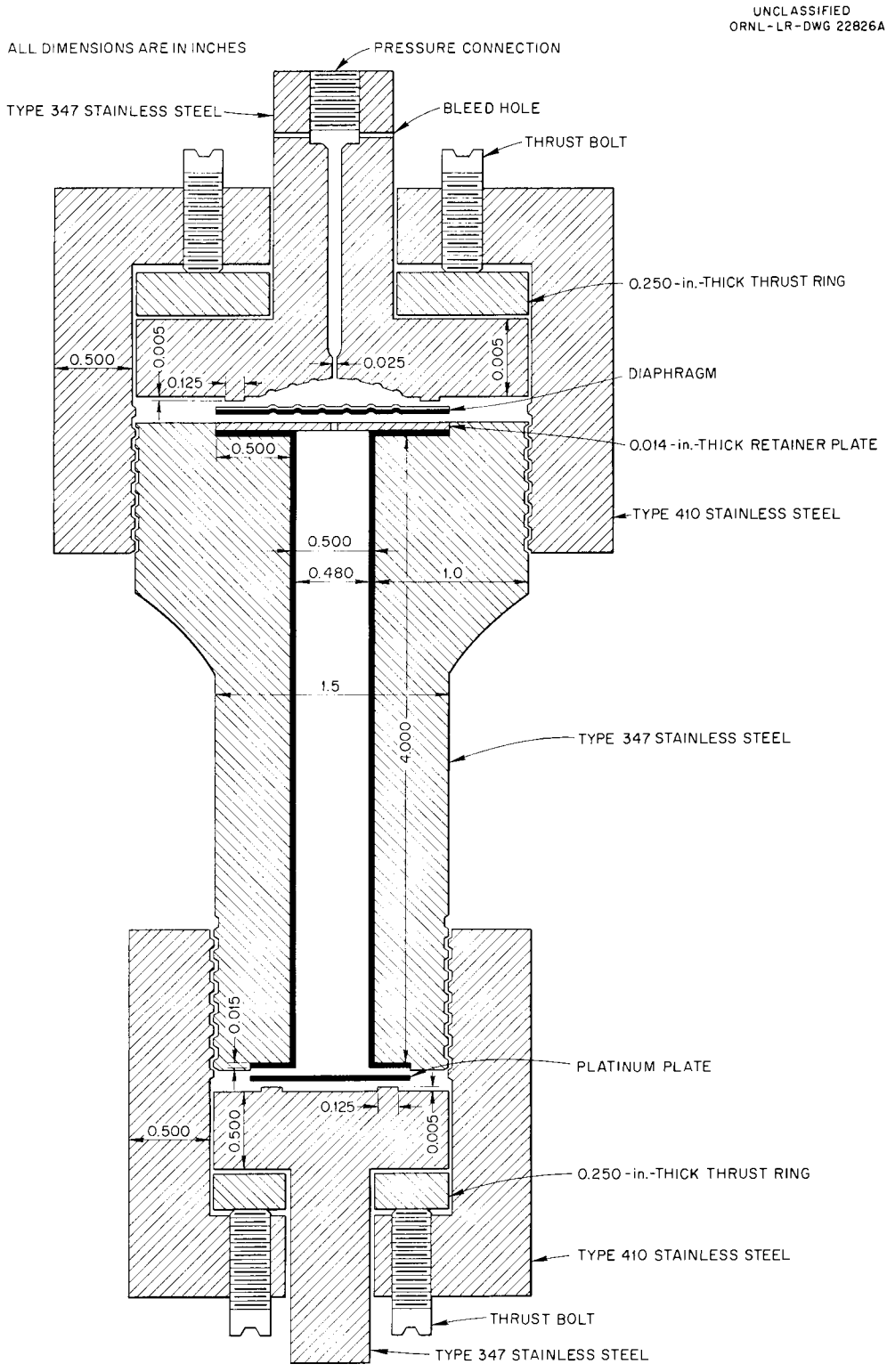

Fig. 20.2. High-Pressure Bomb.

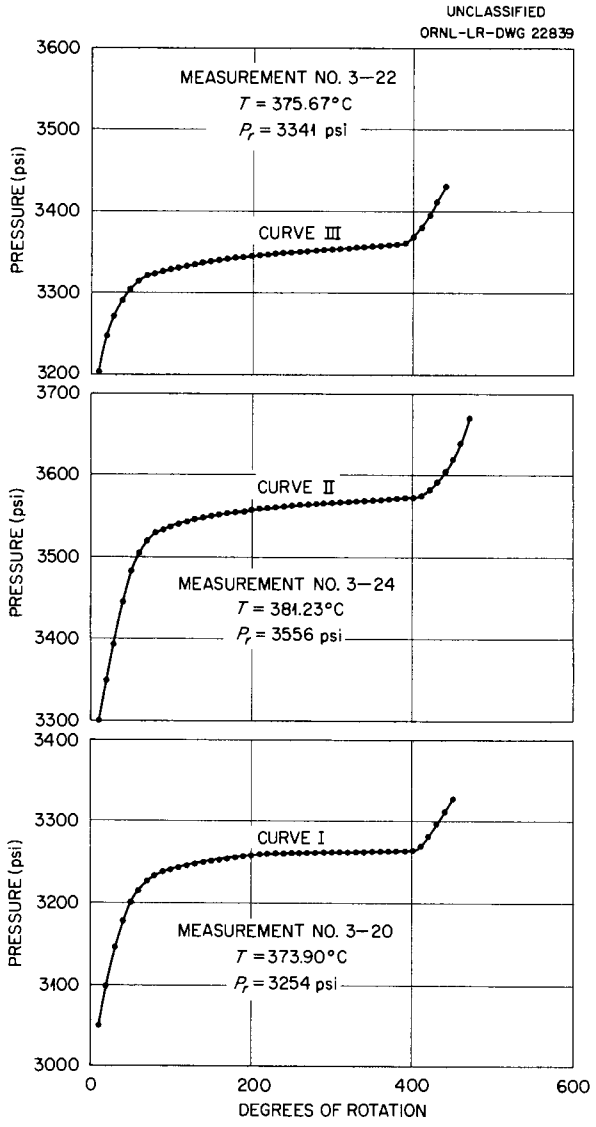

Fig. 20.3. Pressure as a Function of Volume Reduction.

20.2 THE DENSITIES OF HEAVY-WATER LIQUID AND SATURATED VAPOR AT ELEVATED TEMPERATURES

In connection with studies of the homogeneous catalysis of the deuterium-oxygen reaction in heavy-water systems, it became desirable to know the densities for the liquid and saturated vapor of heavy water at temperatures above 250°C. Previous studies of the density of heavy water had provided data for the density[5] of the liquid up to 250°C and for the critical properties of heavy water.[6] No data concerning the vapor density of heavy water over the temperature range appeared to be available.

The experimental method used for determining the volume of uranyl sulfate solutions as a function of concentration, temperature, and fractional filling of sealed quartz tubes[7] appeared suitable for application to the determination of the fractional filling at various temperatures of tubes containing heavy water. It is easily shown, by mass-balance equations, that the relationship between the fractional filling at room temperature, F_0, and that at some temperature, F_T, is expressed by:

$$F_0\left(d_{l_0} - d_{v_0}\right) + d_{v_0} = F_T\left(d_{l_T} - d_{v_T}\right) + d_{v_T} ,$$

where

d = density,
l = liquid,
v = vapor.

The reasonable assumption that $d_{v_0} \cong 0$ reduces the expression to a simple linear relationship:

$$F_0 d_{l_0} = F_T\left(d_{l_T} - d_{v_T}\right) + d_{v_T} .$$

It is also assumed that only one component (D_2O) is present in the tubes and that the air included when the tubes were sealed has only a negligible effect. Values for d_{v_T} and d_{l_T} were obtained by graphical or mathematical extrapolation of this relationship to the extremes where $F_T = 0$ and 1, respectively. Four quartz tubes, of differing F_0 values, were used for all determinations except for those at 367°C, where only two of the tubes retained observable liquid phases. As an internal check of the experimental method and interpretation, two tubes containing light water were included for comparison with the known data for

[5] J. R. Heiks *et al.*, *J. Phys. Chem.* **58**, 488 (1954).

[6] P. A. Lottes, chap. 1.3, sec. 1, p 22 in *Reactor Handbook*, vol II, Technical Information Service, AEC, 1953.

[7] G. M. Hebert, D. W. Sherwood, and C. H. Secoy, *HRP Quar. Prog. Rep. Oct. 31, 1954*, ORNL-1813, p 164.

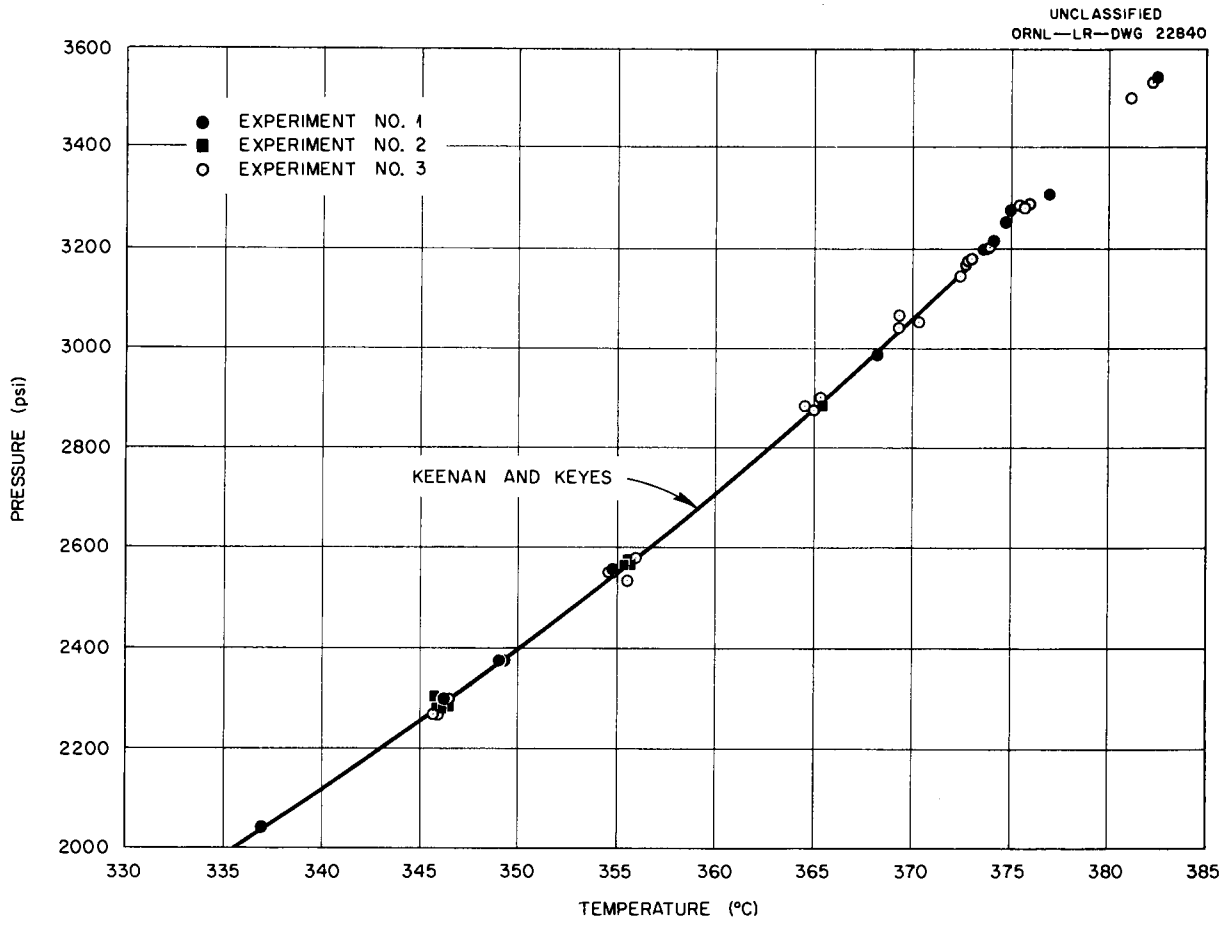

Fig. 20.4. Pressure-Temperature Isochore of Water.

water. The experimentally determined values for both light and heavy water are presented in Fig. 20.5, together with accepted values for each.

20.3 HOMOGENEOUS CATALYSIS OF THE HYDROGEN-OXYGEN REACTION IN AQUEOUS SOLUTIONS

During the past quarter, additional[8,9] studies of homogeneous catalysis were concentrated on the sulfate system at 200°C in order to reduce the uncertainty in the estimation of catalytic activity, k_{sol}, and apparent hydrogen solubility, $10^4/\alpha$, from the experimentally determined relationship between the time constant for pressure decrease, $1/k_{\pi}$, and the gas-to-liquid volume ratio in the experiment.

Table 20.2 presents the experimentally determined 200°C values of $1/k_{sol}$ and α/RTk_{sol} for solutions containing 0.01 and 0.02 *M* $CuSO_4$ plus 0.01 to 0.20 *M* sulfuric acid (at room temperature), together with the derived values of catalytic activity k_{Cu} ($k_{sol}/[Cu]$) and apparent solubility (corrected for its dependence on the square root of the copper concentration),

$$\frac{10^4}{\alpha\,[Cu]^{1/2}}.$$

Figures 20.6 and 20.7 illustrate the dependence of these quantities on the acidity; Figs. 20.8 and 20.9 provide comparison with the data previously obtained at 175°C. It is seen that increasing the temperature has altered the influence of changes

[8] C. H. Secoy *et al.*, *HRP Quar. Prog. Rep. Jan. 31, 1957*, ORNL-2272, p 165.

[9] C. H. Secoy *et al.*, *HRP Quar. Prog. Rep. April 30, 1957*, ORNL-2331, p 173.

in the acidity; although the maximum apparent solubility still occurs at about 0.05 *M* acid, the effects of changing to higher and lower acidity are much smaller at 200°C; the catalytic activity appears to be inversely related to the acidity over the whole range at 200°C, whereas at 175°C the inverse relationship disappeared above 0.05 *M* acid. These changes must be due to the effect of temperature on the as-yet-unknown species which are involved in the apparent hydrogen solubility and the catalytic activity.

Preliminary experiments in the perchlorate system (cupric perchlorate–perchloric acid) indicate that the relationships are different from those in the sulfate system; further work with perchlorates and mixtures of perchlorates and sulfates is in progress.

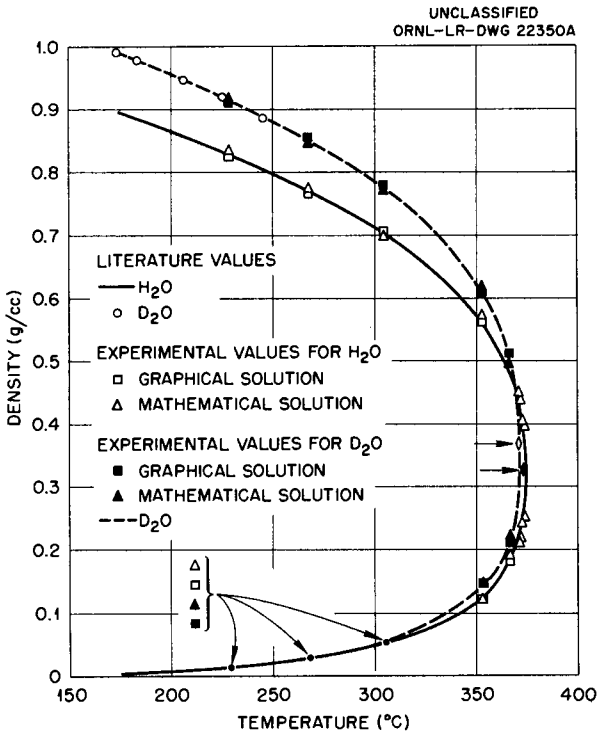

Fig. 20.5. Liquid and Saturated Vapor Density of H_2O and D_2O.

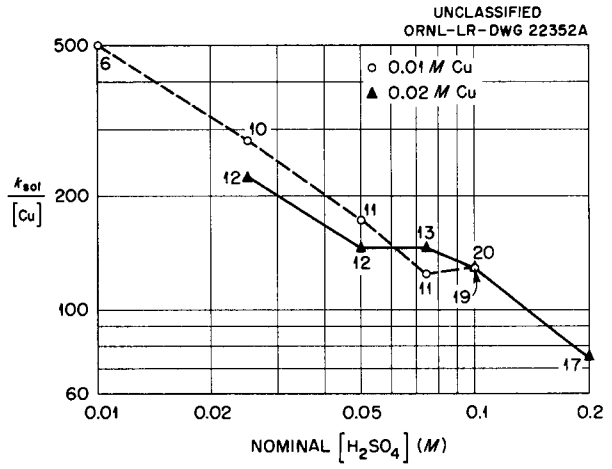

Fig. 20.6. Homogeneous Catalytic Activity at 200°C.

Table 20.2. Homogeneous Catalysis in the Sulfate System at 200°C

Solution Composition, at Room Temperature		Number of Experiments	Experimental Data, from Least-Squares Line		Derived Values	
$CuSO_4$ (*M*)	H_2SO_4 (*M*)		Slope, $\frac{\alpha}{RTk_{sol}}$	Intercept, $\frac{1}{k_{sol}}$	Apparent Solubility, $\frac{10^4}{\alpha[Cu]^{1/2}}$	Catalytic Activity, $\frac{k_{sol}}{[Cu]}$
0.01	0.01	6	1.522	0.230	28.5	503
	0.025	10	2.029	0.413	38.3	280
	0.050	11	3.079	0.667	40.8	173
	0.075	11	3.992	0.923	43.6	125
	0.100	19	4.690	0.899	36.1	128
0.02	0.025	18	0.909	0.183	26.8	315
	0.050	12	1.172	0.396	45.0	146
	0.075	16	1.597	0.401	33.4	144
	0.100	20	1.995	0.455	30.4	127
	0.200	20	3.501	0.928	35.3	62

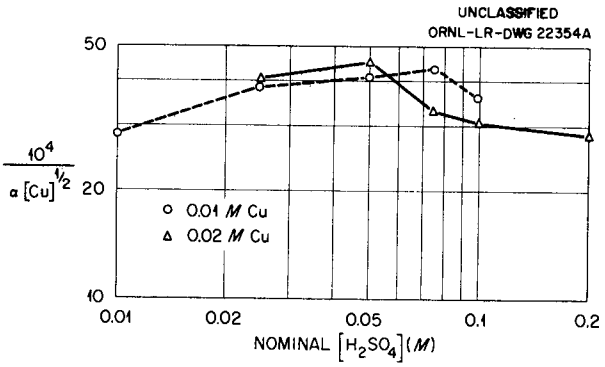

Fig. 20.7. Experimental Solubility Parameter at 200°C.

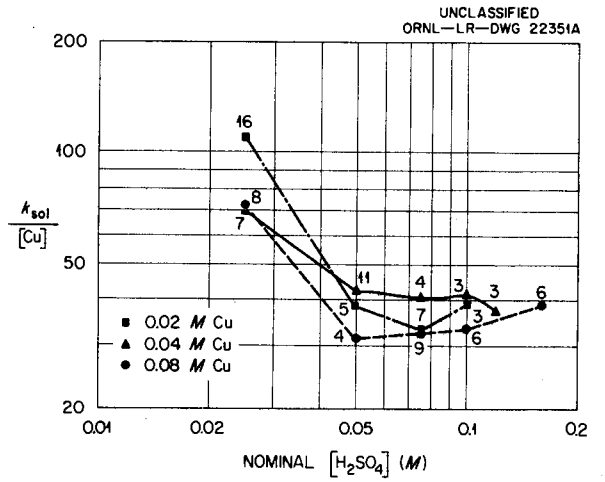

Fig. 20.8. Homogeneous Catalytic Activity at 175°C.

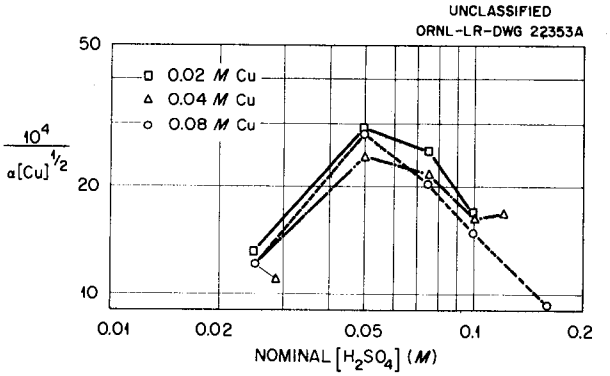

Fig. 20.9. Experimental Solubility Parameter at 175°C.

20.4 PRECIPITATION TEMPERATURES FOR DILUTE SOLUTIONS IN THE SYSTEM UO_2SO_4-$CuSO_4$-$NiSO_4$-H_2SO_4-H_2O

Further work was done in the determination of temperatures of precipitation in the five-component system UO_2SO_4-$CuSO_4$-$NiSO_4$-H_2SO_4-H_2O, using the static or equilibrium method described and explained in an earlier report.[10] The new measurements are principally an extension of those already presented on solutions 0.04 *m* in UO_2SO_4 and 0.01 *m* in excess H_2SO_4. A few runs were also made with 0.02 *m* excess H_2SO_4.

The earlier report gave an example[11] showing the precipitation of a copper-containing solid at 186°C from solution No. 4421, having the composition 0.04 *m* UO_2SO_4, 0.04 *m* $CuSO_4$, 0.02 *m* $NiSO_4$ and 0.01 *m* excess H_2SO_4. This solid has now been identified, on the basis of its x-ray diffraction pattern, as the basic copper sulfate $3CuO{\cdot}SO_3{\cdot}2H_2O$, known as antlerite. The additional experiments which have since been made were intended to explore further the field of precipitation of this solid phase, and to attempt to obtain similar information for the field of precipitation of the uranium-containing solid phase $2UO_3{\cdot}SO_3{\cdot}5H_2O$, mineral name – zippeite.

The data are presented in Table 20.3, which includes also the results previously reported.[12] Column 4 refers to the range of temperatures covered, in intervals of approximately 10°C, in the successive equilibrations and samplings upon the one solution. Column 5 shows the metals whose concentrations were determined at the successive temperatures. Column 6 is the temperature at which one of these concentrations showed a distinct break, followed by a continued fall in value, when plotted against the temperature. The next two columns (7,8) list the solids observed when the titanium tube was opened after quenching from the temperature indicated. In almost all cases the solids were not only observed visually as

[10] C. H. Secoy *et al.*, *HRP Quar. Prog. Rep. Oct. 31, 1956*, ORNL-2222, p 161.

[11] *Ibid.*, Fig. 19.3, p 164.

[12] *Ibid.*, Table 19.1, p 164.

Table 20.3. Precipitation Temperatures in the System UO_2SO_4-$CuSO_4$-$NiSO_4$-H_2SO_4-H_2O

Solution No.	Composition		Temperature Range of Analysis (°C)	Metals Determined	Precipitation Temperature, Break in Curve (°C)	Quenching Observations		Visually Observed Precipitation Temperature[b] (°C)
	$CuSO_4$ (*m*)	$NiSO_4$ (*m*)				Temperature of Quenching (°C)	Solids Found[a]	
				0.04 *m* UO_2SO_4; 0.01 *m* H_2SO_4				
4031 I	0	0.03	198–282	U, Ni	261 (U)	282	Z (N)	<288
4031 J	0	0.03	205–280	Cu, Ni	None	249	None	
4041 I	0	0.04	198–282	U, Ni	None	282	(Z) N	247
4041 J	0	0.04	205–280	U, Ni	None	249	Z	
4531 I	0.005	0.03	198–282	U, Cu, Ni	None	282	Z, N	265
4531 J	0.005	0.03	205–280	U, Cu, Ni	None	249	None	
4541 I	0.005	0.04	198–282	U, Cu, Ni	None	282	(Z) N (U_3O_8)	231
4541 J	0.005	0.04	180–280	U, Cu, Ni	None	249	Z	
4541[c]						250	Z	
4541[c]						275	Z, C	
4131 I	0.01	0.03	198–282	U, Cu, Ni	None	282	Z, N	<273
4131[c]						275	Z, N, U_3O_8	
4131[c]						249	None	
4141 I	0.01	0.04	198–282	U, Cu, Ni	None	282	(Z) N	
4141 J	0.01	0.04	205–280	U, Cu, Ni	None	249	Z, N	
4141[c]						275	Z, N, C	
4221 J	0.02	0.02	205–250	U, Cu, Ni	240 (Cu)	250	A	277
4231 G	0.02	0.03	150–275	Cu, Ni	215 (Cu)	275	A (C)	255
4231 H	0.02	0.03	150–275	Cu, Ni	229 (Cu)	275	A (C)	
4241 H	0.02	0.04	165–265	Cu, Ni	220 (Cu)	265	A, N	
4241 I	0.02	0.04	190–285	U, Cu, Ni	200 (Cu)	285	A, N	
4241 J	0.02	0.04	190–250	U, Cu, Ni	215 (Cu)	250	A, N	
4311 G	0.03	0.01	150–275	Cu, Ni	215 (Cu)		Not examined	255
4321 G	0.03	0.02	148–265	Cu, Ni	211 (Cu)	265	A (C)	238
4321 H	0.03	0.02	148–265	Cu, Ni	216 (Cu)	265	A (C)	
4331 G	0.03	0.03	148–275	Cu, Ni	197 (Cu)	275	A	220
4341 H	0.03	0.04	170–265	Cu, Ni	186 (Cu)	265	A (C)	
4401 G	0.04	0.00	148–262	Cu	199 (Cu)	262	A, C	256
4411 G	0.04	0.01	148–262	Cu, Ni	189 (Cu)	262	A, C	226
4421 G	0.04	0.02	148–262	Cu, Ni	186 (Cu)	262	A	215
4421[c]						190	A	
4431 G	0.04	0.03	148–262	Cu, Ni	185 (Cu)	262	A	208
4431[c]						165	None	
4431[c]						190	Green solid	
4431[c]						230	Green and red solids	
4431[c]						255	A	
4441 G	0.04	0.04	160–265	Cu, Ni	175 (Cu)	265	A (C)	

Table 20.3 (continued)

Solution No.	Composition $CuSO_4$ (*m*)	Composition $NiSO_4$ (*m*)	Temperature Range of Analysis (°C)	Metals Determined	Precipitation Temperature, Break in Curve (°C)	Quenching Observations: Temperature of Quenching (°C)	Quenching Observations: Solids Found[a]	Visually Observed Precipitation Temperature[b] (°C)
				0.04 *m* UO_2SO_4; 0.02 *m* H_2SO_4				
4422 H	0.04	0.02	165–265	Cu, Ni	245 (Cu)	265	A (C)	313
4432 H	0.04	0.03	165–265	Cu, Ni	223 (Cu)	265	A (C)	241
4442 H	0.04	0.04	165–265	Cu, Ni	218 (Cu)	265	A (C)	

[a]Symbols for solids; minor constituents in parentheses: Z: $2UO_3 \cdot SO_3 \cdot 5H_2O$, zippeite; N: $NiSO_4 \cdot H_2O$; A: $3CuO \cdot SO_3 \cdot 2H_2O$, antlerite; C: $CuSO_4 \cdot H_2O$

[b]From data reported by F. E. Clark *et al.*, *HRP Quar. Prog. Rep. April 30, 1956*, ORNL-2096, p 130.

[c]In these experiments, the systems were quenched after being maintained for long periods of time (up to 1 month) at the indicated temperatures.

distinct types of crystals (zippeite as red crystals, $NiSO_4 \cdot H_2O$ and antlerite as green crystals) but also identified by x-ray examination. The last column of the table lists the temperatures of precipitation as observed visually in quartz tubes.[13]

The only break which may be taken as indicating a temperature of precipitation for zippeite was observed in experiment No. 4031 I, given in the first line of the table. The optical density curves for this run are given in Fig. 20.10, which shows that the solution became saturated at 261°C. While the uranium curve shows this break, the nickel concentration is seen to be approximately constant within the experimental scattering. The solid found in the bomb after quenching from 282°C consisted of red crystals mixed with small amounts of green crystals, and x-ray examination showed these to be $2UO_3 \cdot SO_3 \cdot 5H_2O$ (zippeite) and $NiSO_4 \cdot H_2O$, respectively. The precision of the nickel concentration curve (Fig. 20.10) is not sufficient to show whether the $NiSO_4 \cdot H_2O$ solid formed before the zippeite or appeared as a second solid phase after the initial precipitation of zippeite. At any rate, neither solid is found if the same solution is quenched from 249°C, as shown in the second line of the table. In this run, dealing with the same initial composition, no breaks appeared in the concentration/temperature plots for copper and nickel up to 280°C, but the solution was not analyzed for uranium. The temperature of the bomb was brought back to 249°C

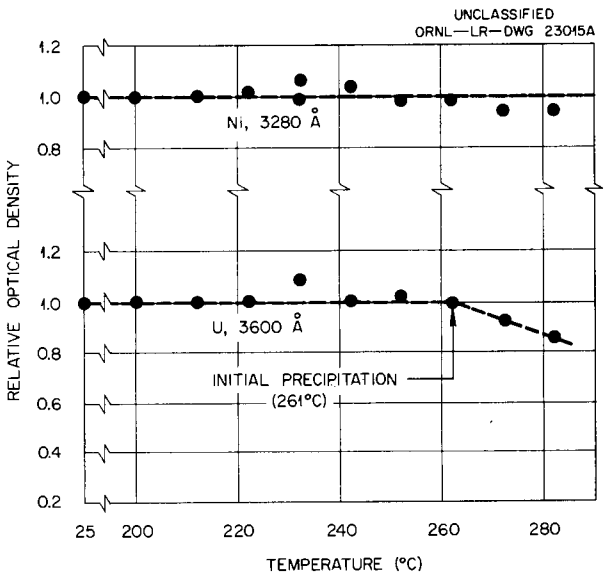

Fig. 20.10. Temperature of Precipitation, Solution 4031 I. Ordinate plots optical density of sample relative to that of original solution.

[13]F. E. Clark *et al.*, *HRP Quar. Prog. Rep. April 30, 1956*, ORNL-2096, p 130.

and held there with shaking for six days before quenching; the absence of solid phase after quenching would suggest redissolving of the solid (or solids) on cooling from 280 to 249°C.

Consistency is not maintained, however, in the remaining runs (solutions 4041 to 4141 of the table), in which zippeite appeared as a final solid after quenching. The method fails to show the expected break in the concentration/temperature curve for the precipitation of the uranium-containing solid. Essentially, the observations show simply that an increase in the concentration of $NiSO_4$ lowers the temperature of precipitation, and that $NiSO_4 \cdot H_2O$ appears as a second solid phase. Zippeite was found either alone or with the $NiSO_4 \cdot H_2O$, whereas the latter was never found as the only solid.

Beginning with solution 4221 in the table, the primary solid produced on heating is the green $3CuO \cdot SO_3 \cdot 2H_2O$, antlerite; and the method consistently shows a break in the concentration/temperature plot for copper content, corresponding to temperature of precipitation. Duplicate runs on the same initial composition gave fairly good agreement for these temperatures, as seen in solutions 4231, 4241, and 4321 (within 5 to 15°C). X-ray examination showed the presence of $CuSO_4 \cdot H_2O$ as a second solid phase in many of the solids of this region.

The temperatures for the appearance of nonhomogeneity in solutions 0.04 *m* in UO_2SO_4 and 0.01 *m* in H_2SO_4 are roughly mapped out in Fig. 20.11. At low copper and nickel concentrations the initial phase separation is the appearance of a second liquid phase. The information for the boundaries and the contours of this region comes from an earlier report.[13] The rest of the figure is divided into two areas. With <0.02 *M* $CuSO_4$ and with >0.01 *M* $NiSO_4$ the first and principal solid phase is zippeite, $2UO_3 \cdot SO_3 \cdot 5H_2O$, which is then accompanied by $NiSO_4 \cdot H_2O$ as a second solid. The precipitation temperature is lowered considerably by $NiSO_4$ (especially at low $NiSO_4$ concentration near the two-liquid region) and somewhat less by $CuSO_4$; but no significant temperature contours can be drawn from the data. In the remaining area of the diagram, $3CuO \cdot SO_3 \cdot 2H_2O$ (antlerite) is the first and principal precipitate, accompanied in many cases by $CuSO_4 \cdot H_2O$ as a second solid. In this area the precipitation temperature falls steeply from its maximum at the

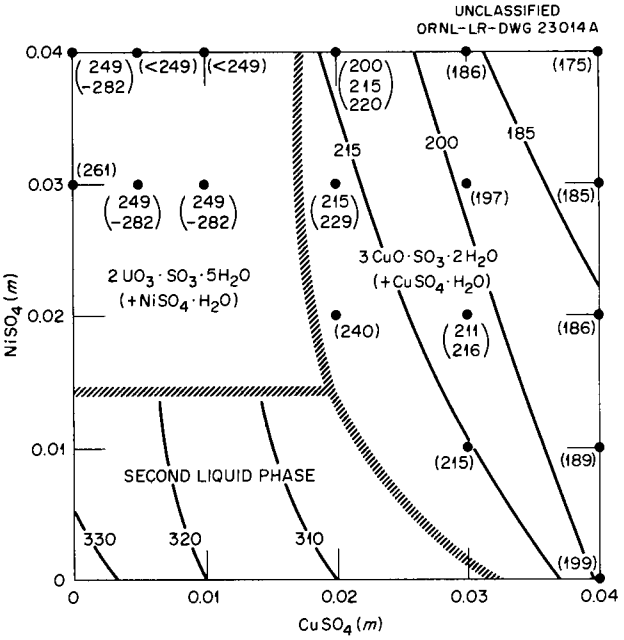

Fig. 20.11. The Effect of $CuSO_4$ and $NiSO_4$ on Phase Transition Temperatures: 0.04 *m* UO_2SO_4; 0.01 *m* H_2SO_4.

border of the two-liquid region, and the effect of $CuSO_4$ is greater than that of $NiSO_4$, as expected for a precipitate containing copper but not nickel.

The results for the antlerite region seem to be on the whole both consistent and dependable. The procedure avoids reaction with quartz and also evidently avoids the supersaturation encountered in the earlier work with the visual method,[13] inasmuch as the new precipitation temperatures are in general considerably lower than those observed visually (last column of Table 20.3). For the zippeite region, however, the method has not been successful. Among the faults or difficulties which may account for the failure, one may be the insufficient precision of the spectrophotometric analytical values. Another is probably inherent in the system, involving persistent and variable supersaturation with respect to zippeite as solid phase. Still another is the fact that continued removal of successive samples for analysis is bound to cause ultimately a significant change in the residual liquid composition as the vapor-to-liquid volume ratio increases. If the method is resumed at all, it will be modified by the use of a number of simultaneous fillings for one solution, so that only a few samples will have

to be removed from each bomb to cover a considerable temperature range for a given initial composition.

The last three lines of Table 20.3 give the temperatures of precipitation of antlerite in solutions with higher concentration of excess H_2SO_4 (0.02 *M*). Comparison with solutions 4421, 4431, and 4441 of the first part of the table shows that increasing the excess acid from 0.01 to 0.02 *m* in this region raises the temperature of precipitation by 40 to 60 degrees.

In the course of the x-ray examination of the solid phases reported, the diffraction pattern for the compound $2UO_3 \cdot SO_3 \cdot 5H_2O$, zippeite, was determined and it was found to be slightly different from the pattern available in the literature.[14] The two patterns are given in Table 20.4 for comparison. The differences are considered to be significant and to constitute a correction of the older pattern.

[14] C. Frondel, *Am. Mineralogist* **37**, 950 (1952).

Table 20.4. X-Ray Diffraction Spacings for $2UO_3 \cdot SO_3 \cdot 5H_2O$ (Zippeite)

Observed (Tracing Pattern)		Literature*		Observed (Tracing Pattern)		Literature*	
d (Å)	*I*	*d* (Å)	*I*	*d* (Å)	*I*	*d* (Å)	*I*
8.58	2	8.65	4	2.00	?		
7.02	8	7.06	10	1.936	5	1.935	6
		6.45	2			1.876	2
5.43	1	5.44	4	1.843	1	1.856	2
4.28	2	4.27	5	1.814	2	1.816	5
3.90	2	3.88	3	1.763	1		
		3.63	4	1.743	3	1.745	6
3.52	9	3.51	8	1.691	4	1.694	1
3.45	4			1.672	2	1.666	1
3.26	1			1.633	1	1.632	1
3.10	10	3.12	9			1.598	5
2.86	4	2.86	6	1.567	2	1.563	2
		2.71	2	1.545	1		
2.64	4	2.65	5			1.519	2
2.46	4	2.47	5	1.49	1	1.494	1
2.35	1	2.34	2			1.458	2
2.27	1					1.424	4
2.22	2	2.21	4	1.397	2	1.396	1
2.14	1	2.14	3	1.369	1	1.367	1
2.07	2	2.09	2	1.32	1	1.326	1
2.04	2	2.05	5				

*Ref 14.

21. RADIATION CHEMISTRY

H. A. Mahlman J. W. Boyle

21.1 HYDROGEN YIELDS IN AQUEOUS SODIUM NITRATE SOLUTIONS BY COBALT-60 GAMMA RAY RADIOLYSIS

In the decomposition of aqueous solutions by ionizing radiations, hydrogen atoms and hydroxyl radicals have been assumed to be intermediate products.[1] The observed molecular products, hydrogen and hydrogen peroxide, have been assumed to be produced by the reaction of hydrogen atoms and hydroxyl radicals with themselves as they diffuse out of the "hot spots" where they are formed. The suppression of molecular yields by solutes is in agreement with these assumptions. Evidence is presented below that the nitrate ion will lower the hydrogen yield.

The water used was purified and stored in silica vessels.[2] The chemicals were Baker and Adamson reagent grade and were used without purification. Aliquots of the solutions, containing 10^{-3} *M* KBr to ensure radical recombination,[3] were degassed by alternately freezing, applying a 10^{-6} mm vacuum, and thawing. Five cycles reduced the residual gas volume to less than 0.001 cc STP per sample.

All irradiations were made by utilizing a Co^{60} gamma-ray source supplying a dose rate of 7×10^{20} ev·liter^{-1}·min^{-1} relative to the ferrous dosimeter value of 15.6 molecules oxidized per 100 ev of absorbed energy.[4] This annularly loaded cylindrical source provided homogeneous irradiation for centrally placed samples.[5] Hydrogen determinations were made by ignition with oxygen on a platinum filament.[6] Determinations of ferric ion were made spectrophotometrically with a Cary recording spectrophotometer at 3050 Å and calculated by using a molar extinction coefficient of 2240 at 25°C (ref 4).

The hydrogen yields, $G(H_2)$, are the number of molecules formed per 100 ev of absorbed energy. In Fig. 21.1 are plotted the initial hydrogen yields as a function of the cube root of the nitrate ion molarity. Assuming the radical mechanism for the formation of molecular hydrogen, the observed suppression (postulated by Boyle and Mahlman[7] and demonstrated by Sowden's[8] mixed neutron and gamma-ray irradiations of $Ca(NO_3)_2$ solutions) may be interpreted as substantiating evidence for the reaction of hydrogen atoms with nitrate ion. This reaction has been postulated by Bakh.[9]

The dependence of the hydrogen yield on the cube root of the nitrate ion concentration is similar to the cube-root dependence found by Sworski[2] on the H_2O_2 yield in KBr solution and supports the radical diffusion hypothesis for molecular hydrogen formation. A least-squares analysis of the data gave the equation

$$G(H_2) = -0.40\,[NO_3^-]^{1/3} + 0.45 \ .$$

The sodium nitrate solutions studied were 6.35×10^{-4}, 1.09×10^{-3}, 3.33×10^{-3}, 7.96×10^{-3}, 2.68×10^{-2}, 6.05×10^{-2}, 0.15 and 0.31 *M*.

[1] A. O. Allen, *Discussions Faraday Soc.* **12**, 79 (1952).

[2] T. J. Sworski, *J. Am. Chem. Soc.* **76**, 4687 (1954).

[3] C. J. Hochanadel, *J. Phys. Chem.* **56**, 587 (1952).

[4] C. J. Hochanadel and J. A. Ghormley, *J. Chem. Phys.* **21**, 880 (1953).

[5] J. A. Ghormley and C. J. Hochanadel, *Rev. Sci. Instr.* **22**, 473 (1951).

[6] K. W. Saunders and H. A. Taylor, *J. Chem. Phys.* **9**, 616 (1941).

[7] J. W. Boyle and H. A. Mahlman, *Radiation Chemistry of Thorium Nitrate Breeder-Blanket Solutions*, paper presented at the Second Annual Meeting of the American Nuclear Society, Chicago, 1956.

[8] R. G. Sowden, *J. Am. Chem. Soc.* **79**, 1263 (1957).

[9] N. A. Bakh, *Conf. Acad. Sci. U.S.S.R. Peaceful Uses of Atomic Energy. Sess. Div. Chem. Sci.*, p 23 (1955).

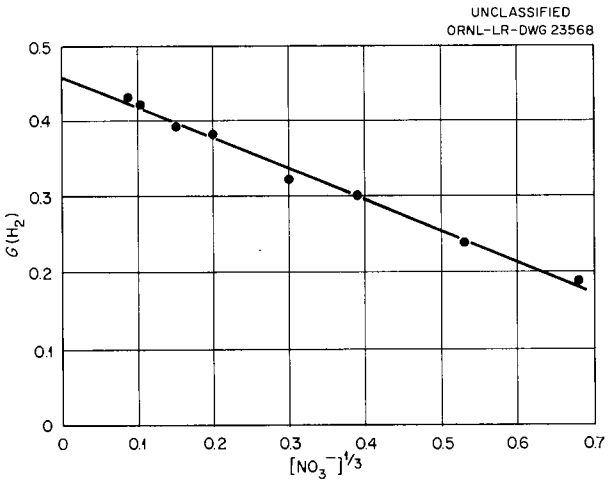

Fig. 21.1. Suppression of Hydrogen Yields by Nitrate Ion.

Part VII

ANALYTICAL CHEMISTRY

M. T. Kelley

22. ANALYTICAL CHEMISTRY

O. Menis

R. G. Ball
C. M. Boyd
G. Goldstein
H. P. House
D. L. Manning
R. H. Powell
T. C. Rains
I. B. Rubin

22.1 ANALYSIS OF THORIUM OXIDE

22.1.1 Colorimetric Estimation of Aluminum

A multiple solvent-extraction procedure was developed for use in the isolation and subsequent colorimetric estimation of low concentrations of aluminum in slurries of thorium oxide which are contaminated with corrosion products of stainless steel, additives, and impurities. The isolation of aluminum is achieved by first extracting a dilute perchloric acid solution of the slurry with thenoyltrifluoroacetone in chloroform, followed by subsequent extractions of the raffinates with diethyldithiocarbamate in chloroform and 8-quinolinol in chloroform. The absorption of the aluminum complex of 8-quinolinol in chloroform is then measured at a wavelength of 390 mμ, from which the aluminum is calculated. The method is suitable for the evaluation of aluminum concentrations in the range of 10 to 150 μg/ml, with a coefficient variation of about 3%. Although complex, the procedure is satisfactory for the separation of aluminum from a thorium matrix contaminated with trace quantities of uranium, iron, nickel, chromium, titanium, zirconium, vanadium, molybdenum, copper, zinc, manganese, cobalt, and tin. In the absence of manganese, cobalt, tin, and zinc, the second step, with diethyldithiocarbamate in chloroform, need not be made; but in this case, however, the organic phase, containing complexes of 8-quinolinol, is washed with an aqueous solution of sodium cyanide to eliminate nickel and copper.

22.1.2 Flame Photometric Determination of Aluminum

As a consequence of the complexity of the preceding and other methods for determining the aluminum content of thorium oxide slurries, a successful application of the flame-photometric method has been made. This procedure is based on the solvent extraction of an acetate solution of the slurry with thenoyltrifluoroacetone in hexone, after which the aluminum is estimated from measurements of the radiant intensity of the organic phase, in a flame spectrophotometer, at a wavelength of 484 mμ. Hexavalent uranium and chromium, thorium, potassium, calcium, and magnesium in concentrations from 0.04 to 1 mg/ml do not interfere; however, sodium, lithium, and titanium interfere when present in similar concentrations. Barium and trivalent iron interfere only at the 1-mg/ml level, while molybdenum, tungsten, copper, and nickel interfere when present in concentrations from 0.02 to 1 mg/ml. Except for the presence of impurities in the concentrations noted above, this method can be used satisfactorily over the range from 5 to 50 μg of aluminum per milliliter with a coefficient of variation of 10%.

22.2 ANALYSIS OF URANYL SULFATE SOLUTIONS

22.2.1 Polarographic Determination of Zinc

A polarographic method was developed for the determination of low concentrations of zinc in solutions of uranyl sulfate, for which the ORNL, high-sensitivity, derivative polarograph is utilized. Zinc is separated from uranium by extracting it from a basic carbonate solution with a chloroform solution of diethyldithiocarbamate. The zinc is then extracted from the organic phase with 0.1 *M* HCl, after which the concentration of the element is measured polarographically. The polarographic measurement is based on the reduction of divalent zinc at a half-wave potential of −1.0 v vs the standard calomel electrode. Concentrations, of the order of 0.5 μg of zinc per milliliter in a volume of 10 ml, can be estimated by the use of this procedure with a coefficient of variation of about 5%.

22.2.2 Flame Photometry of Ruthenium

A flame-photometric method is being examined for the determination of ruthenium in solutions of uranyl sulfate. The radiant intensity of an RuO band at a wavelength of 374 mμ was found to be sufficient for the estimation of this element in solutions that contain at least 10 μg of ruthenium per milliliter. Within the range, 10 to 50 μg/ml,

the radiant energy is a linear function of the concentration of either $RuCl_3$ or the ruthenium nitroso salt in solution. Flame photometry can, therefore, be applied to the determination of ruthenium as the nitroso salt, thus giving this method a distinct advantage over colorimetric methods, which are inapplicable if the ruthenium is present as this salt. Uranium and iron, which interfere in the flame-photometric method, must first be separated from ruthenium by extraction; but, for solutions of uranyl sulfate very low in ruthenium, 20 ppm or less, the concentration of ruthenium in the raffinate is below the detectable level of 10 μg/ml of the ORNL flame photometer. An attempt will be made to utilize the Beckman flame photometer, which is more sensitive than the ORNL instrument in the ultraviolet region, for this purpose.

OAK RIDGE NATIONAL LABORATORY
HOMOGENEOUS REACTOR PROJECT

AUGUST 1, 1957

PROJECT DIRECTOR
R. B. BRIGGS — O

ASSOCIATE PROJECT DIRECTOR
C. E. WINTERS** — D
A. L. GUNNELS, SEC. — D

PROJECT EDITOR
W. D. REEL — TI

DESIGN AND ENGINEERING
J. A. LANE, DIRECTOR — REE
R. N. LYON, ASSISTANT DIRECTOR — REE
T. S. CARLSMITH, SEC. — REE

DESIGN
W. R. GALL, SECTION CHIEF — REE
M. I. LUNDIN, ASSISTANT SECTION CHIEF — REE

MECHANICAL DESIGN
F. C. ZAPP, GROUP LEADER — REE
F. C. BOWEN — VITRO
C. A. BURCHSTED — REE
C. J. CLAFFEY — REE
C. W. COLLINS — REE
E. M. GUGLIELMO — VITRO
R. C. HOREN — WESTINGHOUSE
A. C. PHILLIPS — VITRO
R. G. PITKIN — VITRO
J. N. ROBINSON — REE
D. D. TARR — VITRO
W. L. WRIGHT — REE

PROCESS DESIGN
R. C. ROBERTSON, GROUP LEADER — REE
J. C. BOLGER — REE
E. H. GIFT — REE
H. A. MCLAIN — REE
R. O. MAAK — FOSTER-WHEELER

STRESS ANALYSIS
R. D. CHEVERTON, GROUP LEADER — REE
R. H. CHAPMAN — REE
T. H. MALMEY — REE
R. E. SCHAPPEL — REE

PLANT LAYOUT AND DRAFTING
C. L. SEGASER, GROUP LEADER — REE
W. ROBINSON — REE
W. TERRY* — REE
H. M. BRADFORD — REE
R. L. CAUBLE — REE
C. W. DAY — REE
J. P. DILORENZO — REE
W. B. KRICK — REE
A. S. LUDLOW — REE
C. A. ROBERTS — REE
R. D. SATTERFIELD — REE
R. H. SIGLER — REE
W. G. STERLING — REE

REACTOR ANALYSIS
P. R. KASTEN, SECTION CHIEF — REE

REACTOR PHYSICS
T. B. FOWLER — REE
C. W. NESTOR, JR. — REE
M. W. ROSENTHAL — REE
M. TOBIAS — REE

LONG RANGE STUDIES
S. JAYE — REE
M. P. LIETZKE — REE
B. E. PRINCE — REE

SPECIAL ASSIGNMENT
H. C. CLAIBORNE — REE

ENGINEERING DEVELOPMENT
I. SPIEWAK, SECTION CHIEF — REE

HEAT EXCHANGERS, TITANIUM PROGRAM, MISCELLANEOUS EQUIPMENT
J. S. CULVER, GROUP LEADER — REE
B. D. DRAPER — TVA
P. P. HOLZ* — REE
I. K. NAMBA — REE
H. C. ROLLER — REE

PUMPS
C. H. GABBARD, GROUP LEADER — REE
J. M. BAKER — REE
R. BLUMBERG — REE
E. C. HISE — REE
J. C. MOYERS — REE
H. R. PAYNE — REE
J. P. HURST — REE
R. J. LOCKETT — REE
T. R. WILSON — REE

MRT MOCKUP, RECOMBINERS
P. H. HARLEY, GROUP LEADER — REE
B. A. HANNAFORD — REE
O. L. SNYDER — REE
D. E. WILLIS — REE
T. L. CASTILE — REE
A. B. DAFFRON — REE
R. GOODMAN — REE
W. M. PARKS — REE

SPECIAL ASSIGNMENT
P. P. HOLZ* — REE
T. W. CATE — REE
C. C. HURT — REE
L. E. PENTON — REE
S. R. WEST — REE

ENGINEERING RESEARCH
R. B. KORSMEYER, SECTION CHIEF — REE
F. N. PEEBLES, ASSISTANT SECTION CHIEF — REE

SLURRY PROPERTIES
D. G. THOMAS, GROUP LEADER — REE
L. L. BENNETT — REE
R. B. GALLAHER — REE
C. H. GIBSON — REE
W. R. MIXON — REE
C. S. MORGAN — REE
R. H. NINMO — REE

SLURRY BLANKET SYSTEM DEVELOPMENT
L. F. PARSLY, GROUP LEADER — REE
V. L. KENYON † — REE

SPECIAL ASSIGNMENT
H. L. FALKENBERRY — TVA
C. G. LAWSON — REE
M. RICHARDSON — REE
C. F. VANDEN BULCK — UCNC

SERVICES
A. N. SMITH — REE
T. L. BOSWELL — REE
R. E. CARNES — REE
B. R. CHILCOAT — REE
J. T. DICKIE — REE
C. M. FITZPATRICK — REE
C. A. GIFFORD — REE
P. H. HAYES — REE
C. A. MCLAUGHLIN — REE
H. G. MOORE — REE
R. E. POTTER — REE
R. M. SUMMERS — REE
B. J. SUTTON — REE
D. H. WALLACE — REE

INSTRUMENTATION AND CONTROLS
D. S. TOOMB, SECTION CHIEF — I&C

MRT
J. R. BROWN, GROUP LEADER — I&C
R. M. PIERCE* — TVA
H. D. WILLS — I&C
R. W. BORGERS — I&C

HRP SUPPORTING FACILITIES
D. G. DAVIS, GROUP LEADER — I&C
S. J. BALL — I&C
G. W. GREENE — I&C
J. D. GRIMES — TVA
P. G. HERNDON — I&C
J. A. RUSSELL — I&C
R. M. BURNETT — I&C
M. A. MEADHAM — I&C
P. E. SMITH — I&C

VALVES AND ACTUATORS
A. M. BILLINGS, GROUP LEADER — I&C
E. H. BELL — I&C
B. J. JONES — I&C
P. F. MURAY — I&C
A. J. SHARENBERGER* — I&C

INSTRUMENT DEVELOPMENT
R. L. MOORE, GROUP LEADER — I&C

REACTOR MATERIALS RESEARCH
E. G. BOHLMANN, ASSISTANT DIRECTOR — REE
T. F. KELLEY, SEC. — REE
R. E. WACKER, RECORDS — REE

SOLUTIONS
J. C. GRIESS, ASSISTANT SECTION CHIEF — REE

LOOPS
R. S. GREELEY — REE
S. R. BUXTON — REE
J. E. EVE — REE
W. H. HINDS — REE

LABORATORY STUDIES
J. L. ENGLISH, GROUP LEADER — REE
D. N. HESS — REE
P. D. NEUMANN — REE
L. L. FAIRCHILD — REE
H. L. BARKER — REE
P. B. DAVIS — REE
B. L. JOHNSON — REE
H. R. TINCH — REE
J. L. UNDERWOOD — REE

SLURRIES
E. L. COMPERE, ASSISTANT SECTION CHIEF — REE

LOOPS
S. A. REED,* GROUP LEADER — REE

TOROIDS
S. A. REED* — REE
R. F. BENSON — REE
F. E. MCDANIEL — REE

ENGINEERING
H. C. SAVAGE, ASSISTANT SECTION CHIEF — REE

SOLUTIONS
S. E. BOLT, GROUP LEADER — REE
D. W. HUBBARD — REE
W. C. ULRICH — REE

IN-PILE MOCKUPS
J. R. HART, LEADER — REE
C. H. BURBAGE — REE
H. F. HENDERSON — REE
B. H. PARKS — REE
B. W. SCOTT — REE

100A LOOP OPERATIONS
J. F. WINESETTE* — REE
L. L. ALLEN — REE
C. M. BURCHELL — REE
C. L. FRANCIS — REE
J. B. FRENCH — REE
D. G. GATES — REE
J. W. GOOCH — REE
J. E. JACKSON — REE
T. R. RAYBURN — REE
W. A. WAGNER — REE

SLURRIES
D. T. JONES, GROUP LEADER — REE
R. M. WARNER — REE

IN-PILE TOROIDS
J. D. BARNES — REE

100A LOOP OPERATIONS
J. F. WINESETTE* — REE
C. R. BENSON — REE
G. A. MOORE — REE
L. G. PHELPS — REE
A. E. PUGH — REE

REACTOR OPERATIONS
R. A. LORENZ, GROUP LEADER — REE
J. W. BROWN — REE
V. A. DECARLO — REE
F. J. WALTER — REE
V. R. BULLINGTON — REE
W. E. TEICHERT, A SHIFT LEADER — REE
C. E. ROBERTS — REE
E. H. GUINN, B SHIFT LEADER — REE
J. P. GORDON — REE
D. M. SMITH — REE
A. L. SUTTON, C SHIFT LEADER — REE
R. A. JONES — REE
R. M. WALLER — REE
J. W. MYERS, D SHIFT LEADER — REE
J. W. MOSIER — REE
R. G. ROSS — REE

RADIATION
G. H. JENKS, SECTION CHIEF — REE

IN-PILE LOOPS
J. R. MCWHERTER, GROUP LEADER — REE
J. E. BAKER — REE
S. H. WHEELER — REE

IN-PILE BOMBS
R. J. DAVIS, GROUP LEADER — C
K. S. WARREN — C
J. L. RUTHERFORD — REE
R. L. PLEMONS — REE

SUPPORTING RESEARCH
A. L. BACARELLA — C
M. D. SILVERMAN — C
W. C. YEE — C

REMOTE EVALUATION
A. R. OLSEN — REE
B. W. MCCOLLUM, SHIFT LEADER — REE
W. J. SCHILL — REE
W. H. SMITH, JR. — REE
J. C. THOMPSON — REE

METALLURGY
G. M. ADAMSON, SECTION CHIEF — M

METALLURGICAL RESEARCH
M. L. PICKLESIMER, LEADER — M
P. L. RITTENHOUSE — M
R. L. STEPHENSON — M
P. J. JONES — M
G. C. NELSON — M
M. A. WHEELER — M

METALLURGICAL ENGINEERING
E. S. BOMAR, LEADER — M
F. W. COOKE — M
E. A. FRANCO-FERREIRA** — M
W. J. LEONARD — M
J. J. PRISLINGER — M
J. K. WHITE — M
C. M. SMITH — M
J. J. WOODHOUSE — M

METALLOGRAPHY
R. S. CROUSE,** LEADER — M
T. M. KEGLEY, JR. — M
W. J. WERNER** — M
E. R. BOYD — M
B. F. DAY** — M
R. L. FITZGERALD — M
T. J. HENSON** — M
L. G. SHRADER** — M

RADIATION DAMAGE
R. C. BERGGREN — SS
J. C. WILSON — SS
F. M. GRIZZEL — SS

PERSONNEL SUMMARY

	FULL TIME	PART TIME	INDUSTRIAL PARTICIPANTS
ADMINISTRATION	7	4	
ANALYTICAL CHEMISTRY	40		
CHEMICAL RESEARCH	8	10	
CHEMICAL TECHNOLOGY	45	13	
DESIGN AND ENGINEERING	113		6
HOMOGENEOUS REACTOR TEST	38		5
REACTOR MATERIALS RESEARCH	96	6	
TOTAL	347	33	11

CHEMICAL TECHNOLOGY
O. E. FERGUSON,* PROGRAM LEADER — CT
I. LOOPE, SEC. — CT
R. WILLIAMS, SEC. — CT

CHEMICAL DEVELOPMENT
O. E. FERGUSON,* SECTION CHIEF — CT

BLANKET PROCESSING
R. E. LEUZE, PROBLEM LEADER — CT
R. D. BAYBARZ — CT
J. M. CHILTON — CT
S. S. KIRSLIS — CT
J. M. DELOZIER — CT
R. L. HICKEY — CT
O. K. TALLENT — CT

CORE PROCESSING
R. A. MCNEES, PROBLEM LEADER — CT
M. N. LLOYD — CT
S. PETERSON — CT
W. B. HOWERTON — CT

THORIUM BLANKET STUDIES
J. P. MCBRIDE, PROBLEM LEADER — CT
E. V. JONES — C
N. A. KROHN — CT
L. E. MORSE — CT
R. L. PEARSON — CT
C. E. SCHILLING — CT
C. W. GREENE — CT
P. P. MAYDON — CT
W. L. PATTISON — CT
H. F. SOARD — CT

DESIGN
W. E. UNGER, ASSISTANT SECTION CHIEF — CT

PROCESS DESIGN
H. O. WEEREN — CT

PROJECT DESIGN
G. B. BERRY** — E&M
F. C. MCCULLOUGH — CT
E. B. BRIDGES** — E&M
J. D. CUPP** — E&M
H. W. FALLON** — E&M
P. P. FERBO** — E&M
W. J. LEE** — CO-OP, GA. TECH.
J. H. MANNEY** — E&M
J. P. NICHOLS** — CO-OP, UNIV. OF TENN.
F. L. PEISHEL** — E&M
J. PHILLIPS** — E&M
K. F. STOOKSBURY** — CT
J. N. WHEELER** — E&M

LOOP DESIGN
T. A. ARehART — CT
B. B. KLIMA — CT
W. F. SCHAFFER — CT

INSTRUMENTATION
C. S. LISSER — I&C

PILOT PLANT
R. B. LINDAUER,** SECTION CHIEF — CT

SLURRY PREPARATION
E. M. SHANK, PROBLEM LEADER — CT
C. V. ELLISON — CT

UNIT OPERATIONS
P. A. HAAS, GROUP LEADER — CT

CORE PROCESSING
R. W. HORTON — CT
E. L. YOUNGBLOOD — CT
R. D. ARTHUR — CT
R. C. EARLY — CT
S. G. KENT — CT

UO_2SO_4 BLANKET PROCESSING
S. O. CLINTON — CT
J. W. SNIDER — CT
F. N. MCLAIN — CT
D. A. MCMINTER — CT
G. E. WOODALL — CT

THORIUM BLANKET STUDIES
C. C. HAWS — CT
W. W. PITTS, JR. — CT
W. M. WOODS — CT
V. L. FOWLER — CT

CHEMICAL RESEARCH
E. H. TAYLOR,** DIRECTOR — C
E. SCHAPPEL, SEC. — C

FUEL SOLUTION CHEMISTRY
H. F. MCDUFFIE, GROUP LEADER — C
W. L. MARSHALL, GROUP LEADER — C
F. E. CLARK — C
J. S. GILL — C
G. M. HEBERT — C
R. SLUSHER — C
H. H. STONE — C
F. H. SWEETON — C

RADIATION CHEMISTRY
C. J. HOCHANADEL,** GROUP LEADER — C
J. W. BOYLE** — C
N. A. MAHLMANN** — C

HEAVY ELEMENT CHEMISTRY
R. W. STOUGHTON,** GROUP LEADER — C
J. HALPERIN** — C
M. H. LIETZKE** — C
W. C. WAGGENER** — C

INORGANIC SOLUTION CHEMISTRY
K. A. KRAUS,** GROUP LEADER — C
T. A. CARLSON** — C
H. O. PHILLIPS** — C

ANALYTICAL CHEMISTRY
MYRON T. KELLEY,** DIRECTOR
C. D. SUSANO,** ASSOCIATE DIRECTOR
K. ODOM, SEC. — AC

CORROSION ANALYTICAL LABORATORY
O. MENIS,* SUPERVISOR — AC
H. P. HOUSE, ASSISTANT SUPERVISOR — AC

RESEARCH
O. MENIS,* GROUP LEADER — AC
R. G. BALL — AC
C. M. BOYD — AC
G. GOLDSTEIN — AC
D. L. MANNING — AC
R. H. POWELL — AC
T. C. RAINS — AC
I. B. RUBIN — AC

SERVICES
C. K. TALBOTT, GROUP LEADER — AC
N. M. FERGUSON — AC
F. L. LAYTON — AC
T. P. BACON — AC
W. D. CLAPP, JR. — AC
C. A. CLERK — AC
P. S. GOODWIN — AC
B. D. HICKS — AC
T. G. MILLER — AC
V. S. NORMAN — AC
E. ONKST — AC

HRT AND IN-PILE LOOP ANALYSES
U. KOSKELA, SUPERVISOR — AC
L. G. FARRAR, ASSISTANT SUPERVISOR — AC
J. E. ATTRILL — AC
C. P. ARTHUR — AC
R. E. CORCORAN — AC
S. R. DINSMORE — AC
J. L. MOTTERN — AC
G. M. CAMPBELL — AC
G. I. GAULT — AC
M. N. MCCORQUODALE — AC
J. SLESSINGER, JR. — AC
W. W. WARREN — AC
H. L. WEBB — AC
H. L. WHITTINGTON — AC

HRT DEVELOPMENT
P. F. THOMASON, GROUP LEADER — AC
R. E. BIGGERS — AC
F. J. MILLER — AC
S. A. REYNOLDS, GROUP LEADER — AC
T. H. HANDLEY — AC

HIGH RADIATION LABORATORY
C. L. BURROS — AC

HOMOGENEOUS REACTOR TEST
S. E. BEALL, PROJECT ENGINEER — REE
B. EUBANK, SEC. — REE
M. SWANK, SEC. — CT

OPERATIONS PLANNING
S. I. KAPLAN, GROUP LEADER — REE
J. R. BUCHANAN — CT

SPECIAL ASSIGNMENT
H. M. MCLEOD — CT

REACTOR TEST PROGRAM
J. W. HILL, JR., CHIEF — REE
R. SMITH — REE
J. R. ENGEL, SUPERVISOR — CT
R. J. HARVEY — REE
H. K. SEARCH — PA. POWER AND LIGHT CO.
H. D. CURTIS — REE
D. T. GODWIN — REE
A. L. JOHNSON — REE
J. D. FLYNN, SUPERVISOR — REE
H. F. BAUMAN — CT
N. C. BRADLEY — CT
W. T. BOSTIC — CT
E. W. BROWN — CT
T. G. HILL — REE
J. O. KOLB, SUPERVISOR — REE
N. A. BROWN — TVA
O. F. FRECH — REE
H. L. BROWN — REE
R. J. SHANNON — CT
J. E. WOLFE — REE
G. W. RIVENBARK, SUPERVISOR — REE
T. H. GLADNEY — TVA
R. H. GUYMON — CT
R. J. HUNTER — REE
L. J. SHERSKY — CT
J. L. STEPP — REE

CHEMICAL PLANT COORDINATION
W. D. BURCH, GROUP LEADER — CT
W. L. ALBRECHT — TVA
R. H. WINGET — CT
W. A. LINDSEY — CT

REACTOR COORDINATION
R. VAN WINKLE, GROUP LEADER — REE
J. A. WATTS — REE

REACTOR ANALYSIS
P. N. HAUBENREICH, GROUP LEADER — REE

MAINTENANCE PLANNING
W. TERRY,* SUPERVISOR — REE
T. E. HAYNES — REE
G. H. JOHNSTONE — REE

REACTOR MATERIALS AND CHEMISTRY
D. M. RICHARDSON, GROUP LEADER — C
J. D. JONES — REE

INSTRUMENTATION
K. W. WEST, GROUP LEADER — I&C
R. M. PIERCE* — TVA
A. J. SHARONBERGER* — I&C

SUBCONTRACTS
AEROJET-GENERAL CORPORATION
ARMOUR RESEARCH FOUNDATION
HOUDRY PROCESS CORPORATION
OHIO STATE UNIVERSITY
STANFORD RESEARCH INSTITUTE
SYRACUSE UNIVERSITY
TULANE UNIVERSITY
UNIVERSITY OF FLORIDA
UNIVERSITY OF TENNESSEE
UNIVERSITY OF UTAH
UNIVERSITY OF VIRGINIA
VITRO LABORATORIES

INDUSTRIAL PARTICIPATION
FOSTER-WHEELER
PENNSYLVANIA POWER AND LIGHT COMPANY
TENNESSEE VALLEY AUTHORITY
UNION CARBIDE NUCLEAR COMPANY, NEW YORK
WESTINGHOUSE ELECTRIC CORPORATION

AC ANALYTICAL CHEMISTRY
C CHEMISTRY DIVISION
CT CHEMICAL TECHNOLOGY DIVISION
D DIRECTOR'S DIVISION
E&M ENGINEERING AND MECHANICAL DIVISION
I&C INSTRUMENTATION AND CONTROLS DIVISION
M METALLURGY DIVISION
REE REACTOR EXPERIMENTAL ENGINEERING DIVISION
SS SOLID STATE DIVISION
TI TECHNICAL INFORMATION DIVISION
† DUAL CAPACITY
** PART TIME ON PROJECT
* ON SABBATICAL LEAVE FROM DUKE UNIVERSITY